

A Discrete-Continuous Algorithm for Globally Optimal Free Flight Trajectory Optimization

Dissertation

zur Erlangung des Grades eines
Doktors der Naturwissenschaften (Dr. rer. nat.)
am Fachbereich Mathematik und Informatik
der Freien Universität Berlin

vorgelegt von

Fabian Danecker

2023

Datum der Verteidigung: 29. April 2024

Supervisoren: Prof. Dr. Ralf Borndörfer und
Dr. Martin Weiser

Gutachter

Erstgutachter: Prof. Dr. Ralf Borndörfer

Zweitgutachter: Prof. Dr. Anton Schiela

Selbstständigkeitserklärung

Ich erkläre hiermit, dass ich die vorliegende Dissertation selbstständig und ohne Benutzung anderer als der angegebenen Quellen und Hilfsmittel angefertigt habe. Diese Dissertation wurde in gleicher oder ähnlicher Form noch in keinem früheren Promotionsverfahren eingereicht.

Darüber hinaus bestätige ich hiermit, dass die Mitautoren der dieser Arbeit zugrunde liegenden wissenschaftlichen Artikel der detaillierten Zuordnung der individuellen Beiträge am Ende jedes Artikel zustimmen.

Ort, Datum

Fabian Danecker

Acknowledgements

Personal

I would like to express my deepest gratitude to my thesis supervisors, Martin Weiser and Ralf Borndörfer, for their unwavering support, guidance, and mentorship throughout my doctoral journey. Their expertise, dedication, and patience have been invaluable in shaping the research presented in this thesis.

I am also indebted to my colleagues at ZIB, who have been a constant source of inspiration and joy. In particular, I would like to extend my heartfelt thanks to Adam Schienle, Arturas Jocas, Berenike Masing, Boris Grimm, Denise Rings, Elmar Swarat, Enrico Bortoletto, Fabian Löbel, Fatemeh Chegini, Felix Baumann, Grégoire Portier, Hazim Saleh, Julia Ullrich, Karlotta Kruschke, Lea Strubberg, Luitgart Kraus, Marco Blanco Sandoval, Niels Lindner, Paolo Villani, Patricia Ebert, Pedro Maristany de las Casas, Phillip Semler, Ricardo Euler, Stefan Schwartz, Stefan Zachow, Torsten Klug, Thomas Schlechte, Wai Tang Victor Chan, and William Suarau. Their enthusiastic collaboration have enriched my academic experience and played a pivotal role in the development of this work.

Funding

This research was funded by the DFG Research Center of Excellence MATH+ – Berlin Mathematics Research Center, Projects AA3-3 and TrU-4.

Zusammenfassung

In dieser Dissertation wird der neuartige hybride Algorithmus DisCOptER für global optimale Flugplanung vorgestellt.

DisCOptER (Discrete-Continuous Optimization for Enhanced Resolution) verbindet diskrete und kontinuierliche Optimierung in einem zweistufigen Ansatz um optimale Trajektorien unter strengen Genauigkeitsanforderungen in endlicher Zeit zu finden. Im ersten Schritt wird ein gerichteter Graph erzeugt und damit implizit eine Menge potentieller Pfade definiert, die den relevanten Teil des Trajektorienraumes gleichmäßig abdeckt. Vielversprechende Kandidaten werden mithilfe von Yen's Algorithmus identifiziert. Diese dienen als Startpunkte für die zweite Stufe, in welcher lokal konvergente Methoden der Optimalsteuerung eingesetzt werden um kontinuierliche Lösungen zu generieren.

Die Korrektheit, Genauigkeit und Komplexität der DisCOptER Methode sind untrennbar verknüpft mit der Wahl des Umschaltpunktes, definiert durch die Dichte des Graphen. Nur auf einem ausreichend dichten Graphen kann ein Pfad gefunden werden, der innerhalb des Konvergenzbereichs um ein globales Optimum liegt. Ausgehend von einem solchen Pfad konvergiert die zweite Stufe schnell zum Optimum. Demgegenüber birgt ein übermäßig dichter Graph das Risiko für aufwändige und redundante Berechnungen.

Die Identifikation dieses Umschaltpunktes verlangt nach einem tiefgehenden Verständnis des lokalen Problemverhaltens, der Approximationseigenschaften des benutzten Graphen, sowie der Konvergenzeigenschaften der eingesetzten kontinuierlichen Optimierungsmethode. Diese Aspekte werden in der vorliegenden Arbeit ausführlich untersucht.

Eine zentrale Stärke des vorgestellten diskret-kontinuierlichen Ansatzes ist, dass die nötige Graphendichte ausschließlich von den Umgebungsbedingungen, jedoch nicht von der geforderten Lösungsgüte, abhängt. Dies hat zur Folge, dass asymptotisch die vorteilhaften Konvergenzeigenschaften der kontinuierlichen Optimierung beibehalten werden.

Die Effizienz der vorgestellten Methode wird unter realistischen Bedingungen praktisch nachgewiesen. Es wird demonstriert, dass der DisCOptER Algorithmus mit minimalem Aufwand konsistent hochpräzise global optimale Lösungen erzielt und so einen doppelten Vorteil im Vergleich zu bestehenden Methoden bietet. Einerseits wird eine gesteigerte algorithmische Effizienz erreicht. Andererseits trägt die verbesserte Qualität der Trajektorien wesentlich dazu bei, den Luftfahrtsektor effizienter und umweltfreundlicher zu gestalten.

Abstract

This thesis introduces the novel hybrid algorithm DisCOptER for globally optimal flight planning.

DisCOptER (Discrete-Continuous Optimization for Enhanced Resolution) combines discrete and continuous optimization in a two-stage approach to find optimal trajectories up to arbitrary precision in finite time. In the discrete phase, a directed auxiliary graph is created in order to define a set of candidate paths that densely covers the relevant part of the trajectory space. Then, Yen's algorithm is employed to identify a set of promising candidate paths. These are used as starting points for the subsequent stage in which they are refined with a locally convergent optimal control method.

The correctness, accuracy, and complexity of DisCOptER are intricately linked to the choice of the switch-over point, defined by the discretization coarseness. Only a sufficiently dense graph enables the algorithm to find a path within the convex domain surrounding the global minimizer. Initialized with such a path, the second stage rapidly converges to the optimum. Conversely, an excessively dense graph poses the risk of overly costly and redundant computations.

The determination of the optimal switch-over point necessitates a profound understanding of the local behavior of the problem, the approximation properties of the graph, and the convergence characteristics of the employed optimal control method. These topics are explored extensively in this thesis.

Crucially, the density of the auxiliary graph is solely dependent on the environmental conditions, yet independent of the desired solution accuracy. As a consequence, the algorithm inherits the superior asymptotic convergence properties of the optimal control stage.

The practical implications of this computational efficiency are demonstrated in realistic environments, where the DisCOptER algorithm consistently delivers highly accurate globally optimal trajectories with exceptional computational efficiency. This notable improvement upon existing approaches underscores the algorithm's significance. Beyond its technical prowess, the DisCOptER algorithm stands as a valuable tool contributing to the reduction of costs and the overall enhancement of flight operations efficiency.

Contents

1	Introduction	17
1.1	Motivation	19
1.2	Free Flight Model	21
1.2.1	Spatial Restrictions	21
1.2.2	Collaboration	23
1.2.3	Open VS. Closed Loop Optimization	24
1.2.4	Cost Factors	25
1.2.5	Traffic Flow Restrictions (TFRs)	26
1.2.6	Aircraft Physics	27
1.3	The Free Flight Trajectory Optimization Problem	29
1.4	Solution Approaches	31
1.4.1	Dynamic Programming (DP)	33
1.4.2	Indirect Methods	39
1.4.3	Direct Methods	41
1.4.4	Stochastic Methods	45
1.5	Contributions of this Work	54
1.5.1	Published Articles	54
1.5.2	The DisCOptER Algorithm	55
1.5.3	Approximation Properties of Graphs	57
1.5.4	Towards Global Optimality	58
1.5.5	Proof of Convergence	59
1.5.6	Practical Convergence Properties	60
1.5.7	Harvesting the Benefits of Free Flight	61
2	A Discrete-Continuous Algorithm for Free Flight Planning	85
2.1	Introduction	87
2.2	Materials & Methods	89
2.2.1	Free Flight Planning	89
2.2.2	Continuous Approach: Optimal Control	90

2.2.3	Discrete Approach: Shortest Paths in Airway Networks . . .	94
2.2.4	DisCOptER Algorithm	100
2.3	Results	102
2.3.1	Test Problems	102
2.3.2	Computational Complexity	106
2.3.3	Minimum Graph Requirements	106
2.3.4	Optimal Crossover Point	108
2.3.5	Computational Complexity	109
2.4	Conclusion	110
3	Error Bounds for Discrete-Continuous Free Flight Trajectory	
	Optimization	117
3.1	Introduction	119
3.2	Shortest Flight Planning: Continuous & Discrete	121
3.2.1	Continuous: Optimal Control	121
3.2.2	Discrete: Airway Networks	125
3.3	Approximation Error Bounds	125
3.3.1	A Posteriori Error	126
3.3.2	Trajectory Approximation in Locally Dense Graphs	128
3.3.3	Computable Error Bounds	132
3.4	Numerical Examples	135
3.4.1	Test Instances	135
3.4.2	Results	136
3.5	Conclusion	141
3.A	Appendix	144
4	A Discrete-Continuous Algorithm for Globally Optimal Free Flight	
	Trajectory Optimization	151
4.1	Introduction	153
4.2	The Free Flight Trajectory Optimization Problem	155
4.2.1	Continuous Point of View: Optimal Control	155

4.2.2	Discrete Point of View: Shortest Paths	159
4.2.3	Discrete-Continuous Point of View: DisCOptER	160
4.3	Towards Global Optimality	162
4.4	Conclusion	167
5	Newton's Method for Global Free Flight Trajectory Optimization	173
5.1	Introduction	175
5.2	The Free Flight Trajectory Optimization Problem	177
5.2.1	Notation	177
5.2.2	Problem Statement	177
5.3	Continuous Optimization: Newton-KKT	179
5.3.1	Optimality Conditions	179
5.3.2	Newton's Method	183
5.4	Proof of Convergence	183
5.4.1	Inf-Sup Condition	185
5.4.2	Positive Definiteness of the Lagrangian	187
5.4.3	Upper Bound for the Lagrangian	190
5.4.4	Invertibility of the KKT-Operator	193
5.4.5	Lipschitz Constant	194
5.4.6	Convergence of Newton's Method	199
5.5	Conclusion	201
5.A	Appendix	204
5.A.1	Global Bounds	204
5.A.2	Bounds in a Neighborhood of a Minimizer	217
6	Convergence Properties of Newton's Method for Globally Optimal Free Flight Trajectory Optimization	223
6.1	Introduction	225
6.2	The Free Flight Trajectory Optimization Problem	226
6.3	Numerical Results	227
6.3.1	Size of the Convergence Radius	229

6.3.2	Relevance of the Error Terms	230
6.3.3	Algorithmic Improvement	231
6.4	Conclusion	232
7	Appendix	235
7.1	A Priori Estimates	237
7.1.1	Still Air	238
7.1.2	Moderate Wind Conditions	239
7.2	Efficiently Harvesting the Benefits of Free Flight	249
7.2.1	Graph-Based Routing	249
7.2.2	DisCOptER	252
7.2.3	Wind Conditions	253
7.2.4	Origin-Destination Pairs	254
7.2.5	Results	254
7.2.6	Supplementary Material	258
7.3	Errata	261
7.3.1	Notational improvements	261
7.3.2	Continuity of the objective function	261
8	Conclusion	263

CHAPTER **1**

Introduction

Contents

1.1	Motivation	19
1.2	Free Flight Model	21
1.2.1	Spatial Restrictions	21
1.2.2	Collaboration	23
1.2.3	Open VS. Closed Loop Optimization	24
1.2.4	Cost Factors	25
1.2.5	Traffic Flow Restrictions (TFRs)	26
1.2.6	Aircraft Physics	27
1.3	The Free Flight Trajectory Optimization Problem	29
1.4	Solution Approaches	31
1.4.1	Dynamic Programming (DP)	33
1.4.2	Indirect Methods	39
1.4.3	Direct Methods	41
1.4.4	Stochastic Methods	45
1.5	Contributions of this Work	54
1.5.1	Published Articles	54
1.5.2	The DisCOptER Algorithm	55
1.5.3	Approximation Properties of Graphs	57
1.5.4	Towards Global Optimality	58
1.5.5	Proof of Convergence	59
1.5.6	Practical Convergence Properties	60
1.5.7	Harvesting the Benefits of Free Flight	61

1.1 Motivation

In the early stages of air travel, landmarks and radio navigational beacons played an indispensable role in navigation. Over time, these elements evolved into an intricate three-dimensional global network consisting of 400,000 predefined waypoints connected by 900,000 arcs, shaping the routes that aircraft operate on today [6].

While the graph-based system has served as a reliable foundation for air traffic management (ATM), it also has inherent limitations. Most importantly, it can only roughly approximate efficient routes which are likely continuous curves rather than polygonal chains. Consequently, this system inherently yields suboptimal solutions, resulting in excessive fuel consumption, as well as emissions of carbon dioxides (CO_2), methane (CH_4), nitrogen oxides (NO_x), water vapor, soot, and sulfate aerosols [7, 8].

As highlighted in the European Environment Agency (EEA) report, the aviation sector was responsible for 1.7% of global CO_2 emissions in 2019 [9]. This statistic is projected to triple by 2050 if no interventions are undertaken, as indicated by the International Civil Aviation Organization (ICAO) [10]. If this trajectory continues, aviation could consume as much as 25% of the global carbon budget. Furthermore, recent research suggests that aviation is poised to contribute approximately 1.5% of the cumulative global warming effects between 2015 and 2100 [11]. Given these projections, there exists a compelling motivation to investigate and harness the potential of alternative approaches.

Especially as air travel continues its expansion, these limitations manifest as costly challenges. The demand for passenger kilometers surged by 4.9% between 2018 and 2019 alone, continuing a consistent trend resulting in a striking 75% growth between 2010 and 2019, as reported by the ICAO Annual Report [12]. Despite a temporary halt caused by the COVID-19 pandemic, this upward trajectory is anticipated to endure, inevitably resulting in increased airspace congestion [13–15].

Harnessing the capabilities of modern navigation and communication technology, such as e.g., a network of low earth orbit satellites [16, 17], the aviation industry is addressing these challenges through the implementation of Free Flight Airspaces

[18, 19]. Integral to comprehensive overhauls of air traffic management systems, such as Europe’s *Single European Sky ATM Research* (SESAR [20]), the U.S.’s *Next Generation Air Transportation System* (NextGen [21]), or Japan’s *Collaborative Actions for Renovation of Air Traffic Systems* (CARATS [22]) is the replacement of the highly structured ATM system with a more trajectory-centric framework. Airlines shall be granted significantly larger freedom in route planning.

Expectations for these changes are substantial [19]. The European Organisation for the Safety of Air Navigation (EUROCONTROL) anticipates savings of 1 billion nautical miles, 6 million tonnes of fuel, 20 million tonnes of CO₂ emissions, and €5 billion in fuel costs [23]. Research indicated potential savings of up to 16.4% in extreme cases [24, 25]. These projected benefits underscore the potential transformative impact of embracing Free Flight Airspaces.

This chapter is organized as follows: we begin in Section 1.2 by discussing various aspects of Free Flight currently under investigation in both research and industry communities. Concurrently, we define the precise setting discussed in this thesis, which is formally stated in Section 1.3. In Section 1.4 we provide an overview of existing solution approaches, before we introduce our algorithm DisCOptER in Section 1.5. Furthermore, we outline the articles comprising this work and emphasize their individual contributions.

1.2 Free Flight Model

The implementation of true Free Flight necessitates significant transformations across numerous institutions and processes within the ATM framework [26, 27]. As a result, transitional solutions arise between the conventional graph-based routing and the ultimate realization of Free Flight.

In this section, we delve into specific facets of Free Flight currently being explored within the research community, simultaneously outlining the assumptions underpinning this study. These chosen simplifications are strategically designed to facilitate theoretical analysis, straightforward expansion to more intricate scenarios, and early integration within the existing ATM framework.

1.2.1 Spatial Restrictions

The most apparent dimension of Free Flight revolves around the degree of spatial constraints. In the traditional system, aircraft are compelled to conform to a three-dimensional directed graph comprised of 400,000 nodes (called waypoints) on 43 flight levels and 900,000 arcs (called airway segments) [28, 29].

A first step towards Free Flight is conducted by introducing so called Free Route Airspaces (FRAs). Within these designated airspaces, users are granted the freedom to chart a route between predetermined entry and exit points, with the added option of including intermediate waypoints in their trajectory [23].

The subsequent progression involves merging several FRAs and thus eliminating spatial limitations along the horizontal plane, while still necessitating aircraft to adhere to specific (discrete) flight levels. The switching of flight levels follows a defined procedure.

It has been shown that the two problems of optimizing the horizontal and the vertical flight profile are only weakly coupled. While the former is mainly dependent of the horizontal wind gradients, the latter is primarily dictated by the interplay of aircraft-performance and the fuel-burn induced weight reduction [30, 31]. Hence, a common approach is to first obtain the vertical profile and then optimize the

horizontal path on piecewise constant flight levels. This is usually referred to as 2+2D approach. Both sub-problems are by themselves subject to active research. While the vertical part is studied e.g., in [32–35], this work focuses on the horizontal part.

With the background of this approach, we assume travelling at constant flight levels and reduce the problem to a two-dimensional context. This includes that take-off and landing are not optimized.

Approaches aimed at optimizing these flight phases, e.g., with *continuous descent operations* (CDO) [22, 36], have considerably enhanced flight efficiency. However, they often encounter significant operational restrictions and are guided by different objectives, e.g., noise reduction [37]. As a result, these approaches are frequently studied separately [38] or as part of multiphase strategies [39, 40].

The ultimate vision of Free Flight encompasses an aviation landscape where aircraft possess the autonomy to navigate according to their own preferences in the four-dimensional space (3D and time), devoid of imposed restrictions. It has been demonstrated that continuous cruise climb following a straightforward physical principle leads to significant increase in operating efficiency [30, 41–44]. During a flight, aircraft lose significant amounts of weight due to fuel consumption. Consequently, they require less lift to counterbalance the gravitational force, which allows them to climb and reduce drag.

Moreover, greater flexibility in choosing flight altitudes can have a notable positive impact on reducing the environmental footprint of a flight. The environmental consequences of aircraft emissions are intricately linked to their precise geographical occurrence. For instance, the impact of NO_x emissions varies considerably with altitude, and areas where contrails are prone to form are often confined to specific thin layers [45]. According to findings in [46], significant reductions in these effects – up to 10% – can be achieved with a mere 1% increase in cost (attributed to fuel consumption due to route detouring) by strategically avoiding high-impact regions. However, this way of operating is not compliant with the current ATM concept.

Remark 1.1. — *Research has demonstrated that employing a periodic pattern of repetitive climb and descent cycles, rather than maintaining a constant altitude*

cruise, can result in improved fuel efficiency [47]. However, as this approach might lead to passenger discomfort, it is not a preferred option for human-operated flights. Therefore, we will exclude such operations from our consideration, reserving them for the optimization of unmanned flights.

1.2.2 Collaboration

In a nutshell, the process of aircraft routing within the current centralized system unfolds as follows: airlines optimize routes for each aircraft individually. These planned routes are then submitted to the relevant air traffic control (ATC) agency (e.g., EUROCONTROL) as a list of waypoints, altitudes, times, etc. [48]. Here, all submissions from various airlines are checked for potential conflicts. Upon approval, the route is granted, and airlines are required to adhere to the established plan. Deviation from the route is only permissible in emergency situations and necessitates approval from the respective airspace security agency.

Aligned with these current circumstances, our investigation focuses on optimizing the trajectory of a single aircraft, without considering competing interests from other parties.

It is important to note that the potential for significantly enhancing the overall efficiency of the aviation industry through centralized trajectory optimization for multiple aircraft simultaneously has been recognized [49–52].

One plausible explanation for the absence of such an implementation thus far lies in the sensitivity of aircraft performance data and operating cost functions, which are considered valuable proprietary information that airlines prefer to retain control over.

Moreover, the complexity of the combined optimization problem tends to increase exponentially with the number of conflicting aircraft [52, 53], making this approach practically challenging to implement.

Looking ahead, the concept of Free Flight will advance with a more promising approach involving decentralized individual routeplanning and en-flight reoptimization [54]. This shift entails transferring control from central agencies to cockpit crews,

who, aided by an Airborne Separation System (ASS), will take over the responsibility for real-time airborne route adjustments and conflict resolution [55–57].

Maintaining airspace safety presents a substantial challenge in this context [58, 59]. However, research suggests that decentralized trajectory optimization can handle even higher traffic densities than centralized ATC [60] and even enhance airspace security. Hoekstra et al. aptly summarize this: *"better a safe chaos, than a dangerous order"* [55, 61]. The development of efficient algorithms will be pivotal in addressing these challenges effectively. Nonetheless, the anticipated economical advantages of Free Flight are expected to outweigh any additional complexities [62]. Early studies indicate that such collaborative routing has the potential to reduce fuel consumption by a significant margin [27, 54, 63, 64].

1.2.3 Open VS. Closed Loop Optimization

As previously discussed, the existing system mandates aircraft to adhere to routes that are predefined prior to take-off, with minimal to no flexibility for in-flight alterations. This way of route planning is commonly referred to as open-loop approach.

Consequently, route planning hinges heavily on highly accurate weather forecasts [65]. Moreover, given that route determination usually occurs at the latest time possible before take-off (about one hour [48]), computational efficiency becomes paramount.

The weather forecast alongside indicators of the reliability of the forecast in terms of so-called ensemble forecast data with different look-ahead times may be provided by global weather data services such as the World Area Forecast System (WAFS) [66] or the Global Forecast System (GFS) [67]. Wind data (speed and direction) is available for each 1.25° of latitude and longitude and for several altitudes, yielding a 3D grid of geodesic points that is updated every one to six hours. Typically, the prediction accuracy of a one-hour forecast stands at around 3%, in comparison to the actual weather state modeled for the subsequent six hours [68].

To address this uncertainty, probabilistic optimization has been proposed. These methods are based on meteorological forecasts provided by so-called Ensemble

Prediction Systems (EPS) [69–74]. However, when the forecast extends beyond one hour, the margin of weather prediction error grows markedly, rendering it unsuitable for reliable input data in trajectory optimization [75].

Consequently, the concept of en-route re-optimization (a closed-loop approach) emerges as a promising remedy, embedded within the broader vision of Free Flight [25]. A recent study reports fuel savings of 0.5% up to 7% [48] by updating the route multiple times during the flight. On the other hand, this requires more intricate tools to uphold airspace security.

In this study, we work within the limitations of the current system and assume the weather conditions to be well known, disregarding introduced uncertainties. Additionally, we consider wind as stationary (i.e., time-independent) for the majority of our analysis. With these premises in place, we proceed with the open-loop approach for our research.

1.2.4 Cost Factors

Our objective is to determine the most cost-efficient route, with the exact definition of "cost-efficient" varying according to the criteria set by individual airlines. For a comprehensive understanding of the diverse conflicting objectives and constraints airlines encounter in their operations, we refer interested readers to [76].

This study specifically focuses on trajectory-dependent cost, which is usually a combination of two major components: fuel cost (making up for roughly 30% of all operating cost [77]) and time cost (incl. wages (around 20%), aircraft rentals (around 3%), etc.).

This led to a recent investigation of multiobjective approaches in order to yield a Pareto front regarding these individual objectives [78, 79].

Most often, however, airlines define the ratio of time and fuel cost individually, based on their business models. This ratio is referred to as Cost-Index (CI) [65, 80] and directly translates to the most economic air speed (ECON speed). Assuming constant altitude, while ignoring weight reduction due to fuel burn, this results in constant air speed and establishes a direct proportionality of fuel and time cost [24].

With a growing awareness of aviation’s environmental impact, airlines now also consider additional factors in their trajectory planning strategies, such as the emission of climate-active gases like CO₂, CH₄ (methane), and NO_x (nitrogen oxides), which are likewise proportional to the overall fuel consumption [81]. As a result, our primary focus is on minimizing total travel time as a singular objective, encompassing all these contributing elements.

Furthermore, there exists a wide variety of other factors that can be taken into consideration during the optimization of a flight trajectory. Notable examples include overflight cost [82, 83] – fees for traversing an airspace – and penalties for the creation of persistent contrails [84–88]. Both factors are dependent on the spatial route arrangement and are not directly proportional to the travel time. However, these considerations go beyond the scope of the current study.

1.2.5 Traffic Flow Restrictions (TFRs)

Especially in high-traffic regions such as Europe or North America, flight trajectories are heavily constrained by so-called Traffic Flow Restrictions (TFRs), [6, 89]. The most prominent sources of such restrictions in the European airspace are Notice(s) to Airmen (NOTAMs) [90] and the Route Availability Document (RAD) [91].

NOTAMs are restrictions issued by government agencies and airport operators, which limit the usage of certain parts of the airway network on short notice. They regulate the availability of waypoints, segments, runways, airspaces, etc., possibly only within given time or altitude ranges. Some common motivations for the implementation of these restrictions are military exercises, flights by heads of state, extreme weather phenomena or technical issues at an airport.

Remarkably, many of these constraints can be seamlessly adapted to the Free Flight context. For instance, preliminary research suggests that no-fly zones can be effectively represented as obstacles and readily integrated into conventional trajectory optimization frameworks [92, 93].

The RAD is a collection of restrictions updated in 28-day cycles. These constraints aim to enhance airspace utilization by predefining traffic flows. As of August

2023, the RAD document is presented as a PDF of more than six hundred pages, embodying over ten thousand constraints [91].

One notably complex set of constraints is known as *forbidden pairs* [94]. In essence, these pairs signify that the usage of one waypoint prohibits the usage of another (not necessarily neighboring) waypoint. As these restrictions inherently revolve around waypoints and airway segments within the airway network, their representation within the Free Flight paradigm remains uncertain. Therefore, TFRs will be disregarded in this study. Notably, for the comparative analysis between graph-based routing and Free Flight, TFRs will be excluded on both fronts.

1.2.6 Aircraft Physics

Optimal control problems (not solely aircraft trajectory optimization) are often solved with a hierarchical strategy, which involves optimizing the route on a macroscopic scale first, followed by determining the control of actuators on a finer scale based on the previously optimized route. This principle is extensible in both directions and can incorporate any number of intermediate levels.

In our investigation, we focus on the macroscopic optimization of a single aircraft trajectory. Depending on the chosen strategy, two popular aircraft and atmospheric models are commonly utilized.

The first model is documented in the User Manual for the Base of Aircraft Data (BADA) [95] and has found application in research on aircraft trajectory optimization (e.g., [30, 49, 85]). It involves rather intricate aircraft dynamics, describing the state in seven dimensions (3D-coordinates, air speed, climb angle, course angle and mass), controlled by three variables (angle of attack, bank angle, and thrust lever position). The atmosphere is not only described by wind speed and direction, but also by air pressure and temperature.

Under the previous assumptions, most notably constant altitude and air speed, the problem can be simplified significantly. Finally, an aircraft can be conceptualized as a self-propelled point mass that maintains a constant airspeed (velocity relative to the surrounding air) and experiences advection by the prevailing airflow. This

permits to calculate motion in an earth-fixed coordinate system by vector addition of airspeed and wind vectors. In this form the problem was originally presented by Ernst Zermelo in the 1930s [96, 97] and has since been studied in numerous publications (e.g., [51, 98–100]).

Although the real-world turn radius of an aircraft is physically constrained, this limitation is not reflected in the model. Instantaneous changes in direction are possible, which allows for direct comparison of continuous curves with theoretical polygonal chains (e.g., paths on a graph). Since wind-optimal trajectories usually have significantly broader curves, however, this model limitation is rarely violated.

Due to its simplicity, which nevertheless captures the essential aspects of the problem, this model is well-suited for theoretical analysis. Consequently, it is employed in the present study.

1.3 The Free Flight Trajectory Optimization Problem

In the preceding section, an in-depth exploration of various assumptions was conducted, ultimately shaping the problem framework that forms the basis of this study. Concisely recapped, our objective is to determine the minimum-time trajectory for an aircraft within a two-dimensional plane, departing at an origin x_O and arriving at a destination x_D . During this trajectory, the aircraft maintains a constant airspeed \bar{v} , while traversing through a multiple times continuously differentiable stationary wind field $w \in C^3(\mathbb{R}^2, \mathbb{R}^2)$. Additionally, a simplified kinematic model governs the aircraft's behavior, allowing the problem to be expressed in a classical optimal control formulation:

$$\min_{T,x,v} T \tag{1.1a}$$

$$\text{subject to} \quad \dot{x}(t) = v(t) + w(x(t)) \tag{1.1b}$$

$$v(t)^T v(t) = \bar{v}^2 \tag{1.1c}$$

$$x(0) = x_O \tag{1.1d}$$

$$x(T) = x_D, \tag{1.1e}$$

where T denotes the travel time, $x, \dot{x} : [0, T] \rightarrow \mathbb{R}^2$ represent the aircraft position (the state variables) and its time derivative, respectively, and $v : [0, T] \rightarrow \mathbb{R}^2$ stands for the air speed (the control variable). The departure time is fixed at $t = 0$, which does not impose a restriction in a time-invariant wind field. Finally, the route shall be generated before take-off, i.e., in an open loop or offline approach.

This problem is commonly known as Zermelo's navigation problem, named after the scientist who initially introduced it already in the 1930s. However, it did not receive considerable attention until after the second world war, when the air travel industry began to evolve rapidly.

Today, the aviation sector is a fiercely competitive market characterized by narrow profit margins and increasing urges to reduce the environmental footprint.

As a result, airlines have high standards regarding the efficiency of planned flights, necessitating routes that are (globally) optimal.

The overall goal of this work is to find an ϵ -globally optimal aircraft trajectory, for which we use the following notation. Given a function $f : X \rightarrow \mathbb{R}$, we call x^{**} a global optimizer of the problem $\min_{x \in X} f(x)$, if $f(x^{**}) \leq f(x) \forall x \in X$, contrary to a local optimizer x^* for which the inequality only holds in a certain neighborhood, $f(x^*) \leq f(x) \forall x \in \mathcal{N}(x^*) \subseteq X$. Further, we call \tilde{x} an ϵ -globally optimal solution, if $f(\tilde{x}) \leq f(x^{**}) + \epsilon$ for some small $\epsilon > 0$.

Remark 1.2. — *It is essential to recognize that there can be multiple equivalent global optima (as illustrated, for instance, in test problem d) in Section 2.3, Figure 2.5). Hence, we refer to "a" global minimizer rather than "the" global minimizer.*

As we will demonstrate later in Section 2.2, the quality of the solution with respect to the overall objective (the travel time), denoted as ϵ , is inherently linked to the discretization length ℓ employed by the solution technique, which might be a characteristic arc length within a graph or the step length in a direct collocation approach. This correlation enables us to compare the efficiency of different methods concerning the objective of identifying an ϵ -globally optimal trajectory. Therefore, we will use ℓ as a measure for the solution quality rather than ϵ .

1.4 Solution Approaches

This section provides an overview of existing solution approaches to the Trajectory Optimization Problem, with a particular emphasis on Free Flight but not exclusively limited to it.

Inspiration can be drawn from related fields, such as trajectory optimization for Autonomous Underwater Vehicles (AUVs) or ships [101–103]. Since these vehicles operate in the presence of ambient currents, these problems closely resemble the Free Flight Trajectory Optimization Problem discussed above.

Furthermore, the realm of designing interplanetary space missions represents an active research area that motivates the development of various novel methods. In this case, control are usually executed on a very short timescale compared to the overall mission duration. Consequently, maneuvers are often modeled as instantaneous actions rather than continuous controls [104], which introduces a slightly different optimization challenge.

Given that the simplified aircraft model allows for any Lipschitz-continuous route (refer to Section 1.2.6), we can approach the problem from a path planning perspective and employ methods commonly used for robots, unmanned aerial vehicles (UAVs), or drones [105–109]. In these applications, the vehicle’s velocity is typically isotropic, the primary focus is on obstacle avoidance, and the objective is to minimize path length. Nevertheless, anisotropic velocity can often be accounted for by factoring in travel time as the cost of a path.

We categorize existing solution approaches into four main groups:

- **Dynamic Programming.** These methods focus on optimizing the trajectory by considering sequences of optimal decisions. This category encompasses techniques such as graph-based shortest path algorithms and methods for solving the Hamilton-Jacobi-Bellman equation.
- **Indirect Methods.** These methods adopt the principle of "*optimize then discretize*". They apply Pontryagin’s maximum principle to derive necessary

conditions for the control variables, which leads to the formulation of a two-point boundary value problem.

- **Direct Methods.** Direct methods, on the other hand, follow the principle of "*discretize then optimize*". They discretize both the state and control variables, transforming the continuous problem into a structured constrained nonlinear optimization problem.
- **Stochastic Methods.** These methods incorporate randomness or probabilistic elements into the optimization process.

It will become evident that these categories are not rigidly defined, and numerous approaches, including the algorithm presented in this work, incorporate techniques from multiple categories.

Furthermore, it is essential to acknowledge that the discussion provided here is not exhaustive. For different perspectives, we recommend consulting survey articles such as [110] or [111].

We will examine the strengths and limitations of each approach in detail, with focus on the criteria computational efficiency aiming at global optimality and extensibility to the more complex problem. Ultimately, the observation emerges that there exists a deficiency in methods capable of providing globally optimal solutions with a high degree of accuracy in finite time. Dynamic programming solutions, while valuable, tend to suffer from scalability issues as the resolution increases. Conversely, direct and indirect methods excel at providing highly accurate solutions but run the risk of getting trapped in local minima. Both challenges can be alleviated by resorting to stochastic approaches, albeit at the expense of potentially unbounded runtime.

This very gap underscores the significance of the discrete-continuous hybrid algorithm introduced in this study. Our algorithm bridges the gap between the strengths of dynamic programming and optimal control, aiming to provide efficient and accurate solutions to the Free Flight Trajectory Optimization Problem.

1.4.1 Dynamic Programming (DP)

Dynamic programming is a set of methods that are grounded in Bellman's principle of optimality, which can be concisely stated as follows: "*In an optimal sequence of decisions, every subsequence must also be optimal.*" [112].

We will now delve into the development of various methods applicable to the Free Flight Trajectory Optimization Problem, commencing with classical shortest path algorithms, such as Dijkstra's. Subsequently, we will introduce the Hamilton-Jacobi-Bellman equation which motivates the fast marching method, an extension of Dijkstra's algorithm tailored for continuous spaces. However, it is important to note that this approach is only suitable for isotropic problems and not able to address the complexities of the Free Flight Trajectory Optimization Problem. Consequently, we will turn our attention to ordered upwind methods as a potential solution to this deficiency.

1.4.1.1 Shortest Path Algorithms

Shortest path algorithms typically generate routes on the basis of a spatially fixed graph. The classical airway network is the primal example for a deterministically created graph. As it has been predefined with respect to multiple criteria aside of route efficiency and is altered only slightly in response to current weather situation or air traffic conditions, it is not surprising that it often leads to suboptimal results.

A natural approach to harvest the flexibility offered by Free Flight is to expand the existing airway network by introducing additional nodes and arcs. This enables the problem to be addressed within the existing framework using well-established algorithms.

In an idealized way, this approach will serve as benchmark in this work (outlined in Section 2.2.3). To represent it, we define an isotropic, locally densely connected graph and calculate time-optimal paths using the A* algorithm (explained below).

A similar approach has been proposed by Cheung [71]. As discussed by the author, static graphs suffer from limited angular resolution, which makes them incapable of approximating continuous curves adequately. The issue can be reduced

by increasing the connectivity, which, however, quickly increases the number of arcs, leading to exploding computational times. An improvement on this approach is offered by Jensen et al., who suggest to divide the space into cells with arcs being defined by subdividing the borders in small steps [113].

Determining the optimal path on a weighted graph is typically accomplished using a variant of Dijkstra's algorithm [114], most prominently the A* algorithm [115].

Remark 1.3. — *The term "shortest path" is commonly used to denote the minimum-weight path on a weighted graph. Since we are not optimizing for the euclidean distance, but for the travel time or a more complex cost function as discussed in Section 1.2.4, the term "most cost-efficient path" would be more appropriate.*

Dijkstra's algorithm operates by systematically expanding a front of nodes reachable within a receding time horizon. During this process, a priority queue is employed to manage "considered" nodes that have not yet been accepted into the optimal path. These nodes are assigned labels representing their estimated earliest arrival times and the parent node through which they may be reached. As soon as the destination node gets accepted, the optimal path can be traced back to the origin by following the stored parent nodes.

The A* variant incorporates a lower bound on the travel time from a given node to the destination in order to guide the exploration and increase the overall efficiency.

A detailed discussion of further variants of Dijkstra's algorithm is offered by Souissi et al. [116]. These general approaches can be further enhanced through recent problem-specific advancements such as search space pruning [117–120] or the implementation of tight lower bounds [28, 29, 121, 122]. These refinements significantly contribute to remarkably fast computational runtimes, even for moderately large and dense graphs [6, 118, 123–126].

Moreover, the challenge of limited angle resolution can also be addressed at this level. A promising approach that is closely related to the algorithm proposed in the present work, is to employ a distinct post-processing step [127] which can be realized via nonlinear optimization methods [128, 129].

Alternatively, smoothing can be directly interleaved with the A*-search using *any-angle* pathfinding algorithms [130], like *Field D** [131] or *Theta** [132]. Another approach is to allow for non-straight arcs which are created by solving nonlinear optimization problems [129].

These strategies may improve the paths beyond the approximation capabilities of the underlying graph. However, attaining convergence to a global minimizer is not guaranteed.

The level of detail considered in the aircraft model introduces a significant challenge for label-setting algorithms such as Dijkstra's. The shortest path problem on graphs is known to be solvable in polynomial time provided that the *First-In-First-Out* (FIFO) property is satisfied [133]. Put simply, this dictates that when an aircraft departs from a node, it cannot be overtaken by another aircraft departing from the same node at a later time. However, it is entirely possible that an aircraft arrives at a node later and at a lighter weight, allowing it to fly faster and overtake another aircraft that arrived earlier, but was heavier and slower. This leads to a violation of the FIFO property, resulting in a NP-hard problem, as a total ordering of labels is no longer possible [134]. Nevertheless, research has shown that even if this issue is disregarded, satisfactory results can still be achieved [32].

A more critical challenge concerning the overarching objective of this study is that graph search algorithms face scalability issues when dealing with high resolutions.

Global optimization is usually not explicitly addressed in this context, since Dijkstra's algorithm inherently yields the globally optimal solution in the subset of the trajectory space that is implicitly defined by the graph. It is evident that a continuous solution can be approximated to an arbitrary degree of accuracy by increasing the graph-density. Consequently, an ϵ -global optimal solution can be achieved for any given ϵ by employing a sufficiently fine graph.

However, it is important to note that shortest path algorithms often inherit the computational complexity of Dijkstra's algorithm. With efficient heap data structures, this complexity scales as $\mathcal{O}(|A| + |V| \log(|V|))$, where A and V denote the sets of segments (arcs) and waypoints (vertices), respectively.

What may seem intuitive will be analytically confirmed in this study. It will be shown that the computational complexity of the purely graph-based approach is in $\mathcal{O}(\ell^{-6})$, where ℓ indicates the connectivity length of a locally densely connected digraph, rendering this approach inefficient for achieving highly accurate optimization (refer to Chapter 2).

1.4.1.2 Solving the Hamilton-Jacobi-Bellman Equation

The Hamilton-Jacobi-Bellman (HJB) equation follows as a direct consequence of Bellman's principle of optimality. This partial differential equation (PDE) of the so-called value function provides a necessary condition for optimality. In our specific context, the value function indicates the earliest possible arrival time at a given point. The optimal trajectory finally follows the characteristics of the PDE.

In the isotropic case, i.e., if the ground speed of the aircraft was independent of the travel direction, this leads to the Eikonal equation [135]. The most well known approach to solve the Eikonal equation numerically is the *Fast Marching* (FM) method. Obviously, the velocity of an aircraft is inherently anisotropic due to the influence of wind. For such problems *Ordered Upwind* (OU) methods have been developed as extension of the FM method.

The Fast Marching (FM) Method, introduced in [136], is an algorithm that can be viewed as an extension of Dijkstra's algorithm to the continuous domain. It involves two main steps in order to find a viscosity solution to isotropic trajectory optimization problems.

First, the HJB equation is solved in a forward manner on a defined grid. While this initially seems to lead to a large coupled system of PDEs, it can be efficiently decoupled. This decoupling requires an ordering of grid points in terms of increasing value (arrival time), which is not known a priori. An efficient approach is to solve the PDE by gradually expanding the wavefront of the value function, similar to how Dijkstra's algorithm operates.

Various update schemes have been proposed for the purpose of estimating the value function and its gradient at a grid point x by solving the PDE locally, considering simplices (x, x_1, x_2) that include two already accepted grid points x_1, x_2 .

Finally, the optimal trajectory is extracted in a backward manner by tracing the estimated characteristic from the destination to the origin. In the isotropic case, the characteristics of the PDE coincide with the gradients of the viscosity solution.

As such, FM closely resembles Dijkstra's algorithm but differs in two crucial aspects: Dijkstra's algorithm assigns labels to nodes to indicate the earliest arrival time. In contrast, the FM labels include gradient information.

Moreover, Dijkstra's algorithm provides a sequence of nodes on a predefined graph as the solution. Angular resolution may only be enhanced by increasing the graph's connectivity, which in turn leads to larger computational effort, since the complexity scales with $\mathcal{O}(|A| + |V| \log |V|)$, where A and V indicate the sets of arcs and vortices (nodes), respectively.

On the other hand, during the wavefront expansion in the FM method, only the spatially closest neighbors of the grid are considered. This results in a complexity similar to Dijkstra's on a graph with limited node-degree, $\mathcal{O}(|V| \log |V|)$. However, the FM solution is not bound to the underlying graph and provides a better approximation of the actual continuous optimum.

Similar to Dijkstra's algorithm, the FM method can incorporate a heuristic lower bound on the cost to reach the destination from a given point, guiding the search space exploration towards the destination. This approach is known as FM*, drawing an analogy to A* [137].

It is important to emphasize that FM is applicable solely to isotropic problems, e.g., situations where the aircraft's ground speed remains independent of the travel direction. However, when confronted with significant wind conditions, complications arise: under such circumstances, the characteristics of the PDE may no longer align with the gradient of the viscosity solution. Consequently, the gradient becomes an inadequate indicator for determining the characteristic. This can even result in situations where the value function for a given node is smaller than the value function

for its accepted neighbors on the grid, a scenario that violates the fundamental principle of causality.

Ordered Upwind (OU) Methods have been developed by Vladimirsky and the inventor of the FM method, Sethian, as an extension designed to tackle general anisotropic problems while maintaining a similar computational complexity [138–140].

These methods operate on the basis of an upper bound on the difference between the characteristics of the PDE and the gradient of the value function, which is dependent on the maximum wind speed in our case. In contrast to FM, not only the directly neighboring nodes on the grid are considered when estimating the value function at a specific query point. Instead, the upper bound is employed to select all nodes from the accepted front that could potentially be part of the simplex containing the gradient of the value function.

Remark 1.4. — *The term "upwind" can be somewhat deceptive in this context. It does not refer to the wind conditions, but describes that the finite difference approximation of the gradient of the value function at a given point is determined based on data points that have already been accepted considering the flow of information (referred to as "upwind").*

As the number of nodes considered in each update is bounded, the asymptotic complexity is inherited from the FM method. Nevertheless, the practical computational cost does increase by a constant factor related to the degree of anisotropy (the absolute wind speed in our specific case).

These methods have been rigorously proven to converge to the viscosity solution when the underlying grid is refined [138]. Furthermore, it is expected that the rate of convergence follows a first-order behavior concerning the mesh-width ℓ . This translates to an overall complexity of approximately $\mathcal{O}(\ell^{-2} \log(\ell^{-2}))$, as established in [138].

In [51, 100], Girardet et al. demonstrated that Ordered Upwind methods are a viable approach to solve the Free Flight Trajectory Optimization Problem, capable of handling additional difficulties, such as obstacles and spherical coordinates.

1.4.1.3 Conclusion

In 1975, Bryson and Ho expressed skepticism about the practicality of dynamic programming, referring to what they called the "curse of dimensionality." They noted that even solving moderately complex problems using DP required a vast amount of storage and found it impractical to compute a field of extremals when only one optimal path was needed [141].

However, in recent years, there has been a resurgence of interest in dynamic programming, largely due to the substantial increase in affordable computational capacity. As demonstrated in this section, DP remains a powerful global optimization approach, capable of finding good solutions for various problems.

1.4.2 Indirect Methods

Indirect methods involve transforming the continuous trajectory optimization problem into a two-point boundary value problem by considering the necessary conditions for optimality, known as the Euler-Lagrange equations. Solutions to this problem are referred to as extremals, and it is evident that an optimal trajectory qualifies as an extremal.

Historically, these methods were developed prior to the existence of computers capable of numerically solving problems as complex as the Free Flight Trajectory Optimization Problem. For instance, Zermelo derived the necessary conditions for aircraft control in a two-dimensional planar case in his original work [96]. This work was later extended to the spherical case [142], and further adaptations were made for more intricate aircraft models [30, 85, 87]. However, attempting to encompass all the aspects discussed in Section 1.2 appears to be a daunting task.

Numerically, extremals are often determined using a shooting approach, which transforms the boundary value problem into an initial value problem [30, 85, 87,

143, 144]. This involves forward integration ("*shooting*") from the initial boundary conditions trying to meet the final boundary conditions (or vice versa, which has been observed to improve practical performance [145]). In the present case (continuously differentiable wind conditions) this leads to a nonlinear optimization problem over the initial control variables (the initial heading angle in our case) [144].

Approaching this problem with a general-purpose solver is prone to yielding suboptimal results. Therefore, more specialized methods have been developed.

Built on the assumptions of relatively minor wind gradients and the close proximity of the optimal trajectory to the great circle, an approach named *Neighboring Optimal Wind Routing* was developed by Jardin and Bryson [99, 146, 147]. Applying the principles of *Neighboring Optimal Control*, the problem is simplified by linearization of the kinematic equations (1.1b) and the differential equation that describes the optimal heading angle based on a nominal route (usually the great circle segment from origin to destination).

In principle, this technique also allows for the variation of both the origin and destination, enabling the derivation of routes for numerous origin-destination pairs with marginal additional effort. Nonetheless, its effectiveness is bound to delivering "*near-optimal*" outcomes and is seldom capable of identifying a global optimum. A later study by the same authors even demonstrated a scenario in which the method produced significantly suboptimal results [145].

Generally, the quality of the solution strongly diminishes with increasing nonlinearity of the wind conditions, which led to the development of another approach designed to achieve global optimality [148]. The authors advocate for simultaneously tracing multiple trajectories, each initiated with varying initial heading angles. The intention is to encompass all local minima by ensuring that adjacent trajectories do not diverge too much. If the distance exceeds a threshold, an additional trajectory is introduced.

This way, a network is built up containing points that can be reached along minimal-time tracks (the resemblance to the dynamic programming approaches discussed earlier is readily apparent). The final trajectory from origin to destination

is obtained by selecting the one extremal which ends closest to the destination. Given that derived trajectories might intersect, a spatially fixed grid is employed to monitor which trajectory arrived first at a given point.

This approach may be beneficial if the objective is to calculate routes from the same origin to multiple destinations (or from multiple origins to the same destination). Another advantage is that extremals can be pre-computed offline and used for a quick airborne re-optimization of the route after a deviation from the originally planned path.

For adequate spatial coverage, roughly $\mathcal{O}(\ell^{-1})$ trajectories are necessary, with ℓ denoting the discretization length of the solution. Simultaneously, the computational effort per trajectory is in $\mathcal{O}(\ell^{-1})$. Consequently, the overall computational complexity in relation to solution accuracy scales as $\mathcal{O}(\ell^{-2})$.

1.4.3 Direct Methods

In contrast to indirect methods, direct methods adopt the strategy of "*discretize then optimize*". In other words, they transform the original infinite-dimensional problem into a finite-dimensional constrained nonlinear problem (NLP) [149, 150].

1.4.3.1 Transcription

In order to transform the optimal control problem into a NLP, the time interval is broken down into smaller steps. From this point, there are two popular strategies that are commonly followed:

Direct (Single) Shooting treats only the control variable at the discretization points as independent variables. The state variables are subsequently determined by integrating the dynamics equations (1.1b).

Direct Collocation, on the other hand, treats both the state and control variables as independent variables, while the dynamics equations are incorporated as constraints. This results in a larger yet highly structured nonlinear programming problem. Direct collocation is often considered the state-of-the-art approach and is employed in numerous research articles [39–41, 49, 151–156].

Additionally, there is an approach known as *Direct Multiple Shooting*, which applies elements of both methods. It involves applying the single shooting approach individually to several subintervals. The states at the endpoints of these subintervals are treated as independent variables subject to continuity constraints [155, 157–159].

Direct methods, in comparison to indirect methods, often involve higher computational demands. Nevertheless, their applicability extends to a broader range of problems, making them better suited for real-world flight planning scenarios. Notably, these methods can even accommodate discrete variables, such as discrete flight levels, with relative ease [39, 40].

1.4.3.2 Solving the Nonlinear Problem

While the process of transcription is well understood [160], the intricacy of these approaches primarily lies in solving the resultant constrained nonlinear problem, which is the focal point of our attention. While it is technically viable to address the problem using general-purpose local solvers, numerous numerical challenges are likely to arise [160, 161]. Most importantly, such solvers heavily rely on a well-informed initial guess.

In essence, most common approaches follow a multi-start approach, incorporating not only one but multiple starting points, and share a two-step structure. In the first step, the global exploration phase, potential solutions are generated, which serve as starting points for a locally convergent nonlinear programming solver in a subsequent local exploitation phase.

The algorithm proposed in this work is no exception. As we will elaborate later, candidates are derived as shortest paths on a suitable graph, which is designed to guarantee the existence of a viable candidate.

For the purpose of analysis, we use the arguably most straightforward approach to solve the NLP and apply the ordinary Newton’s method to the necessary conditions for optimality known as the *Karush-Kuhn-Tucker* (KKT) conditions. This approach is referred to as *Newton-KKT* or also *Sequential Quadratic Programming*

(SQP). While it excels in terms of convergence speed, it is very sensitive to the initial conditions.

Alternative state-of-the-art solvers, such as Trust-Region methods, offer increased robustness in expense for computational speed.

Moreover, while the standard Newton-KKT method is limited to handling equality constraints, the inclusion of inequality constraints can be managed through *Interior-Point*, *Penalty*, or *Augmented Lagrangian* methods. For an excellent introduction in this domain, we recommend consulting the textbook by Nocedal and Wright [162].

The mentioned methods operate in a deterministic manner. However, it is essential to recognize the existence of stochastic techniques designed to prevent solvers from becoming trapped in local minima. One such technique is *Monotonic Basin Hopping* (MBH), which introduces random perturbations to potential solutions followed by another local optimization step. If this results in an improved trajectory, it is accepted and replaces the original one [163–165].

Another technique is *Simulated Annealing* (SA), which is very similar to MBH, but allows for the acceptance of non-improving solutions with a certain (decreasing) probability [166]. This can further be enhanced by adjusting the perturbation radius based on the acceptance rate of the series of minimizers. This method is referred to as *Simulated Annealing with Adaptive Neighborhood* (SA-AN). For a comprehensive discussion we refer to [167].

1.4.3.3 Generating Starting Points

We will now turn our focus onto the initial step, which involves the candidate generation. Naively sampling the search space in a uniform way (grid search) is a rigorous approach, but inefficient when applied to high-dimensional problems. Practically relevant methods can be characterized as either deterministic or stochastic.

Deterministic Methods are often based on the principle of Branch & Bound (B&B). This technique involves iteratively subdividing the search space into smaller subproblems called branches. Solving the actual problem locally with a suitable candidate yields an upper bound for each branch. Lower bounds are obtained by solving a convex relaxation of the problem. During the process a non-decreasing sequence of lower bounds and a non-increasing sequence of upper bounds on the global optimum is generated. The process continues until no more feasible solutions remain or all branches are pruned. The best known solution is guaranteed to be optimal.

An example of this approach is the α BB method [168], which constructs a quadratic lower bound using the second order sensitivities of the state variables with respect to the control. In combination with multiple shooting, this method has shown reasonable success in solving optimal control problems [157–159].

B&B methods provide a rigorous sampling of the search space. However, they encounter limitations due to the curse of dimensionality, since the computational effort scales exponentially with the number of decision variables, which in turn scales linearly with the solution quality ℓ^{-1} .

Stochastic Methods have been developed over the past years with the goal of sampling the search space more efficiently. They have proven to perform well for many practically relevant tasks.

Methods like *Probabilistic Roadmaps* (PRMs) and *Rapidly Exploring Random Trees* (RRTs), which will be discussed in the next section, have proven to be effective tools for path planning when used on their own, but can also be used in a hybridization with local NLP solvers.

In Section 1.4.1 we have introduced the concept of combining coarser methods with a subsequent smoothing operation, aimed at improving angular resolution and overall solution quality. Karatas and Bullo proposed a related method that initially generates a candidate solution using a RRT, which is then utilized as a starting point for a nonlinear optimization stage addressing the optimal control problem

through a direct method [128]. A similar approach was proposed by Bouffard and Waslander using a PRM to generate an initial guess [169].

Due to the local convergence of the NLP solver, this hybridization inherits the probabilistic optimality of RRT* or PRM*, respectively.

1.4.4 Stochastic Methods

Stochastic optimization methods have experienced significant attention in recent years due to their effectiveness in tackling challenging optimization problems characterized by high-dimensionality, ill-behavior, noise, non-convexity, or limited prior knowledge about the objective function. Unlike traditional deterministic optimization methods that rely on gradients or derivatives to navigate the search space, stochastic methods introduce an element of randomness into the optimization process.

This field of research is vast and continually evolving, and a comprehensive survey is beyond the scope of this work. For those seeking further references and a more extensive overview, we recommend consulting works such as [104, 170–172]. In the following, we will explore two categories of stochastic optimization methods and delve into specific approaches to highlight their respective strengths and weaknesses, which often generalize to related methods.

Population-based approaches center around a set of candidate solutions that collectively traverse the search space in search of the optimal solution.

Sampling-based methods, on the other hand, primarily focus on the creation of a roadmap or tree-like structure within the configuration space. This structure enables an efficient exploration of feasible paths or solutions.

1.4.4.1 Population-Based Algorithms

The following methods share the characteristic, that multiple candidate solutions are considered simultaneously. During the optimization process, they evolve with a combination of individualistic behavior, aimed at exploring unknown areas of

the search space, and social behavior, aimed at exploiting promising areas of the search space.

This category encompasses a wide range of techniques, including *Genetic Algorithms*, *Differential Evolution*, *Simulated Annealing*, and *Monotonic Basin Hopping*, among others. Many of these methods draw inspiration from natural processes and are classified as nature-inspired metaheuristics.

Their effectiveness in the context of flight planning has been demonstrated [31, 173–177]. Moreover, they have proven to be valuable tools for related applications, such as interplanetary space mission design [104, 165, 178, 179].

We will delve into two specific approaches in greater detail: *Particle Swarm Optimization* (PSO) and *Ant Colony Optimization* (ACO). PSO is a nonlinear programming (NLP) solver that operates across the entire search space, employing direct communication between candidate solutions. On the other hand, ACO has originally been designed for solving combinatorial problems and can be utilized for path planning by operating on a discretized version of the search space. This method relies on indirect communication among candidate solutions.

Particle Swarm Optimization (PSO), developed by Eberhart and Kennedy in 1995 [180–182], is a versatile method for solving nonlinear finite-dimensional optimization problems. It operates based on a finite-dimensional representation of trajectories, which can take various forms.

In its most straightforward application, PSO deals with trajectories represented by waypoints that create piecewise linear routes [183]. Alternatively, trajectories can be represented using sequences of circular arcs [183], cubic splines [184], or what so-called "Motion Primitives".

Motion primitives are fundamental, predefined motion segments or building blocks that can be combined to achieve more complex and varied movements. One prominent application is the design of interplanetary space missions using (multiple) gravity assist maneuvers. In this case, the trajectory from one planet

to the next can be precomputed based on the initial and final state by solving Lambert's problem [185].

The PSO algorithm works as follows: a set of candidates, referred to as particles, forms a swarm. Each particle maintains a state and a velocity, both of which are initialized randomly. Until a termination criterion is met or until the computational budget is exhausted, particles move according to their velocities in discrete time steps. These velocities are updated in each step through a combination of individualistic and social behaviors. The velocity update is influenced by the particle's current velocity (inertia), its individually best-encountered state, and the overall best-encountered state among all particles in the swarm.

Constraints can be handled in PSO either by simply discarding infeasible solutions [186] or by imposing a penalty for constraint-violation [187]. These approaches usually work well for inequality constraints, but severely impact the practical performance if multiple equality constraints are involved [188].

In a related approach, called Multi-Swarm PSO, the particle set is divided into several smaller swarms [189]. Each swarm concentrates on exploring a specific area of the solution space, allowing for more focused exploitation. Particles can be periodically regrouped between swarms to further enhance exploration.

The PSO algorithm involves several crucial parameters that significantly affect its performance. These parameters include the population size, initial velocities, initial states, and the weights used for velocity updates, which are commonly known as cognitive and social scaling parameters. Additionally, there is an optional parameter that defines the neighborhood influence of particles, a concept introduced to prevent the swarm from becoming trapped in a single local optimum [190].

It is important to note that these parameters have a direct impact on the practical performance of the PSO algorithm [191, 192] and that it is not trivial to provide an *"off-the-shelf"* version of the algorithm [193, 194]. Moreover, these parameters need not remain static. Adaptive versions of the algorithm, known as Adaptive Particle Swarm Optimization (APSO), have demonstrated improved exploration efficiency and convergence [195, 196].

Numerous extensions and variations of PSO have been developed to address different problem domains and challenges. For a comprehensive overview of these extensions, we recommend referring to the survey conducted by Bonyadi and Michalewicz [197].

In its original form, PSO cannot guarantee optimality, neither locally nor globally. Moreover, it does not even satisfy the criteria for stability, meaning there is no guarantee that particles will converge to the same point.

An improvement called *Guaranteed Convergence PSO* (GCPSO) was introduced in [198] to overcome this limitation. GCPSO achieves local convergence by modifying the update mechanism for the particle with the best-known state. Instead of being influenced by the swarm, this particle focuses on the local exploration of the vicinity around the best-known state. Its velocity is updated based on this best-known state combined with a random perturbation.

Furthermore, GCPSO has two straightforward extensions: *Randomized PSO* (RPSO) and *Multi-Start PSO* (MPSO), both aimed at ensuring probabilistic optimality [198]. In other words, they will find the global optimum given an infinite number of iterations.

RPSO introduces random state resets for particles after a certain number of iterations, in order to maintaining a minimum level of exploration. On the other hand, MPSO employs a simple multi-start approach, running GCPSO with different initial states to enhance the probability of reaching the global optimum.

PSO has been successfully used for closely related Flight Planning problems in [183] and [199]. Moreover, its frequent use in various related applications demonstrates that it holds potential as an efficient tool for numerous practical problems, particularly when limited insight is available [188, 200–202].

One of its notable strengths lies in its ability to tackle problems without relying on gradient information. However, in scenarios where this information is available, as we assume in this work, it is expected that the previously discussed methods may outperform PSO.

Ant Colony Optimization (ACO), introduced by Dorigo in 1992 [203], draws inspiration from the foraging behavior of ants in search of food [204–206].

In nature, ants engage in a decentralized exploration strategy. When an ant locates a food source, it returns to the colony while depositing a trail of pheromones along its path. The strength of this pheromone trail influences the behavior of other ants. A stronger trail attracts more ants, who follow the same path and contribute to the pheromone deposition, ultimately reinforcing the trail. Importantly, these trails are not binding; ants continue to explore alternative paths. Over time, the most efficient path accumulates the highest pheromone concentration.

The ACO algorithm has originally been proposed for combinatorial optimization problems, such as the Travelling Salesman Problem (TSP). In order to use it for trajectory optimization problems, the search space is discretized into a weighted digraph with the pheromone levels on all arcs initialized to zero. The algorithm proceeds in iterations simulating a batches of "ants" exploring the graph. After the exploration phase, the pheromone trails are updated. This process repeats until a termination criterion is met or the computational resources are exhausted.

During exploration, ants construct paths through the graph starting from the given origin. At each step, an ant selects its next node from available successor nodes based on a probability distribution, which considers both the attractiveness of the arc (determined by the pheromone level) and the cost associated with that arc. Inspired by the classic A* algorithm, arc-costs may optionally include a heuristic lower bound on the cost to reach the target [207]. Ants continue to build paths until they reach their destination.

The path quality is evaluated concerning the overall objective, and the pheromone levels on the arcs are updated accordingly. This update involves two key processes: "evaporation", where pheromone levels naturally decrease over time, and "pheromone deposition", where new pheromones are added to arcs based on the quality of the path in which they were used. Arcs that were part of more efficient paths receive more pheromones.

In essence, ACO harnesses the individual curiosity of simulated ants to explore the space and the collective intelligence to exploit paths, gradually converging toward optimal solutions through pheromone reinforcement and evaporation.

ACO has seen various extensions, such as the (*strong*) *elitist strategy*, which allows only the best generated solution to update pheromone trails. This can be the best solution within the current iteration or the globally best solution [204].

The *Max-Min Ant System* (MMAS) additionally introduces upper and lower bounds on pheromone trail values and initializes pheromone trails to their upper limit, accompanied by periodic reinitialization, aiming at enhanced exploration [208, 209].

On the other hand, *Ant Colony System* (ACS) amplifies the importance of exploiting information collected by previous ants over exploration by altering the probability distribution for choosing the next arcs in favor of the currently best path [210].

The ACO algorithm involves several parameters, such as weights to balance the effects of pheromone levels on arcs and their costs, the rate of pheromone evaporation, the number of ants in each batch, and more. Further extensions introduce additional parameters, all of which significantly impact both the theoretical and practical convergence speed of the algorithm. Research has shown that adjusting parameters dynamically over time can lead to better convergence [211, 212].

It has been shown that several versions of the ACO algorithm converge probabilistically to an optimal solution [211–214]. The convergence rate, however, is again difficult to assess [215]. Also, defining a termination criterion can be challenging. However, in many cases, including the Free Flight Trajectory Optimization Problem discussed here, a first feasible solution is rapidly reached and continuously improved upon. This flexibility allows for a direct trade-off between the computational budget allocated and the quality of the solution obtained.

Another notable advantage of ACO algorithms is their adaptability to dynamic environments and evolving problem landscapes, such as changing weather conditions, as they can continuously update pheromone levels to reflect changes [216, 217].

In contrast, classical shortest path algorithms like Dijkstra’s would require rerunning on a modified graph in order to adapt to such changes (refer to Section 1.4.1). However, it is essential to note that on well-defined, deterministic, and static graphs classical algorithms shine as highly efficient solutions and are often the superior choice to ACO [218].

Due to the approximation error of the underlying graph, ACO, similar to its deterministic counterparts, is subject to the curse of dimensionality. Nonetheless, ACO has proven its effectiveness not only in addressing the TSP but also in solving flight planning [219] and related problems [220, 221].

1.4.4.2 Sampling-Based Methods

Sampling-based methods for path planning are a class of algorithms that approach the problem by incrementally constructing a graph structure through random sampling of points within the state space [109, 222]. The most prominent methods are *Probabilistic Roadmaps* (PRMs) [223] and *Rapidly Exploring Random Trees* (RRTs) [224, 225]. These techniques have been developed especially for scenarios involving high-dimensional state spaces, where constructing a conventional isotropic graph becomes impractical due to its sheer size.

Although closely related, these two approaches differ in two key aspects. For a PRM, random samples are drawn from the state space, and efforts are made to establish feasible connections among them. This process generates clusters that eventually merge into a connected graph. On the other hand, a RRT expands a graph from its origin by randomly sampling states from the search space and linking them to the growing graph. This characteristic allows for determination of paths to each node on the fly. A path on a PRM, in turn, must be derived in a secondary step using standard shortest path algorithms (refer to Section 1.4.1).

This quality is particularly advantageous when calculating routes for multiple origin-destination pairs, as query times on a constructed roadmap are typically very low. For single-query tasks, which this work focuses on, usually RRTs are used. Therefore, we focus more on this method.

Both PRMs and RRTs are probabilistically complete, implying they will eventually identify a feasible solution if one exists. More precisely, the probability of failing to yield a solution decays exponentially to zero. Extensions of these methods, specifically PRM* and RRT*, have even been proven to be even asymptotically optimal, meaning they will eventually find an optimal solution [226]. However, achieving this requires an additional step where the graph is rewired after adding a new node. This process increases the computational complexity only by a constant factor, which, however, can be significant in practice.

The balance between exploration and exploitation in these methods depends mostly on how new random samples are generated. In the original version points are sampled uniformly from the state space, but by altering the probability distribution, the balance can be biased in one direction or the other.

For enhancing exploration, the probability distribution can be biased explicitly towards unexplored areas [227].

To boost exploitation, the graph creation can be guided towards the destination, either by incorporating a lower bound on the cost to reach the destination, similar to the A* algorithm (known as informed RRT* [228, 229]), or by using a coarse initial guess of the optimal route [230].

Another way to enhance computational efficiency are approaches like *Bidirectional RRT* or *RRT-Connect*, which involve growing a second tree from the destination allowing for more efficient exploration of the search space [231]. However, this comes with a certain overhead to correctly connect these trees and is not probabilistically optimal. This deficiency was addressed later in [232]. A more comprehensive overview of extensions of the RRT can be found in [233] or [234].

PRMs and RRTs have found successful applications in flight planning [235–237], as well as various related tasks [226, 238, 239], and may serve as valuable tools for addressing the Free Flight Trajectory Optimization Problem from the perspective of a path planning problem. However, it is worth noting that incorporating more complex non-holonomic physics, as discussed in Section 1.2.6, presents a significant challenge [233].

Further advantages and disadvantages overlap with those of PSO and ACO. Therefore, we discuss them in a final concluding remark.

1.4.4.3 Conclusion

Stochastic methods have found success in several trajectory optimization and path planning problems. The discussed approaches exemplify their notable strengths.

One of the key advantages of these methods is their ability to operate without the need for in-depth problem understanding or strict adherence to problem regularity conditions. They do not rely on gradient information and can handle problems that may lack smoothness or have complex characteristics. This adaptability makes them versatile tools suitable for a wide range of problem domains.

Moreover, these methods are known for their simplicity of implementation and user-friendliness, although optimizing the various parameters involved can significantly enhance their practical efficiency. This ease of use contributes to their applicability across a broad spectrum of problems.

However, it is crucial to acknowledge that these methods do not provide a formal certificate of optimality, which can be a limitation in specific situations, particularly for safety-critical operations. In the best-case scenario, they converge to an optimal solution in a probabilistic sense. Conversely, some methods or extensions prioritize practical efficiency but do not offer any guarantee of optimality whatsoever.

Furthermore, considering our assumption of having detailed problem insight, it would be inefficient not to harness gradient information, as emphasized by Betts [111]. This realization has motivated the development of hybrid methods, which combine stochastic algorithms with local optimization, such as direct methods (refer to Section 1.4.3).

1.5 Contributions of this Work

In this work, we present an algorithm designed to deterministically find an ϵ -globally optimal solution to the Free Flight Trajectory Optimization Problem in finite time.

As discussed in Sections 1.2 and 1.3, this setting introduces several simplifications. Most importantly, we focus on the trajectory of a single aircraft, which is restricted to travel at constant air speed and altitude. Additionally, we assume the wind field to be stationary and defined by a multiple times continuously differentiable function. Despite these simplifications, our exploration of various sophisticated approaches, that have been developed to address the additional complexities of the real-world scenario, leads us to anticipate that our findings will be transferrable to practical applications.

The preceding section underscores the wide and deep landscape of methods devised to solve the Free Flight Trajectory Optimization Problem and related tasks, each with its unique strengths and weaknesses. Especially satisfying the criteria for global optimality and bounded computation time at the same time and in an efficient way remains a challenge.

Our approach combines the strengths of discrete and continuous optimization while mitigating their individual limitations. To rigorously prove the claimed convergence properties, we conduct a thorough analysis of various aspects of the problem. This includes investigating the approximation properties of graphs, understanding the local behavior of the optimization problem, and analyzing the convergence properties of Newton's method.

1.5.1 Published Articles

This thesis comprises five peer-reviewed and published research articles: [1–5], listed in Table 1.1 below. These articles are presented as individual chapters within this thesis, organized in the order of their preparation, which may not perfectly align with their publication sequence.

In order to enhance the readability and cohesiveness of this thesis, cross-references between these articles have been adjusted for clarity. Each article is accompanied by a distinct statement that outlines the authors’ individual contributions.

Additionally, this thesis includes an appendix containing supplementary theoretical findings and a numerical study.

-
-
- [1] R. Borndörfer, F. Danecker, and M. Weiser, “A Discrete-Continuous Algorithm for Free Flight Planning,” *Algorithms*, vol. 14, no. 1, p. 4, 2021. DOI: 10.3390/a14010004.
 - [2] R. Borndörfer, F. Danecker, and M. Weiser, “A Discrete-Continuous Algorithm for Globally Optimal Free Flight Trajectory Optimization,” in *22nd Symposium on Algorithmic Approaches for Transportation Modelling, Optimization, and Systems (ATMOS 2022)*, vol. 106, Schloss Dagstuhl – Leibniz-Zentrum für Informatik, 2022, pp. 1–13. DOI: 10.4230/OASIcs.ATMOS.2022.2.
 - [3] R. Borndörfer, F. Danecker, and M. Weiser, “Error Bounds for Discrete-Continuous Free Flight Trajectory Optimization,” *Journal of Optimization Theory and Applications*, vol. 198, no. 2, pp. 830–856, 2023. DOI: 10.1007/s10957-023-02264-7.
 - [4] R. Borndörfer, F. Danecker, and M. Weiser, “Newton’s Method for Global Free Flight Trajectory Optimization,” *Operations Research Forum*, vol. 4, no. 3, p. 63, 2023. DOI: 10.1007/s43069-023-00238-z.
 - [5] R. Borndörfer, F. Danecker, and M. Weiser, “Convergence Properties of Newton’s Method for Globally Optimal Free Flight Trajectory Optimization,” in *23rd Symposium on Algorithmic Approaches for Transportation Modelling, Optimization, and Systems (ATMOS 2023)*, vol. 115, Schloss Dagstuhl – Leibniz-Zentrum für Informatik, 2023, 3:1–3:6. DOI: 10.4230/OASIcs.ATMOS.2023.3.
-
-

Table 1.1: Articles of this work.

We will now guide through this thesis by introducing the developed algorithm and highlighting the individual contribution of each chapter.

1.5.2 The DisCOptER Algorithm

Akin to most global optimization algorithms, the proposed algorithm comprises two fundamental components: global exploration and local exploitation.

In order to explore the search space globally, we create a graph that adequately covers the region relevant for the given problem instance. This graph implicitly defines a finite sample of feasible paths from the origin to the destination. The minimum-cost path can efficiently be identified using shortest path algorithms, such as A*. In this process we employ a lower bound on the travel time from any node to the destination by considering an a priori known upper bound on the wind speed.

This path is exploited in a second step, in which we use classical optimal control methods to generate a (locally) optimal continuous solution and overcome the limited resolution of the graph. This step can be realized either with direct or with indirect methods, both of which were discussed in Section 1.4. In this work, we use a direct collocation approach and solve the resulting constrained nonlinear optimization problem using the Newton-KKT method (also known as Sequential Quadratic Programming, SQP). This entails applying the ordinary Newton's method to the first order necessary conditions for optimality, known as the *Karush-Kuhn-Tucker* (KKT) conditions.

This algorithm was proposed in [1] (Chapter 2) under the name *DisCOptER* (Discrete-Continuous Optimization for Enhanced Resolution). Theoretical analysis and practical demonstrations have shown that this hybrid approach clearly outperforms purely graph-based routing for high-precision requirements.

Routing on a graph is realized with a special class of (h, ℓ) -dense graphs, characterized by the node spacing h and the local connectivity radius ℓ , which simultaneously serves as a measure for the resolution of the solution. By varying these parameters, the graph is isotropically refined. It was shown that this way of routing carries a time complexity of $\mathcal{O}(\ell^{-6})$.

The enhancement of the DisCOptER algorithm is achieved by effectively decoupling the complexity of the problem instance from the requested accuracy of the solution. The rougher the wind conditions, the denser the graph needs to be in order to contain a path that is sufficiently close to the continuous optimum. Of course, this incurs higher computational costs for graph construction and

shortest path determination. Importantly, however, this cost is independent of the desired solution accuracy.

This requested accuracy, in turn, exclusively impacts the computational effort required for the local optimization stage. Consequently, the algorithm inherits the asymptotical convergence rate of the incorporated method (in this case direct collocation combined with Newton-KKT). It was shown that this computational effort scales with $\mathcal{O}(\ell^{-1})$, with ℓ denoting the collocation discretization length, hence serving as a comparable indicator of the solution quality.

In this first publication, it has been shown that the novel algorithm is based on a promising theoretical foundation and works efficiently in practical application. Several aspects, however, remain to be defined precisely. These evolve around the key question *where is the right switch-over point from discrete to continuous optimization?* Or *what is the right graph density?* The right balance must be struck: the graph should be as sparse as possible to avoid excessive computation yet as dense as necessary to approximate the continuous global optimum sufficiently well.

This involves considering two facets: the approximation error of the incorporated graph (mainly covered in [3], Chapter 3) and the size of the convergence region for the employed local optimization method (primarily discussed in [4], Chapter 5). However, it is crucial to recognize that having a graph fine enough to encompass a path within the convergence region does not guarantee that it is the best path available on the graph (as illustrated in Figure 4.2). As a result, multiple paths on the graph need to be considered as potential candidates (discussed in [2], Chapter 4).

1.5.3 Approximation Properties of Graphs

In [3] (Chapter 3), we establish an upper bound for the suboptimality in terms of overall travel time when routing on (h, ℓ) -dense graphs. This analysis comprises three key steps:

Firstly, we introduce an alternative problem formulation that facilitates the comparison of different trajectories, and therefore serves as an important tool throughout this work. This involves mapping trajectories from the time interval

$[0, T]$ to the unit interval $[0, 1]$ while incorporating the dynamics equation and the constraint for constant ground speed into the objective. While this formulation removes most formal constraints, it introduces a new degree of freedom, which we eliminate by restricting the problem to trajectories of constant ground speed within the transformed time. In [3] (Chapter 3), we accomplished this through the definition of the admissible set, while in subsequent works we incorporate a separate constraint for the same purpose.

Secondly, in order to evaluate the approximation error of an (h, ℓ) -dense graph within the trajectory space, we introduce a rounding procedure to map a continuous trajectory onto a given graph, quantifying the overall error in terms of distance and angular error. Notably, higher-order derivatives like curvature error are not considered since they do not influence the overall travel time in the current model. This analysis also allows us to optimize the combination of the two parameters h and ℓ .

Lastly, to understand the impact of distance within the trajectory space on the overall travel time, we explore the local behavior of the objective near a minimizer. Due to the smoothness of the wind field, and the fact that the gradient vanishes at a minimizer, we can bound the objective function by considering its Hessian. Additionally, we demonstrate that incorporating local wind information can significantly enhance the derived bounds, motivating future work toward adaptive approaches.

1.5.4 Towards Global Optimality

In [2] (Chapter 4) we introduce an extension of the DisCOptER algorithm, which is small but crucial in order to guarantee global optimality of the provided solution. This extension also necessitates a minor adjustment in notation. While we previously used the subscript "C" to denote a (continuous) local solution, we now distinguish between local and global solutions using superscripts "*" and "**", respectively.

Crucially, we formalize a qualitative understanding that has been previously recognized, specifically, how to select the appropriate graph density. This process involves three key steps:

Firstly, we address the restricted admissible set, mentioned above, by introducing an explicit constraint and articulate the necessary and sufficient conditions for optimality. In the following, we operate under the assumption that these conditions hold at a global minimizer and that the characteristics are known quantitatively. This assumption will later be resolved (refer to Section 7.1). Leveraging the smoothness of the problem, we establish a lower bound on the size of the convex region around the minimizer. This lays the groundwork for the subsequent chapter, in which a rigorous proof of convergence will be conducted.

Secondly, we formally derive the minimum graph density that guarantees the presence of a path within this defined convex region, based on the approximation error bounds from [3] (Chapter 3).

Lastly, we consider the possibility that the path contained in this region might not be the best path on the graph. To address this, we propose an iterative approach using Yen's algorithm to evaluate paths in order of ascending travel time. This iteration process involves applying the same shortest path algorithm as before on slightly modified graphs, encouraging the creation of alternative routes. A termination condition is established by bounding the travel time within the convex region, again building upon the results from [3] (Chapter 3).

1.5.5 Proof of Convergence

In [4] (Chapter 5) our primary focus centers on the local optimization through the ordinary Newton-KKT method. We prove the existence of a quantifiable region surrounding a global minimizer from within which the Newton-KKT method does converge. Specifically, two essential criteria must be met within this region:

First, the KKT-operator must be invertible. To establish this result, we scrutinize the LBB (Ladyzhenskaya-Babuška-Brezzi) condition, comprising two pivotal components. Firstly, the inf-sup condition must be satisfied. Secondly, the second partial derivative of the Lagrangian with respect to the state variables should be positive definite on the kernel of the constraints. Furthermore, this derivative needs to be bounded from above.

Secondly, the KKT-operator needs to be sufficiently smooth within the neighborhood. This is accomplished by providing a suitable Lipschitz condition.

In the final theorem of this chapter, we continue to make certain assumptions about the characteristics of the global minimizer. Specifically, we rely on the availability of a lower bound for the Hessian of the objective function. This lower bound plays a crucial role in determining the size of the convergence domain, which, in turn, influences the necessary graph density.

In practice, obtaining such a lower bound is often a non-trivial task. However, in Section 7.1, we demonstrate that under moderate wind conditions, we can provide this lower bound. We achieve this based on the usual global wind characteristics, making it a valuable addition to our theoretical framework.

It is important to note that all the bounds we derive are based on a few mild a priori assumptions regarding the wind field, merely requiring that the wind speed and its spatial derivatives remain globally bounded.

1.5.6 Practical Convergence Properties

It is no surprise that a priori bounds based on global characteristics of the wind situation are rather conservative. In [5] (Chapter 6) we empirically validate our previous theoretical findings in a numerical investigation and subject the Newton-KKT method to a challenging scenario, demonstrating that the convergence region is notably larger than theoretically anticipated. Simultaneously, we confirm the validity and importance of the distance measure introduced in [3] (Chapter 3), which encompassed both distance and angular error.

To execute this empirical examination, we construct a two-dimensional subspace within the infinite-dimensional trajectory space by introducing two types of deviations onto the optimal trajectory. With a low frequency deviation we induce primarily distance error and minimum angular error. With a high frequency deviation, we conversely induce primarily angular and minimum distance error.

While it is intuitive that the domain of convergence is bounded in terms of distance error due to the potential presence of nearby local optima, the same does

not hold true for angular deviations. This motivates the utilization of an overlapping domain decomposition method to significantly enhance convergence.

Our approach capitalizes on two key properties of the problem. Firstly, in line with Bellman's principle of optimality, sub-paths of an optimal trajectory remain optimal. Secondly, for short-haul flights, the trajectory stays relatively close to the straight path (or the great circle on the sphere), with "short" being relative to the wind phenomena.

In essence, our approach operates as follows: the initial trajectory, which may exhibit oscillations or zigzag patterns, is segmented into equally sized "short" segments. The endpoints of these segments remain fixed, and routes between adjacent points are optimized individually. This process is then repeated with shifted segments. The resultant smoothed route serves as the initial guess for an overall optimization.

Our research conclusively demonstrates that this smoothing approach significantly enlarges the overall domain of convergence. Consequently, less angular resolution is required from the graph utilized in the first stage of the DisCOptER method. This, in turn, allows for a reduction in the connectivity radius, making this stage less computationally expensive and rendering the entire algorithm more practically efficient.

1.5.7 Harvesting the Benefits of Free Flight

In addition to the theoretical findings discussed in Section 7.1, the appendix presents a comprehensive numerical study conducted under realistic conditions. This study, presented in Section 7.2, carries a twofold significance.

Firstly, we investigate a graph-based routing approach aimed at emulating the current state-of-the-art in Free Route Airspaces. In this scenario, we assume a predefined set of waypoints and allow valid paths to consist of any combination of these waypoints. Under these conditions, we introduce a method for constructing a graph that prioritizes angular resolution. Our findings reveal that this approach offers significantly improved scalability when compared to the conventional method of constructing a locally dense graph.

Secondly, this study serves as compelling evidence of the exceptional performance of the DisCOptER algorithm. Remarkably, the algorithm consistently identifies the global optimum in the first iteration for every instance, even when using a very sparse graph. This outcome underscores that the strategy of iterating through multiple paths, which is necessary for guaranteeing global optimality, is, in practice, more of a precautionary measure than a fundamental requirement. Furthermore, the provided routes significantly reduced flight costs. These findings highlight the practical efficiency of the developed algorithm as a highly effective tool for Free Flight Trajectory Optimization.

References

- [1] R. Borndörfer, F. Danecker, and M. Weiser, “A Discrete-Continuous Algorithm for Free Flight Planning,” *Algorithms*, vol. 14, no. 1, p. 4, 2021. DOI: 10.3390/a14010004.
- [2] R. Borndörfer, F. Danecker, and M. Weiser, “A Discrete-Continuous Algorithm for Globally Optimal Free Flight Trajectory Optimization,” in *22nd Symposium on Algorithmic Approaches for Transportation Modelling, Optimization, and Systems (ATMOS 2022)*, vol. 106, Schloss Dagstuhl – Leibniz-Zentrum für Informatik, 2022, pp. 1–13. DOI: 10.4230/OASIcs.ATMOS.2022.2.
- [3] R. Borndörfer, F. Danecker, and M. Weiser, “Error Bounds for Discrete-Continuous Free Flight Trajectory Optimization,” *Journal of Optimization Theory and Applications*, vol. 198, no. 2, pp. 830–856, 2023. DOI: 10.1007/s10957-023-02264-7.
- [4] R. Borndörfer, F. Danecker, and M. Weiser, “Newton’s Method for Global Free Flight Trajectory Optimization,” *Operations Research Forum*, vol. 4, no. 3, p. 63, 2023. DOI: 10.1007/s43069-023-00238-z.
- [5] R. Borndörfer, F. Danecker, and M. Weiser, “Convergence Properties of Newton’s Method for Globally Optimal Free Flight Trajectory Optimization,” in *23rd Symposium on Algorithmic Approaches for Transportation Modelling, Optimization, and Systems (ATMOS 2023)*, vol. 115, Schloss Dagstuhl – Leibniz-Zentrum für Informatik, 2023, 3:1–3:6. DOI: 10.4230/OASIcs.ATMOS.2023.3.
- [6] M. D. Blanco Sandoval, “Optimization Algorithms for the Flight Planning Problem,” Ph.D. dissertation, Free University of Berlin, 2023.

- [7] V. Grewe, S. Matthes, and K. Dahlmann, “The Contribution of Aviation NO_x Emissions to Climate Change: Are We Ignoring Methodological Flaws?” *Environmental Research Letters*, vol. 14, no. 12, p. 121003, 2019. DOI: 10.1088/1748-9326/ab5dd7.
- [8] D. Lee, D. Fahey, A. Skowron, M. Allen, U. Burkhardt, Q. Chen, S. Doherty, S. Freeman, P. Forster, J. Fuglestvedt, A. Gettelman, R. De León, L. Lim, M. Lund, R. Millar, B. Owen, J. Penner, G. Pitari, M. Prather, R. Sausen, and L. Wilcox, “The Contribution of Global Aviation to Anthropogenic Climate Forcing for 2000 to 2018,” *Atmospheric Environment*, vol. 244, p. 117834, 2021. DOI: 10.1016/j.atmosenv.2020.117834.
- [9] European Environmental Agency (EEA), *European Aviation Environmental Report 2022 – Executive Summary and Recommendations*. [Online]. Available: https://www.easa.europa.eu/eco/sites/default/files/2022-09/EnvironmentalReport_EASA_summary_12.pdf (visited on 09/22/2023).
- [10] B. Graver, K. Zhang, and D. Rutherford, “CO₂ Emissions from Commercial Aviation, 2018,” *International Council on Clean Transportation*, 2019. [Online]. Available: https://theicct.org/sites/default/files/publications/ICCT_CO2-commercial-aviation-2018_20190918.pdf (visited on 09/22/2023).
- [11] C. Varotsos, V. Krapivin, F. Mkrtychyan, and X. Zhou, “On the Effects of Aviation on Carbon-Methane Cycles and Climate Change During the Period 2015-2100,” *Atmospheric Pollution Research*, vol. 12, no. 1, pp. 184–194, 2021. DOI: 10.1016/j.apr.2020.08.033.
- [12] International Civil Aviation Organization (ICAO), *The World of Air Transport in 2019*. [Online]. Available: <https://www.icao.int/annual-report-2019/Pages/the-world-of-air-transport-in-2019.aspx> (visited on 09/22/2023).
- [13] D. Oxley and C. Jain, “Global Air Passenger Market: Riding Out Periods of Turbulence,” in *Travel and Tourism Competitiveness Report 2015*, International Air Transport Association. World Economic Forum, 2015, ch. 1.4. [Online]. Available: <https://www.iata.org/en/iata-repository/publications/economic-reports/global-air-passenger-markets-riding-out-periods-of-turbulence/> (visited on 09/22/2023).
- [14] International Air Transport Association (IATA), *Air Passenger Numbers to Recover in 2024*, 2022. [Online]. Available: <https://www.iata.org/en/pressroom/2022-releases/2022-03-01-01/> (visited on 09/22/2023).
- [15] B. Vaaben and J. Larsen, “Mitigation of Airspace Congestion Impact on Airline Networks,” *Journal of Air Transport Management*, vol. 47, pp. 54–65, 2015. DOI: 10.1016/j.jairtraman.2015.04.002.
- [16] Aireon, *Operations Overview*. [Online]. Available: <https://www.aireon.com/resources/overview-materials/operations-overview/> (visited on 09/22/2023).

- [17] B. Elder, “Free Flight: The Future of Air Transportation Entering the Twenty-First Century,” *Journal of Air Law and Commerce*, vol. 62, p. 871, 1996.
- [18] R. Schultz, D. Shaner, Y. Zhao, R. Schultz, D. Shaner, and Y. Zhao, “Free-Flight Concept,” in *Guidance, Navigation, and Control Conference*. 1997. DOI: 10.2514/6.1997-3677.
- [19] D. Chin and F. Melone, “Using Airspace Simulation to Assess Environmental Improvements from Free Flight and CNS/ATM Enhancements,” in *WSC’99. 1999 Winter Simulation Conference Proceedings. ‘Simulation – A Bridge to the Future’ (Cat. No.99CH37038)*, vol. 2, 1999, pp. 1295–1301. DOI: 10.1109/WSC.1999.816856.
- [20] *Single European Sky ATM Research 3 Joint Undertaking (SESAR 3 JU)*. [Online]. Available: <https://www.sesarju.eu/discover-sesar> (visited on 09/22/2023).
- [21] *Next Generation Air Transportation System (NextGen)*. [Online]. Available: <https://www.faa.gov/nextgen> (visited on 09/22/2023).
- [22] Ministry of Land, Infrastructure, Transport and Tourism (MLIT), *Collaborative Actions for Renovation of Air Traffic Systems (CARATS)*. [Online]. Available: https://www.mlit.go.jp/en/koku/koku_fr13_000000.html (visited on 09/22/2023).
- [23] EUROCONTROL, *Free Route Airspace (FRA)*. [Online]. Available: <https://www.eurocontrol.int/concept/free-route-airspace> (visited on 09/22/2023).
- [24] C. A. Wells, P. D. Williams, N. K. Nichols, D. Kalise, and I. Poll, “Reducing Transatlantic Flight Emissions by Fuel-Optimised Routing,” *Environ. Res. Letters*, vol. 16, no. 2, p. 025002, 2021. DOI: 10.1088/1748-9326/abce82.
- [25] S. Altus, “Effective Flight Plans Can Help Airlines Economize,” *Boeing Aero*, 2009. [Online]. Available: https://www.boeing.com/commercial/aeromagazine/articles/qtr_03_09/article_08_1.html (visited on 09/22/2023).
- [26] M. Kodera, J. Hospodka, and M. Chleboun, “Flight Planning and Flexible Use of Airspace in Free Route Airspace Area,” *MAD-Magazine of Aviation Development*, vol. 2, no. 7, pp. 4–7, 2014. DOI: 10.14311/MAD.2014.07.01.
- [27] W. Zhang, M. Kamgarpour, D. Sun, and C. J. Tomlin, “A Hierarchical Flight Planning Framework for Air Traffic Management,” *Proceedings of the IEEE*, vol. 100, no. 1, pp. 179–194, 2012. DOI: 10.1109/JPROC.2011.2161243.
- [28] M. Blanco, R. Borndörfer, N.-D. Hoang, A. Kaier, A. Schienle, T. Schlechte, and S. Schlobach, “Solving Time Dependent Shortest Path Problems on Airway Networks Using Super-Optimal Wind,” in *16th Workshop on Algorithmic Approaches for Transportation Modelling, Optimization, and Systems (ATMOS 2016)*, vol. 54, Schloss Dagstuhl–Leibniz-Zentrum fuer Informatik, 2016, pp. 1–15. DOI: 10.4230/OASICS.ATMOS.2016.12.

- [29] A. Schienle, “Solving the Time-Dependent Shortest Path Problem Using Super-Optimal Wind,” in *Operations Research Proceedings 2017*, Springer International Publishing, 2018, pp. 3–9. DOI: 10.1007/978-3-319-89920-6.
- [30] H. K. Ng, B. Sridhar, and S. Grabbe, “Optimizing Aircraft Trajectories with Multiple Cruise Altitudes in the Presence of Winds,” *Journal of Aerospace Information Systems*, vol. 11, no. 1, pp. 35–47, 2014. DOI: 10.2514/1.I010084.
- [31] R. S. Félix Patrón and R. M. Botez, “Flight Trajectory Optimization Through Genetic Algorithms Coupling Vertical and Lateral Profiles,” vol. Volume 1: Advances in Aerospace Technology, 2014. DOI: 10.1115/IMECE2014-36510.
- [32] A. N. Knudsen, M. Chiarandini, and K. S. Larsen, “Vertical Optimization of Resource Dependent Flight Paths,” in *ECAI*, IOS Press, 2016, pp. 639–645. DOI: 10.3233/978-1-61499-672-9-639.
- [33] L. A. Moreno, Z. Yuan, A. Fügenschuh, A. Kaier, and S. Schlobach, “Combining NLP and MILP in Vertical Flight Planning,” in *Operations Research Proceedings 2015*, Springer, 2017, pp. 273–278. DOI: 10.1007/978-3-319-42902-1_37.
- [34] L. A. Moreno, A. Fügenschuh, A. Kaier, and S. Schlobach, “A Nonlinear Model for Vertical Free-Flight Trajectory Planning,” in *Operations Research Proceedings 2017*, Springer International Publishing, 2018, pp. 445–450. DOI: 10.1007/978-3-319-89920-6_59.
- [35] B. D. Dancila and R. Botez, “Construction of an Aircraft’s VNAV Flight Envelope for in-FMS Flight Trajectory Computation and Optimization,” in *14th AIAA Aviation Technology, Integration, and Operations Conference*. 2014, p. 2291. DOI: 10.2514/6.2014-2291.
- [36] S. Khardi, L. Abdallah, O. Konovalova, and M. Houacine, “Optimal Approach Minimizing Aircraft Noise and Fuel Consumption,” *Acta Acustica united with Acustica*, vol. 96, no. 1, pp. 68–75, 2010. DOI: 10.3813/AAA.918257.
- [37] M. Houacine and S. Khardi, “Gauss Pseudospectral Method for Less Noise and Fuel Consumption of Aircraft Operations,” *Journal of Aircraft*, vol. 47, no. 6, pp. 2152–2158, 2010. DOI: 10.2514/1.C031007.
- [38] R. Torres, J. Chaptal, C. Bès, and J.-B. Hiriart-Urruty, “Optimal, Environmentally Friendly Departure Procedures for Civil Aircraft,” *Journal of Aircraft*, vol. 48, no. 1, pp. 11–22, 2011. DOI: 10.2514/1.C031012.
- [39] M. Soler, A. Olivares, and E. Staffetti, “Multiphase Optimal Control Framework for Commercial Aircraft Four-Dimensional Flight-Planning Problems,” *Journal of Aircraft*, vol. 52, no. 1, pp. 274–286, 2015. DOI: 10.2514/1.C032697.
- [40] P. Bonami, A. Olivares, M. Soler, and E. Staffetti, “Multiphase Mixed-Integer Optimal Control Approach to Aircraft Trajectory Optimization,” *Journal of Guidance, Control, and Dynamics*, vol. 36, no. 5, pp. 1267–1277, 2013. DOI: 10.2514/1.60492.

- [41] R. Dalmau Codina and X. Prats Menéndez, “How Much Fuel and Time can be Saved in a Perfect Flight Trajectory? Continuous Cruise Climbs vs. Conventional Operations,” in *Proceedings of the 6th International Congress on Research in Air Transportation (ICRAT)*, 2014. [Online]. Available: <http://hdl.handle.net/2117/23151> (visited on 09/22/2023).
- [42] J. Lovegren and R. J. Hansman, “Estimation of Potential Aircraft Fuel Burn Reduction in Cruise via Speed and Altitude Optimization Strategies,” Tech. Rep., 2011. [Online]. Available: <http://hdl.handle.net/1721.1/62196> (visited on 09/22/2023).
- [43] R. Howe-Veenstra, “Commercial Aircraft Trajectory Optimization and Efficiency of Air Traffic Control Procedures,” M.S. thesis, University of Minnesota, 2011. [Online]. Available: https://conservancy.umn.edu/bitstream/handle/11299/119038/1/Howe-Veenstra_Ryan_November2011.pdf (visited on 09/22/2023).
- [44] L. E. Miller, “Optimal Cruise Performance,” *Journal of Aircraft*, vol. 30, no. 3, pp. 403–405, 1993. DOI: 10.2514/3.46349.
- [45] S. Gössling and P. Upham, *Climate Change and Aviation: Issues, Challenges and Solutions*, 1st ed. Rutledge, 2009. DOI: 10.4324/9781849770774.
- [46] V. Grewe, S. Matthes, C. Frömming, S. Brinkop, P. Jöckel, K. Gierens, T. Champougny, J. Fuglestvedt, A. Haslerud, E. Irvine, and K. Shine, “Feasibility of Climate-Optimized Air Traffic Routing for Trans-Atlantic Flights,” *Environmental Research Letters*, vol. 12, no. 3, p. 034003, 2017. DOI: 10.1088/1748-9326/aa5ba0.
- [47] J. L. Speyer, “Periodic Optimal Flight,” *Journal of Guidance, Control, and Dynamics*, vol. 19, no. 4, pp. 745–755, 1996. DOI: 10.2514/3.21695.
- [48] J. Rosenow, M. Lindner, and J. Scheiderer, “Advanced Flight Planning and the Benefit of In-Flight Aircraft Trajectory Optimization,” *Sustainability*, vol. 13, no. 3, 2021. DOI: 10.3390/su13031383.
- [49] A. Dreves, M. Gerdts, M. Sama, and A. D’Ariano, *Free Flight Trajectory Optimization and Generalized Nash Equilibria in Conflicting Situations*, 2017.
- [50] A. K. Agogino and K. Tumer, “A Multiagent Approach to Managing Air Traffic Flow,” *Autonomous Agents and Multi-Agent Systems*, vol. 24, no. 1, pp. 1–25, 2012. DOI: 10.1007/s10458-010-9142-5.
- [51] B. Girardet, L. Lapasset, D. Delahaye, C. Rabut, and Y. Brenier, “Generating Optimal Aircraft Trajectories with respect to Weather Conditions,” in *2nd International Conference on Interdisciplinary Science for Innovative Air Traffic Management (ISIATM)*, 2013. [Online]. Available: <https://hal-enac.archives-ouvertes.fr/hal-00867818> (visited on 09/22/2023).
- [52] B. Hoch and F. Liers, “An Integrated Rolling Horizon and Adaptive-Refinement Approach for Disjoint Trajectories Optimization,” *Optimization and Engineering*, vol. 24, no. 2, pp. 1017–1055, 2023. DOI: 10.1007/s11081-022-09719-2.

- [53] J. Schmidt and A. Fügenschuh, “A Two-Time-Level Model for Mission and Flight Planning of an Inhomogeneous Fleet of Unmanned Aerial Vehicles,” *Computational Optimization and Applications*, vol. 85, no. 1, pp. 293–335, 2023. DOI: 10.1007/s10589-023-00450-x.
- [54] M. Pechoucek and D. Sislak, “Agent-Based Approach to Free-Flight Planning, Control, and Simulation,” *IEEE Intelligent Systems*, vol. 24, no. 1, pp. 14–17, 2009. DOI: 10.1109/MIS.2009.1.
- [55] J. Hoekstra, “Designing for Safety: The Free Flight Air Traffic Management Concept,” Ph.D. dissertation, Technical University Delft, 2001. [Online]. Available: <http://resolver.tudelft.nl/uuid:d9f6078a-0961-403f-871e-cad365ee46a9> (visited on 09/22/2023).
- [56] J. M. Hoekstra, R. van Gent, and R. C. J. Ruigrok, “Designing for Safety: The ‘Free Flight’ Air Traffic Management Concept,” *Reliability Engineering & System Safety*, vol. 75, pp. 215–232, 2002. DOI: 10.1016/S0951-8320(01)00096-5.
- [57] D. Šišlák, “Agent-Based Approach to Air-Traffic Modeling, Simulation and Collision Avoidance,” Ph.D. dissertation, Czech Technical University in Prague, 2013. [Online]. Available: <https://core.ac.uk/download/pdf/47172463.pdf> (visited on 09/22/2023).
- [58] K. Palopo, R. D. Windhorst, S. Suharwardy, and H.-T. Lee, “Wind-Optimal Routing in the National Airspace System,” *Journal of Aircraft*, vol. 47, no. 5, pp. 1584–1592, 2010. DOI: 10.2514/1.C000208.
- [59] A. Barnett, “Air Safety: End of the Golden Age?” *The Journal of the Operational Research Society*, vol. 52, no. 8, pp. 849–854, 2001. [Online]. Available: <http://www.jstor.org/stable/822945> (visited on 09/22/2023).
- [60] J. Hoekstra and F. Bussink, “Free Flight: How Low Can You Go? [ATC],” in *Proceedings. The 21st Digital Avionics Systems Conference*, vol. 1, 2002. DOI: 10.1109/DASC.2002.1067889.
- [61] J. M. Hoekstra, R. C. J. Ruigrok, and R. N. H. W. van Gent, “Free Flight in a Crowded Airspace?” In *Air Transportation Systems Engineering*. 2000, pp. 533–545. DOI: 10.2514/5.9781600866630.0533.0545.
- [62] M. V. Clari, R. Ruigrok, and J. Hoekstra, “Cost-Benefit Study of Free Flight with Airborne Separation Assurance,” in *AIAA Guidance, Navigation, and Control Conference and Exhibit*. 2000. DOI: 10.2514/6.2000-4361.
- [63] M. Bittner, M. Rieck, B. Grüter, and F. Holzapfel, “Optimal Approach Trajectories for Multiple Aircraft Considering Disturbances and Configuration Changes,” in *30th Congress of the International Council of the Aeronautical Sciences (ICAS)*, The International Council of the Aeronautical Sciences, 2016, pp. 25–30. [Online]. Available: https://www.icas.org/ICAS_ARCHIVE/ICAS2016/data/papers/2016_0051_paper.pdf (visited on 09/22/2023).

- [64] C. Layton, P. J. Smith, and C. E. McCoy, “Design of a Cooperative Problem-Solving System for En-Route Flight Planning: An Empirical Evaluation,” *Human Factors*, vol. 36, no. 1, pp. 94–119, 1994. DOI: 10.1177/001872089403600106.
- [65] A. Alizadeh, M. Uzun, E. Koyuncu, and G. Inalhan, “Optimal En-Route Trajectory Planning based on Wind Information,” *IFAC-PapersOnLine*, vol. 51, no. 9, pp. 180–185, 2018, 15th IFAC Symposium on Control in Transportation Systems (CTS). DOI: 10.1016/j.ifacol.2018.07.030.
- [66] International Civil Aviation Organization (ICAO), *The World Area Forecast System (WAFS) Internet File Service (WIFS) Users Guide*. [Online]. Available: https://www.icao.int/NACC/Documents/eDOCS/MET/Final%5C%20WIFS_Users_Guide_v4%5C%201-2.pdf (visited on 09/22/2023).
- [67] National Oceanic and Atmospheric Administration, *Global Forecast System*. [Online]. Available: <https://vlab.noaa.gov/web/gfs/home> (visited on 09/22/2023).
- [68] M. Lindner, J. Rosenow, T. Zeh, and H. Fricke, “In-Flight Aircraft Trajectory Optimization within Corridors Defined by Ensemble Weather Forecasts,” *Aerospace*, vol. 7, no. 10, 2020. DOI: 10.3390/aerospace7100144.
- [69] J. C. H. Cheung, J.-L. Brenguier, J. Heijstek, A. Marsman, and O. Wells, “Sensitivity of Flight Durations to Uncertainties in Numerical Weather Prediction,” 2014. [Online]. Available: https://www.sesarju.eu/sites/default/files/SID_2014-32.pdf (visited on 09/22/2023).
- [70] J. Cheung, A. Hally, J. Heijstek, A. Marsman, and J.-L. Brenguier, “Recommendations on Trajectory Selection in Flight Planning based on Weather Uncertainty,” *Proc. 5th SESAR Innovation Days (SID2015), Bologna, Italy*, pp. 1–8, 2015. [Online]. Available: https://www.sesarju.eu/sites/default/files/documents/sid/2015/SIDs_2015_paper_24.pdf (visited on 09/22/2023).
- [71] J. C. H. Cheung, “Flight Planning: Node-Based Trajectory Prediction and Turbulence Avoidance,” *Meteorological Applications*, vol. 25, no. 1, pp. 78–85, 2018. DOI: 10.1002/met.1671.
- [72] D. González Arribas, M. F. Soler Arnedo, and M. Sanjurjo Rivo, “Wind-Based Robust Trajectory Optimization using Meteorological Ensemble Probabilistic Forecasts,” *6th Cesar Innovation days*, 2016. [Online]. Available: https://www.sesarju.eu/sites/default/files/documents/sid/2016/SIDs_2016_paper_58.pdf (visited on 09/22/2023).
- [73] D. González-Arribas, M. Soler, and M. Sanjurjo-Rivo, “Robust Aircraft Trajectory Planning under Wind Uncertainty using Optimal Control,” *Journal of Guidance, Control, and Dynamics*, vol. 41, no. 3, pp. 673–688, 2017. DOI: 10.2514/1.G002928.

- [74] J.-H. Kim, W. N. Chan, B. Sridhar, and R. D. Sharman, “Combined Winds and Turbulence Prediction System for Automated Air-Traffic Management Applications,” *Journal of Applied Meteorology and Climatology*, vol. 54, no. 4, pp. 766–784, 2015. DOI: 10.1175/JAMC-D-14-0216.1.
- [75] M. Lindner, J. Rosenow, and H. Fricke, “Aircraft Trajectory Optimization with Dynamic Input Variables,” *CEAS Aeronautical Journal*, vol. 11, no. 2, pp. 321–331, 2020. DOI: 10.1007/s13272-019-00430-0.
- [76] S. E. Karisch, S. S. Altus, G. Stojković, and M. Stojković, “Operations,” in *Quantitative Problem Solving Methods in the Airline Industry*, Springer, 2011, ch. 6 – Operations, pp. 283–383. DOI: 10.1007/978-1-4614-1608-1_6.
- [77] International Air Transport Association (IATA), *Airline Fuel and Labour Cost Share*, 2010. [Online]. Available: <https://www.iata.org/en/iata-repository/publications/economic-reports/airline-fuel-labour-costs/#:~:text=Labour%20accounted%20for%2024.8%2025%20of,%20while%20fuel%20about%2025.3%2025>. (visited on 09/22/2023).
- [78] P. Maristany de las Casas, R. Borndörfer, L. Kraus, and A. Sedeño-Noda, “An FPTAS for Dynamic Multiobjective Shortest Path Problems,” *Algorithms*, vol. 14, no. 2, pp. 1–22, 2021. DOI: 10.3390/a14020043.
- [79] P. Maristany de las Casas, L. Kraus, A. Sedeno-Noda, and R. Borndörfer, “Targeted Multiobjective Dijkstra Algorithm,” *Networks*, vol. 82, no. 3, pp. 277–298, 2023. DOI: 10.1002/net.22174.
- [80] W. Rumler, T. Günther, U. Weißhaar, and H. Fricke, “Flight Profile Variations due to the Spreading Practice of Cost Index Based Flight Planning,” in *4th International Conference on Research in Air Transportation, Budapest*, 2010. [Online]. Available: <https://de.scribd.com/document/150317383/Flight-Profile-Variations-Due-to-Spreading-Practice-of-CI-Planning> (visited on 09/22/2023).
- [81] B. Sridhar, N. Chen, H. Ng, and A. Morando, “Modeling and Simulation of the Impact of Air Traffic Operations on the Environment,” *AIAA Modeling and Simulation Technologies Conference 2011*, 2011. DOI: 10.2514/6.2011-6376.
- [82] M. Blanco, R. Borndörfer, N. D. Hoàng, A. Kaier, S. Thomas, and S. Schlobach, “The Shortest Path Problem with Crossing Costs,” *ZIB Report*, 2016. [Online]. Available: <https://nbn-resolving.org/urn:nbn:de:0297-zib-61240> (visited on 09/22/2023).
- [83] M. Blanco, R. Borndörfer, N. D. Hoàng, A. Kaier, P. Maristany de las Casas, S. Thomas, and S. Schlobach, “Cost Projection Methods for the Shortest Path Problem with Crossing Costs,” in *17th Workshop on Algorithmic Approaches for Transportation Modelling, Optimization, and Systems (ATMOS 2017)*, vol. 59, Schloss Dagstuhl–Leibniz-Zentrum fuer Informatik, 2017, pp. 1–14. DOI: 10.4230/OASIcs.ATMOS.2017.15.

- [84] H. Mannstein, P. Spichtinger, and K. Gierens, “A Note on How to Avoid Contrail Cirrus,” *Transportation Research Part D: Transport and Environment*, vol. 10, no. 5, pp. 421–426, 2005. DOI: 10.1016/j.trd.2005.04.012.
- [85] H. K. Ng, B. Sridhar, S. Grabbe, and N. Chen, “Cross-Polar Aircraft Trajectory Optimization and the Potential Climate Impact,” in *IEEE/AIAA 30th Digital Avionics Systems Conference*, 2011, pp. 1–15. DOI: 10.1109/DASC.2011.6096060.
- [86] S. Campbell, N. Neogi, and M. Bragg, “An Optimal Strategy for Persistent Contrail Avoidance,” in *AIAA Guidance, Navigation and Control Conference and Exhibit*. 2012. DOI: 10.2514/6.2008-6515.
- [87] B. Sridhar, H. Ng, and N. Chen, “Aircraft Trajectory Optimization and Contrails Avoidance in the Presence of Winds,” *Journal of Guidance, Control, and Dynamics*, vol. 34(5), pp. 1577–1584, 2011. DOI: 10.2514/1.53378.
- [88] D. I. A. Poll, “On the Relationship Between Non-Optimum Operations and Fuel Requirement for Large Civil Transport Aircraft, with Reference to Environmental Impact and Contrail Avoidance Strategy,” *The Aeronautical Journal*, vol. 122, no. 1258, pp. 1827–1870, 2018. DOI: 10.1017/aer.2018.121.
- [89] A. N. Knudsen, M. Chiarandini, and K. S. Larsen, “Constraint Handling in Flight Planning,” in *Principles and Practice of Constraint Programming – 23rd International Conference*, 2017, pp. 354–369. DOI: 10.1007/978-3-319-66158-2_23.
- [90] International Civil Aviation Organization (ICAO), *Global Repository of actual NOTAMs*. [Online]. Available: <https://www.icao.int/safety/istars/pages/notams.aspx> (visited on 09/22/2023).
- [91] EUROCONTROL, *Road Availability Document (RAD)*. [Online]. Available: <https://www.nm.eurocontrol.int/RAD/> (visited on 09/22/2023).
- [92] B. Li, C. Xu, K. Teo, and J. Chu, “Time Optimal Zermelo’s Navigation Problem with Moving and Fixed Obstacles,” *Applied Mathematics and Computation*, vol. 224, pp. 866–875, 2013. DOI: 10.1016/j.amc.2013.08.092.
- [93] M. Mattei and L. Blasi, “Smooth Flight Trajectory Planning in the Presence of No-Fly Zones and Obstacles,” *Journal of Guidance, Control, and Dynamics*, vol. 33, no. 2, pp. 454–462, 2010. DOI: 10.2514/1.45161.
- [94] H. Yinnone, “On Paths Avoiding Forbidden Pairs of Vertices in a Graph,” *Discrete Applied Mathematics*, vol. 74, no. 1, pp. 85–92, 1997. DOI: 10.1016/S0166-218X(96)00017-0.
- [95] EUROCONTROL, *User Manual for the Base of Aircraft Data (BADA) Revision 3.12*.

- [96] E. Zermelo, “Über die Navigation in der Luft als Problem der Variationrechnung ‘On the Navigation in the Air as a Problem of the Calculus of Variations’,” *Jahresbericht der Deutschen Mathematiker-Vereinigung*, vol. 39, pp. 44–48, 1930.
- [97] E. Zermelo, “Über das Navigationsproblem bei ruhender oder veränderlicher Windverteilung,” *ZAMM-Journal of Applied Mathematics and Mechanics/Zeitschrift für Angewandte Mathematik und Mechanik*, vol. 11(2), pp. 114–124, 1931. DOI: 10.1002/zamm.19310110205.
- [98] T. Levi-Civita, “Über Zermelo’s Luftfahrtproblem,” *ZAMM – Journal of Applied Mathematics and Mechanics / Zeitschrift für Angewandte Mathematik und Mechanik*, vol. 11, no. 4, pp. 314–322, 1931. DOI: 10.1002/zamm.19310110404.
- [99] M. R. Jardin and A. E. Bryson, “Neighboring Optimal Aircraft Guidance in Winds,” *Journal of Guidance, Control and Dynamics*, vol. 24, no. 4, 2001. DOI: 10.2514/2.4798.
- [100] B. Girardet, L. Lapasset, D. Delahaye, and C. Rabut, “Wind-Optimal Path Planning: Application to Aircraft Trajectories,” in *13th International Conference on Control Automation Robotics Vision (ICARCV)*, 2014, pp. 1403–1408. DOI: 10.1109/ICARCV.2014.7064521.
- [101] M. Eichhorn, “Solutions for Practice-Oriented Requirements for Optimal Path Planning for the AUV ‘SLOCUM Glider’,” in *OCEANS 2010 MTS/IEEE SEATTLE*, 2010, pp. 1–10. DOI: 10.1109/OCEANS.2010.5664082.
- [102] B. Garau, A. Alvarez, and G. Oliver, “Path Planning of Autonomous Underwater Vehicles in Current Fields with Complex Spatial Variability: an A* Approach,” in *Proceedings of the 2005 IEEE International Conference on Robotics and Automation*, 2005, pp. 194–198. DOI: 10.1109/ROBOT.2005.1570118.
- [103] T. P. Zis, H. N. Psaraftis, and L. Ding, “Ship Weather Routing: A Taxonomy and Survey,” *Ocean Engineering*, vol. 213, 2020. DOI: 10.1016/j.oceaneng.2020.107697.
- [104] M. Vasile, E. Minisci, and M. Locatelli, “Analysis of Some Global Optimization Algorithms for Space Trajectory Design,” *Journal of Spacecraft and Rockets*, vol. 47, no. 2, pp. 334–344, 2010. DOI: 10.2514/1.45742.
- [105] C. Goerzen, Z. Kong, and B. Mettler, “A Survey of Motion Planning Algorithms from the Perspective of Autonomous UAV Guidance,” *Journal of Intelligent and Robotic Systems*, vol. 57, no. 1, pp. 65–100, 2010. DOI: 10.1007/s10846-009-9383-1.
- [106] L. Quan, L. Han, B. Zhou, S. Shen, and F. Gao, “Survey of UAV Motion Planning,” *IET Cyber-Systems and Robotics*, vol. 2, no. 1, pp. 14–21, 2020. DOI: 10.1049/iet-csr.2020.0004.

- [107] T. T. Mac, C. Copot, D. T. Tran, and R. De Keyser, “Heuristic Approaches in Robot Path Planning: A Survey,” *Robotics and Autonomous Systems*, vol. 86, pp. 13–28, 2016. DOI: 10.1016/j.robot.2016.08.001.
- [108] K. Karur, N. Sharma, C. Dharmatti, and J. E. Siegel, “A Survey of Path Planning Algorithms for Mobile Robots,” *Vehicles*, vol. 3, no. 3, pp. 448–468, 2021. DOI: 10.3390/vehicles3030027.
- [109] M. Elbanhawi and M. Simic, “Sampling-Based Robot Motion Planning: A Review,” *IEEE Access*, vol. 2, pp. 56–77, 2014. DOI: 10.1109/ACCESS.2014.2302442.
- [110] J. García-Heras, M. Soler, and F. J. Sáez, “A Comparison of Optimal Control Methods for Minimum Fuel Cruise at Constant Altitude and Course with Fixed Arrival Time,” *Procedia Engineering*, vol. 80, pp. 231–244, 2014. DOI: 10.1016/j.proeng.2014.09.083.
- [111] J. T. Betts, “Survey of Numerical Methods for Trajectory Optimization,” *Journal of Guidance, Control, and Dynamics*, vol. 21, no. 2, pp. 193–207, 1998. DOI: 10.2514/2.4231.
- [112] R. Bellman, *Dynamic Programming*. Princeton University Press, 1957.
- [113] C. K. Jensen, M. Chiarandini, and K. S. Larsen, “Flight Planning in Free Route Airspaces,” in *17th Workshop on Algorithmic Approaches for Transportation Modelling, Optimization, and Systems (ATMOS 2017)*, vol. 59, Schloss Dagstuhl–Leibniz-Zentrum fuer Informatik, 2017, pp. 1–14. DOI: 10.4230/OASIcs.ATMOS.2017.14.
- [114] E. Dijkstra, “A Note on two Problems in Connexion with Graphs,” *Numerische Mathematik*, vol. 1, pp. 269–271, 1959. DOI: 10.1007/BF01386390.
- [115] P. E. Hart, N. J. Nilsson, and B. Raphael, “A Formal Basis for the Heuristic Determination of Minimum Cost Paths,” *IEEE Transactions on Systems Science and Cybernetics*, vol. 4, no. 2, pp. 100–107, 1968. DOI: 10.1109/TSSC.1968.300136.
- [116] O. Souissi, R. Benatitallah, D. Duvivier, A. Artiba, N. Belanger, and P. Feyzeau, “Path Planning: A 2013 Survey,” in *Proceedings of the 2013 International Conference on Industrial Engineering and Systems Management (IESM)*, 2013, pp. 1–8. [Online]. Available: <https://ieeexplore.ieee.org/document/6761521> (visited on 09/22/2023).
- [117] A. Schienle, P. Maristany de las Casas, and M. Blanco, “A Priori Search Space Pruning in the Flight Planning Problem,” in *19th Symposium on Algorithmic Approaches for Transportation Modelling, Optimization, and Systems (ATMOS 2019)*, vol. 75, Schloss Dagstuhl–Leibniz-Zentrum fuer Informatik, 2019, pp. 1–14. DOI: 10.4230/OASIcs.ATMOS.2019.8.
- [118] H. Bast, D. Delling, A. Goldberg, M. Müller-Hannemann, T. Pajor, P. Sanders, D. Wagner, and R. F. Werneck, “Route Planning in Transportation Networks,” in *Algorithm Engineering*, Springer, 2016, pp. 19–80. DOI: 10.1007/978-3-319-49487-6_2.

- [119] Y. Miyazawa, N. K. Wickramasinghe, A. Harada, and Y. Miyamoto, “Dynamic Programming Application to Airliner Four Dimensional Optimal Flight Trajectory,” in *AIAA Guidance, Navigation, and Control (GNC) Conference*. 2013. DOI: 10.2514/6.2013-4969.
- [120] P. Hagelauer and F. Mora-Camino, “A Soft Dynamic Programming Approach for On-Line Aircraft 4D-Trajectory Optimization,” *European Journal of Operations Research*, vol. 107, no. 1, pp. 87–95, 1998. DOI: 10.1016/S0377-2217(97)00221-X.
- [121] D. Šišlák, P. Volf, and M. Pechoucek, “Flight Trajectory Path Planning,” in *Proc. of Intl. Scheduling and Planning Applications Workshop*, 2009, pp. 76–83.
- [122] M. Blanco, R. Borndörfer, and P. Maristany de las Casas, “An A* Algorithm for Flight Planning Based on Idealized Vertical Profiles,” in *22nd Symposium on Algorithmic Approaches for Transportation Modelling, Optimization, and Systems (ATMOS 2022)*, vol. 106, 2022, 1:1–1:15. DOI: 10.4230/OASIcs.ATMOS.2022.1.
- [123] A. Knudsen, M. Chiarandini, and K. Larsen, “Heuristic Variants of A* Search for 3D Flight Planning,” in *Integration of Constraint Programming, Artificial Intelligence, and Operations Research*, Springer International Publishing, 2018, pp. 361–376. DOI: 10.1007/978-3-319-93031-2_26.
- [124] D. Delling and D. Wagner, “Time-Dependent Route Planning,” in *Robust and Online Large-Scale Optimization: Models and Techniques for Transportation Systems*. Springer Berlin Heidelberg, 2009, pp. 207–230. DOI: 10.1007/978-3-642-05465-5_8.
- [125] D. Delling, “Route Planning in Transportation Networks: From Research to Practice,” in *Proceedings of the 26th ACM SIGSPATIAL International Conference on Advances in Geographic Information Systems*, Association for Computing Machinery, 2018, p. 2. DOI: 10.1145/3274895.3282802.
- [126] E. Rippel, A. Bar-Gill, and N. Shimkin, “Fast Graph-Search Algorithms for General-Aviation Flight Trajectory Generation,” *Journal of Guidance, Control, and Dynamics*, vol. 28, no. 4, pp. 801–811, 2005. DOI: 10.2514/1.7370.
- [127] A. Botea, M. Müller, and J. Schaeffer, “Near Optimal Hierarchical Path-Finding,” *Journal of Game Development*, vol. 1, no. 1, pp. 1–30, 2004. [Online]. Available: https://papersdb.cs.ualberta.ca/~papersdb/uploaded_files/585/paper_jogd.pdf (visited on 09/22/2023).
- [128] T. Karatas and F. Bullo, “Randomized Searches and Nonlinear Programming in Trajectory Planning,” in *Proceedings of the 40th IEEE Conference on Decision and Control (Cat. No.01CH37228)*, vol. 5, 2001, pp. 5032–5037. DOI: 10.1109/CDC.2001.981008.
- [129] S. Stoneman and R. Lampariello, “Embedding Nonlinear Optimization in RRT* for Optimal Kinodynamic Planning,” 2014, pp. 3737–3744. DOI: 10.1109/CDC.2014.7039971.

- [130] A. Nash and S. Koenig, “Any-Angle Path Planning,” *AI Magazine*, vol. 34, no. 4, pp. 85–107, 2013. DOI: 10.1609/aimag.v34i4.2512.
- [131] D. Ferguson and A. Stentz, “Field D*: An Interpolation-Based Path Planner and Replanner,” in *Robotics Research*, Springer, 2007, pp. 239–253. DOI: 10.1007/978-3-540-48113-3_22.
- [132] K. Daniel, A. Nash, S. Koenig, and A. Felner, “Theta*: Any-Angle Path Planning on Grids,” 1, vol. 39, AI Access Foundation, 2010, pp. 533–579.
- [133] D. E. Kaufman and R. L. Smith, “Fastest Paths in Time-Dependent Networks for Intelligent Vehicle-Highway Systems Application,” *Journal of Intelligent Transportation Systems: Technology, Planning, and Operations*, vol. 1, no. 1, pp. 1–11, 1993. DOI: 10.1080/10248079308903779.
- [134] A. Orda and R. Rom, “Shortest-Path and Minimum-Delay Algorithms in Networks with Time-Dependent Edge-Length,” *J. ACM*, vol. 37, no. 3, pp. 607–625, 1990. DOI: 10.1145/79147.214078.
- [135] E. Bruns, *Das Eikonal*. S. Hirzel, 1895.
- [136] J. A. Sethian, “A Fast Marching Level Set Method for Monotonically Advancing Fronts,” *Proceedings of the National Academy of Sciences of the United States of America*, vol. 93, no. 4, pp. 1591–1595, 1996. [Online]. Available: <http://www.jstor.org/stable/38628> (visited on 09/22/2023).
- [137] C. Petres, Y. Pailhas, P. Patron, Y. Petillot, J. Evans, and D. Lane, “Path Planning for Autonomous Underwater Vehicles,” *IEEE Transactions on Robotics*, vol. 23, no. 2, pp. 331–341, 2007. DOI: 10.1109/TR0.2007.895057.
- [138] A. B. Vladimirsky, “Fast Methods for Static Hamilton-Jacobi Partial Differential Equations,” English, Research Org.: Lawrence Berkeley National Lab. (LBNL), Berkeley, CA (United States), Ph.D. dissertation, 2001. DOI: 10.2172/827572.
- [139] J. A. Sethian and A. Vladimirsky, “Ordered Upwind Methods for Static Hamilton–Jacobi Equations,” *Proceedings of the National Academy of Sciences*, vol. 98, no. 20, pp. 11 069–11 074, 2001. DOI: 10.1073/pnas.201222998.
- [140] J. A. Sethian and A. Vladimirsky, “Ordered Upwind Methods for Static Hamilton–Jacobi Equations: Theory and Algorithms,” *SIAM Journal on Numerical Analysis*, vol. 41, no. 1, pp. 325–363, 2003. DOI: 10.1137/S0036142901392742.
- [141] A. E. J. Bryson and Y.-C. Ho, *Applied Optimal Control*. Hemisphere Publishing Corporation, 1975.
- [142] K. J. Arrow, “On the Use of Wind in Flight Planning,” *Journal of Atmospheric Sciences*, vol. 6, no. 2, pp. 150–159, 1949. DOI: 10.1175/1520-0469(1949)006<0150:OTUOWI>2.0.CO;2.
- [143] R. W. Lunnion and A. D. Marklow, “Optimization of Time Saving in Navigation Through an Area of Variable Flow,” *Journal of Navigation*, vol. 45, no. 3, pp. 384–399, 1992. DOI: 10.1017/S037346330001095X.

- [144] S. J. Bijlsma, “Optimal Aircraft Routing in General Wind Fields,” *Journal of Guidance, Control, and Dynamics*, vol. 32, no. 3, pp. 1025–1029, 2009. DOI: 10.2514/1.42425.
- [145] M. R. Jardin and A. E. Bryson, “Methods for Computing Minimum-Time Paths in Strong Winds,” *Journal of Guidance, Control, and Dynamics*, vol. 35(1), pp. 165–171, 2012. DOI: 10.2514/1.53614.
- [146] M. R. Jardin, “Toward Real-Time En Route Traffic Control Optimization,” Ph.D. dissertation, Stanford University, 2003. [Online]. Available: <https://web.stanford.edu/group/scpnt/gpslab/pubs/theses/MatthewJardinThesis03.pdf> (visited on 09/22/2023).
- [147] M. R. Jardin, “Analytical Solutions for Minimum-Time Neighboring Optimal Aircraft Guidance in Winds,” *American Institute of Aeronautics and Astronautics*, 2008. DOI: 10.2514/6.2008-6977.
- [148] A. Marchidan and E. Bakolas, “Numerical Techniques for Minimum-Time Routing on a Sphere with Realistic Winds,” *American Institute of Aeronautics and Astronautics*, 2016. DOI: 10.2514/1.G001389.
- [149] O. von Stryk and R. Bulirsch, “Direct and Indirect Methods for Trajectory Optimization,” *Annals of Operations Research*, vol. 37, pp. 357–373, 1992. DOI: 10.1007/BF02071065.
- [150] P. J. Enright and B. A. Conway, “Discrete Approximations to Optimal Trajectories using Direct Transcription and Nonlinear Programming,” *Journal of Guidance, Control, and Dynamics*, vol. 15, no. 4, pp. 994–1002, 1992. DOI: 10.2514/3.20934.
- [151] F. Fahroo and I. M. Ross, “Direct Trajectory Optimization by a Chebyshev Pseudospectral Method,” *Journal of Guidance, Control, and Dynamics*, vol. 25, no. 1, pp. 160–166, 2002. DOI: 10.2514/2.4862.
- [152] D. Gonzalez Arribas, M. S. Arnedo, and M. S. Rivo, “Wind-Optimal Cruise Trajectories Using Pseudospectral Methods and Ensemble Probabilistic Forecasts,” in *Proceedings of the 5th International Conference on Application and Theory of Automation in Command and Control Systems (ATACCS)*, Association for Computing Machinery, 2015, pp. 160–167. DOI: 10.1145/2899361.2899378.
- [153] C. Hargraves and S. Paris, “Direct Trajectory Optimization Using Nonlinear Programming and Collocation,” *Journal of Guidance, Control, and Dynamics*, vol. 10, no. 4, pp. 338–342, 1987. DOI: 10.2514/3.20223.
- [154] B. Geiger, J. Horn, A. DeLullo, A. Niessner, and L. Long, “Optimal Path Planning of UAVs Using Direct Collocation with Nonlinear Programming,” in *AIAA Guidance, Navigation, and Control Conference and Exhibit*, American Institute of Aeronautics and Astronautics, Inc., 2006. DOI: 10.2514/6.2006-6199.

- [155] M. Soler, A. Olivares, and E. Staffetti, “Hybrid Optimal Control Approach to Commercial Aircraft Trajectory Planning,” *Journal of Guidance, Control, and Dynamics*, vol. 33, no. 3, pp. 985–991, 2010. DOI: 10.2514/1.47458.
- [156] M. Soler, A. Olivares, E. Staffetti, and D. Zapata, “Framework for Aircraft Trajectory Planning Toward an Efficient Air Traffic Management,” *Journal of Aircraft*, vol. 49, no. 1, pp. 341–348, 2012. DOI: 10.2514/1.C031490.
- [157] H. Diedam, “Global Optimal Control Using Direct Multiple Shooting,” Ph.D. dissertation, University of Heidelberg, 2015. DOI: 10.11588/heidok.00019744.
- [158] H. Diedam and S. Sager, “Global Optimal Control with the Direct Multiple Shooting Method,” *Optimal Control Applications and Methods*, vol. 39, no. 2, pp. 449–470, 2018. DOI: 10.1002/oca.2324.
- [159] H. Diedam and S. Sager, “Global Optimal Control with the Direct Multiple Shooting Method,” *Optim Control Appl Meth.*, pp. 1–22, 2017. DOI: 10.1002/oca.2324.
- [160] J. T. Betts, *Practical Methods for Optimal Control and Estimation Using Nonlinear Programming (Second Edition)*. Siam (Society for Industrial and Applied Mathematics, Philadelphia), 2011. DOI: 10.1137/1.9780898718577.
- [161] A. Rao, “A Survey of Numerical Methods for Optimal Control,” *Advances in the Astronautical Sciences*, vol. 135, 2010. [Online]. Available: <https://www.anilvrao.com/Publications/ConferencePublications/trajectorySurveyAAS.pdf> (visited on 09/22/2023).
- [162] J. Nocedal and S. J. Wright, *Numerical Optimization*. Springer, 2006. DOI: 10.1007/978-0-387-40065-5.
- [163] D. J. Wales and J. P. K. Doye, “Global Optimization by Basin-Hopping and the Lowest Energy Structures of Lennard-Jones Clusters Containing up to 110 Atoms,” *The Journal of Physical Chemistry A*, vol. 101, no. 28, pp. 5111–5116, 1997. DOI: 10.1021/jp970984n.
- [164] R. H. Leary, “Global Optimization on Funneling Landscapes,” *Journal of Global Optimization*, vol. 18, no. 4, pp. 367–383, 2000. DOI: 10.1023/A:1026500301312.
- [165] B. Addis, A. Cassioli, M. Locatelli, and F. Schoen, “A Global Optimization Method for the Design of Space Trajectories,” *Computational Optimization and Applications*, vol. 48, pp. 635–652, 2011. DOI: 10.1007/s10589-009-9261-6.
- [166] M. Locatelli, “Simulated Annealing Algorithms for Continuous Global Optimization,” in *Handbook of Global Optimization*, Springer, 2002, pp. 179–229. DOI: 10.1007/978-1-4757-5362-2_6.
- [167] A. Cassioli, D. Izzo, D. Di Lorenzo, M. Locatelli, and F. Schoen, “Global Optimization Approaches for Optimal Trajectory Planning,” in *Modeling and Optimization in Space Engineering*. Springer New York, 2012, ch. 5, pp. 111–140. DOI: 10.1007/978-1-4614-4469-5_5.

- [168] I. P. Androulakis, C. D. Maranas, and C. A. Floudas, “ α BB: A Global Optimization Method for General Constrained Nonconvex Problems,” *Journal of Global Optimization*, vol. 7, no. 4, pp. 337–363, 1995. DOI: 10.1007/BF01099647.
- [169] P. Bouffard and S. Waslander, “A Hybrid Randomized/Nonlinear Programming Technique for Small Aerial Vehicle Trajectory Planning in 3D,” *Planning, Perception and Navigation for Intelligent Vehicles (PPNIV)*, vol. 63, 2009. [Online]. Available: https://www.researchgate.net/profile/Patrick-Bouffard/publication/228716707_A_Hybrid_RandomizedNonlinear_Programming_Technique_For_Small_Aerial_Vehicle_Trajectory_Planning_in_3D/links/0a85e52fff4d1a062f000000/A-Hybrid-Randomized-Nonlinear-Programming-Technique-For-Small-Aerial-Vehicle-Trajectory-Planning-in-3D.pdf (visited on 09/22/2023).
- [170] A. Žilinskas and A. Zhigljavsky, “Stochastic Global Optimization: A Review on the Occasion of 25 Years of Informatica,” *Informatica*, vol. 27, no. 2, pp. 229–256, 2016. DOI: 10.15388/Informatica.2016.83.
- [171] J. Hu, Y. Wang, E. Zhou, M. C. Fu, and S. I. Marcus, “A Survey of Some Model-Based Methods for Global Optimization,” in *Optimization, Control, and Applications of Stochastic Systems: In Honor of Onésimo Hernández-Lerma*. Birkhäuser Boston, 2012, pp. 157–179. DOI: 10.1007/978-0-8176-8337-5_10.
- [172] M. Khajezadeh, M. R. Taha, A. El-Shafie, and M. Eslami, “A Survey on Meta-Heuristic Global Optimization Algorithms,” *Research Journal of Applied Sciences, Engineering and Technology*, vol. 3, no. 6, pp. 569–578, 2011. [Online]. Available: <https://maxwellsci.com/print/rjaset/v3-569-578.pdf> (visited on 09/22/2023).
- [173] R. Chai, A. Savvaris, A. Tsourdos, and S. Chai, “Overview of Trajectory Optimization Techniques,” in *Design of Trajectory Optimization Approach for Space Maneuver Vehicle Skip Entry Problems*. Springer Singapore, 2020, pp. 7–25. DOI: 10.1007/978-981-13-9845-2_2.
- [174] R. S. Félix Patron, A. Kessaci, and R. M. Botez, “Flight Trajectories Optimization under the Influence of Winds using Genetic Algorithms,” in *AIAA Guidance, Navigation, and Control (GNC) Conference*. 2013. DOI: 10.2514/6.2013-4620.
- [175] R. S. Félix Patrón, A. Kessaci, and R. M. Botez, “Horizontal Flight Trajectories Optimisation for Commercial Aircraft through a Flight Management System,” *The Aeronautical Journal*, vol. 118, no. 1210, pp. 1499–1518, 2014. DOI: 10.1017/S0001924000010162.
- [176] R. S. Félix Patrón, Y. Berrou, and R. M. Botez, “New Methods of Optimization of the Flight Profiles for Performance Database-Modeled Aircraft,” *Proceedings of the Institution of Mechanical Engineers, Part G: Journal of Aerospace Engineering*, vol. 229, 2014. DOI: 10.1177/0954410014561772.

- [177] R. S. Félix Patrón, M. Schindler, and R. M. Botez, “Aircraft Trajectories Optimization by Genetic Algorithms to Reduce Flight Cost using a Dynamic Weather Model,” in *15th AIAA Aviation Technology, Integration, and Operations Conference*. 2015. DOI: 10.2514/6.2015-2281.
- [178] M. Vasile and M. Locatelli, “A Hybrid Multiagent Approach for Global Trajectory Optimization,” *Journal of Global Optimization*, vol. 44, no. 4, pp. 461–479, 2009. DOI: 10.1007/s10898-008-9329-3.
- [179] K. Subbarao and B. M. Shippey, “Hybrid Genetic Algorithm Collocation Method for Trajectory Optimization,” *Journal of Guidance, Control, and Dynamics*, vol. 32, no. 4, pp. 1396–1403, 2009. DOI: 10.2514/1.41449.
- [180] J. Kennedy and R. Eberhart, “Particle Swarm Optimization,” in *Proceedings of ICNN’95 – International Conference on Neural Networks*, vol. 4, 1995, pp. 1942–1948. DOI: 10.1109/ICNN.1995.488968.
- [181] R. Eberhart and J. Kennedy, “A New Optimizer using Particle Swarm Theory,” in *MHS’95. Proceedings of the Sixth International Symposium on Micro Machine and Human Science*, 1995, pp. 39–43. DOI: 10.1109/MHS.1995.494215.
- [182] J. Kennedy, “The Particle Swarm: Social Adaptation of Knowledge,” in *Proceedings of 1997 IEEE International Conference on Evolutionary Computation (ICEC ’97)*, 1997, pp. 303–308. DOI: 10.1109/ICEC.1997.592326.
- [183] L. Blasi, S. Barbato, and M. Mattei, “A Particle Swarm Approach for Flight Path Optimization in a Constrained Environment,” *Aerospace Science and Technology*, vol. 26, no. 1, pp. 128–137, 2013. DOI: 10.1016/j.ast.2012.02.021.
- [184] M. Saska, M. Macas, L. Preucil, and L. Lhotska, “Robot Path Planning using Particle Swarm Optimization of Ferguson Splines,” in *2006 IEEE Conference on Emerging Technologies and Factory Automation*, 2006, pp. 833–839. DOI: 10.1109/ETFA.2006.355416.
- [185] D. Izzo, V. Becerra, D. Myatt, S. Nasuto, and J. Bishop, “Search Space Pruning and Global Optimisation of Multiple Gravity Assist Spacecraft Trajectories,” *Journal of Global Optimization*, vol. 38, pp. 283–296, 2007. DOI: 10.1007/s10898-006-9106-0.
- [186] X. Hu and R. Eberhart, “Solving Constrained Nonlinear Optimization Problems with Particle Swarm Optimization,” *Citeseer*, vol. 2002, pp. 203–206, 2002. [Online]. Available: <http://www.swarmintelligence.org/papers/SCI2002Constrained.pdf> (visited on 09/22/2023).
- [187] K. Parsopoulos and M. Vrahatis, “Particle Swarm Optimization Method for Constrained Optimization Problem,” in 2002, vol. 76, pp. 214–220. [Online]. Available: <https://www.cs.cinvestav.mx/~constraint/papers/eisci.pdf> (visited on 09/22/2023).

- [188] M. Pontani and B. A. Conway, “Swarming Theory Applied to Space Trajectory Optimization,” in *Spacecraft Trajectory Optimization*. Cambridge University Press, 2010, pp. 263–294. DOI: 10.1017/CB09780511778025.011.
- [189] J. Jie, W. Wang, C. Liu, and B. Hou, “Multi-Swarm Particle Swarm Optimization based on Mixed Search Behavior,” in *5th IEEE Conference on Industrial Electronics and Applications*, 2010, pp. 605–610. DOI: 10.1109/ICIEA.2010.5517044.
- [190] P. Suganthan, “Particle Swarm Optimiser with Neighbourhood Operator,” in *Proceedings of the 1999 Congress on Evolutionary Computation-CEC99 (Cat. No. 99TH8406)*, vol. 3, 1999, pp. 1958–1962. DOI: 10.1109/CEC.1999.785514.
- [191] Y. Shi and R. C. Eberhart, “Parameter Selection in Particle Swarm Optimization,” in *Evolutionary Programming VII*, Springer Berlin Heidelberg, 1998, pp. 591–600. DOI: 10.1007/BFb0040810.
- [192] F. Marini and B. Walczak, “Particle Swarm Optimization (PSO). A Tutorial,” *Chemometrics and Intelligent Laboratory Systems*, vol. 149, pp. 153–165, 2015. DOI: 10.1016/j.chemolab.2015.08.020.
- [193] A. Carlisle and G. Dozier, “An off-the-shelf pso,” in *Proceedings of the workshop on particle swarm optimization*, Indianapolis, USA, vol. 1, 2001, pp. 1–6. [Online]. Available: <https://citeseerx.ist.psu.edu/viewdoc/download;jsessionid=E00B21C8BE6A0F1D2B396FF4D3E57EFA?doi=10.1.1.589.485%5C&rep=rep1%5C&type=pdf> (visited on 09/22/2023).
- [194] J. F. Schutte and A. A. Groenwold, “A Study of Global Optimization Using Particle Swarms,” *Journal of Global Optimization*, vol. 31, no. 1, pp. 93–108, 2005. DOI: 10.1007/s10898-003-6454-x.
- [195] Z.-H. Zhan, J. Zhang, Y. Li, and H. S.-H. Chung, “Adaptive Particle Swarm Optimization,” *IEEE Transactions on Systems, Man, and Cybernetics, Part B (Cybernetics)*, vol. 39, no. 6, pp. 1362–1381, 2009. DOI: 10.1109/TSMCB.2009.2015956.
- [196] O. N. Almasi and M. H. Khooban, “A Parsimonious SVM Model Selection Criterion for Classification of Real-World Data Sets via an Adaptive Population-Based Algorithm,” *Neural Computing and Applications*, vol. 30, no. 11, pp. 3421–3429, 2018. DOI: 10.1007/s00521-017-2930-y.
- [197] M. R. Bonyadi and Z. Michalewicz, “Particle Swarm Optimization for Single Objective Continuous Space Problems: A Review,” *Evolutionary Computation*, vol. 25, no. 1, pp. 1–54, 2017. DOI: 10.1162/EVC0_r_00180.
- [198] F. van den Bergh and A. P. Engelbrecht, “A Convergence Proof for the Particle Swarm Optimiser,” *Fundamenta Informaticae*, vol. 105, pp. 341–374, 2010, 4. DOI: 10.3233/FI-2010-370.
- [199] A. Murrieta Mendoza, H. Ruiz, and R. Botez, “Vertical Reference Flight Trajectory Optimization with the Particle Swarm Optimisation,” in *Modelling, Identification and Control*, 2017. DOI: 10.2316/P.2017.848-032.

- [200] C. R. Bessette and D. B. Spencer, "Optimal Space Trajectory Design: A Heuristic-Based Approach," *Advances in the Astronautical Sciences*, vol. 124, pp. 1611–1628, 2006. [Online]. Available: <https://www.engr.psu.edu/ce/Divisions/Hydro/Reed/Education/CE%5C%20563%5C%20Projects/Bessette.pdf> (visited on 09/22/2023).
- [201] C. R. Bessette and D. B. Spencer, "Identifying Optimal Interplanetary Trajectories through a Genetic Approach," in *AIAA/AAS Astrodynamics Specialist Conference and Exhibit*, 2006. DOI: 10.2514/6.2006-6306.
- [202] M. Dileep, S. Kamath, and V. G. Nair, "Particle Swarm Optimization Applied to Ascent Phase Launch Vehicle Trajectory Optimization Problem," *Procedia Computer Science*, vol. 54, pp. 516–522, 2015. DOI: 10.1016/j.procs.2015.06.059.
- [203] M. Dorigo, "Optimization, Learning and Natural Algorithms," *Ph. D. Thesis, Politecnico di Milano*, 1992.
- [204] M. Dorigo, V. Maniezzo, and A. Colorni, "Ant System: Optimization by a Colony of Cooperating Agents," *IEEE Transactions on Systems, Man, and Cybernetics, Part B (Cybernetics)*, vol. 26, no. 1, pp. 29–41, 1996. DOI: 10.1109/3477.484436.
- [205] A. Colorni, M. Dorigo, and V. Maniezzo, "An Investigation of some Properties of an "Ant Algorithm"," in *Parallel Problem Solving from Nature*, 1992. [Online]. Available: <http://faculty.washington.edu/paymana/swarm/colorni92-ppsn.pdf> (visited on 09/22/2023).
- [206] A. Colorni, M. Dorigo, and V. Maniezzo, "Distributed Optimization by Ant Colonies," vol. 142, 1991, pp. 134–142. [Online]. Available: <https://citeseerx.ist.psu.edu/document?repid=rep1%5C&type=pdf%5C&doi=c2be957583ba0a6008baa22cc42bd9cfea8cbc69> (visited on 09/22/2023).
- [207] X. Dai, S. Long, Z. Zhang, and D. Gong, "Mobile Robot Path Planning Based on Ant Colony Algorithm with A* Heuristic Method," *Frontiers in Neurorobotics*, vol. 13, 2019. DOI: 10.3389/fnbot.2019.00015.
- [208] T. Stützle and H. H. Hoos, "MAX–MIN Ant System," *Future Generation Computer Systems*, vol. 16, no. 8, pp. 889–914, 2000. DOI: 10.1016/S0167-739X(00)00043-1.
- [209] T. Stützle and H. H. Hoos, "MAX-MIN Ant System and Local Search for the Traveling Salesman Problem," in *Proceedings of 1997 IEEE International Conference on Evolutionary Computation (ICEC '97)*, 1997, pp. 309–314. DOI: 10.1109/ICEC.1997.592327.
- [210] M. Dorigo and L. Gambardella, "Ant Colony System: A Cooperative Learning Approach to the Traveling Salesman Problem," *IEEE Transactions on Evolutionary Computation*, vol. 1, no. 1, pp. 53–66, 1997. DOI: 10.1109/4235.585892.

- [211] W. J. Gutjahr, “A Graph-Based Ant System and its Convergence,” *Future Generation Computer Systems*, vol. 16, no. 8, pp. 873–888, 2000. DOI: 10.1016/S0167-739X(00)00044-3.
- [212] W. J. Gutjahr, “ACO Algorithms with Guaranteed Convergence to the Optimal Solution,” *Information Processing Letters*, vol. 82, no. 3, pp. 145–153, 2002. DOI: 10.1016/S0020-0190(01)00258-7.
- [213] Dorigo, Marco and Stützle, Thomas, *Ant Colony Optimization*. MIT Press, 2004.
- [214] T. Stützle and M. Dorigo, “A Short Convergence Proof for a Class of Ant Colony Optimization Algorithms,” *IEEE Transactions on Evolutionary Computation*, vol. 6, no. 4, pp. 358–365, 2002. DOI: 10.1109/TEVC.2002.802444.
- [215] W. J. Gutjahr, “Mathematical Runtime Analysis of ACO Algorithms: Survey on an Emerging Issue,” *Swarm Intelligence*, vol. 1, no. 1, pp. 59–79, 2007. DOI: 10.1007/s11721-007-0001-1.
- [216] M. Á. P. García, O. Montiel, O. Castillo, R. Sepúlveda, and P. Melin, “Path Planning for Autonomous Mobile Robot Navigation with Ant Colony Optimization and Fuzzy Cost Function Evaluation,” *Applied Soft Computing*, vol. 9, no. 3, pp. 1102–1110, 2009. DOI: 10.1016/j.asoc.2009.02.014.
- [217] F. H. Ajeil, I. K. Ibraheem, A. T. Azar, and A. J. Humaidi, “Grid-Based Mobile Robot Path Planning Using Aging-Based Ant Colony Optimization Algorithm in Static and Dynamic Environments,” *Sensors*, vol. 20, no. 7, 2020. DOI: 10.3390/s20071880.
- [218] M. Dramski, “A Comparison between Dijkstra Algorithm and Simplified Ant Colony Optimization in Navigation,” *Scientific Journals of the Maritime University of Szczecin, Zeszyty Naukowe Akademii Morskiej w Szczecinie*, vol. 29, pp. 25–29, 2012. [Online]. Available: <https://repository.am.szczecin.pl/handle/123456789/422> (visited on 09/22/2023).
- [219] A. Murrieta-Mendoza, A. Hamy, and R. M. Botez, “Four- and Three-Dimensional Aircraft Reference Trajectory Optimization Inspired by Ant Colony Optimization,” *Journal of Aerospace Information Systems*, vol. 14, no. 11, pp. 597–616, 2017. DOI: 10.2514/1.I010540.
- [220] A. Lazarowska, “Ant Colony Optimization based Navigational Decision Support System,” *Procedia Computer Science*, vol. 35, pp. 1013–1022, 2014, Knowledge-Based and Intelligent Information & Engineering Systems 18th Annual Conference. DOI: 10.1016/j.procs.2014.08.187.
- [221] Z. J. Kiyak, R. J. Hartfield, and T. W. Ledlow, “Missile Trajectory Optimization Using a Modified Ant Colony Algorithm,” in *2014 IEEE Aerospace Conference*, 2014, pp. 1–8. DOI: 10.1109/AERO.2014.6836264.
- [222] P. Švestka and M. H. Overmars, “Probabilistic Path Planning,” in *Robot Motion Planning and Control*. Springer, 1998, pp. 255–304. DOI: 10.1007/BFb0036074.

- [223] L. Kavraki, P. Svestka, J.-C. Latombe, and M. Overmars, “Probabilistic Roadmaps for Path Planning in High-Dimensional Configuration Spaces,” *IEEE Transactions on Robotics and Automation*, vol. 12, no. 4, pp. 566–580, 1996. DOI: 10.1109/70.508439.
- [224] S. M. LaValle, “Rapidly-Exploring Random Trees: A New Tool for Path Planning,” *The Annual Research Report*, 1998. [Online]. Available: <http://msl.cs.illinois.edu/~lavelle/papers/Lav98c.pdf> (visited on 09/22/2023).
- [225] S. M. LaValle and J. J. Kuffner Jr, “Randomized Kinodynamic Planning,” *The International Journal of Robotics Research*, vol. 20, no. 5, pp. 378–400, 2001. DOI: 10.1177/02783640122067453.
- [226] S. Karaman and E. Frazzoli, “Sampling-Based Algorithms for Optimal Motion Planning,” *The International Journal of Robotics Research*, vol. 30, no. 7, pp. 846–894, 2011. DOI: 10.1177/0278364911406761.
- [227] C. Urmson and R. Simmons, “Approaches for Heuristically Biasing RRT Growth,” in *Proceedings 2003 IEEE/RSJ International Conference on Intelligent Robots and Systems (IROS 2003) (Cat. No.03CH37453)*, vol. 2, 2003, pp. 1178–1183. DOI: 10.1109/IROS.2003.1248805.
- [228] I. Ardiyanto and J. Miura, “Heuristically Arrival Time Field-Biased (HeAT) Random Tree: An Online Path Planning Algorithm for Mobile Robot Considering Kinodynamic Constraints,” in *2011 IEEE International Conference on Robotics and Biomimetics*, 2011, pp. 360–365. DOI: 10.1109/ROBIO.2011.6181312.
- [229] J. D. Gammell, S. S. Srinivasa, and T. D. Barfoot, “Informed RRT*: Optimal Sampling-Based Path Planning Focused via Direct Sampling of an Admissible Ellipsoidal Heuristic,” in *2014 IEEE/RSJ International Conference on Intelligent Robots and Systems*, 2014, pp. 2997–3004. DOI: 10.1109/IROS.2014.6942976.
- [230] M. Brunner, B. Brüggemann, and D. Schulz, “Hierarchical Rough Terrain Motion Planning using an Optimal Sampling-Based Method,” in *2013 IEEE International Conference on Robotics and Automation*, IEEE, 2013, pp. 5539–5544. DOI: 10.1109/ICRA.2013.6631372.
- [231] J. Kuffner and S. LaValle, “RRT-Connect: An Efficient Approach to Single-Query Path Planning,” in *Proceedings 2000 ICRA. Millennium Conference. IEEE International Conference on Robotics and Automation. Symposia Proceedings (Cat. No.00CH37065)*, vol. 2, 2000, pp. 995–1001. DOI: 10.1109/ROBOT.2000.844730.
- [232] B. Akgun and M. Stilman, “Sampling Heuristics for Optimal Motion Planning in High Dimensions,” in *2011 IEEE/RSJ International Conference on Intelligent Robots and Systems*, 2011, pp. 2640–2645. DOI: 10.1109/IROS.2011.6095077.

- [233] I. Noreen, A. Khan, and Z. Habib, “Optimal Path Planning using RRT* based Approaches: A Survey and Future Directions,” *International Journal of Advanced Computer Science and Applications*, vol. 7, 2016. DOI: 10.14569/IJACSA.2016.071114.
- [234] Z. Tahir, A. H. Qureshi, Y. Ayaz, and R. Nawaz, “Potentially Guided Bidirectionalized RRT* for Fast Optimal Path Planning in Cluttered Environments,” *Robotics and Autonomous Systems*, vol. 108, pp. 13–27, 2018. DOI: 10.1016/j.robot.2018.06.013.
- [235] E. Andrés, D. Gonzalez-Arribas, M. Sanjurjo-Rivo, M. Soler, and M. Kamgarpour, “GPU-Accelerated RRT for Flight Planning Considering Ensemble Forecasting of Thunderstorms,” *10th SESAR Innovation Days*, 2020. [Online]. Available: https://www.sesarju.eu/sites/default/files/documents/sid/2020/papers/SIDs_2020_paper_49red.pdf (visited on 09/22/2023).
- [236] Y. Guo, X. Liu, X. Liu, Y. Yang, and W. Zhang, “FC-RRT*: An Improved Path Planning Algorithm for UAV in 3D Complex Environment,” *ISPRS International Journal of Geo-Information*, vol. 11, no. 2, 2022. DOI: 10.3390/ijgi11020112.
- [237] W. Pan, Q. He, Y. Huang, and L. Qin, “Four-Dimensional Trajectory Planning for Urban Air Traffic Vehicles Based on Improved RRT* Algorithm,” *IEEE Access*, vol. 11, pp. 81 113–81 123, 2023. DOI: 10.1109/ACCESS.2023.3300374.
- [238] Á. Madridano, A. Al-Kaff, D. Martín, and A. de la Escalera, “3D Trajectory Planning Method for UAVs Swarm in Building Emergencies,” *Sensors*, vol. 20, no. 3, 2020. DOI: 10.3390/s20030642.
- [239] Q. Li, C. Wei, J. Wu, and X. Zhu, “Improved PRM Method of Low Altitude Penetration Trajectory Planning for UAVs,” in *Proceedings of 2014 IEEE Chinese Guidance, Navigation and Control Conference*, 2014, pp. 2651–2656. DOI: 10.1109/CGNCC.2014.7007587.

CHAPTER **2**

A Discrete-Continuous Algorithm for Free Flight Planning

Borndörfer, R., Danecker, F., and Weiser, M.
Algorithms 2021, 14(1), 4.
DOI: 10.3390/a14010004.

This article is licensed under a Creative Commons Attribution 4.0
International License (<http://creativecommons.org/licenses/by/4.0/>).

Abstract We propose a hybrid discrete-continuous algorithm for flight planning in free flight airspaces. In a first step, our DisCOptER method (discrete-continuous optimization for enhanced resolution) computes a globally optimal approximate flight path on a discretization of the problem using the A* method. This route initializes a Newton method that converges rapidly to the smooth optimum in a second step. The correctness, accuracy, and complexity of the method are governed by the choice of the crossover point that determines the coarseness of the discretization. We analyze the optimal choice of the crossover point and demonstrate the asymptotic superiority of DisCOptER over a purely discrete approach.

Contents

2.1	Introduction	87
2.2	Materials & Methods	89
2.2.1	Free Flight Planning	89
2.2.2	Continuous Approach: Optimal Control	90
2.2.3	Discrete Approach: Shortest Paths in Airway Networks	94
2.2.4	DisCOptER Algorithm	100
2.3	Results	102
2.3.1	Test Problems	102
2.3.2	Computational Complexity	106
2.3.3	Minimum Graph Requirements	106
2.3.4	Optimal Crossover Point	108
2.3.5	Computational Complexity	109
2.4	Conclusion	110

2.1 Introduction

Flight planning is concerned with the computation of time and fuel efficient flight paths with respect to the weather, see [1] for a comprehensive survey. In particular, wind conditions make a big difference: flying with a headwind of 60 kts increases flight time and fuel consumption of an Airbus A321 by as much as 20% over a tailwind of 60 kts [2]. To exploit this potential, and to mitigate airspace congestion, free flight aircraft routing has been suggested since 1995 [3], and projects to complement, enhance, and finally replace the airway network that is currently used to organize all air traffic are now under way all over the world. Europe is introducing so-called free route airspaces (FRAs), in which one can fly on arbitrary straight lines between defined entry and exit points, and between more and more intermediate points, moving ever closer towards free flight. According to EUROCONTROL, FRA projects are now in place in three quarters of all European airspaces, and, once fully implemented, will save total fuel burn, CO₂, and H₂O emissions by 1.6–2.3%, which amounts to 3,000 tonnes of fuel/day, 10,000 tonnes of CO₂/day, 3€ million in fuel costs/day, and 500,000 nautical miles/day [4].

The flight planning problem can be seen as a special type of time-dependent shortest path problem. A large number of algorithms has been developed in this general context, including contraction hierarchies, hub labeling, and arc flags for route planing in road networks, see [5, 6] for surveys, RAPTOR, transfer patterns, and connection scan for journey planning in public transport networks [6], the isochrones method and dynamic programming for ship weather routing [7], and sampling-based algorithms like rapidly exploring random graphs and trees (RRT), probabilistic road maps (PRM), artificial potential fields as well as graph-based algorithms such as A*, D*, theta*, etc. for robot path planning [8]. The variety of these methods reflects the different characteristics of the respective problems.

The best flight planning methods are currently super-fast A*/Dijkstra algorithms that employ efficient problem specific speed-up techniques such as cost projection [9], super-optimal wind [10], and active constraint propagation [11]. They can find

globally optimal solutions of basic problem variants on the world wide airway network with its 100,000 nodes and 600,000–700,000 edges within milliseconds. A* methods can in principle be extended to deal with FRAs or free flight by excessive graph augmentation, but only up to a certain point, when the graphs become too large and dense.

On the other hand, numerical methods of optimal control are able to compute optimal free flight trajectories to high precision with great efficiency, either with indirect methods based on Pontryagin’s maximum principle [12–14], or by direct methods using a collocation discretization to reformulate the problem as a nonlinear program (NLP) [15, 16]. These methods compute a smooth trajectory independently of any a priori network discretization, i.e., the desired free flight path. The computational complexity of solving the optimality systems by Newton’s method is asymptotically much smaller than for graph discretizations. If measured in terms of accuracy, higher order discretizations of the underlying ordinary differential equations exhibit even larger asymptotic gains. The drawback is that continuous optimal control methods converge only locally, and towards any local optimum, without providing any guarantee of global optimality. Approaches to compute globally optimal solutions to optimal control problems include global optimal control [17], mixed-integer optimal control [18], and various heuristics [19]. Applications to flight planning exist, but consider only very small networks [20] or vertical profiles [21].

We propose in this paper the novel hybrid algorithm DisCOptER (discrete-continuous optimization for enhanced resolution) that combines the strengths of discrete and continuous approaches to flight planning, and provide a numerical study of its efficiency and accuracy. The discrete component of our method provides global optimality, the continuous component high accuracy and asymptotic efficiency. The idea of the method is to do a discrete search for a global optimum on a coarse, approximate, artificial network, and to use the resulting approximate solution to initialize a Newton’s method for the solution of a continuous optimal control problem. The correctness and effectiveness of this strategy depends on the choice of the crossover point between the discrete and the continuous part of the algorithm.

The network for the discrete part must be coarse enough to be searched efficiently, and fine enough to guarantee sufficient proximity to the continuous optimum, such that a subsequent Newton iteration will converge to the latter. Clearly, the convergence radius of the continuous method strongly depends on the gradients of the wind field and affects, together with the approximation error associated with the graph, the computational complexity of both methods. We shall show that this idea is ideally suited for free flight settings.

Our aim in this paper is to demonstrate the potential of combining discrete and continuous optimization methods for the solution of problems that involve space or time discretizations. The goal is to achieve global optimality and rapid convergence at the same time. The model that we consider is simple, and the special characteristics of flight planning have left their imprint. The basic idea, however, should, with suitable modifications, be applicable to various problems of similar nature. In this vein, our paper intends to give a first indication of the usefulness of such approaches.

The paper is structured as follows. Sections 2.2.1–2.2.3 describe the free flight problem that we consider. The DisCOptER algorithm is introduced in Section 2.2.4 including error and complexity estimates. Finally, Section 2.3 provides a computational study and analyzes the choice of the switch over point.

2.2 Materials & Methods

2.2.1 Free Flight Planning

We consider in this paper an idealized version of the flight planning problem in 2D Euclidean space subject to a stationary wind field. We want to compute a flight path $x : [0, T] \rightarrow \mathbb{R}^2, \tau \mapsto x(\tau)$ that connects an origin and a destination $x_O, x_D \in \mathbb{R}^2$; the path parameter τ measures the flight time. The path is influenced by a smooth field of stationary wind $w : \mathbb{R}^2 \rightarrow \mathbb{R}^2$ of bounded magnitude $\|w\| \leq \bar{w}$. Flying at an airspeed $v : [0, T] \rightarrow \mathbb{R}^2, \tau \mapsto v(\tau)$ of constant magnitude $\|v\| = \bar{v} > \bar{w}$, the aircraft arrives at time $T \in \mathbb{R}_{\geq 0}$, which we seek to minimize. Our setting is chosen for ease of

exposition, but our method carries over to more complex 3D and/or time dependent versions, or other objectives, in particular, minimization of fuel consumption.

2.2.2 Continuous Approach: Optimal Control

In free flight, the flight path is not restricted to a predefined airway network of waypoints and segments. Instead, any Lipschitz-continuous path $x : [0, T] \rightarrow \mathbb{R}^2$, with $\|x_t - w\| = \bar{v}$ almost everywhere, connecting origin x_O and destination x_D , is a valid trajectory. Among those, we shall find one of minimal flight duration T . This classic of optimal control is known as Zermelo's navigation problem [22].

In order to formulate the problem over a fixed interval $[0, 1]$ independent of the actual flight duration, we scale time by T^{-1} as usual in free end time problems and arrive at the following optimal control problem for the flight duration $T \in \mathbb{R}$, the flight path $x \in H^1([0, 1])^2$, and the airspeed $v \in L^2([0, 1])^2$:

$$\min_{T, x, v} T \quad \text{s.t.} \quad c(T, x, v) = \begin{bmatrix} x(0) - x_O \\ x(1) - x_D \\ \dot{x}(\tau) - T(v(\tau) + w(x(\tau))) \\ v(\tau)^T v(\tau) - \bar{v}^2 \end{bmatrix} = 0. \quad (2.1)$$

Here, the constraint $c : Z \rightarrow \Lambda$ maps from the primal domain $Z := \mathbb{R} \times H^1([0, 1])^2 \times L^2([0, 1])^2$ to the image space $\Lambda := \mathbb{R}^2 \times \mathbb{R}^2 \times L^2([0, 1])^2 \times L^2([0, 1])$.

2.2.2.1 Optimality Conditions

Let us briefly recall the necessary and sufficient optimality conditions for the optimal control problem (2.1). With $z = (T, x, v) \in Z$ and $\lambda \in \Lambda$, the Lagrangian is defined as

$$L(z, \lambda) = T - \langle \lambda, c(z) \rangle_{\Lambda, \Lambda}. \quad (2.2)$$

If z is a (local) minimizer, the necessary first order or *Karush-Kuhn-Tucker* (KKT) condition

$$L'(z, \lambda) = 0 \quad (2.3)$$

and the necessary second order condition

$$\langle L_{zz}\zeta, \zeta \rangle_{Z^*, Z} \geq 0 \quad \forall \zeta \in \ker c'(z)$$

hold [23], since $c'(z)$ is surjective due to $\|w\|_{L^\infty(0,1)} < \bar{v}$. Moreover, if the KKT conditions (2.3) are satisfied at z for some λ and the sufficient second order condition (SSC)

$$\langle L_{zz}\zeta, \zeta \rangle_{Z^*,Z} \geq \alpha \|z\|_Z^2 \quad \forall \zeta \in \ker c'(z) \quad (2.4)$$

holds for some $\alpha > 0$, then z is a locally unique solution of (2.1) and stable under perturbations of the problem, e.g., due to sufficiently fine discretization. Let us point out that for wind fields with non-vanishing second derivative, in general there is no closed form solution of the necessary conditions (2.3), such that solutions must be approximated numerically.

Approaches to computing solutions of (2.1) generally fall into two classes: indirect methods relying on Pontryagin's maximum principle [12, 24] and direct methods based on discretization of the minimization problem (2.1) [25, 26]. Indirect methods lead to a boundary value problem for state x and adjoint state λ together with a pointwise optimality condition for the control v , which can be solved by shooting type methods, collocation, or spectral discretization approaches [27, 28]. The discretization of direct methods, usually by collocation or spectral methods, translates the optimal control problem in a finite dimensional nonlinear program to be solved by corresponding optimization problems [15, 16, 29]. While indirect methods using multiple shooting lead to smaller problem sizes than direct methods based on collocation in particular for high accuracy requirements, the latter are widely seen as being easier to implement and use, in particular in the presence of state constraints.

In both approaches, Newton-type methods for solving either discretized boundary value problems or nonlinear programming problems converge in general only locally towards a close-by minimizer. Thus, sufficiently good initial iterates need to be provided. The domain of convergence can be extended using line search methods or trust region methods, but without guarantee of global optimality. Special care has to be taken in case of non-convex problems, since the Newton direction need not be a descent direction if far away from a minimizer satisfying the sufficient second

order conditions. Convexification, truncation of iterative solvers [30–32], or solvers for non-convex quadratic programs can be used to address this.

2.2.2.2 Collocation Discretization

Exemplarily, we consider a discretize-then-optimize approach based on direct collocation with the midpoint rule. Let $0 = \tau_0 < \dots < \tau_n = 1$ be a time grid,

$$X_h = \{x \in H^1([0, 1]) \mid x|_{[\tau_i, \tau_{i+1}]} \in \mathbb{P}_1, i = 0, \dots, n-1\} \quad \text{and} \quad (2.5)$$

$$V_h = \{v \in L^2([0, 1]) \mid v|_{[\tau_i, \tau_{i+1}]} \in \mathbb{P}_0, i = 0, \dots, n-1\} \quad (2.6)$$

the piecewise linear and piecewise constant ansatz spaces for positions and velocities, respectively. We discretize (2.1) by looking for solutions $x_h \in X_h^2$ and $v_h \in V_h^2$ and require the state equation $\dot{x}(\tau) - T(v(\tau) + w(x(\tau))) = 0$ to be satisfied only at the interval midpoints $\tau_{i+1/2} := (\tau_i + \tau_{i+1})/2$ for $i = 0, \dots, n-1$. Representing x_h by its nodal values $x_i = x_h(\tau_i)$ and v_h by its midpoint values $v_i = v_h(\tau_{i+1/2})$, we obtain the large nonlinear program

$$\begin{aligned} & \min_{T, x_h, v_h} T \\ \text{s.t.} \quad & c_h(T, x_h, v_h) = \begin{bmatrix} x_0 - x_O \\ x_n - x_D \\ x_1 - x_0 - (\tau_1 - \tau_0)T(v_0 + w((x_0 + x_1)/2)) \\ \vdots \\ x_n - x_{n-1} - (\tau_n - \tau_{n-1})T(v_{n-1} + w((x_{n-1} + x_n)/2)) \\ v_0^\top v_0 - \bar{v}^2 \\ \vdots \\ v_{n-1}^\top v_{n-1} - \bar{v}^2 \end{bmatrix} = 0. \end{aligned} \quad (2.7)$$

2.2.2.3 Discretization Error

The discretization error introduced by the midpoint rule is well-known to be of second order. For given $w \in C^1([0, 1])^2$ and $T > 0$ there is some constant $C(T, \|w_x\|_{L^\infty(\mathbb{R}^2)})$ independent of v such that

$$\|x_h - x\|_{L^\infty([0, 1])} \leq C\delta\tau^2, \quad (2.8)$$

where $\delta\tau = \max_{i=0,\dots,n-1} \tau_{i+1} - \tau_i$ is the mesh width, see, e.g., [33]. This translates into a corresponding error in the objective, i.e., the flight time T . Different goal-oriented error concepts have been investigated [34, 35] for equality constrained optimal control problems. The excess in actual flight time when the computed path is implemented depends quadratically on the path deviation $\|x_h - x\|_{L^\infty([0,1])}$, and is therefore of order $\mathcal{O}(\delta\tau^4)$. In any case, the error depends directly on the mesh width $\delta\tau$, which we therefore use as a coarse but simple qualitative measure of accuracy.

2.2.2.4 Newton-KKT Solver

Analogous to the continuous Lagrangian (2.2), we may formulate its discretized counterpart

$$L_h(z_h, \lambda_h) = T - \lambda_h^T c_h(z_h)$$

and the corresponding necessary first order optimality condition

$$L'_h(z_h, \lambda_h) = 0. \quad (2.9)$$

Writing $\chi = [z_h, \lambda_h]^T$, this can be solved using Newton's method by computing

$$L''_h(\chi_k) \delta\chi_k = -L'_h(\chi_k), \quad \chi_{k+1} = \chi_k + \delta\chi_k. \quad (2.10)$$

For smooth wind fields, there is some $\omega < \infty$ related to an affine invariant Lipschitz constant of L''_h , such that

$$\|\chi_{k+1} - \chi^*\| \leq \omega \|\chi_k - \chi^*\|^2 \quad (2.11)$$

holds [36]. Thus, Newton's method converges quadratically if started sufficiently close to a locally unique solution point χ^* , i.e., if $\|\chi_0 - \chi^*\| < \omega^{-1}$. This convergence radius is in general mesh-independent [36, 37], and does not depend on the final accuracy in terms of mesh width $\delta\tau$, but only on problem parameters such as derivatives of the wind w .

2.2.2.5 Time Complexity

The run time of the Newton-KKT solver is determined by the number of steps and the cost of each step. The computational effort of a Newton step is dominated by the cost of solving the linear equation (2.10). Due to the ODE structure, $L_h''(\chi)$ is an arrow-shaped matrix with band width independent of $\delta\tau$. Assuming quasi-uniform meshes, i.e., there is a generic constant $C > 0$ such that $\tau_{i+1} - \tau_i \geq C\delta\tau$, this structure allows for an efficient solution in $\mathcal{O}(\delta\tau^{-1})$ time using direct band solvers.

Starting sufficiently close to the solution, say $\omega\|\chi_0 - \chi^*\| < 1$, allows to bound the truncation error by linear convergence as

$$\|\chi_k - \chi^*\| \leq (\omega\|\chi_0 - \chi^*\|)^k \|\chi_0 - \chi^*\|,$$

which is of course rather pessimistic. A tolerance of $\|\chi_k - \chi^*\| \leq \mathcal{O}(\delta\tau^2)$ to match the discretization error is therefore reached after at most $\mathcal{O}(\log \delta\tau / \log(\omega\|\chi_0 - \chi^*\|))$ iterations. Thus, the overall complexity in terms of mesh width $\delta\tau$ is

$$R_C = \mathcal{O}\left(\delta\tau^{-1} \frac{\log \delta\tau}{\log(\omega\|\chi_0 - \chi^*\|)}\right). \quad (2.12)$$

Remark 2.1. — *If an inexact Newton method based on a geometrically refined sequence of meshes with mesh width $\delta\tau_k = \beta^k \ell$ for some $\ell \gg \delta\tau$ and $\beta < 1$ is used, the number of iterations is determined by the linear convergence of the collocation discretization, while the truncation error is quickly diminished by the quadratic convergence of Newton's method [36]. Since the effort per Newton step grows geometrically to its final value, the complexity reduces to*

$$R_C = \mathcal{O}(\delta\tau^{-1}) \quad (2.13)$$

provided the initial error is sufficiently small, i.e. $\omega\|\chi_0 - \chi^\| \leq \beta^2$.*

2.2.3 Discrete Approach: Shortest Paths in Airway Networks

If flight paths are restricted to a predefined airway network of waypoints and segments, flight planning becomes a special kind of shortest path problem on

a digraph. Let $V \subset \mathbb{R}^2$ be a finite set of waypoints including x_O and x_D , and $A \subset V \times V$ a set of arcs such that $G = (V, A)$ is a strongly connected directed graph. A discrete flight path is a finite sequence $(x_i)_{0 \leq i \leq n}$ of waypoints with $(x_i, x_{i+1}) \in A$ for $i = 0, \dots, n-1$, connecting $x_0 = x_O$ with $x_n = x_D$. We denote the set of all flight paths by P . The total flight duration $T(p)$ for a path $p = (x_0, \dots, x_n) \in P$ is given in terms of the flight duration $T(e_i)$ for an arc $e_i = (x_i, x_{i+1})$ by

$$T(p) = \sum_{i=0}^{n-1} T(e_i).$$

The travel time on the arc e_i can be computed from the local ground speed

$$s = v + w = \|s\| \frac{x_{i+1} - x_i}{\|x_{i+1} - x_i\|} =: \|s\| \bar{e}_i,$$

at $x = (1 - \tau)x_i + \tau x_{i+1}$ and the constant airspeed $\|v\| = \bar{v}$ by solving the quadratic equation

$$(\|s\| \bar{e}_i - w)^T (\|s\| \bar{e}_i - w) = \bar{v}^2.$$

This yields

$$\|s\| = \bar{e}_i^T w + \sqrt{(\bar{e}_i^T w)^2 + \bar{v}^2 - \|w\|^2}$$

and thus

$$T(e_i) = \|e_i\| \int_{\tau=0}^1 \|s\|^{-1} \delta\tau. \quad (2.14)$$

The discrete optimization problem to be solved is now

$$\min_{p \in P} T(p).$$

2.2.3.1 Graph Construction.

Discrete approaches to (flight) path planning fall into two classes. The first class are sampling-based algorithms. They construct the search graph by some kind of sampling during the execution of the shortest path algorithm, which is usually an A*-method. This class includes rapidly exploring random trees (RRT) and graph (RRG) algorithms, that are often used in robot path planning [8]. There are versions

that guarantee convergence to a global optimum with probability one [38], however, although undoubtedly often extremely efficient in practice, these methods do not provide a priori error bounds or complexity estimates.

The second class are graph-based algorithms, that take the search graph as an input. Impressive super-fast performance in practice, and also theoretically for special classes of graphs, has been achieved by making use of preprocessing as well as sophisticated data structures. However, “proving better running time bounds than those of Dijkstra’s algorithm is unlikely for general graphs” [6]. In many applications, including traditional flight planning on airway networks, the search graph is canonical. In applications involving space and time discretization, like in free flight, graph construction is a degree of freedom. Using an appropriate discretization, a priori bounds on the runtime and the accuracy of the solutions can be derived. This is the approach that we take.

We cover free flight zones with “locally densely” connected digraphs, i.e., digraphs with a certain density of vertices and arcs.

Definition 2.1. — *A digraph $G = (V, A)$ is said to be (h, ℓ) -dense in a convex set $\Omega \subset \mathbb{R}^2$ for some $h, \ell > 0$, if it satisfies the following conditions:*

1. containment: $V \subset \Omega$
2. vertex density: $\forall x \in \Omega : \exists v \in V : \|x - v\| \leq h$
3. arc density: $\forall x, y \in V, \|x - y\| \leq 2h + \ell : (x, y) \in A$.

We call h the vertex density and $2h + \ell$ the connectivity radius of an (h, ℓ) -dense graph.

With this definition, $|V| \in \mathcal{O}(h^{-2})$ and $|E| \in \mathcal{O}((2h + \ell)^2 h^{-4})$ hold. Furthermore, it is easy to see that this graph structure implies that G is strongly connected and therefore P is nonempty, i.e. a path from x_O to x_D exists.

2.2.3.2 Discretization Error

Similar to the collocation error (2.8), the error due to graph discretization depends on the vertex density h and the connectivity radius $2h + \ell$. We restrict our exposition in this paper to a plausible argument for the error order in terms of h and ℓ and refer the reader to [39] (Chapter 3) for rigorous error bounds of the same orders.

Spatial deviation due to vertex spacing is bounded by $\epsilon_1 = \mathcal{O}(h)$, while the linear interpolation error depending on the curvature of the continuous optimal path is bounded by $\epsilon_2 = \mathcal{O}((2h + \ell)^2)$, as illustrated in Figure 2.1a. Together, the deviation measured as pointwise normal distance is bounded by $\mathcal{O}(\ell^2 + h)$. As mentioned in Section 2.2.2 above, this translates quadratically into a flight time error of order $\mathcal{O}(\ell^4 + h^2)$.

Assuming that the path actually contains arcs of length around $\ell + 2h$, this order of error is not only an upper bound, but also the expected error. The existence of arcs of length $2h + \ell$ in the optimal discrete path is likely, as the following argument based on Figure 2.1b shows. With quasi-uniform vertex spacing, the number of adjacent vertices within a distance $2h + \hat{\ell} \leq 2h + \ell$ is of order $\mathcal{O}((2h + \hat{\ell})^2/h^2)$, such that the average angle between arcs of length up to $2h + \hat{\ell}$, and thus the expected angular deviation α between the discrete path and the optimal continuous path is of order $\mathcal{O}((2 + \hat{\ell}/h)^{-2})$. The geometric length difference between the discrete path and the continuous path is of order $\mathcal{O}(1 - \cos \alpha) = \mathcal{O}(\alpha^2) = \mathcal{O}((2 + \hat{\ell}/h)^{-4})$. The expected length and therefore travel time error induced by angular deviation is smallest if $\hat{\ell}$ is largest, i.e., arcs of maximum length $2h + \ell$ are to be preferred.

This analysis also implies that the total flight time error is of order $\mathcal{O}(\ell^4 + h^2 + (h/\ell)^4)$ and that $h = o(\ell^2)$ ensures convergence for $\ell \rightarrow 0$.

2.2.3.3 A* Shortest Path Algorithm

The state-of-the-art for finding shortest paths in airway networks is the A* algorithm [10], which extends Dijkstra's algorithm by a (heuristic) lower bound for the distance of some vertex x_i to the destination x_D in order to prioritize the search. Depending on the tightness of the heuristic bound, A* can discard a substantial

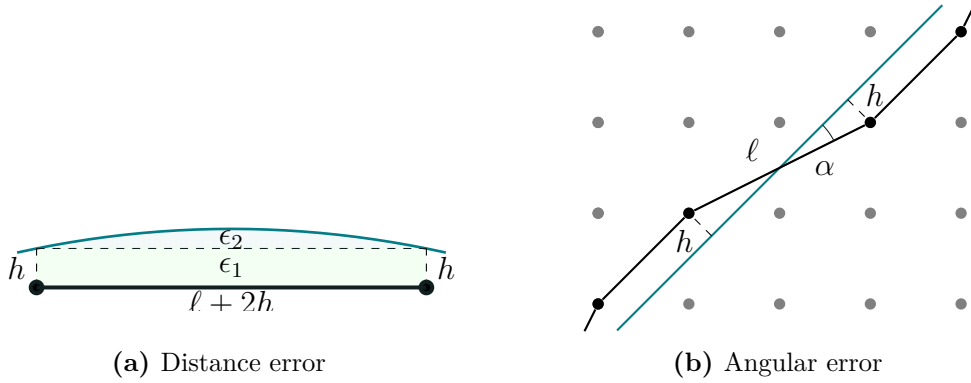


Figure 2.1: Geometrical error bounds. Blue line: continuous optimal solution. Black line: discrete optimal solution. Gray dots: graph nodes.

part of the graph and reduce the run time considerably. As a particularly fast and simple heuristic we employ the travel time along a straight line between x_i and x_D , assuming maximum tail wind, i.e.,

$$d(x_i, x_D) = \frac{\|x_i - x_D\|}{\bar{v} + \bar{w}}.$$

Tighter and more complex heuristics exploiting local bounds on the wind have been proposed for flight planning, also for time-dependent wind fields [10].

The travel time for each arc is again calculated via numerical integration of (2.14) using the same method as for the collocation with a fixed discretization. In order to draw up a fair comparison, we process arcs on the fly and thus eliminate any major preprocessing. This also makes the approach extendable to the time dependent case.

2.2.3.4 Time Complexity

Using a Fibonacci heap for the priority queue, A* can be implemented to run in time

$$R_D \in \mathcal{O}(|A| + |V| \log |V|), \quad (2.15)$$

where $|A|$ and $|V|$ are the numbers of arcs and vertices, respectively. As outlined above, we may assume $\ell \gg h$. If we – conservatively – assume $\ell^2 \geq h^2 \log h^{-1}$, the total complexity becomes

$$R_D = \mathcal{O}(\ell^2 h^{-4}).$$

2.2.3.5 Graph Structure

Given the above considerations, we now address the question of which graph structure in terms of h and ℓ is the most efficient, i.e., which structure achieves a minimal error for a given computational budget b or, equivalently, a desired accuracy with minimal effort. Models for computational work and accuracy are

$$W(h, \ell) = \ell^2 h^{-4} \quad \text{and} \quad \epsilon(h, \ell) = \ell^4 + h^2 + h^4 \ell^{-4}.$$

We are hence interested in solving the optimization problem

$$\min \epsilon(h, \ell) \quad \text{s.t.} \quad W(h, \ell) = b.$$

The constraint $W(h, \ell) = b$ yields $\ell^2 = h^4 b$, which, when inserted into the objective, leads to the unconstrained problem

$$\min_h b^2 h^8 + h^2 + b^{-2} h^{-4} \quad \Leftrightarrow \quad \min_H BH^4 + H + B^{-1} H^{-2}.$$

The necessary optimality condition $4BH^3 + 1 - 2B^{-1}H^{-3} = 0$ is a quadratic equation in H^3 with solution

$$h^6 = \frac{-1 + \sqrt{33}}{8b^2} \quad \Leftrightarrow \quad b = \sqrt{\frac{-1 + \sqrt{33}}{8h^6}}.$$

Inserting this into the constraint yields $\ell^2 = h\sqrt{\frac{-1 + \sqrt{33}}{8}}$. We conclude that graphs of optimal efficiency should follow the law

$$h = \mathcal{O}(\ell^2), \tag{2.16}$$

such that the computational complexity of the discrete optimization can be expressed as

$$R_D \in \mathcal{O}(h^{-3}) \quad \Leftrightarrow \quad R_D \in \mathcal{O}(\ell^{-6}) \tag{2.17}$$

with an associated error of $\mathcal{O}(\ell^4)$ in flight time and of $\mathcal{O}(\ell^2)$ in path approximation.

2.2.4 DisCOptER Algorithm

Due to their superior angular resolution, arcs of length ℓ will occur in the optimal discrete path, while the length of flight path segments in the collocation solution is around $\delta\tau T\bar{v}$. Hence, we expect the accuracy of continuous and discrete optimization approaches to be comparable if $\ell = \delta\tau T\bar{v}$. Obviously, for increasing accuracy $\ell \rightarrow 0$, the collocation effort of order $\mathcal{O}(\delta\tau^{-1} \log \delta\tau / \log(\omega \|\chi_0 - \chi^*\|))$ grows much slower than the A* effort of complexity $\mathcal{O}(\ell^{-6})$. On the other hand, the collocation approach converges only locally.

We therefore propose a hybrid algorithm that combines the strengths of discrete optimization and optimal control, see Algorithm 1. First, a discrete shortest path of low accuracy is calculated using the A* algorithm as described in Section 2.2.3. This is used as initial iterate for solving the KKT system (2.7) to the desired final accuracy using the ordinary Newton's method. Employing line search or trust region globalization would enlarge the convergence domain of Newton's method and allow for coarser graphs to be used, but at the cost of less robust and efficient convergence. In favor of robustness and simplicity, we restrict the attention to the ordinary Newton's method.

Algorithms that combine methods from discrete and continuous optimization have been proposed before. A reverse deterministic combination going from continuous to discrete has been proposed in [40] based on dynamic programming principles. Other combinations involve a stochastic discrete stage, like rapidly-exploring random trees (RRT, RRT*) (see, e.g., [41]) or Probabilistic Roadmaps (PRM) [42] in combination with a second NLP stage. Another approach was taken in [43], where the authors use a combination of A* and RRT* to find an optimal trajectory. These algorithms reveal remarkable performance when it comes to obstacle avoidance. Since our goal is, however, to develop an algorithm with a priori error estimates and bounded runtime, we do not make use of any stochastic approaches in the DisCOptER algorithm.

Algorithm 1: DisCOptER Algorithm**Input** : $x_O, x_D \in \mathbb{R}^2$, $w \in C^2(\mathbb{R}^2)^2$, $\bar{v} > 0$, $\text{TOL} > 0$ **Output** : approximate solution $(T, x, v) \in \mathbb{R} \times C^0([0, 1])^2 \times L^2([0, 1])^2$
of (2.1) with error of order $\text{TOL}^2, \text{TOL}, \text{TOL}$, respectively

- 1 Choose $\delta\tau = \mathcal{O}(\sqrt{\text{TOL}})$
- 2 Define (h, ℓ) -dense graph G with $\ell > \delta\tau\|x_D - x_O\|$, but sufficiently small, and $h = \mathcal{O}(\ell^2)$
- 3 Calculate shortest path on G using the A* algorithm (see Section 2.2.3)
- 4 Interpolate path onto collocation discretization (see Section 2.2.4.1)
- 5 Calculate a continuous solution by solving the nonlinear problem (2.7), via direct collocation and Newton's method (see Section 2.2.2)

2.2.4.1 Initialization

Let $(x_0, \dots, x_n) \in P$ be a shortest path from x_O to x_D in the graph G . Let t_i denote the time at which waypoint x_i is passed, and define the relative passage time $\tau_i = t_i/T(p) \in [0, 1]$. We define a mapping $\Xi : P \rightarrow C^{0,1}([0, 1])^2$ of discrete flight paths $(x_0, \dots, x_n) \in P$ to continuous paths $x \in C^{0,1}([0, 1])^2$ by piecewise linear interpolation:

$$x(\tau) = x_i + \frac{T(p)\tau - t_i}{t_{i+1} - t_i}(x_{i+1} - x_i) \quad \text{if } t_i \leq T(p)\tau \leq t_{i+1}. \quad (2.18)$$

The initial collocation iterate is then obtained by evaluating $x(\tau_i)$ on the collocation grid $0=\tau_0, \dots, \tau_n=1$ and defining the airspeeds

$$v_i = \frac{x(\tau_{i+1}) - x(\tau_i)}{T(p)(\tau_{i+1} - \tau_i)} - w((x(\tau_{i+1}) + x(\tau_i))/2)$$

at the interval midpoints $\tau_{i+1/2}$.

2.2.4.2 Complexity

The runtime of this hybrid algorithm is comprised of the runtime of the A* algorithm (2.15) and the runtime (2.12) of the KKT-Newton solver for the collocation system. Provided that the initial iterate based on the discrete solution p is sufficiently close to the continuous optimum, i.e., $\omega\|\chi_0 - \chi^*\| < 1$, Newton's method converges locally as described by (2.12). For the path approximation error, we

expect $\|\chi_0 - \chi^*\| \approx C\ell^2$, which leads to an overall complexity of

$$R_H = R_D + R_C \in \mathcal{O}\left(\ell^{-6} + \delta\tau^{-1} \frac{\log \delta\tau}{\log(\omega C\ell^2)}\right), \quad (2.19)$$

or $R_H = \mathcal{O}(\ell^{-6} + \delta\tau^{-1})$ subject to $\omega C\ell^2 < 1$ if an inexact Newton method is used. Both complexity bounds essentially suggest to choose a graph as sparse as possible ($\ell \rightarrow \infty$), only restricted from above by the accuracy necessary for the Newton-KKT solver to converge locally, i.e. $\omega C\ell^2 < 1$, which is independent of the final accuracy $\delta\tau$.

2.3 Results

We validate in this section the effectiveness and the efficiency of our algorithm on a test set of four problems of increasing difficulty. Our aim is to demonstrate that our hybrid approach is asymptotically superior to a purely graph-based alternative. We discuss the convergence properties of the method in relation to the choice of the crossover point and its dependence on the minimum required graph density. Based on these results, we evaluate the DisCOptER algorithm for varying graph densities, using the theoretically optimal graph structure of $h = \ell^2$, cf. (2.16). We will see that – as expected – the best performance is achieved on very sparse graphs. The chapter concludes with a computational comparison of the hybrid algorithm with a purely discrete approach.

2.3.1 Test Problems

We test our algorithm on a set of simple, but representative examples that are well suited to demonstrate our method, and not far from real world situations or arguably even more difficult. The instances live in a square $[0, 1]^2$ or $[0, 1] \times [-1, 1]$, and the origin and the destination are $x_O = [0, 0]^T$ and $x_D = [1, 0]^T$, respectively. All values are chosen dimensionless. The wind fields are constructed in a such a way that the straight line from the origin to the destination is particularly unfavorable. The wind speed is limited to $\bar{w} = \frac{1}{2}\bar{v}$, which is rather strong, but not unrealistic. Even though not formally required, the graph nodes are positioned on a uniform

Cartesian grid, such that the diagonal distance of two adjacent nodes is $2h$. For the sake of simplicity the graph structure will be described based on the node spacing in x-direction $h_x = \sqrt{2}h$. This directly defines $\ell = \sqrt{h}$ by (2.16).

In the first test problem a), the wind field is a laminar flow of opposing parallel currents, namely,

$$w(x) = \begin{bmatrix} \bar{w} \min(\max(2\frac{x_2}{H} - 1, -1), 1) \\ 0 \end{bmatrix},$$

with $H = 0.5$, see Figure 2.2; a similar problem is discussed in [44]. Due to its simplicity, this problem has only one distinct minimum, a property that we make use of in the next section.

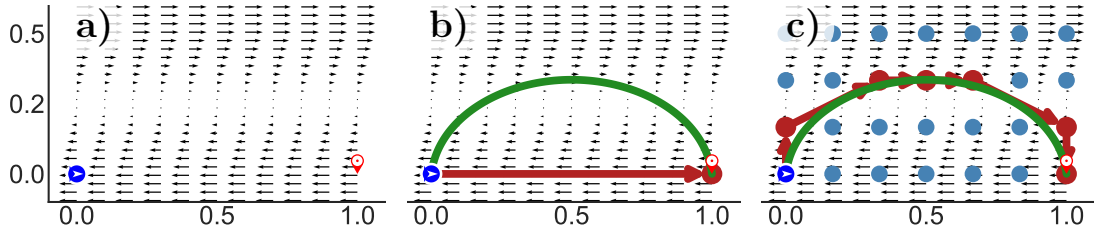


Figure 2.2: Test problem a) with $H = 0.5$, $x_O = (0, 0)$, $x_D = (1, 0)$, $\bar{w} = \frac{1}{2}\bar{v}$. Blue dots: network-graph with $h = \ell^2$ and $1/h_x = 1$ and 6 , respectively, Red: discrete optimal trajectory, Green: continuous optimal trajectory.

In problems b)-d), the wind w is the sum of an increasing number of vortices w_i , each of which is described by

$$w_i(x) = \begin{bmatrix} -s\tilde{w}(r) \sin(\alpha) \\ s\tilde{w}(r) \cos(\alpha) \end{bmatrix},$$

where s is the spin of the vortex ($s=+1$: counter-clockwise, $s=-1$: clockwise), $r = \|x - z\|_2$ is the distance from the vortex center z_i , α is the angle with respect to the center and the x-axis with $\tan(\alpha) = \frac{(x-z_i)_2}{(x-z_i)_1}$ and the absolute vortex wind speed \tilde{w} is a function of r and the vortex radius R :

$$\tilde{w}(r) = \begin{bmatrix} \bar{w} \exp\left(\frac{r^2}{r^2 - R^2}\right) & \text{if } r \leq R \\ 0 & \text{otherwise} \end{bmatrix}. \quad (2.20)$$

Problem b) involves one large vortex with $R = 1/2$ at $z = [0.5, -0.1]^T$, see Figure 2.3. This causes Newton's method to converge to a suboptimal trajectory

(above the vortex) if initialized with the straight trajectory. That is the case if the DisCOptER algorithm is used with a minimally sparse graph with $h_x = 1$ (see second subfigure). We observed, that the discrete shortest path passes below the vortex for any $h_x > 1$. From there the globally optimal solution shown in the third subfigure was found for $h_x = 1/6$.

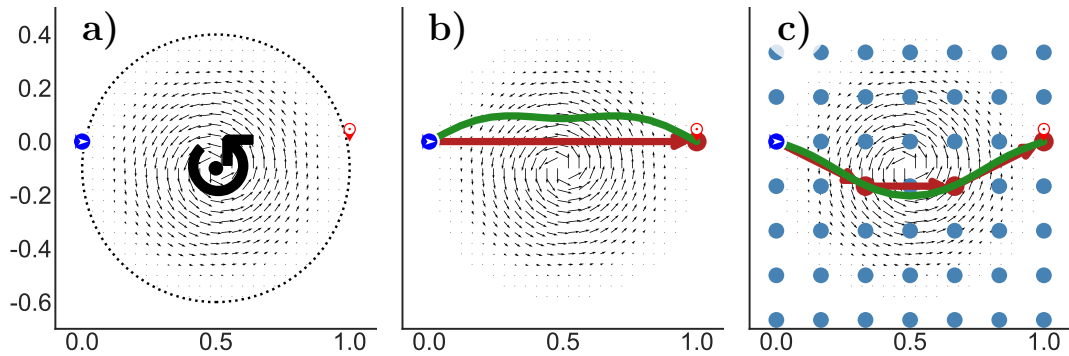


Figure 2.3: Test problem b) with counterclockwise spinning vortex centered at $z = [0.5, -0.1]^T$, $R = 0.5$. $x_O = [0, 0]^T$, $x_D = [1, 0]^T$, $\bar{w} = \frac{1}{2}\bar{v}$. Blue dots: network graph with $h = \ell^2$ and $1/h_x = 1$ and 6, respectively, Red: discrete optimal trajectory, Green: continuous optimal trajectory.

Problem c) involves 15 vortices with $R=1/8$. One is centered at $z=[1/2, -R/2]^T$, the others are regularly aligned as seen in Figure 2.4. Vortices with positive spin (clockwise) are colored green, vortices with negative spin (anti-clockwise) are colored red. Due to the turbulence of this wind field, a plain application of Newton's method is not guaranteed to converge. As an example, Subfigure b) shows again the result with the trivial initialization. Further, there are several local minima, Subfigures c)-d) show two of them. A relatively high graph density ($h_x \leq 1/17$) is required to find the globally optimal trajectory (see Subfigure e)).

Problem d) involves 50 regularly aligned vortices of radius $R = 1/16$ (Figure 2.5). This is clearly an exaggeration, and no commercial plane would ever try to traverse a wind field like this. We use the instance to show that the proposed algorithm outperforms existing methods even under the most adverse conditions. In fact, the high level of non-convexity exacerbates the situation regarding the convergence of Newton's method. Note that, the magnitude of derivatives of (2.20) is coupled directly to the vortex radius. With $R = 1/16$ the vortices here are half as large as

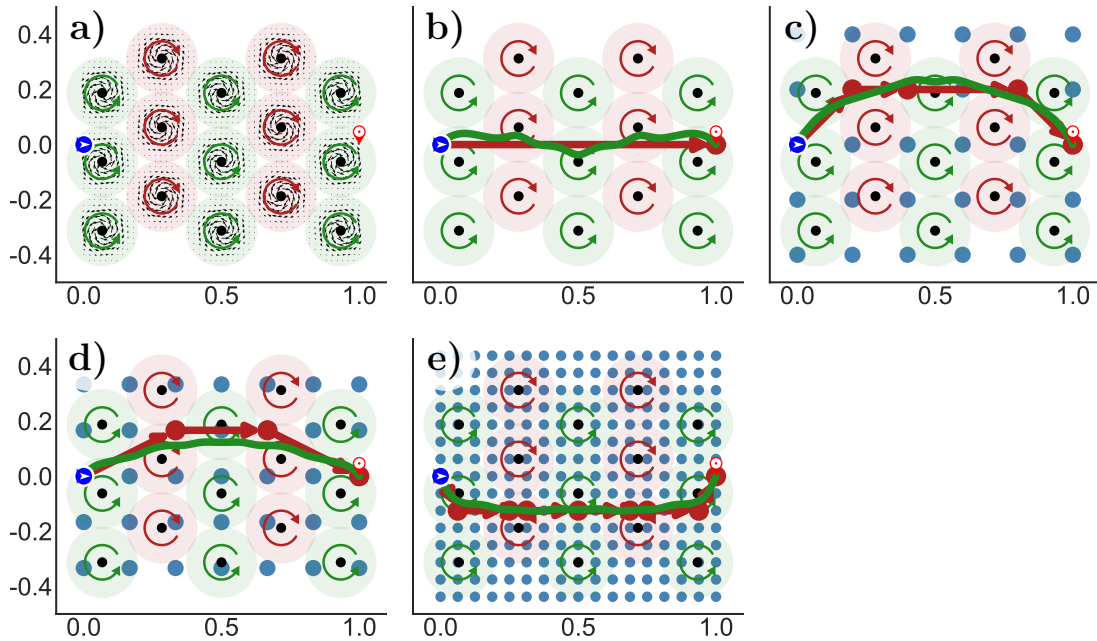


Figure 2.4: Test problem c) with 15 vortices, $R = 1/8$. One is centered at $z = [0.5, -R/2]$, the others are regularly positioned as seen above. $x_O = [0, 0]^T$, $x_D = [1, 0]^T$, $\bar{w} = \frac{1}{2}\bar{v}$. Blue dots: graph with $h = l^2$ and $1/h_x = 1, 5, 6$, and 16 , respectively, Red: discrete optimal trajectory, Green: continuous optimal trajectory. Note that the straight trajectory is particularly unfavorable.

in the previous example. In turn, the first and second order derivatives are 2 and 4 times larger, respectively. Consequently, a quite dense graph with $h_x \leq 1/60$ is required to make Newton's method converge reliably. Note that this wind field is point-symmetric with respect to $[0.5, 0]^T$, which allows for two equivalent global optima (see Subfigures b) and c)). It is a priori not obvious which one will be found. This depends on the discrete optimum.

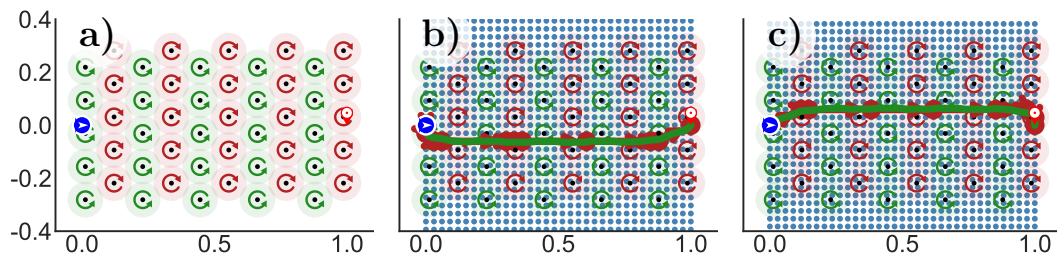


Figure 2.5: Test problem d) with 50 vortices (10 columns of 5 vortices each), $R = 1/16$, regularly positioned. $x_O = [0, 0]^T$, $x_D = [1, 0]^T$, $\bar{w} = 0.5\bar{v}$. Blue dots: graph with $h = l^2$ and $1/h_x = 33$ and 34 , respectively, Red: discrete optimal trajectory, Green: continuous optimal trajectory. Note that, again, the straight trajectory is particularly unfavorable. This problem is point-symmetric w.r.t. $[0.5, 0]^T$. The two shown solutions are equivalent.

2.3.2 Computational Complexity

Before discussing the DisCOptER algorithm, we validate that the optimal control methods are asymptotically more efficient than a purely graph-based approach. This can be investigated only for the first test problem. Due to the simplicity of this wind field, Newton's method will converge from a trivial initialization, i.e., the straight line from x_O to x_D . On the other hand, discrete flight paths were calculated with varying accuracy, that is, with varying ℓ , which is, according to Section 2.2.3.2, a measure for the accuracy of the calculated path. For the sake of consistency, we indicate the accuracy of the continuous solution by $l_C := \delta\tau L$, where L is the path length. Figure 2.6 clearly confirms the estimated time complexities of $\mathcal{O}(\ell^{-6})$ for the discrete approach (see (2.15)) and $\mathcal{O}(\delta\tau^{-1})$ for the continuous approach (see (2.12)).

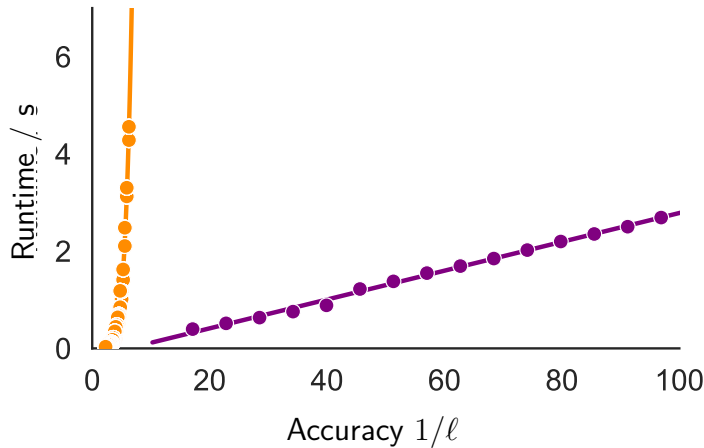


Figure 2.6: Test case a). Orange: Discrete-only approach, polynomial trend line of order 6. Purple: Newton-KKT initialized with straight line, $\ell \doteq l_C = \delta\tau L$, linear trend line.

2.3.3 Minimum Graph Requirements

Figure 2.7 shows the runtime of the DisCOptER algorithm for various graph parameters (h, ℓ) . Some key observations can be made for all four test problems. Towards the top right of each figure the graph density increases, which comes with an increased runtime dictated by the graph searching part of the algorithm. The black dashed line represents the theoretically optimal graph structure $h = \ell^2$,

cf. (2.16); it is shown for orientation as the results in the following sections are computed with this setting.

From left to right the wind fields become increasingly more non-convex. As these plots reveal, this comes with generally higher runtimes, but more importantly with a region of low graph densities where the algorithm converges either to a local minimum or not at all (gray areas). As discussed before, this is not an issue in case a) since this problem is convex and Newton's method converges even from a trivial initialization. Even in case b) we found that a graph with $h_x < 1$ is good enough such that we find the optimal flight path (only one additional column of nodes between start and destination is required). This outcome is not visible here due to the limited resolution of the plot. The convergence problem becomes all the more apparent with instances c) and d). In both cases, a good number of local minima exists, each of which has a rather small radius of convergence such that Newton's method fails if not initialized with sufficient accuracy. Especially in case d) we see a patchwork of runs that converge presumably by chance in an unpredictable way. Some of this might be compensated by globalization techniques and an explicit treatment of non-convexity, which, however, would affect the efficiency of Newton's method. In order to provide reliable results, we need to use a graph density of at least $\ell < 0.15$ and 0.11 for case c) and d), respectively.

Interestingly, the node distance h appears to have a much stronger effect on the convergence than the connectivity width ℓ . This might be explained to some extent in terms of the distance and angular error (cf. Section 2.2.3.2). Low ℓ decreases the angular resolution and thus induces an increased angular error. The discrete flight path then tends to zig-zag along the optimum. This can easily be smoothed by Newton's method. However, if the discrete flight path is parallelly offset from the optimum (distance error due to large node distance h), it might quickly leave the convergence radius of Newton's method.

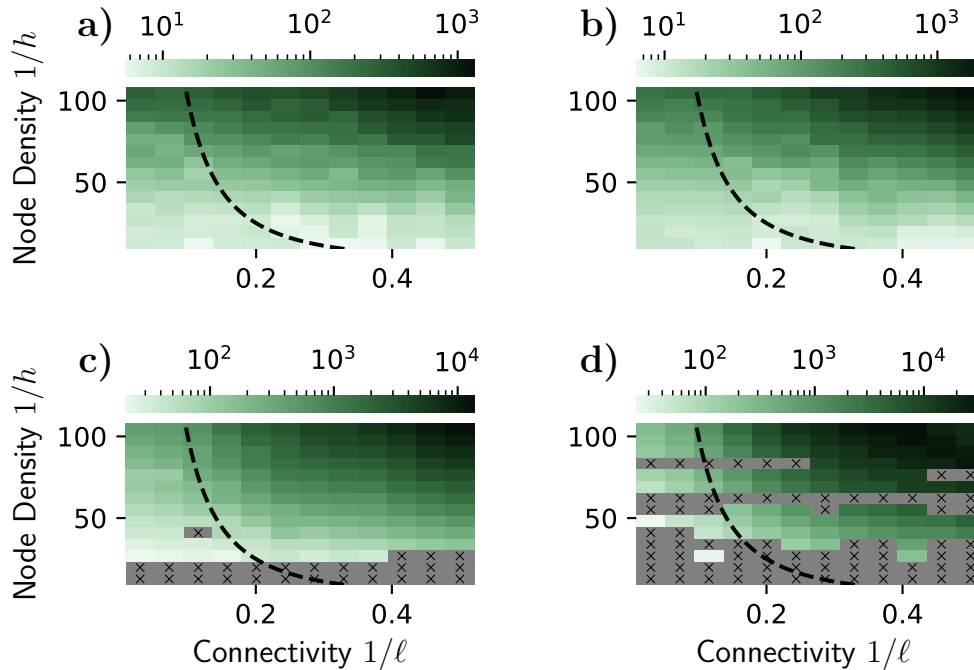


Figure 2.7: Runtime of the DisCOptER algorithm in seconds. Top right corner: dense graph. Bottom left corner: sparse graph. Gray areas: not converged or converged to local minimum. Black dashed line: $h = \ell^2$.

2.3.4 Optimal Crossover Point

In Section 2.2.3.2 we derived $h = \ell^2$ as the optimal graph structure, cf. (2.16). Using this setting and sampling over various graph densities for the test problems leads to the results presented in Figure 2.8. Obviously, an increased graph density comes with a computationally more expensive graph searching task (pink, top, cf. (2.17)). In turn the NLP part of the algorithm (green, bottom) becomes cheaper following (2.12), since the initial guess gets closer to the optimum.

From test problem a) it can be seen that the best performance is achieved – independently of the overall accuracy $\delta\tau$ – with a relatively low graph density of $1/\ell \approx 5$, where the graph search is still negligibly cheap but the graph is already dense enough for Newton’s method to converge with only one iteration. The exact numbers depend strongly on implementation details. We do not claim to have an optimal realization of either part of the algorithm. The trend towards low graph densities, however, is confirmed by the following examples.

As it turns out, the lower bound on the required graph density imposed by the non-convexity of the wind field is the more important criterion. Looking at examples c) and d), where we excluded the area that we identified as not trustworthy in the previous section, we conclude that we want the graph to be as sparse as possible and only as dense as necessary.

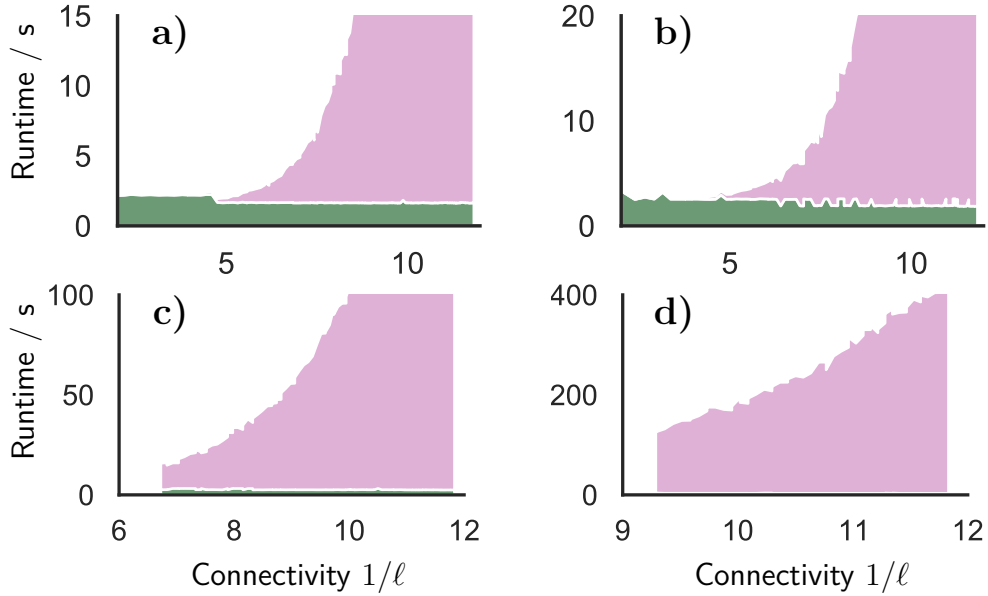


Figure 2.8: Runtimes of the DisCOptER algorithm in seconds, split into the discrete part (pink, top) and the continuous part (green, bottom), sampled with $h = \ell^2$. Constant accuracy $\delta\tau = 1/300$.

2.3.5 Computational Complexity

We finally show that globally optimal shortest paths can be calculated more efficiently using the proposed DisCOptER algorithm than with a purely graph based approach, see Figure 2.9. In the previous section we showed that the algorithm performs best if the graph is chosen rather sparse while respecting the problem-specific minimum density. Consequently, the calculation of the discrete solution is relatively cheap and we can benefit from the computational efficiency of Newton's algorithm. We can also confirm that the time complexity of the DisCOptER Algorithm is $\mathcal{O}(\delta\tau^{-1})$, see (2.19), and that the time complexity of the purely graph-based approach is $\mathcal{O}(\ell^{-6})$, see (2.15).

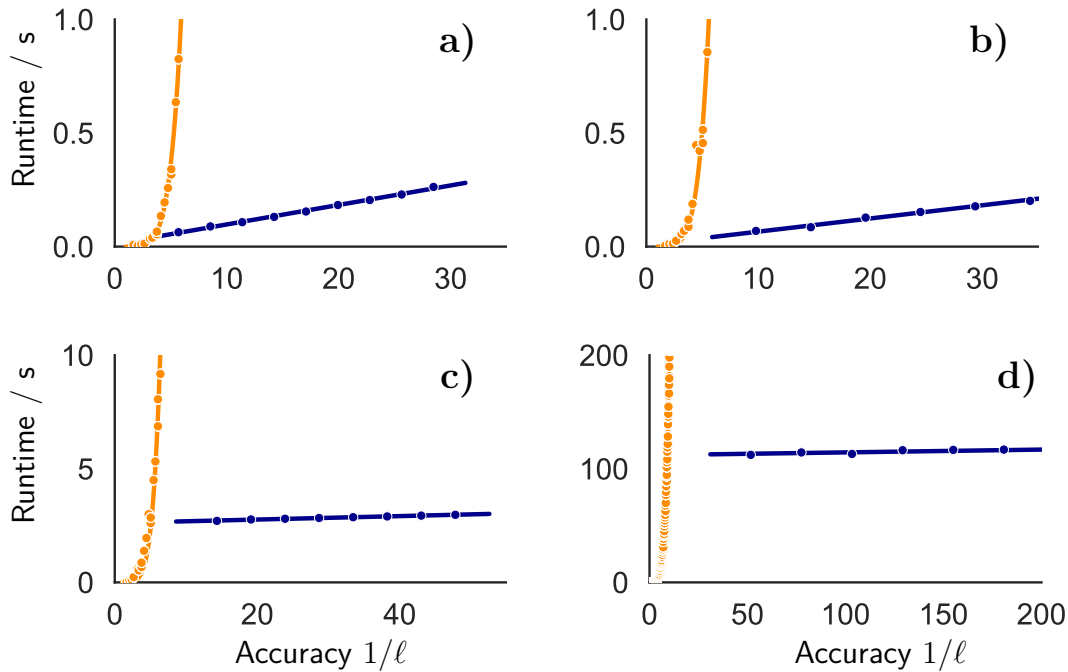


Figure 2.9: Minimum runtime in seconds taken experiments similar to Figure 2.8. Blue: DisCOptER Algorithm with $\ell_c := \delta\tau L$, linear trend line. Orange: Purely discrete, polynomial trend line of order 6.

2.4 Conclusion

In this paper we presented the novel DisCOptER algorithm to calculate flight paths in free flight airspaces utilizing a combination of discrete and continuous optimization. We demonstrated that the achieved efficiency is asymptotically much better than the conventional purely discrete alternative. Even though the algorithm was described for the static two-dimensional case it is strongly promising also for more complex cases, to which it can directly be transferred.

Our study also reveals a need for more theoretical analysis of the problem. In order to design a one-shot algorithm with theoretical efficiency guarantees, a priori error estimates allowing the determination of a minimum required crossover graph density is needed. This will of course depend mainly on the characteristics of the wind field including first and second order derivatives. On the other hand, a posteriori error estimates and adaptive coarse-to-fine graph refinement strategies will be necessary for robustness and efficiency in practice. We investigate some

of these questions in [39] (Chapter 3).

Authors' Contributions

Conceptualization, R.B and M.W.; methodology, M.W.; software, F.D.; validation, F.D.; formal analysis, M.W.; investigation, F.D. and M.W.; resources, R.B., F.D. and M.W.; data curation, F.D.; writing—original draft preparation, F.D. and M.W.; writing—review and editing, R.B.; visualization, F.D.; supervision, R.B.; project administration, R.B. and M.W.; funding acquisition, R.B. and M.W..

All authors have read and agreed to the published version of the manuscript.

References

- [1] S. E. Karisch, S. S. Altus, G. Stojković, and M. Stojković, “Operations,” in *Quantitative Problem Solving Methods in the Airline Industry*, Springer, 2011, ch. 6 – Operations, pp. 283–383. DOI: 10.1007/978-1-4614-1608-1_6.
- [2] Airbus Industries, *Getting to Grips with Fuel Economy*, Issue 4, 2004. [Online]. Available: <https://ansperformance.eu/library/airbus-fuel-economy.pdf> (visited on 09/22/2023).
- [3] Radio Technical Commission for Aeronautics, *Final Report of RTCA Task Force 3 Free Flight Implementation*. RTCA, 1995.
- [4] F. Jelinek, S. Carlier, J. Smith, and A. Quesne, *The EUR RVSM Implementation Project Environmental Benefit Analysis*, Technical Report, 2019. [Online]. Available: <https://www.eurocontrol.int/publication/eur-rvsm-implementation-project-environmental-benefit-analysis> (visited on 09/22/2023).
- [5] D. Delling and D. Wagner, “Time-Dependent Route Planning,” in *Robust and Online Large-Scale Optimization: Models and Techniques for Transportation Systems*. Springer Berlin Heidelberg, 2009, pp. 207–230. DOI: 10.1007/978-3-642-05465-5_8.
- [6] H. Bast, D. Delling, A. Goldberg, M. Müller-Hannemann, T. Pajor, P. Sanders, D. Wagner, and R. F. Werneck, “Route Planning in Transportation Networks,” in *Algorithm Engineering*, Springer, 2016, pp. 19–80. DOI: 10.1007/978-3-319-49487-6_2.
- [7] T. P. Zis, H. N. Psaraftis, and L. Ding, “Ship Weather Routing: A Taxonomy and Survey,” *Ocean Engineering*, vol. 213, 2020. DOI: 10.1016/j.oceaneng.2020.107697.

- [8] L. Yang, J. Qi, D. Song, J. Xiao, J. Han, and Y. Xia, “Survey of Robot 3D Path Planning Algorithms,” *Journal of Control Science and Engineering*, pp. 1687–5249, 2016. DOI: 10.1155/2016/7426913.
- [9] M. Blanco, R. Borndörfer, N. D. Hoàng, A. Kaier, P. Maristany de las Casas, S. Thomas, and S. Schlobach, “Cost Projection Methods for the Shortest Path Problem with Crossing Costs,” in *17th Workshop on Algorithmic Approaches for Transportation Modelling, Optimization, and Systems (ATMOS 2017)*, vol. 59, Schloss Dagstuhl–Leibniz-Zentrum fuer Informatik, 2017, pp. 1–14. DOI: 10.4230/OASIcs.ATMOS.2017.15.
- [10] M. Blanco, R. Borndörfer, N.-D. Hoang, A. Kaier, A. Schienle, T. Schlechte, and S. Schlobach, “Solving Time Dependent Shortest Path Problems on Airway Networks Using Super-Optimal Wind,” in *16th Workshop on Algorithmic Approaches for Transportation Modelling, Optimization, and Systems (ATMOS 2016)*, vol. 54, Schloss Dagstuhl–Leibniz-Zentrum fuer Informatik, 2016, pp. 1–15. DOI: 10.4230/OASIcs.ATMOS.2016.12.
- [11] K. Larsen, A. Knudsen, and M. Chiarandini, “Constraint Handling in Flight Planning,” in *Principles and Practice of Constraint Programming*, vol. 10416, 2017, pp. 354–369. DOI: 10.1007/978-3-319-66158-2_23.
- [12] O. von Stryk and R. Bulirsch, “Direct and Indirect Methods for Trajectory Optimization,” *Annals of Operations Research*, vol. 37, pp. 357–373, 1992. DOI: 10.1007/BF02071065.
- [13] A. Marchidan and E. Bakolas, “Numerical Techniques for Minimum-Time Routing on a Sphere with Realistic Winds,” *American Institute of Aeronautics and Astronautics*, 2016. DOI: 10.2514/1.G001389.
- [14] M. R. Jardin and A. E. Bryson, “Methods for Computing Minimum-Time Paths in Strong Winds,” *Journal of Guidance, Control, and Dynamics*, vol. 35(1), pp. 165–171, 2012. DOI: 10.2514/1.53614.
- [15] J. Betts and E. Cramer, “Application of Direct Transcription to Commercial Aircraft Trajectory Optimization,” *Journal of Guidance, Control and Dynamics*, vol. 18, no. 1, pp. 151–159, 1995. DOI: 10.2514/3.56670.
- [16] J. García-Heras, M. Soler, and F. J. Sáez, “A Comparison of Optimal Control Methods for Minimum Fuel Cruise at Constant Altitude and Course with Fixed Arrival Time,” *Procedia Engineering*, vol. 80, pp. 231–244, 2014. DOI: 10.1016/j.proeng.2014.09.083.
- [17] H. Diedam and S. Sager, “Global Optimal Control with the Direct Multiple Shooting Method,” *Optimal Control Applications and Methods*, vol. 39, no. 2, pp. 449–470, 2018. DOI: 10.1002/oca.2324.
- [18] S. Sager, G. Reinelt, and H. Bock, “Direct Methods with Maximal Lower Bound for Mixed-Integer Optimal Control Problems,” *Mathematical Programming*, vol. 118, no. 1, pp. 109–149, 2009. DOI: 10.1007/s10107-007-0185-6.

- [19] A. Rao, “A Survey of Numerical Methods for Optimal Control,” *Advances in the Astronautical Sciences*, vol. 135, 2010. [Online]. Available: <https://www.anilvraro.com/Publications/ConferencePublications/trajectorySurveyAAS.pdf> (visited on 09/22/2023).
- [20] P. Bonami, A. Olivares, M. Soler, and E. Staffetti, “Multiphase Mixed-Integer Optimal Control Approach to Aircraft Trajectory Optimization,” *Journal of Guidance, Control, and Dynamics*, vol. 36, no. 5, pp. 1267–1277, 2013. DOI: 10.2514/1.60492.
- [21] L. A. Moreno, A. Fügenschuh, A. Kaier, and S. Schlobach, “A Nonlinear Model for Vertical Free-Flight Trajectory Planning,” in *Operations Research Proceedings 2017*, Springer International Publishing, 2018, pp. 445–450. DOI: 10.1007/978-3-319-89920-6_59.
- [22] E. Zermelo, “Über das Navigationsproblem bei ruhender oder veränderlicher Windverteilung,” *ZAMM-Journal of Applied Mathematics and Mechanics/Zeitschrift für Angewandte Mathematik und Mechanik*, vol. 11(2), pp. 114–124, 1931. DOI: 10.1002/zamm.19310110205.
- [23] H. Maurer and J. Zowe, “First and Second Order Necessary and Sufficient Optimality Conditions for Infinite-Dimensional Programming Problems,” *Math. Programming*, vol. 16, pp. 98–110, 1979. DOI: 10.1007/BF01582096.
- [24] L. Pontrjagin, V. Boltyansky, V. Gamkrelidze, and E. Mischenko, *Mathematical Theory of Optimal Processes*. Wiley-Interscience, 1962.
- [25] J. T. Betts, “Survey of Numerical Methods for Trajectory Optimization,” *Journal of Guidance, Control, and Dynamics*, vol. 21, no. 2, pp. 193–207, 1998. DOI: 10.2514/2.4231.
- [26] C. Hargraves and S. Paris, “Direct Trajectory Optimization Using Nonlinear Programming and Collocation,” *Journal of Guidance, Control, and Dynamics*, vol. 10, no. 4, pp. 338–342, 1987. DOI: 10.2514/3.20223.
- [27] F. Fahroo and I. M. Ross, “Direct Trajectory Optimization by a Chebyshev Pseudospectral Method,” *Journal of Guidance, Control, and Dynamics*, vol. 25, no. 1, pp. 160–166, 2002. DOI: 10.2514/2.4862.
- [28] U. Ascher, R. Mattheij, and R. Russell, *Numerical Solution of Boundary Value Problems for Ordinary Differential Equations*. Prentice Hall, 1988. DOI: 10.1137/1.9781611971231.
- [29] P. Hagelauer and F. Mora-Camino, “A Soft Dynamic Programming Approach for On-Line Aircraft 4D-Trajectory Optimization,” *European Journal of Operations Research*, vol. 107, no. 1, pp. 87–95, 1998. DOI: 10.1016/S0377-2217(97)00221-X.
- [30] T. Steihaug, “The Conjugate Gradient Method and Trust Regions in Large Scale Optimization,” *SIAM Journal on Numerical Analysis*, vol. 20, no. 3, pp. 626–637, 1983. DOI: 10.1137/0720042.

- [31] P. Toint, “Towards an Efficient Sparsity Exploiting Newton Method for Minimization,” in *Sparse Matrices and Their Use*, Academic Press, 1981, pp. 57–88.
- [32] M. Weiser, P. Deuffhard, and B. Erdmann, “Affine Conjugate Adaptive Newton Methods for Nonlinear Elastomechanics,” *Optimization Methods and Software*, vol. 22, no. 3, pp. 413–431, 2007. DOI: 10.1080/10556780600605129.
- [33] P. Deuffhard and F. Bornemann, *Scientific Computing with Ordinary Differential Equations*, 2nd ed. Springer, 2002, vol. 42. DOI: 10.1007/978-0-387-21582-2.
- [34] R. Becker, H. Kapp, and R. Rannacher, “Adaptive Finite Element Methods for Optimal Control of Partial Differential Equations: Basic Concepts,” *SIAM Journal on Control and Optimization*, vol. 39, pp. 113–132, 2000. DOI: 10.1137/S0363012999351097.
- [35] M. Weiser, “On Goal-Oriented Adaptivity for Elliptic Optimal Control Problems,” *Optimization Methods and Software*, vol. 28, no. 13, pp. 969–992, 2013. DOI: 10.1080/10556788.2011.651469.
- [36] P. Deuffhard, *Newton Methods for Nonlinear Problems. Affine Invariance and Adaptive Algorithms*. Springer, 2004, vol. 35. DOI: 10.1007/978-3-642-23899-4.
- [37] M. Weiser, A. Schiela, and P. Deuffhard, “Asymptotic Mesh Independence of Newton’s Method Revisited,” *SIAM Journal on Numerical Analysis*, vol. 42, no. 5, pp. 1830–1845, 2005. DOI: 10.1137/S0036142903434047.
- [38] S. Karaman and E. Frazzoli, “Sampling-Based Algorithms for Optimal Motion Planning,” *The International Journal of Robotics Research*, vol. 30, no. 7, pp. 846–894, 2011. DOI: 10.1177/0278364911406761.
- [39] R. Borndörfer, F. Danecker, and M. Weiser, “Error Bounds for Discrete-Continuous Free Flight Trajectory Optimization,” *Journal of Optimization Theory and Applications*, vol. 198, no. 2, pp. 830–856, 2023. DOI: 10.1007/s10957-023-02264-7.
- [40] O. Junge and H. Osinga, “A Set Oriented Approach to Global Optimal Control,” *ESAIM: Contr. Opt. Calc. Var.*, vol. 10, pp. 259–270, 2004. DOI: 10.1051/cocv:2004006.
- [41] T. Karatas and F. Bullo, “Randomized Searches and Nonlinear Programming in Trajectory Planning,” in *Proceedings of the 40th IEEE Conference on Decision and Control (Cat. No.01CH37228)*, vol. 5, 2001, pp. 5032–5037. DOI: 10.1109/CDC.2001.981008.
- [42] P. Bouffard and S. Waslander, “A Hybrid Randomized/Nonlinear Programming Technique for Small Aerial Vehicle Trajectory Planning in 3D,” *Planning, Perception and Navigation for Intelligent Vehicles (PPNIV)*, vol. 63, 2009. [Online]. Available: https://www.researchgate.net/profile/Patrick-Bouffard/publication/228716707_A_Hybrid_RandomizedNonlinear_Programming_Technique_For_Small_Aerial_Vehicle_

Trajectory_Planning_in_3D/links/0a85e52fff4d1a062f000000/A-Hybrid-Randomized-Nonlinear-Programming-Technique-For-Small-Aerial-Vehicle-Trajectory-Planning-in-3D.pdf (visited on 09/22/2023).

- [43] M. Brunner, B. Brüggemann, and D. Schulz, “Hierarchical Rough Terrain Motion Planning using an Optimal Sampling-Based Method,” in *2013 IEEE International Conference on Robotics and Automation*, IEEE, 2013, pp. 5539–5544. DOI: 10.1109/ICRA.2013.6631372.
- [44] L. Techy, “Optimal Navigation in Planar Time-Varying Flow: Zermelo’s Problem Revisited,” *Intelligent Service Robotics 4.4*, pp. 271–283, 2011. DOI: 10.1007/s11370-011-0092-9.

CHAPTER 3

Error Bounds for Discrete-Continuous
Free Flight Trajectory Optimization

Borndörfer, R., Danecker, F., and Weiser, M.
Journal of Optimization Theory and Applications 198, 830–856 (2023).
DOI: 10.1007/s10957-023-02264-7.

This article is licensed under a Creative Commons Attribution 4.0
International License (<http://creativecommons.org/licenses/by/4.0/>).

Abstract Two-stage methods addressing continuous shortest path problems start local minimization from discrete shortest paths in a spatial graph. The convergence of such hybrid methods to global minimizers hinges on the discretization error induced by restricting the discrete global optimization to the graph, with corresponding implications on choosing an appropriate graph density.

A prime example is flight planning, i.e., the computation of optimal routes in view of flight time and fuel consumption under given weather conditions. Highly efficient discrete shortest path algorithms exist and can be used directly for computing starting points for locally convergent optimal control methods. We derive a priori and localized error bounds for the flight time of discrete paths relative to the optimal continuous trajectory, in terms of the graph density and the given wind field. These bounds allow designing graphs with an optimal local connectivity structure.

The properties of the bounds are illustrated on a set of benchmark problems. It turns out that localization improves the error bound by four orders of magnitude, but still leaves ample opportunities for tighter error bounds by a posteriori estimators.

Contents

3.1	Introduction	119
3.2	Shortest Flight Planning: Continuous & Discrete	121
3.2.1	Continuous: Optimal Control	121
3.2.2	Discrete: Airway Networks	125
3.3	Approximation Error Bounds	125
3.3.1	A Posteriori Error	126
3.3.2	Trajectory Approximation in Locally Dense Graphs	128
3.3.3	Computable Error Bounds	132
3.4	Numerical Examples	135
3.4.1	Test Instances	135
3.4.2	Results	136
3.5	Conclusion	141
3.A	Appendix	144

3.1 Introduction

There are applications of numerical optimization that call for the computation of global instead of just local optima. One example is free flight planning, an instance of airborne navigation, where travel time is optimized subject to a given wind field (the travel time T between origin and destination is almost proportional to fuel consumption, CO₂ emission, and cost [1]). Going left or right around obstacles or adverse wind situations gives rise to locally optimal trajectories with considerably different costs [2], and airlines are naturally interested in the best of those.

Various approaches to global optimization have been proposed: stochastic ones like multistart or simulated annealing [3], biologically inspired metaheuristics like genetic algorithms or particle swarms [4], and rigorous ones based on objective bounds and branching [5, 6]. The former approaches converge to a global minimizer only almost surely at increasing computational costs, but provide no guarantees for finiteness. The latter ones usually require in-depth structural knowledge of the objective, or the use of interval arithmetics, and quickly suffer from the curse of dimensionality for practically relevant problems.

In this paper we consider a two-stage multistart approach along the following lines. It (i) defines a sufficiently large set of possible starting points, (ii) selects few promising candidates, and (iii) performs local optimization starting from those candidates. For this to be computationally feasible, the representation and selection of starting points needs to be highly efficient even for large and high-dimensional design spaces. This is, of course, problem-dependent. Some problems allow a discretization in terms of discrete network optimization problems such as minimum cost flow and, in particular, shortest path problems, which can be solved efficiently to global optimality in theory and practice [7]. If such discrete problems are close to their continuous counterpart, their solutions might provide promising starting points for local optimization to converge to a nearby global optimizer.

Obviously, flight planning and discrete shortest path search are related in this way and can hence serve as examples to substantiate the general idea. The starting

points covering the design space of trajectories between origin and destination can be implicitly described as paths in a graph covering the spatial domain. In this discrete approximation of the problem, the selection of promising candidate points can be efficiently performed using Dijkstra’s algorithm or its A* variants. This leads to a hybrid discrete-continuous algorithm combining discrete global optimization methods with continuous local optimal control methods.

A first successful step in this direction has been taken with the development of the hybrid algorithm DisCOptER (Chapter 2, [8]) that has been proposed by the authors of this paper for free flight planning. Even though the potential applications are manifold, no other similar method has been proposed so far. Note that the discrete stage alone is traditionally used as a standalone optimizer for practical flight planning on given airway networks [9, 10], but gets quickly inefficient when the airway networks need to be refined significantly to exploit the potential benefits of free flight [1]. Similarly, for robot path planning, rapidly exploring random graphs and trees (RRT) are used for sampling the trajectory design space at many discrete points [11].

Guaranteed convergence of a hybrid two-stage algorithm to a global minimizer hinges on the one hand on a sufficiently dense sampling of possible starting points in the design space, and on the other hand on the ability of the local optimizer to converge reliably to a nearby local optimum when started from one of these candidate points. The present paper investigates the first aspect, i.e., we derive bounds on the required resolution of the discretization. To this purpose, we introduce a continuous problem formulation that allows a direct comparison of continuous and discrete 2D flight paths (Section 3.2), and derive bounds for the flight duration deviation $T(\xi) - T(\xi_C)$ between different paths ξ and ξ_C in terms of spatial distance $\|\xi - \xi_C\|$, angular distance $\|(\xi - \xi_C)_\tau\|$, and bounds on the stationary wind and its derivatives. Based on the (h, ℓ) graph density property from [8] (Chapter 2), we obtain corresponding flight duration bounds for discrete optimal trajectories (Section 3.3), which also yield a theoretically optimal ratio $h = \mathcal{O}(\ell^2)$ of vertex distance and characteristic edge length. We derive two types of error bounds: an

a priori bound $T(\xi_G) \leq T(\xi_C) + \kappa \ell^2$ depending only on problem quantities but not on a particular solution, and a local bound based on bounds for the wind in a neighborhood of the optimal trajectory. Taking more detailed information into account, the latter one improves on the former one by several orders of magnitude. The theoretical predictions are confirmed by numerical examples for a set of benchmark problems with varying wind complexity (Section 3.4), which reveal that there is still ample room for improvement by using a posteriori error estimators. The flight planning application leaves its imprint on the nature and derivation of these bounds, but the general idea should work for similar applications that have a discrete-continuous nature.

3.2 Shortest Flight Planning: Continuous & Discrete

For simplicity of presentation, we consider flight planning in the Euclidean plane. We aim at minimizing the travel time T between an origin x_O and a destination x_D , with a fixed departure at $t = 0$ and a constant airspeed $\bar{v} > 0$, thus neglecting start and landing phase. Moreover, we assume a spatially heterogeneous, twice continuously differentiable wind field w to be given, with a bounded magnitude $\|w\|_{L^\infty(\mathbb{R}^2)} < \bar{v}$. Focusing on free flight areas, we also neglect any traffic flight restrictions.

3.2.1 Continuous: Optimal Control

In free flight areas, the flight trajectory is not restricted to a predefined set of airways. Instead, we consider any Lipschitz-continuous path $x : [0, T] \rightarrow \mathbb{R}^2$ in the Sobolev space $H^1([0, T])$, connecting origin x_O and destination x_D , as a valid trajectory if it satisfies the following ODE almost everywhere,

$$x_t(t) = v(t) + w(x(t), t), \quad (3.1)$$

where x_t denotes the derivative of x with respect to t and is obtained by adding the vectors of airspeed and wind. The airspeed $v \in L^2([0, T]) : [0, T] \mapsto \mathbb{R}^2$ lives in the Lebesgue space of square integrable functions. Among those trajectories, we need

to find one with minimal flight duration T , since that is essentially proportional to fuel consumption [1]. This classic of optimal control is known as Zermelo's navigation problem [12].

The optimal control problem of finding a trajectory (x, v) that minimizes travel time $T \in \mathbb{R}$ while obeying the dynamics described in (3.1) and travelling at constant airspeed \bar{v} now reads

$$\min_{T, x, v} T \quad \text{s.t.} \quad c(T, x, v) = \begin{bmatrix} x(0) - x_O \\ x(T) - x_D \\ x_t(t) - (v(t) + w(x(t), t)) \\ v(t)^T v(t) - \bar{v}^2 \end{bmatrix} = 0 \quad (3.2)$$

with $c : \mathbb{R} \times H^1([0, T])^2 \times L^2([0, T])^2 \rightarrow \mathbb{R}^2 \times \mathbb{R}^2 \times L^2([0, T])^2 \times L^2([0, T])$. Note that due to $v^T v = \bar{v}^2$, the airspeed v (and therefore also the ground speed $v + w$) is bounded almost everywhere, such that any feasible trajectory x is Lipschitz-continuous, i.e., $x \in C^{0,1}([0, T])$ [13, Thm. 1.36]. Moreover, it is immediately clear that there is an ellipse $\Omega \subset \mathbb{R}^2$ with focal points x_O and x_D , in which any trajectory with minimal flight duration is contained.

Problem (3.2) can be numerically solved efficiently with either direct methods using a discretization of the variables to formulate a finite-dimensional nonlinear programming problem [14], or with indirect methods relying on Pontryagin's maximum principle, leading to a boundary value problem for ordinary differential equations [12, 15–19]. These approaches have also been considered explicitly for free flight planning [20, 21].

While the optimal control formulation (3.2) is convenient for numerically solving the optimization problem, we will consider a different formulation defining trajectories on the unit interval that is better suited for direct comparison with graph-based approaches here. Assume the flight trajectory $x : [0, T] \rightarrow \Omega$ is given by a strictly monotonously increasing parametrization $t(\tau)$ on $(0, 1)$ as $x(t(\tau)) = \xi(\tau)$, and $\xi \in H^1(0, 1) : (0, 1) \rightarrow \Omega$ being a Lipschitz-continuous path with $\xi(0) = x_O$, $\xi(1) = x_D$. Due to Rademacher's theorem, its derivative ξ_τ exists almost everywhere, and we assume it not to vanish. Then, $t(\tau)$ is defined by the

state equation $x_t \stackrel{(3.1)}{=} v + w \neq 0$ and the airspeed constraint $\|v\| = \bar{v}$, since

$$\bar{v} = \|x_t - w\| \quad \text{and} \quad x_t t_\tau = \xi_\tau \neq 0$$

imply

$$\begin{aligned} & (t_\tau^{-1} \xi_\tau - w)^T (t_\tau^{-1} \xi_\tau - w) = \bar{v}^2 \\ \Leftrightarrow & \quad t_\tau^{-2} \xi_\tau^T \xi_\tau - 2t_\tau^{-1} \xi_\tau^T w + w^T w - \bar{v}^2 = 0 \\ \Leftrightarrow & \quad (\bar{v}^2 - w^T w) t_\tau^2 + 2\xi_\tau^T w t_\tau - \xi_\tau^T \xi_\tau = 0 \end{aligned}$$

due to $t_\tau > 0$. Solving the quadratic equation yields

$$t_\tau = \frac{-\xi_\tau^T w + \sqrt{(\xi_\tau^T w)^2 + (\bar{v}^2 - w^T w)(\xi_\tau^T \xi_\tau)}}{\bar{v}^2 - w^T w} =: f(t, \xi, \xi_\tau). \quad (3.3)$$

The flight duration T is then given by integrating the ODE (3.3) from 0 to 1 as $T = t(1)$. For the ease of presentation let us assume that the wind w is stationary, i.e., independent of t , and thus $f(t, \xi, \xi_\tau) = f(\xi, \xi_\tau)$. Doing so, we avoid the more complicated work with an ODE. Instead, we obtain

$$T(\xi) = \int_0^1 f(\xi(\tau), \xi_\tau(\tau)) d\tau. \quad (3.4)$$

We, however, strongly expect our results to directly carry over to the more complex case. Since the flight duration T as defined in (3.4) is based on a reparametrization $x(t) = \xi(\tau(t))$ of the path such that $\|x_t(t) - w(x(t))\| = \bar{v}$, the actual parametrization of ξ is irrelevant for the value of T . Calling two paths $\xi, \hat{\xi}$ equivalent if there exists a Lipschitz-continuous bijection $r : (0, 1) \rightarrow (0, 1)$ such that $\hat{\xi}(r(\tau)) = \xi(\tau)$, we can restrict the optimization to equivalence classes $[\xi]$. Thus, the admissible set is

$$X = \{[\xi] \mid \xi \in C^{0,1}((0, 1), \Omega), \xi(0) = x_O, \xi(1) = x_D\}. \quad (3.5)$$

Example 3.1. — *This is illustrated in Figure 3.1. Consider the case that the wind gets stronger the farther the airplane proceeds to the right with $w(\xi(\tau), \tau) = \begin{bmatrix} \bar{w} & 0 \\ 0 & 0 \end{bmatrix} \xi(\tau)$. Obviously, the optimal route is the straight line. This route can be represented differently, depending on the choice of the time parametrization $\tau(t)$. E.g., with $\tau(t) = t/T$ constant air speed is maintained. Consequently, the distance*

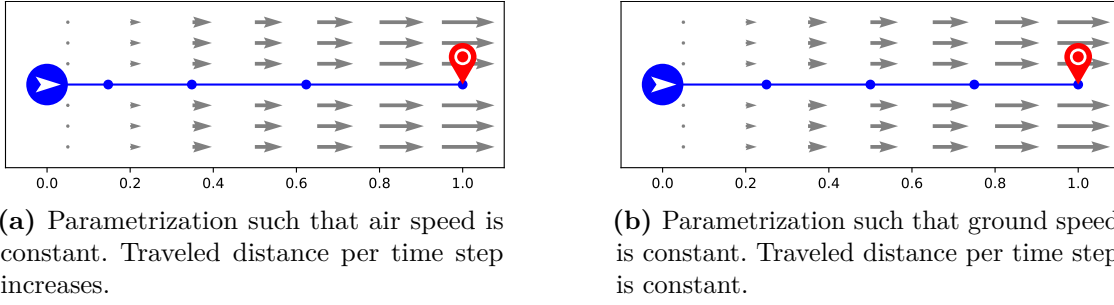


Figure 3.1: Illustration of the effect of the time parametrization $\tau(t)$. Blue dots represent position at equidistant time steps in the normalized time $\tau \in (0, 1)$. Wind is blowing to the right with increasing speed.

traveled in a certain time step increases over the course of the flight, due to the increasing wind speed (Figure 3.1 (a)). Alternatively, one may choose $\tau(t)$ such that the ground speed is constant (Figure 3.1 (b)).

Since every equivalence class contains a representative with constant ground speed $\|\xi_\tau(\tau)\|$, we will subsequently often assume $\|\xi_\tau(\tau)\| = \text{const}$ without loss of generality, such that $\|\xi_\tau\|$ is just the length of the flight trajectory. For convenience, let us define the set of representatives with constant ground speed as

$$\hat{X} = \{\xi \mid [\xi] \in X, \|\xi_\tau\| = \text{const f.a.a. } \tau \in (0, 1)\}. \quad (3.6)$$

The reduced minimization problem, equivalent to (3.2), now reads

$$\min_{[\xi] \in X} T(\xi), \quad \text{or, equivalently,} \quad \min_{\xi \in \hat{X}} T(\xi). \quad (3.7)$$

Remark 3.1. — *Let us interpret this representation of flight duration. In the absence of wind, i.e., $\|w\| = 0$, (3.3) yields $t_\tau = \xi_\tau/\bar{v}$. Integrating over $(0, 1)$ yields just the total path length divided by the velocity (airspeed and ground speed coincide). For low wind, i.e., $\|w\| \ll \bar{v}$, we obtain $t_\tau \approx (\xi_\tau - \xi_\tau^\top w)/\bar{v}$ from (3.3), and hence a reduction of flight duration due to the tail wind component $\xi_\tau^\top w$ (or an increase in the case $\xi_\tau^\top w < 0$ of head wind). For $\|w\| \rightarrow \bar{v}$, we obtain $t_\tau \rightarrow \xi_\tau/(2\|\xi_\tau\|^{-1}|\xi_\tau^\top w|)$ from (3.3) in case of a tailwind component $\xi_\tau^\top w > 0$ and $t_\tau \rightarrow \infty$ otherwise. In any case, flight duration scales linearly with the length of the path.*

In contrast to the optimal control formulation (3.2), the reduced formulation (3.7) allows a direct comparison of continuous and discrete flight trajectories, and is therefore the ideal tool for deriving error bounds in Section 3.3. We point out, however, that it is less suited for actually computing an optimal solution.

3.2.2 Discrete: Airway Networks

If flight trajectories are restricted to certain airways connecting predefined waypoints, flight planning is a special kind of shortest path problem on a graph. Let $V \subset \mathbb{R}^2$ be a finite set of waypoints including x_O and x_D , and $E \subset V \times V$ a set of airways such that $G = (V, E)$ is a connected directed graph. A discrete flight path is a finite sequence $(x_i)_{0 \leq i \leq n}$ of waypoints with $(x_{i-1}, x_i) \in E$ for $i = 1, \dots, n$, connecting $x_0 = x_O$ with $x_n = x_D$.

We define a mapping $\Xi : (x_i)_{0 \leq i \leq n} \mapsto [\xi] \in X$ of discrete flight paths to continuous paths by piecewise linear interpolation

$$\xi(\tau) = x_{\lfloor n\tau \rfloor} + (n\tau - \lfloor n\tau \rfloor)(x_{\lceil n\tau \rceil} - x_{\lfloor n\tau \rfloor}) \quad (3.8)$$

resulting in polygonal chains, which are Lipschitz-continuous with piecewise constant derivative. We denote its image $\text{im } \Xi \subset X$, i.e., the set of flight trajectories in the Euclidean plane that can be realized by adhering to the airway network, by X_G . The discrete flight planning problem then reads

$$\min_{[\xi] \in X_G} T(\xi), \quad (3.9)$$

and differs from its continuous counterpart (3.7) only by the admissible set, effectively acting as a particular discretization.

Shortest path problems on static graphs with non-negative weights are usually solved with the A^* variant of Dijkstra's algorithm [22].

3.3 Approximation Error Bounds

Having established a setting in which discrete and continuous flight trajectories can be directly compared, we are interested in bounding the suboptimality, i.e., the

increase of flight duration T relative to the continuous optimum, due to restricting the flight path to predefined airways. In particular, we aim at relating this approximation error to the airway network density.

3.3.1 A Posteriori Error

For estimating the flight time deviation, we start with a Taylor-based bound in terms of the actual path deviation $\delta\xi$ from a minimizer. This bound will serve as the basis for computable bounds in Section 3.3.3 and, in addition, provide a quantitative idea of the efficiency of a posteriori error estimators using computable estimates of $\|\delta\xi\|$.

At this point we want to point out that ξ , ξ_τ , $\delta\xi$, and $\delta\xi_\tau$ are in general functions of τ . In favor of a more compact notation we will usually omit the argument τ in the remainder of the paper.

Lemma 3.1. — *For any $p \in \Omega$ let $c_0(p) = \|w(p)\|$, $c_1(p) = \|w_x(p)\|$, and $c_2(p) = \|w_{xx}(p)\|$, and assume $c_0 \leq \bar{v}/\sqrt{5}$. Moreover, let $\xi \in \hat{X}$, $L := \|\xi_\tau\| > 0$ and $\underline{v}^2(p) := \bar{v}^2 - c_0^2(p)$. Then the second total directional derivative of f as defined in (3.3) is bounded by*

$$|f''(\xi, \xi_\tau)[\delta\xi, \delta\xi_\tau]^2| \leq \alpha_0(\xi)\|\delta\xi\|^2 + \alpha_1(\xi)\|\delta\xi\| \|\delta\xi_\tau\| + \alpha_2(\xi)\|\delta\xi_\tau\|^2 \quad (3.10)$$

for almost all $\tau \in (0, 1)$, with $\alpha_i : \Omega \rightarrow \mathbb{R}^+$, $i = 0, \dots, 2$, given as

$$\begin{aligned} \alpha_0(p) &= \frac{L}{\underline{v}^3(p)} \left(12c_1^2(p) + 4\underline{v}(p)c_2(p) \right), \\ \alpha_1(p) &= \frac{8c_1(p)}{\underline{v}^2(p)}, \\ \alpha_2(p) &= \frac{2}{L\underline{v}(p)}. \end{aligned}$$

The proof of this lemma is, though not difficult, rather technical and lengthy calculus and is provided in the appendix.

Remark 3.2. — *The assumption of $c_0 \leq \bar{v}/\sqrt{5}$ covers the usually experienced wind velocities, but not the possible extremes.*

Theorem 3.2. — Let $\xi_C \in \hat{X}$ be a minimizer of (3.7) and $\delta\xi := \xi - \xi_C$. Then there is a constant $r > 0$ depending on ξ_C and w , such that the a posteriori bound

$$T(\xi) \leq T(\xi_C) + \int_0^1 \left(\alpha_0(\xi_C) \|\delta\xi\|^2 + \alpha_1(\xi_C) \|\delta\xi\| \|\delta\xi_\tau\| + \alpha_2(\xi_C) \|\delta\xi_\tau\|^2 \right) d\tau \quad (3.11)$$

holds for all paths $\xi \in \hat{X}$ with $\|\xi - \xi_C\|_{C^{0,1}(0,1)} \leq r$ and α_i as defined in Lemma 3.1.

Proof. We note that $T : C^{0,1}(0,1)^2 \rightarrow \mathbb{R}$ as defined in (3.4) is twice continuously Fréchet-differentiable at $\xi_C \in \hat{X}$ due to $\|(\xi_C)_\tau\| \stackrel{(3.6)}{=} L > 0$ for almost all τ . By Lemma 3.1, there are functions $\alpha_0, \alpha_1, \alpha_2$ depending on the local wind w and its derivatives as well as the overall trajectory length L , such that

$$\begin{aligned} f''(\xi_C, (\xi_C)_\tau)[(\delta\xi, \delta\xi_\tau), (\delta\xi, \delta\xi_\tau)] \\ \leq \alpha_0(\xi_C) \|\delta\xi\|^2 + \alpha_1(\xi_C) \|\delta\xi\| \|\delta\xi_\tau\| + \alpha_2(\xi_C) \|\delta\xi_\tau\|^2 \end{aligned}$$

holds for almost all $\delta\xi, \delta\xi_\tau \in \mathbb{R}^2$ and $\tau \in (0,1)$. Integrating over τ yields the bound

$$T''(\xi_C)[\delta\xi, \delta\xi] \leq \int_0^1 \alpha_0(\xi_C) \|\delta\xi\|^2 + \alpha_1(\xi_C) \|\delta\xi\| \|\delta\xi_\tau\| + \alpha_2(\xi_C) \|\delta\xi_\tau\|^2 d\tau$$

for second directional derivatives of the flight duration T in direction $\delta\xi \in C^{0,1}(0,1)^2$ with $\delta\xi(0) = \delta\xi(1) = 0$. Due to continuity of T'' , there exists a neighborhood $B_r(\xi_C)$ of radius $r > 0$, such that $T''(\tilde{\xi})[\delta\xi, \delta\xi] \leq 2 \int_0^1 \alpha_0 \|\delta\xi\|^2 + \alpha_1 \|\delta\xi\| \|\delta\xi_\tau\| + \alpha_2 \|\delta\xi_\tau\|^2 d\tau$ for all $\tilde{\xi} \in B_r(\xi_C)$. Consequently, by Taylor's theorem and using $\delta\xi = \xi - \xi_C$, we can bound

$$\begin{aligned} T(\xi) &= T(\xi_C) + \underbrace{T'(\xi_C)[\delta\xi]}_{=0} + \int_0^1 (1-\nu) T''(\xi_C + \nu\delta\xi)[\delta\xi, \delta\xi] d\nu \\ &\leq T(\xi_C) + \int_0^1 \left(\alpha_0(\xi_C) \|\delta\xi\|^2 + \alpha_1(\xi_C) \|\delta\xi\| \|\delta\xi_\tau\| + \alpha_2(\xi_C) \|\delta\xi_\tau\|^2 \right) d\tau \end{aligned}$$

due to ξ_C being a minimizer. □

3.3.2 Trajectory Approximation in Locally Dense Graphs

The approximation error of the optimal discrete flight path ξ_G according to (3.9) relative to the continuous optimum ξ_C of (3.7) due to the smaller admissible set $X_G \subset X$ depends on the density of the airway network. The discussion will be limited to a certain class of locally dense digraphs as defined in [8] (Chapter 2).

Definition 3.1. — *A digraph $G = (V, E)$ is said to be (h, ℓ) -dense in a convex set $\Omega \subset \mathbb{R}^2$ for $h, \ell \geq 0$, if it satisfies the following conditions:*

1. containment: $V \subset \Omega$
2. vertex density: $\forall p \in \Omega : \exists v \in V : \|p - v\| \leq h$
3. local connectivity: $\forall v, w \in V, \|v - w\| \leq \ell + 2h : (v, w) \in E$

An example for such an airway digraph is shown in Figure 3.2. Note that, even for $\ell \rightarrow 0$, the minimum local connectivity length of $2h$ guarantees that a vertex is connected to its neighbors. It is easy to show that any (h, ℓ) -dense digraph is connected, such that a path from origin to destination exists.

Let $\xi_C \in X$ be a global minimizer of the continuous problem formulation (3.7), and $\xi_G \in X_G$ be a shortest discrete path in the (h, ℓ) -dense airway digraph G satisfying (3.9). For establishing a bound for the excess flight duration in terms of the airway density, we first construct a particular discrete path $\xi_R(\xi_C) \in X_G$ using a rounding procedure, and derive a bound for $T(\xi_R) - T(\xi_C) \leq e(h, \ell)$, from which the actual error bound $T(\xi_G) - T(\xi_C) \leq e(h, \ell)$ immediately follows from optimality of ξ_G .

For defining $\xi_R(\xi) \in X_G$, with an (h, ℓ) -dense digraph G with $\ell > 0$, for a given continuous path $\xi \in \hat{X}$ with $\xi_\tau = \text{const}$, we first choose an equidistant grid $\tau_i = i/n$, $n = \lceil \xi_\tau / \ell \rceil$, for $i = 0, \dots, n$. By construction, the distance of the corresponding trajectory points is bounded by $\|\xi(\tau_i) - \xi(\tau_{i+1})\| \leq \ell$. For each i , there is some $v_i \in V$ with $\|v_i - \xi(\tau_i)\| \leq h$, such that $\|v_i - v_{i+1}\| \leq \ell + 2h$. Consequently, $(v_i, v_{i+1}) \in E$, and $(v_i)_{0 \leq i \leq n}$ is a valid discrete path, for which we define $[\xi_R] = \Xi(v_i)_i$.

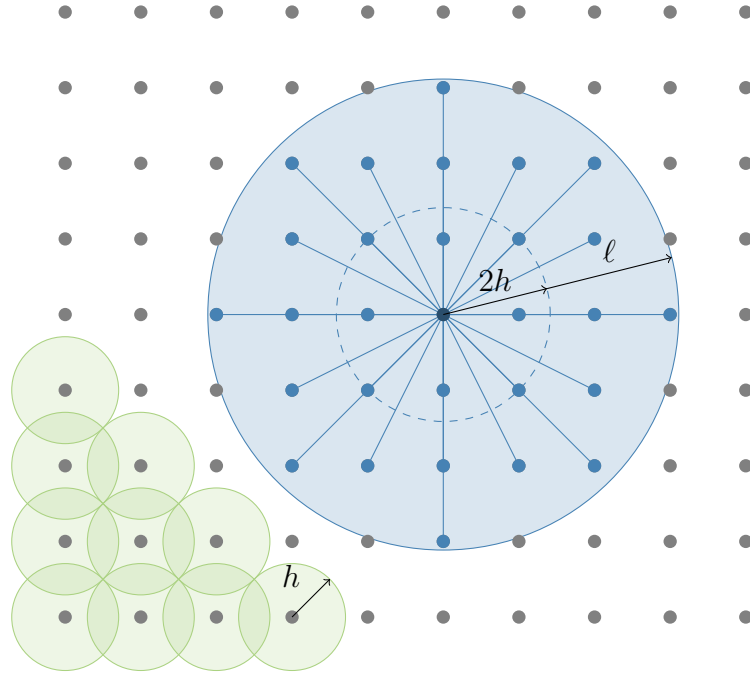


Figure 3.2: A locally densely connected digraph with cartesian structure. The center node (dark blue) is connected to all nodes in a circular neighborhood of radius $2h + \ell$ (light blue) with edges in both directions.

It is intuitively clear – and rigorously confirmed below – that the excess flight duration $T(\xi_R) - T(\xi_C)$ is affected by both, the spatial distance between ξ_R and ξ_C , e.g., taking a longer detour or flying through an area with adverse wind conditions, and the angular deviation, e.g., a zigzag path tends to take longer than a straight trajectory. In order to capture these effects, we will first bound the spatial distance $\|\xi_R - \xi_C\|_{L^\infty(0,1)}$ and the angular deviation $\|(\xi_R - \xi_C)_\tau\|_{L^\infty(0,1)}$, and equip the space of Lipschitz-continuous functions with the norm

$$\|f\|_{C^{0,1}(0,1)} := \|f\|_{L^\infty(0,1)} + \|f_\tau\|_{L^\infty(0,1)}.$$

Theorem 3.3. — Assume $\xi \in \hat{X} \cap C^{1,1}((0,1), \Omega)$ has bounded curvature, i.e., there is some $\bar{\sigma}$ with $\|\xi_\tau(a) - \xi_\tau(b)\| \leq \bar{\sigma}|a - b|$ for $a, b \in (0,1)$, and denote the length of the trajectory by $L = \|\xi_\tau\|$. Then, the following bounds hold for the discrete approximation $\xi_R(\xi)$ in an (h, ℓ) -dense digraph:

$$\text{(distance error)} \quad \|\xi_R(\xi) - \xi\|_{L^\infty(0,1)} \leq \frac{\bar{\sigma}\ell^2}{8L^2} + h, \quad (3.12)$$

$$\text{(angular error)} \quad \|(\xi_R(\xi) - \xi)_\tau\|_{L^\infty(0,1)} \leq \frac{\sqrt{2}\bar{\sigma}\ell}{L} + 2h \left(\frac{L}{\ell} + 1 \right). \quad (3.13)$$

If $\ell \leq L$, we obtain the total error bound

$$\begin{aligned} \|\xi_R(\xi) - \xi\|_{C^{0,1}(0,1)} &\leq \left(\frac{1}{8} + \sqrt{2}\right) \bar{\sigma} \frac{\ell}{L} + 2h \frac{L}{\ell} + 3h \\ &\leq 2\bar{\sigma} \frac{\ell}{L} + 2h \frac{L}{\ell} + 3h. \end{aligned} \quad (3.14)$$

Proof. Let $\hat{\xi}(\tau) = \xi(\tau_{\lfloor n\tau \rfloor}) + (n\tau - \lfloor n\tau \rfloor)(\xi(\tau_{\lceil n\tau \rceil}) - \xi(\tau_{\lfloor n\tau \rfloor}))$ be the linear interpolant of the continuous trajectory ξ on $n = \lceil L/\ell \rceil$ equisized intervals. Standard interpolation error estimates yield

$$\|(\hat{\xi} - \xi)(\tau)\| \leq \bar{\sigma}/(8n^2) \leq \frac{\bar{\sigma}\ell^2}{8L^2}$$

for all τ [23, Ch. 3.1, p. 93 ff.]. Moreover, with $\alpha = (n\tau - \lfloor n\tau \rfloor) \in [0, 1]$,

$$\begin{aligned} \hat{\xi}(\tau) - \xi_R(\tau) &= \xi(\tau_{\lfloor n\tau \rfloor}) - \xi_{R, \lfloor n\tau \rfloor} + \alpha \left(\xi(\tau_{\lceil n\tau \rceil}) - \xi_{R, \lceil n\tau \rceil} - \xi(\tau_{\lfloor n\tau \rfloor}) + \xi_{R, \lfloor n\tau \rfloor} \right) \\ &= (1 - \alpha) \left(\xi(\tau_{\lfloor n\tau \rfloor}) - \xi_{R, \lfloor n\tau \rfloor} \right) + \alpha \left(\xi(\tau_{\lceil n\tau \rceil}) - \xi_{R, \lceil n\tau \rceil} \right) \end{aligned} \quad (3.15)$$

implies $\|(\hat{\xi} - \xi_R)(\tau)\| \leq h$, which yields the distance error bound (3.12) by triangle inequality.

Let $\phi = (\hat{\xi} - \xi)_k$, $k \in \{1, 2\}$, be one of the two components of the difference between continuous trajectory and linear interpolant. By the mean value theorem, there is a point $\hat{\tau} \in]\tau_i, \tau_{i+1}[$ with $\phi_\tau(\hat{\tau}) = 0$. Thus,

$$|\phi_\tau(\tau)| = |\phi_\tau(\tau) - \phi_\tau(\hat{\tau})| \leq \frac{\bar{\sigma}}{n} \quad \forall \tau \in [\tau_i, \tau_{i+1}]$$

holds for all $i = 0, \dots, n-1$ and implies $\|(\hat{\xi} - \xi)_\tau(\tau)\| \leq \sqrt{2}\bar{\sigma}/n \leq \sqrt{2}\bar{\sigma}\ell/L$ for all τ . Moreover, (3.15) implies

$$(\hat{\xi} - \xi_R)_\tau(\tau) = -n \left(\xi(\tau_{\lfloor n\tau \rfloor}) - \xi_{R, \lfloor n\tau \rfloor} \right) + n \left(\xi(\tau_{\lceil n\tau \rceil}) - \xi_{R, \lceil n\tau \rceil} \right)$$

and therefore $\|(\hat{\xi} - \xi_R)_\tau\| \leq 2nh \leq 2h(L/\ell + 1)$ and yields the angular error bound (3.13) by triangle inequality. \square

Of course, if $\ell < \hat{\ell}$, then the (h, ℓ) -dense digraph G is a subgraph of the $(h, \hat{\ell})$ -dense digraph \hat{G} , provided their vertex sets coincide. Thus, the discretization error of a shortest path in \hat{G} is less or equal to one in G – a fact that is not reflected by

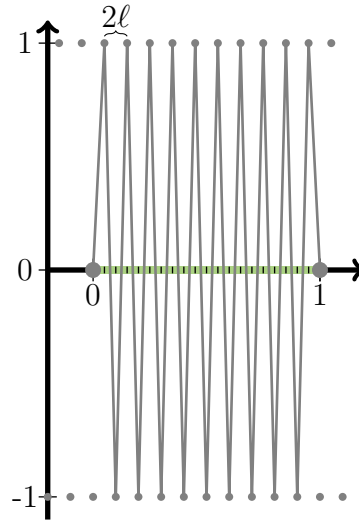


Figure 3.3: Illustration of Example 3.2. Green: continuous trajectory ξ , gray: rounded path ξ_R .

Theorem 3.3. The reason is the explicit rounding procedure, which tends to select arcs of length $\hat{\ell}$ in \hat{G} even if shorter arcs of length ℓ would be better. This effect can be essentially avoided if the connectivity length ℓ is chosen sufficiently small compared to the path length. It should not be chosen too small compared to h , however, because then the angular error can dominate, as the following pathological example shows.

Example 3.2. — Consider $\xi(\tau) = [\tau, 0]^T$ and

$$V = \{[l(2i + j), 2j - 1]^T \mid i, j \in \mathbb{Z}\} \cup \{[0, 0]^T, [1, 0]^T\}$$

with $\ell \ll 1$ and $h = \sqrt{1 + \ell^2/4} \approx 1$. Rounding to the nearest vertex yields a discrete zigzag path with length at least $2h/\ell$, as illustrated in Figure 3.3. Thus, the bounds (3.13) and (3.14) are asymptotically sharp for $\ell \rightarrow 0$.

Hence, we select a theoretically optimal ℓ by minimizing the error bound (3.14).

Theorem 3.4. — Under the assumptions of Theorem 3.3, including $\ell \leq L$, the choice

$$\ell = L\sqrt{\frac{h}{\bar{\sigma}}} \quad \Leftrightarrow \quad h = \bar{\sigma}\frac{\ell^2}{L^2}$$

is optimal with respect to the error bound (3.14) and yields the bounds

$$\|\xi_R(\xi) - \xi\|_{L^\infty(0,1)} \leq \frac{9\bar{\sigma}\ell^2}{8L^2}, \quad (3.16)$$

$$\|(\xi_R(\xi) - \xi)_\tau\|_{L^\infty(0,1)} \leq \frac{11\bar{\sigma}\ell}{2L}, \quad (3.17)$$

$$\|\xi_R(\xi) - \xi\|_{C^{0,1}(0,1)} \leq 7\bar{\sigma}\frac{\ell}{L}. \quad (3.18)$$

Proof. Straightforward minimization of (3.14) yields the given optimal choice of ℓ . Inserting this into (3.12), (3.13), and the bound (3.14) and using $\ell \leq L$ yields the claims. \square

The pathological Example 3.2 reveals a further limitation of the derivation of bounds by employing an explicit rounding procedure: the length of the rounded path ξ_R can be much larger than the length of the discretely optimal path ξ_G . In the example this is $\mathcal{O}(2/\ell) \rightarrow \infty$ compared to $\mathcal{O}(1)$, with ξ_G connecting the vertices along the horizontal line $[0, 1] \times \{1\}$. We point out that this susceptibility of the bound to pathological worst cases is structurally similar to common a priori error estimates for finite element methods [24]. Nevertheless, even if the angular error responsible for the pathological behavior is ignored, the same optimal order of $h = \mathcal{O}(\ell^2)$ is obtained.

3.3.3 Computable Error Bounds

Theorem 3.5. — *Assume that $\xi_C \in \hat{X} \cap C^{1,1}(0, 1)^2$ is a minimizer of (3.7) with bounded curvature, i.e., there is $\bar{\sigma} < \infty$ such that $\|\xi_\tau(a) - \xi_\tau(b)\| \leq \bar{\sigma}|a - b|$ for all $a, b \in (0, 1)$. Let $L = \|(\xi_C)_\tau\|$ denote the length of the optimal flight trajectory and $\bar{\alpha}_i := \max_{\tau \in (0,1)} \alpha_i(\xi_C(\tau))$ with α_i defined in Lemma 3.1. Then, there is a constant $r > 0$, such that the local bound*

$$T(\xi_G) - T(\xi_C) \leq \frac{4\bar{\sigma}^2\ell^2}{3L^2} \left(\frac{\ell^2}{L^2}\bar{\alpha}_0 + 5\frac{\ell}{L}\bar{\alpha}_1 + 23\bar{\alpha}_2 \right) \leq \frac{92\bar{\sigma}^2\bar{\alpha}_2}{3L^2}\ell^2 + \mathcal{O}(\ell^3) \quad (3.19)$$

holds for all (h, ℓ) -dense digraphs with $\ell \leq \min\left\{\frac{r}{7\bar{\sigma}}, 1\right\}L$ and $h \leq \frac{\bar{\sigma}\ell^2}{L^2}$.

Proof. Inserting the bounds (3.16) and (3.17) from Theorem 3.4 into the claim (3.11), we obtain

$$\begin{aligned} T(\xi_R) - T(\xi_C) &\leq \int_0^1 \left(\alpha_0 \frac{81\bar{\sigma}^2\ell^4}{64L^4} + \alpha_1 \frac{9\bar{\sigma}\ell^2}{8L^2} \frac{11\bar{\sigma}\ell}{2L} + \alpha_2 \frac{121\bar{\sigma}^2\ell^2}{4L^2} \right) d\tau \\ &< \frac{4\bar{\sigma}^2\ell^2}{3L^2} \int_0^1 \left(\alpha_0 \frac{\ell^2}{L^2} + 5\alpha_1 \frac{\ell}{L} + 23\alpha_2 \right) d\tau, \end{aligned}$$

since $\ell \leq \min\left\{\frac{r}{7\bar{\sigma}}, 1\right\}L$, where r is the neighborhood radius from Theorem 3.2 and α_i provided by Lemma 3.1. Inserting the upper bounds $\bar{\alpha}_i$ for α_i yields the claim. \square

Note that the bound holds in a certain neighborhood of a continuous minimizer ξ_C and therefore bounds the asymptotic error behavior for $h, \ell \rightarrow 0$, rather than providing a globally reliable error bound.

We can go one step further and eliminate the dependence on the actual optimal path ξ_C by choosing appropriate global bounds on the constants and route properties. For that, we define the global bounds

$$\bar{c}_0 := \|w\|_{L^\infty(\Omega)}, \quad \bar{c}_1 := \|w_x\|_{L^\infty(\Omega)}, \quad \text{and} \quad \bar{c}_2 := \|w_{xx}\|_{L^\infty(\Omega)}$$

for the wind and its derivatives.

Lemma 3.6. — *Let $\xi_C \in \hat{X}$ be a minimizer of (3.7). Further, let $\|w(p)\| \leq \bar{c}_0$ and $\|w_x(p)\| \leq \bar{c}_1 \forall p \in \Omega$. Then, it is twice continuously differentiable and its second derivative is bounded by*

$$\|(\xi_C)_{\tau\tau}\| \leq \bar{\sigma} := \frac{2\bar{v}\bar{c}_1L^2}{(\bar{v} - \bar{c}_0)^3} \left((1 + \sqrt{2})\bar{v} + \bar{c}_0 \right). \quad (3.20)$$

For $\bar{c}_0 \leq \bar{v}/\sqrt{5}$ this simplifies to $\bar{\sigma} \leq 17\frac{\bar{c}_1L^2}{\bar{v}}$.

Again, the proof of this Lemma is rather long and can be found in the appendix.

Lemma 3.7. — *Assume that ξ_C is a global minimizer of (3.7) with path length L and that $\bar{c}_0 \leq \bar{v}/\sqrt{5}$. Then*

$$\|x_D - x_O\| \leq L \leq \frac{\bar{v} + \bar{c}_0}{\bar{v} - \bar{c}_0} \|x_D - x_O\| < \frac{8}{3} \|x_D - x_O\|. \quad (3.21)$$

Proof. The lower bound is clear, since the trajectory can not be shorter than the straight connection. The flight time T_s on the straight line is at most $\frac{\|x_D - x_O\|}{\bar{v} - \bar{c}_0}$. Since ξ_G is optimal, we obtain

$$T_s \geq T(\xi_C) \geq \frac{L}{\bar{v} + \bar{c}_0},$$

which yields the upper bound for L . \square

We can now completely eliminate the need for a posteriori information about ξ_C and derive an *a priori* error bound.

Theorem 3.8. — *Let $\xi_C \in \hat{X} \cap C^{1,1}(0, 1)^2$ be a global continuous minimizer and ξ_G be a shortest path in the (h, ℓ) -dense graph G . Moreover, let $\tilde{L} := \|x_D - x_O\|$ and assume $\bar{c}_0 \leq \bar{v}/\sqrt{5}$. Then, with $\bar{\sigma}$ from Lemma 3.6, the following a priori error bound holds for sufficiently dense graphs:*

$$T(\xi_G) - T(\xi_C) \leq \frac{4\bar{\sigma}^2}{3\tilde{L}^3\bar{v}} \left(14\ell^2 \left(\frac{7}{2}\bar{c}_1^2 + \bar{v}\bar{c}_2 \right) + \frac{51\bar{c}_1\ell}{\bar{v}} + 52 \right) \ell^2 \quad (3.22)$$

$$\leq 1.5 \cdot 10^5 \frac{\bar{c}_1^2 \tilde{L}}{\bar{v}^3} \ell^2 + \mathcal{O}(\ell^3). \quad (3.23)$$

Proof. For $\underline{v}(p) = \sqrt{\bar{v}^2 - c_0^2(p)}$ we obtain $8\bar{v}/9 < \underline{v} \leq \bar{v}$. Lemma 3.7 together with α_i from Lemma 3.1 now yields the global bounds

$$\alpha_0(p) \leq \frac{8\tilde{L}}{3\underline{v}(p)^3} (12\bar{c}_1^2 + 4\underline{v}(p)\bar{c}_2) \leq \frac{14\tilde{L}}{\bar{v}} \left(\frac{7}{2}\bar{c}_1^2 + \bar{c}_2\bar{v} \right) =: \tilde{\alpha}_0,$$

$$\alpha_1(p) \leq \frac{8\bar{c}_1}{\underline{v}(p)^2} \leq \frac{81\bar{c}_1}{8\bar{v}^2} =: \tilde{\alpha}_1, \quad \text{and}$$

$$\alpha_2(p) \leq \frac{2}{\tilde{L}\underline{v}(p)} \leq \frac{9}{4\tilde{L}\bar{v}} =: \tilde{\alpha}_2.$$

Inserting them into (3.19) provides the bound

$$\begin{aligned} T(\xi_G) - T(\xi_C) &\leq T(\xi_R) - T(\xi_C) \\ &\leq \frac{4\bar{\sigma}^2\ell^2}{3\tilde{L}^2} \left(\frac{\ell^2}{\tilde{L}^2} \tilde{\alpha}_0 + 5\frac{\ell}{\tilde{L}} \tilde{\alpha}_1 + 23\tilde{\alpha}_2 \right) \\ &\leq \frac{4\bar{\sigma}^2\ell^2}{3\tilde{L}^2} \left(\frac{14\ell^2}{\tilde{L}\bar{v}} \left(\frac{7}{2}\bar{c}_1^2 + \bar{c}_2\bar{v} \right) + \frac{405\bar{c}_1\ell}{8\bar{v}^2\tilde{L}} + \frac{207}{4\tilde{L}\bar{v}} \right) \\ &\leq \frac{4\bar{\sigma}^2\ell^2}{3\tilde{L}^3\bar{v}} \left(14\ell^2 \left(\frac{7}{2}\bar{c}_1^2 + \bar{c}_2\bar{v} \right) + \frac{51\bar{c}_1\ell}{\bar{v}} + 52 \right), \end{aligned}$$

which completes the proof. \square

3.4 Numerical Examples

In Section 3.3 we derived three error bounds: i) the *a priori* bound (3.22), ii) the *local* bound (3.19), and iii) the computationally in general unavailable *a posteriori* bound (3.11). Now we validate these bounds with the four test problems from [8] (Chapter 2). For this comparison and for evaluating the *a posteriori* bound we compute the optimal continuous trajectory ξ_C numerically using a direct collocation approach to high accuracy.

3.4.1 Test Instances

The goal in all four test instances is to find a time-optimal trajectory from $x_O = [0, 0]^T$ to $x_D = [1, 0]^T$ through wind fields of varying spatial frequency, see Figure 3.4. The wind speed is always bounded by $\|w\| \leq \bar{w} = 0.5\bar{v}$. All values are chosen dimensionless, i.e., $\bar{v} = 1$. For the first test problem a) we define the laminar shear flow

$$w(p) = \left[\bar{w} \min\left(\max\left(\frac{2p_2}{H} - 1, -1\right), 1\right), 0 \right],$$

with $H = 0.5$, and p_2 denoting the y-component of p , see Figure 3.4 a). In problems b)–d), the wind w is the sum of an increasing number of non-overlapping vortices w_i , each of which is described by

$$w_i(p) = s_i \tilde{w}_i(r_i) \begin{bmatrix} -\sin(\alpha_i) \\ \cos(\alpha_i) \end{bmatrix},$$

where s_i is the spin of the vortex ($s_i = +1$: counter-clockwise, $s_i = -1$: clockwise), $r_i = \|p - z_i\|_2$ is the distance from the vortex center z_i , α_i is the angle between p , z_i , and the positive x -axis with $\tan(\alpha_i) = \frac{(p - z_i)_2}{(p - z_i)_1}$ and the absolute vortex wind speed \tilde{w}_i is a function of r and the vortex radius R_i :

$$\tilde{w}_i(r) = \begin{bmatrix} \bar{w} \exp\left(\frac{(r/R_i)^2}{(r/R_i)^2 - 1}\right) & \text{if } r < R_i \\ 0 & \text{otherwise} \end{bmatrix}.$$

More precisely, problems b)–d) involve 1, 15, and 50 regularly aligned vortices with $R = 1/2$, $1/8$, and $1/16$, respectively, see Figure 3.4 b)–d). Vortices with

positive spin (counter-clockwise) are colored green, vortices with negative spin (clockwise) are colored red.

Note that at least problem d) is clearly an exaggeration, as no commercial plane would ever try to traverse a wind field like this. We use this instance to provide evidence that our claims hold even under the most adverse conditions.

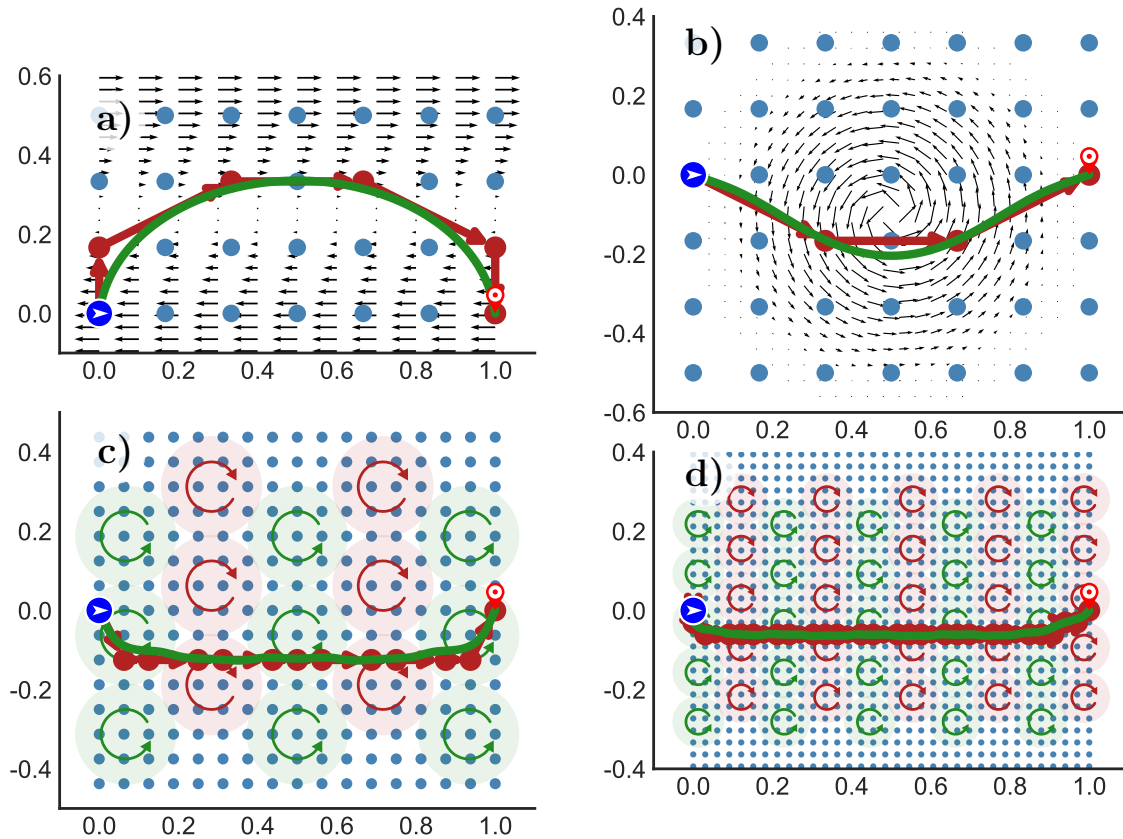


Figure 3.4: Test problems a)-d), $x_O = [0, 0]^T$, $x_D = [1, 0]^T$, $\bar{w} = \frac{1}{2}\bar{v}$. Blue dots: (h, ℓ) -dense rectangular network-graph of some exemplary density and connectivity, satisfying $h = \bar{\sigma}\ell^2/L^2$, red: shortest path on the graph, green: continuous optimal trajectory. Note that in every case the straight trajectory is particularly unfavorable.

3.4.2 Results

The three error bounds (i) *a priori*, ii) *local*, and iii) *a posteriori*) involve an increasing amount of information about the optimal trajectory ξ_C . Hence it is not surprising that the first is far from being sharp and overestimates the actual error by several orders of magnitude. This is mainly due to the worst case estimates that must be considered in several steps finding globally valid constants. Most importantly,

the wind speed and its derivatives need to be bounded globally, even though the conditions experienced along the actually flown path are usually much easier, as can be seen in Figure 3.4. On the other hand, the *a posteriori* requires information about the optimal trajectory, that is not available at the time of calculation. However, it helps us evaluate the more interesting question: how much can be gained by incorporating a posteriori information?

In order to answer this, we evaluate the error between a graph-based shortest path and the continuous optimum for various graph densities, respecting the optimal combination of node density and connectivity $h = \bar{\sigma}\ell^2/L^2$ as stated in Theorem 3.4. The results are shown in the double-logarithmic plots of Figure 3.5 as blue dots together with a linear regression.

The three bounds are illustrated in i) red, ii) purple and iii) gray. In the last case, the *a posteriori* bound (3.11), we depict the three individual parts of the integral by colored areas, from bottom to top: $\int \alpha_0 \|\delta\xi\|^2 d\tau$, $\int \alpha_1 \|\delta\xi\| \|\delta\xi_\tau\| d\tau$, $\int \alpha_2 \|\delta\xi_\tau\|^2 d\tau$. The linearly scaled depiction in Figure 3.6 makes it easier to see that the relative distribution of these parts is more or less stable over a wide range of graph densities. Each part is relevant and none is vanishing even for dense graphs. This suggests that the theoretically optimal choice of (h, ℓ) balances the error terms against each other evenly.

It needs to be mentioned, that, because we have only $\|w\|/\bar{v} \leq 0.5$ here (not $\leq 1/\sqrt{5}$), we cannot use α_i as stated in Lemma 3.1, but must revert to the results from Theorem 3.9 in the appendix. Since the purpose of that Lemma is solely to provide a more compact notation, however, this should not be of any concern. For the same reason, the coefficients in (3.22) also need to be adjusted accordingly.

We show linear trend lines for the *a posteriori* bound iii) and the experimental results, excluding the data of the 10% sparsest graphs (rightmost data points). Results in that region are dominated by effects of local minima (e.g., the continuous optimum goes left, while the discrete path goes right, which results in a large distance error) which vanish quickly and do not contribute to the asymptotical error behavior. As our error bounds were developed to hold in a certain neighborhood

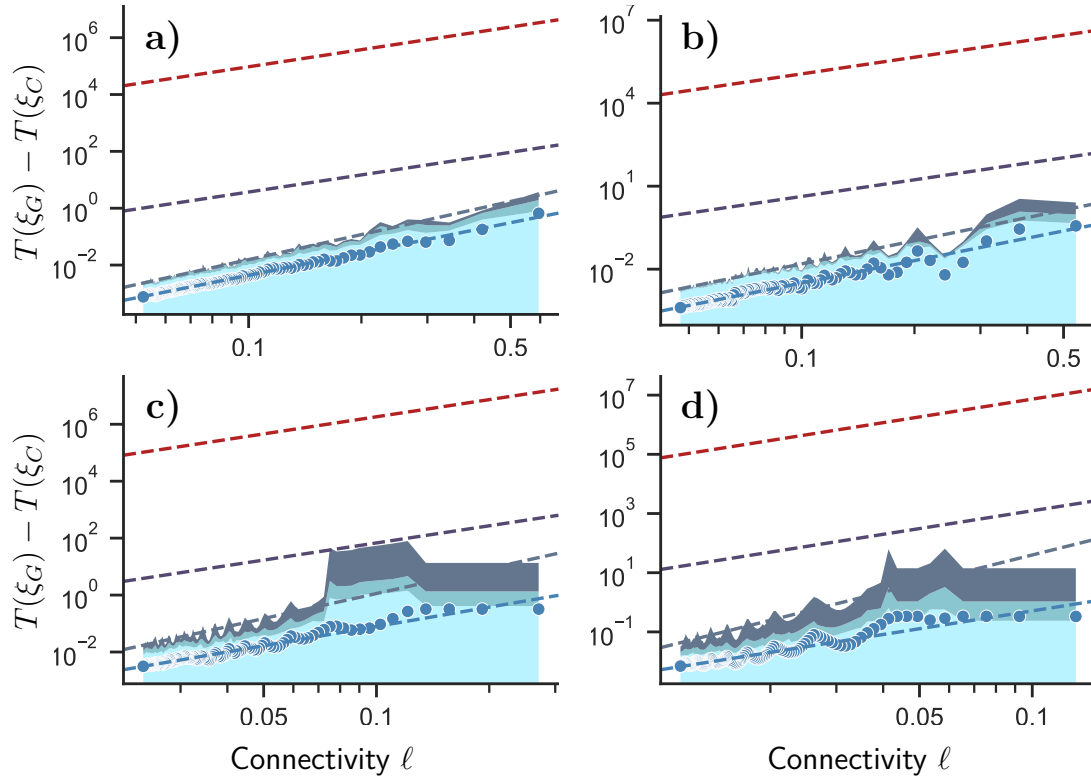


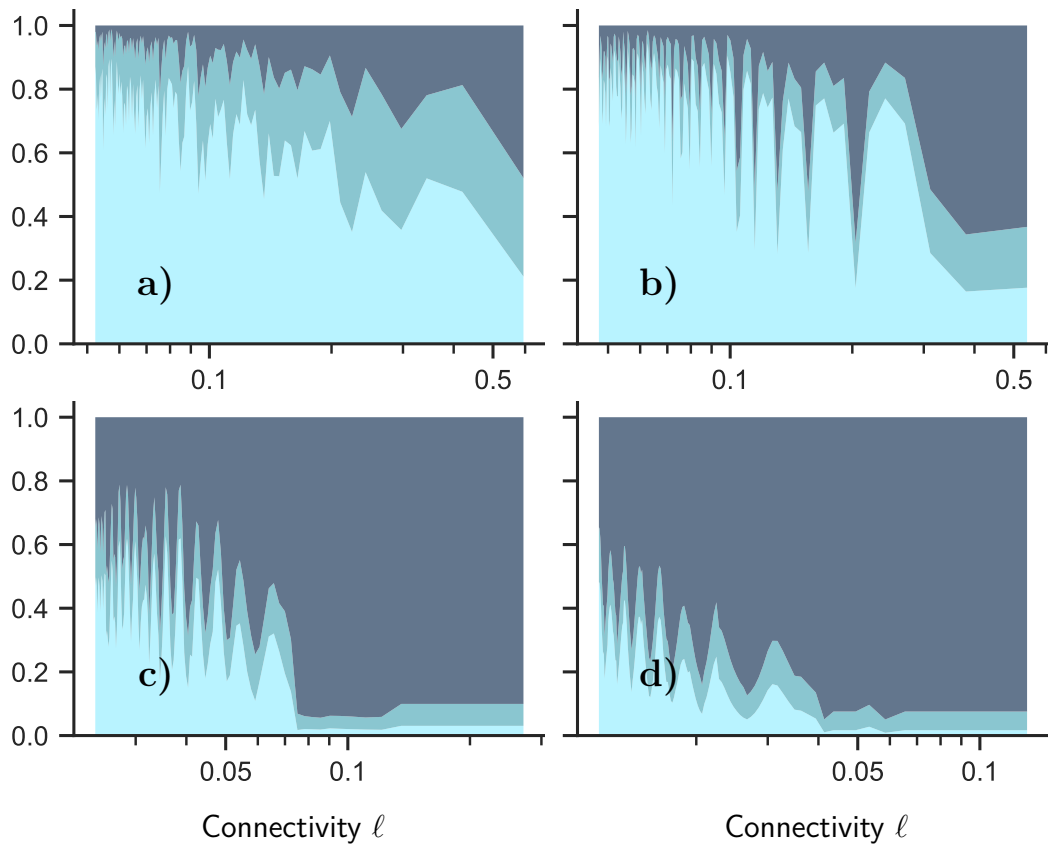
Figure 3.5: Evaluation of the derived error bounds i) *a priori* (top, red), ii) *local* (middle, purple), and iii) *a posteriori* (bottom, gray), comprising three terms visualized by the colored areas. From top to bottom: $\int \alpha_0 \|\delta\xi\|^2 d\tau$, $\int \alpha_1 \|\delta\xi\| \|\delta\xi_\tau\| d\tau$, $\int \alpha_2 \|\delta\xi_\tau\|^2 d\tau$. The blue dots represent results from numerical experiments together with a linear regression line. The sub-figures a)-d) refer to the corresponding test instances.

Table 3.1: Exponent p for the fitted trend lines ℓ^p of the *a posteriori* bound iii) and the numerical results for all four test instances a)-d) as depicted in Figure 3.5.

	a)	b)	c)	d)
theoretical (i) and ii)	2.84	2.65	2.65	2.79
iii) <i>a posteriori</i>	2.84	2.65	2.65	2.79
actual	2.64	2.69	2.25	2.00

Table 3.2: Average ratio between the bounds on $T(\xi_G) - T(\xi_C)$ and the actual differences for all four test cases a)-d).

	a)	b)	c)	d)
i) <i>a priori</i>	$2.6 \cdot 10^7$	$4.9 \cdot 10^7$	$3.1 \cdot 10^7$	$1.5 \cdot 10^7$
ii) <i>local</i>	$1.0 \cdot 10^3$	$1.8 \cdot 10^3$	$1.1 \cdot 10^3$	$2.5 \cdot 10^3$
iii) <i>a posteriori</i>	5.9	8.5	9.3	$1.1 \cdot 10^1$

**Figure 3.6:** Shares of the three parts of the *a posteriori* error bound; from top to bottom: $\int \alpha_0 \|\delta\xi\|^2 d\tau$, $\int \alpha_1 \|\delta\xi\| \|\delta\xi_\tau\| d\tau$, $\int \alpha_2 \|\delta\xi_\tau\|^2 d\tau$. The sub-figures a)-d) refer to the corresponding test instances. Note that on very sparse graphs (large ℓ , right) local minima lead to a dominating distance error term $\int \alpha_0 \|\delta\xi\|^2 d\tau$ (dark, top); this is irrelevant for asymptotic considerations.

of ξ_C , we ignore these effects. It is, however, interesting to see that the bounds hold anyway. This, together with the accumulation of data points on the left side, leads to a noticeable visual bias in the trend lines.

Remember that the i) *a priori* (3.22) and ii) the *local* error bound (3.19) both have the form

$$T(\xi_G) - T(\xi_C) \leq cl^2 + \mathcal{O}(l^3),$$

differing only in the constant c . As a first important result we point out that the quadratic order of these bounds matches the numerical results satisfyingly well. The exponents obtained from fitting a regression line to the numerical data and the evaluated *a posteriori* bound iii) according to (3.11) are listed in Table 3.1.

Further, starting from the *a priori* bound i), we note that the bound can be tightened significantly by incorporating a posteriori knowledge. With the *local* approach, the bound can already be improved by roughly four orders of magnitude, but taking all the *a posteriori* information into account clearly makes the biggest difference. In doing so, the bound comes close to the numerical data up to a factor of 6–11 (see Table 3.2) and can even resolve the aliasing artifacts.

Let us briefly discuss the visible oscillations in the actual errors. We consider the case d), as the effect is most prominent here. The optimal solution is to quickly switch to a mostly horizontal trajectory in the middle between the first and second row of vortices and to switch back very late, using the spin of both the very first and the very last vortex. Since the horizontal part of the trajectory amounts to the majority of the travel time, it is crucial to hit the right level between the two rows.

Graph-based shortest paths, which, unsurprisingly, tend to mimic this strategy, are, however, restricted to certain discrete levels. Consequently, the error is sensitive to the exact node positions. If the optimal level is matched by a row of nodes, the error will attain a minimum. On the other hand, if the nodes are positioned such that the optimal trajectory lies exactly between two rows of nodes, we see a maximum error. Obviously, these are nothing more than local deviations from a clear trend.

Finally, it is interesting to notice that in all four test cases the angular error term of the *a posteriori* bound $\int \alpha_2 \|\delta\xi_\tau\|^2 d\tau$ (light blue in Figure 3.5) would have been enough to bound the numerical data (blue dots) alone, which lets us conclude that, even though the bound is sharp in the worst case, in particular the average angular error is not perfectly captured.

3.5 Conclusion

Discretizing Zermelo’s navigation problem with a graph-based approach for computing global optima inevitably leads to approximation errors depending on the graph as well as the continuous optimal path. For a certain class of locally densely connected graphs we have derived three bounds on the excess flight duration in terms of graph and wind properties.

While the *local* bound improves on the *a priori* bound by four orders of magnitude, stressing the importance of using localized quantities if possible, it still is far from sharp in numerical examples. The – computationally in general unavailable – *a posteriori* bound, in contrast, is quite sharp, and thus indicates that the use of a posteriori error estimators providing rough approximations of the actual path error $\delta\xi$ can be expected to improve the bounds further. The observed convergence rates, however, agree well with the computational bounds in both cases.

The error bounds derived here can on the one hand guide the choice of optimal graph structures – the dependence of vertex density h to connectivity length ℓ as presented here is one example –, and on the other hand help identifying switchover points in hybrid discrete-continuous optimization algorithms [8] (Chapter 2).

Authors’ Contributions

Conceptualization, R.B and M.W.; methodology, M.W.; software, F.D.; validation, F.D.; formal analysis, M.W.; investigation, F.D. and M.W.; resources, R.B., F.D. and M.W.; data curation, F.D.; writing-original draft preparation, F.D. and M.W.; writing-review and editing, R.B.; visualization, F.D.; supervision, R.B.; project

administration, R.B. and M.W.; funding acquisition, R.B. and M.W.

All authors have read and agreed to the published version of the manuscript.

References

- [1] C. A. Wells, P. D. Williams, N. K. Nichols, D. Kalise, and I. Poll, “Reducing Transatlantic Flight Emissions by Fuel-Optimised Routing,” *Environ. Res. Letters*, vol. 16, no. 2, p. 025 002, 2021. DOI: 10.1088/1748-9326/abce82.
- [2] A. Schienle, “Solving the Time-Dependent Shortest Path Problem Using Super-Optimal Wind,” in *Operations Research Proceedings 2017*, Springer International Publishing, 2018, pp. 3–9. DOI: 10.1007/978-3-319-89920-6.
- [3] C. G. E. Boender and H. E. Romeijn, “Stochastic Methods,” in *Handbook of Global Optimization*. Springer US, 1995, pp. 829–869. DOI: 10.1007/978-1-4615-2025-2_15.
- [4] M. A. Lones, “Metaheuristics in Nature-Inspired Algorithms,” in *Proceedings of the Companion Publication of the 2014 Annual Conference on Genetic and Evolutionary Computation (GECCO Comp '14)*, Association for Computing Machinery, 2014, pp. 1419–1422. DOI: 10.1145/2598394.2609841.
- [5] P. Belotti, C. Kirches, S. Leyffer, J. Linderoth, J. Luedtke, and A. Mahajan, “Mixed-Integer Nonlinear Optimization,” *Acta Numerica*, vol. 22, pp. 1–131, 2013. DOI: 10.1017/S0962492913000032.
- [6] C. A. Floudas and C. E. Gounaris, “A Review of Recent Advances in Global Optimization,” *Journal of Global Optimization*, vol. 45, no. 1, pp. 3–38, 2009. DOI: 10.1007/s10898-008-9332-8.
- [7] A. Knudsen, M. Chiarandini, and K. Larsen, “Heuristic Variants of A* Search for 3D Flight Planning,” in *Integration of Constraint Programming, Artificial Intelligence, and Operations Research*, Springer International Publishing, 2018, pp. 361–376. DOI: 10.1007/978-3-319-93031-2_26.
- [8] R. Borndörfer, F. Danecker, and M. Weiser, “A Discrete-Continuous Algorithm for Free Flight Planning,” *Algorithms*, vol. 14, no. 1, p. 4, 2021. DOI: 10.3390/a14010004.
- [9] M. Blanco, R. Borndörfer, N.-D. Hoang, A. Kaier, A. Schienle, T. Schlechte, and S. Schlobach, “Solving Time Dependent Shortest Path Problems on Airway Networks Using Super-Optimal Wind,” in *16th Workshop on Algorithmic Approaches for Transportation Modelling, Optimization, and Systems (ATMOS 2016)*, vol. 54, Schloss Dagstuhl–Leibniz-Zentrum fuer Informatik, 2016, pp. 1–15. DOI: 10.4230/OASIcs.ATMOS.2016.12.

- [10] M. Blanco, R. Borndörfer, N. D. Hoàng, A. Kaier, P. Maristany de las Casas, S. Thomas, and S. Schlobach, “Cost Projection Methods for the Shortest Path Problem with Crossing Costs,” in *17th Workshop on Algorithmic Approaches for Transportation Modelling, Optimization, and Systems (ATMOS 2017)*, vol. 59, Schloss Dagstuhl–Leibniz-Zentrum fuer Informatik, 2017, pp. 1–14. DOI: 10.4230/OASIcs.ATMOS.2017.15.
- [11] L. Yang, J. Qi, D. Song, J. Xiao, J. Han, and Y. Xia, “Survey of Robot 3D Path Planning Algorithms,” *Journal of Control Science and Engineering*, pp. 1687–5249, 2016. DOI: 10.1155/2016/7426913.
- [12] E. Zermelo, “Über das Navigationsproblem bei ruhender oder veränderlicher Windverteilung,” *ZAMM-Journal of Applied Mathematics and Mechanics/Zeitschrift für Angewandte Mathematik und Mechanik*, vol. 11(2), pp. 114–124, 1931. DOI: 10.1002/zamm.19310110205.
- [13] N. Weaver, *Lipschitz Algebras*, 2nd ed. World Scientific, 2018. DOI: 10.1142/9911.
- [14] B. Geiger, J. Horn, A. DeLullo, A. Niessner, and L. Long, “Optimal Path Planning of UAVs Using Direct Collocation with Nonlinear Programming,” in *AIAA Guidance, Navigation, and Control Conference and Exhibit*, American Institute of Aeronautics and Astronautics, Inc., 2006. DOI: 10.2514/6.2006-6199.
- [15] H. K. Ng, B. Sridhar, S. Grabbe, and N. Chen, “Cross-Polar Aircraft Trajectory Optimization and the Potential Climate Impact,” in *IEEE/AIAA 30th Digital Avionics Systems Conference*, 2011, pp. 1–15. DOI: 10.1109/DASC.2011.6096060.
- [16] H. K. Ng, B. Sridhar, and S. Grabbe, “Optimizing Aircraft Trajectories with Multiple Cruise Altitudes in the Presence of Winds,” *Journal of Aerospace Information Systems*, vol. 11, no. 1, pp. 35–47, 2014. DOI: 10.2514/1.I010084.
- [17] M. R. Jardin and A. E. Bryson, “Methods for Computing Minimum-Time Paths in Strong Winds,” *Journal of Guidance, Control, and Dynamics*, vol. 35(1), pp. 165–171, 2012. DOI: 10.2514/1.53614.
- [18] A. Marchidan and E. Bakolas, “Numerical Techniques for Minimum-Time Routing on a Sphere with Realistic Winds,” *American Institute of Aeronautics and Astronautics*, 2016. DOI: 10.2514/1.G001389.
- [19] L. Techy, “Optimal Navigation in Planar Time-Varying Flow: Zermelo’s Problem Revisited,” *Intelligent Service Robotics 4.4*, pp. 271–283, 2011. DOI: 10.1007/s11370-011-0092-9.
- [20] J. Betts and E. Cramer, “Application of Direct Transcription to Commercial Aircraft Trajectory Optimization,” *Journal of Guidance, Control and Dynamics*, vol. 18, no. 1, pp. 151–159, 1995. DOI: 10.2514/3.56670.

- [21] P. Hagelauer and F. Mora-Camino, “A Soft Dynamic Programming Approach for On-Line Aircraft 4D-Trajectory Optimization,” *European Journal of Operations Research*, vol. 107, no. 1, pp. 87–95, 1998. DOI: 10.1016/S0377-2217(97)00221-X.
- [22] A. Madkour, W. G. Aref, F. U. Rehman, M. A. Rahman, and S. Basalamah, “A Survey of Shortest-Path Algorithms,” *Computing Research Repository*, 2017. DOI: 10.48550/arXiv.1705.02044.
- [23] K. Atkinson and W. Han, *Theoretical Numerical Analysis: A Functional Analysis Framework*, 3rd ed. Springer New York, 2009, vol. 39. DOI: 10.1007/978-1-4419-0458-4.
- [24] P. Deuffhard and M. Weiser, *Adaptive Numerical Solution of PDEs*. de Gruyter, 2012. DOI: 10.1515/9783110283112.

3.A Appendix

Recall from (3.3) the derivative

$$f(\xi, \xi_\tau) = \frac{-\xi_\tau^T w(\xi) + \sqrt{(\xi_\tau^T w(\xi))^2 + (\bar{v}^2 - \|w(\xi)\|^2)\xi_\tau^2}}{\bar{v}^2 - \|w(\xi)\|^2}$$

of the time parametrization $t(\tau)$. Here, we will compute and bound its second derivative with respect to ξ and ξ_τ in terms of the wind w and its derivatives.

Theorem 3.9. — *Let $c_0(\xi) = \|w(\xi)\| < \bar{v}$, $c_1(\xi) = \|w_x(\xi)\|$, and $c_2(\xi) = \|w_{xx}(\xi)\|$. Moreover, let $L = \xi_\tau > 0$. Then, the second total directional derivative of f is bounded by*

$$f(\xi, \xi_\tau)''[\delta\xi, \delta\xi_\tau]^2 \leq \alpha_0(\xi)\|\delta\xi\|^2 + \alpha_1(\xi)\|\delta\xi\|\|\delta\xi_\tau\| + \alpha_2(\xi)\|\delta\xi_\tau\|^2$$

with

$$\begin{aligned} \underline{v}^2 &= \bar{v}^2 - c_0^2, \\ \alpha_0 &= L \left[\frac{c_1^2}{\underline{v}^3} \left(1 + 6\frac{c_0}{\underline{v}} + 2\frac{\sqrt{\bar{v}^2 + c_0^2}}{\underline{v}} + 6\frac{c_0^2}{\underline{v}^2} + 8\frac{c_0^3}{\underline{v}^3} + 8\frac{c_0^2\sqrt{\bar{v}^2 + c_0^2}}{\underline{v}^3} \right) \right. \\ &\quad \left. + \frac{c_2}{\underline{v}^2} \left(1 + 2\frac{c_0}{\underline{v}} + 2\frac{c_0^2}{\underline{v}^2} + 2\frac{c_0\sqrt{\bar{v}^2 + c_0^2}}{\underline{v}^2} \right) \right], \\ \alpha_1 &= \frac{c_1}{\underline{v}^2} \left[2 + 8\frac{c_0}{\underline{v}} + 4\frac{c_0^2}{\underline{v}^2} + 8\frac{c_0^3}{\underline{v}^3} \right], \\ \alpha_2 &= \frac{1}{\underline{v}L} \left[1 + 3\frac{c_0^2}{\underline{v}^2} \right]. \end{aligned}$$

Proof. The derivative $f = t_\tau$ of parametrized time consists of two terms, the tailwind term

$$f_1 = -\frac{\xi_\tau^\top w}{g}, \quad g = \bar{v}^2 - w^\top w,$$

and the length term

$$f_2 = g^{-1} \left((\xi_\tau^\top w)^2 + g(\xi_\tau^\top \xi_\tau) \right)^{1/2}.$$

At each time τ , we obtain

$$\underline{v}^2 := \bar{v}^2 - c_0^2 \leq g \leq \bar{v}^2.$$

The directional derivatives of g in direction $(\delta\xi, \delta\xi_\tau)$ read

$$g' \delta\xi = -2w^\top w_x \delta\xi \quad \Rightarrow \quad \|g'\| \leq 2c_0 c_1$$

and, as we are only interested in second order directional derivatives,

$$\delta\xi^\top g'' \delta\xi = -2\delta\xi^\top (w_x^\top w_x + w^\top w_{xx}) \delta\xi \quad \Rightarrow \quad \|g''\| \leq 2(c_1^2 + c_0 c_2).$$

For the tailwind term, we consider

$$f_1' \delta\xi = -g^{-2} \left((\delta\xi_\tau^\top w + \xi_\tau^\top w_x \delta\xi) g - \xi_\tau^\top w g' \delta\xi \right).$$

Again, we are only interested in second directional derivatives and thus consider

$$\begin{aligned} f_1''[\delta\xi, \delta\xi] &= - \left[-2g^{-3} g' \delta\xi \left((\delta\xi_\tau^\top w + \xi_\tau^\top w_x \delta\xi) g - \xi_\tau^\top w g' \delta\xi \right) \right. \\ &\quad + g^{-2} \left((\delta\xi_\tau^\top w_x \delta\xi + \delta\xi^\top (\xi_\tau^\top w_{xx}) \delta\xi + \delta\xi_\tau^\top w_x \delta\xi) g \right. \\ &\quad \quad + (\delta\xi_\tau^\top w + \xi_\tau^\top w_x \delta\xi) g' \delta\xi - \delta\xi_\tau^\top w g' \delta\xi \\ &\quad \quad \left. \left. - \xi_\tau^\top w_x \delta\xi^\top g' \delta\xi - \xi_\tau^\top w \delta\xi^\top g'' \delta\xi \right) \right] \\ &= \delta\xi^\top \left[2g^{-2} w_x^\top \xi_\tau g' - 2g^{-3} g' \xi_\tau^\top w g' - g^{-1} (\xi_\tau^\top w_{xx}) \right. \\ &\quad \quad \left. - g^{-2} w_x^\top \xi_\tau g' + g^{-2} w_x^\top \xi_\tau g' + g^{-2} \xi_\tau^\top w g'' \right] \delta\xi \\ &\quad + \delta\xi_\tau^\top \left[2g^{-2} w g' - 2g^{-1} w_x - g^{-2} w g' + g^{-2} w g' \right] \delta\xi \\ &= \delta\xi^\top \left[2g^{-2} w_x^\top \xi_\tau g' - 2g^{-3} g' \xi_\tau^\top w g' - g^{-1} (\xi_\tau^\top w_{xx}) + g^{-2} \xi_\tau^\top w g'' \right] \delta\xi \\ &\quad + \delta\xi_\tau^\top \left[2g^{-2} w g' - 2g^{-1} w_x \right] \delta\xi. \end{aligned}$$

Now we turn to f_2 , first considering the term $F := (\xi_\tau^\top w)^2 + g(\xi_\tau^\top \xi_\tau)$ with

$$\underline{v}^2 L^2 \leq F \leq L^2(\bar{v}^2 + c_0^2).$$

Then,

$$F' \delta \xi = 2\xi_\tau^\top w (\delta \xi_\tau^\top w + \xi_\tau^\top w_x \delta \xi) + g' \delta \xi \xi_\tau^\top \xi_\tau + 2g \xi_\tau^\top \delta \xi_\tau$$

and

$$\begin{aligned} F''[\delta \xi, \delta \xi] &= 2(\delta \xi_\tau^\top w + \xi_\tau^\top w_x \delta \xi)^2 \\ &\quad + 2\xi_\tau^\top w (\delta \xi_\tau^\top w_x \delta \xi + \delta \xi_\tau^\top w_x \delta \xi + \delta \xi^\top (\xi_\tau^\top w_{xx}) \delta \xi) \\ &\quad + \delta \xi^\top g'' \delta \xi \xi_\tau^\top \xi_\tau + 2g' \delta \xi \xi_\tau^\top \delta \xi_\tau + 2g' \delta \xi \xi_\tau^\top \delta \xi_\tau + 2g \delta \xi_\tau^\top \delta \xi_\tau \\ &= \delta \xi^\top \left[2w_x^\top \xi_\tau \xi_\tau^\top w_x + 2\xi_\tau^\top w (\xi_\tau^\top w_{xx}) + \xi_\tau^\top \xi_\tau g'' \right] \delta \xi \\ &\quad + \delta \xi_\tau^\top \left[4w \xi_\tau^\top w_x + 4\xi_\tau^\top w w_x + 4\xi_\tau g' \right] \delta \xi \\ &\quad + \delta \xi_\tau^\top \left[2w w^\top + 2g \right] \delta \xi_\tau. \end{aligned}$$

For $f_2 = g^{-1} \sqrt{F}$, we thus obtain

$$f_2' \delta \xi = -g^{-2} g' \delta \xi F^{1/2} + \frac{1}{2} g^{-1} F^{-1/2} F' \delta \xi.$$

The second directional derivative is

$$\begin{aligned} f_2''[\delta \xi, \delta \xi] &= 2g^{-3} (g' \delta \xi)^2 F^{1/2} - g^{-2} \delta \xi^\top g'' \delta \xi F^{1/2} - g^{-2} g' \delta \xi \frac{1}{2} F^{-1/2} F' \delta \xi \\ &\quad - \frac{1}{2} g^{-2} g' \delta \xi F^{-1/2} F' \delta \xi - \frac{1}{4} g^{-1} F^{-3/2} (F' \delta \xi)^2 \\ &\quad + \frac{1}{2} g^{-1} F^{-1/2} \delta \xi^\top F'' \delta \xi \\ &= 2g^{-3} (g' \delta \xi)^2 F^{1/2} - g^{-2} \delta \xi^\top g'' \delta \xi F^{1/2} - g^{-2} g' \delta \xi F^{-1/2} F' \delta \xi \\ &\quad - \frac{1}{4} g^{-1} F^{-3/2} (F' \delta \xi)^2 + \frac{1}{2} g^{-1} F^{-1/2} \delta \xi^\top F'' \delta \xi. \end{aligned}$$

Adding f_1'' and f_2'' , we finally obtain

$$\begin{aligned}
f''(\xi, \xi_\tau)[\delta\xi, \delta\xi_\tau]^2 &= (f_1'' + f_2'')[\delta\xi, \delta\xi_\tau]^2 \\
&= -2g^{-3}(g'\delta\xi)^2(\xi_\tau^\top w) && + g^{-2}(\delta\xi^\top g''\delta\xi)(\xi_\tau^\top w) \\
&\quad + 2g^{-2}(g'\delta\xi)(\xi_\tau^\top w_x\delta\xi) && - g^{-1}w_{xx}[\xi_\tau, \delta\xi, \delta\xi] \\
&\quad + 2g^{-2}(g'\delta\xi)(\delta\xi_\tau^\top w) && - 2g^{-1}(\delta\xi_\tau^\top w_x\delta\xi), \\
&\quad + 2g^{-3}(g'\delta\xi)^2F^{1/2} && - g^{-2}(\delta\xi^\top g''\delta\xi)F^{1/2} \\
&\quad - g^{-2}(g'\delta\xi)F^{-1/2}F'[\delta\xi, \delta\xi_\tau] && + \frac{1}{2}g^{-1}F^{-1/2}F''[\delta\xi, \delta\xi_\tau]^2 \\
&\quad - \frac{1}{4}g^{-1}F^{-3/2}(F'[\delta\xi, \delta\xi_\tau])^2,
\end{aligned}$$

which is bounded by

$$\begin{aligned}
|f''(\xi, \xi_\tau)[\delta\xi, \delta\xi_\tau]^2| &\leq L \left[\frac{c_1^2}{\underline{v}^3} \left(1 + 6\frac{c_0}{\underline{v}} + 2\frac{\sqrt{\bar{v}^2 + c_0^2}}{\underline{v}} + 6\frac{c_0^2}{\underline{v}^2} + 8\frac{c_0^3}{\underline{v}^3} + 8\frac{c_0^2\sqrt{\bar{v}^2 + c_0^2}}{\underline{v}^3} \right) \right. \\
&\quad \left. + \frac{c_2}{\underline{v}^2} \left(1 + 2\frac{c_0}{\underline{v}} + 2\frac{c_0^2}{\underline{v}^2} + 2\frac{c_0\sqrt{\bar{v}^2 + c_0^2}}{\underline{v}^2} \right) \right] \|\delta\xi\|^2 \\
&\quad + \frac{c_1}{\underline{v}^2} \left[2 + 8\frac{c_0}{\underline{v}} + 4\frac{c_0^2}{\underline{v}^2} + 8\frac{c_0^3}{\underline{v}^3} \right] \|\delta\xi\| \|\delta\xi_\tau\| \\
&\quad + \frac{1}{\underline{v}L} \left[1 + 3\frac{c_0^2}{\underline{v}^2} \right] \|\delta\xi_\tau\|^2.
\end{aligned}$$

□

Since the claim of Theorem 3.9 is rather unwieldy, we simplify it, finally proving Lemma 3.1.

Lemma 3.1. — *For any $p \in \Omega$ let $c_0(p) = \|w(p)\|$, $c_1(p) = \|w_x(p)\|$, and $c_2(p) = \|w_{xx}(p)\|$, and assume $c_0 \leq \bar{v}/\sqrt{5}$. Moreover, let $\xi \in \hat{X}$, $L := \xi_\tau > 0$ and $\underline{v}^2(p) := \bar{v}^2 - c_0^2(p)$. Then*

$$\begin{aligned}
\alpha_0(p) &\leq \frac{L}{\underline{v}^3(p)} \left(12c_1^2(p) + 4c_2(p)\underline{v}(p) \right), \\
\alpha_1(p) &\leq \frac{8c_1(p)}{\underline{v}^2(p)}, \\
\alpha_2(p) &\leq \frac{2}{L\underline{v}(p)}
\end{aligned}$$

hold in Theorem 3.9.

Proof. Let $s := c_0/\bar{v}$ be the relative wind speed. Then

$$\begin{aligned}\frac{c_0}{\underline{v}} &= \frac{s\bar{v}}{\sqrt{\bar{v}^2 - s^2\bar{v}^2}} = \frac{s}{\sqrt{1 - s^2}} \leq \frac{1}{2}, \\ 1 &\leq \frac{\sqrt{c_0^2 + \bar{v}^2}}{\underline{v}} \leq \sqrt{\frac{3}{2}},\end{aligned}$$

and

$$\frac{\bar{v}}{\underline{v}} = \frac{\bar{v}}{\sqrt{\bar{v}^2 - s^2\bar{v}^2}} = \frac{1}{\sqrt{1 - s^2}} \leq \frac{\sqrt{5}}{2},$$

which allows to bound

$$\begin{aligned}\alpha_0 &:= L \left[\frac{c_1^2}{\underline{v}^3} \left(1 + 6\frac{c_0}{\underline{v}} + 2\frac{\sqrt{\bar{v}^2 + c_0^2}}{\underline{v}} + 6\frac{c_0^2}{\underline{v}^2} + 8\frac{c_0^3}{\underline{v}^3} + 8\frac{c_0^2\sqrt{\bar{v}^2 + c_0^2}}{\underline{v}^3} \right) \right. \\ &\quad \left. + \frac{c_2}{\underline{v}^2} \left(1 + 2\frac{c_0}{\underline{v}} + 2\frac{c_0^2}{\underline{v}^2} + 2\frac{c_0\sqrt{\bar{v}^2 + c_0^2}}{\underline{v}^2} \right) \right] \\ &\leq \left[\frac{c_1^2}{\underline{v}^3} \left(\frac{13}{2} + 4\sqrt{\frac{3}{2}} \right) + \frac{c_2}{\underline{v}^2} \left(\frac{5}{2} + \sqrt{\frac{3}{2}} \right) \right] \\ &\leq L \left(12\frac{c_1^2}{\underline{v}^3} + 4\frac{c_2}{\underline{v}^2} \right),\end{aligned}$$

as well as

$$\alpha_1 := \frac{c_1}{\underline{v}^2} \left[2 + 8\frac{c_0}{\underline{v}} + 4\frac{c_0^2}{\underline{v}^2} + 8\frac{c_0^3}{\underline{v}^3} \right] \leq \frac{8c_1}{\underline{v}^2},$$

and

$$\alpha_2 := \frac{1}{\underline{v}L} \left[1 + 3\frac{c_0^2}{\underline{v}^2} \right] \leq \frac{7}{4\underline{v}L} \leq \frac{2}{L\underline{v}}.$$

□

Lemma 3.6. — *Let $\xi_C \in \hat{X}$ be a minimizer of (3.7). Further, let $\|w(p)\| \leq \bar{c}_0$ and $\|w_x(p)\| \leq \bar{c}_1 \forall p \in \Omega$. Then, it is twice continuously differentiable and its second derivative is bounded by*

$$\|(\xi_C)_{\tau\tau}\| \leq \bar{\sigma} := \frac{2\bar{v}\bar{c}_1L^2}{(\bar{v} - \bar{c}_0)^3} \left((1 + \sqrt{2})\bar{v} + \bar{c}_0 \right). \quad (3.24)$$

For $\bar{c}_0 \leq \bar{v}/\sqrt{5}$ this simplifies to $\bar{\sigma} \leq 17\frac{\bar{c}_1L^2}{\bar{v}}$.

Proof. The optimal control problem (3.2) has originally been formulated by Zermelo [12] in terms of the heading angle φ in unscaled time t instead of the airspeed v in scaled time τ , which are related by

$$v(t) = \bar{v} \begin{bmatrix} \cos \varphi(t) \\ \sin \varphi(t) \end{bmatrix}. \quad (3.25)$$

The Hamiltonian formalism yields an expression for the heading angle rate of an optimal trajectory,

$$\varphi_t = w_x : B, \quad B := \begin{bmatrix} \cos \varphi \sin \varphi & -\cos^2 \varphi \\ \sin^2 \varphi & -\cos \varphi \sin \varphi \end{bmatrix},$$

with “:” denoting tensor contraction, and confirms the regularity of ξ . Note that $\|B\|_F = \sqrt{2}$, where $\|\cdot\|_F$ denotes the Frobenius norm. By the chain rule, (3.25) yields

$$v_t = \bar{v} \begin{bmatrix} -\sin \varphi \\ \cos \varphi \end{bmatrix} \varphi_t$$

and the bound

$$\|v_t\| = \bar{v} |\varphi_t| \leq \bar{v} \|w_x\|_F \|B\|_F \leq \sqrt{2} \bar{v} \bar{c}_1. \quad (3.26)$$

For the ground speed $x_t(t) \stackrel{(3.1)}{=} v(t) + w(x(t))$ we thus obtain

$$\bar{v} - \bar{c}_0 \leq \|x_t\| \leq \bar{v} + \bar{c}_0 \quad (3.27)$$

and

$$\|x_{tt}\| \leq \|v_t + w_x x_t\| \stackrel{(3.26)}{\stackrel{(3.27)}}{\leq} \bar{c}_1 \left((1 + \sqrt{2}) \bar{v} + \bar{c}_0 \right). \quad (3.28)$$

The flight path ξ_C (omitting the subscript C in the following) with constant ground speed $\|\xi_\tau\| = L$ is related to the actual flight path x by $\xi(\tau) = x(t(\tau))$ with $t : [0, T] \rightarrow [0, 1]$ being a monotone bijection. Therefore,

$$\xi_\tau = x_t(t) t_\tau \quad (3.29)$$

yields

$$L = \|\xi_\tau\| = \|x_t\| t_\tau \stackrel{(3.27)}{\geq} (\bar{v} - \bar{c}_0) t_\tau \quad \Rightarrow \quad t_\tau \leq \frac{L}{\bar{v} - \bar{c}_0}. \quad (3.30)$$

For the second derivative, we note that

$$0 = (L^2)_\tau = (\xi_\tau^\top \xi_\tau)_\tau = 2\xi_{\tau\tau}^\top \xi_\tau,$$

which means that the curvature vector $\xi_{\tau\tau}$ is orthogonal to the path and the ground velocity ξ_τ (and x_t). Consequently, we obtain

$$0 = (\xi_\tau^\top \xi_\tau)_\tau \stackrel{(3.29)}{=} (\xi_\tau^\top x_t t_\tau)_\tau = \underbrace{\xi_{\tau\tau}^\top x_\tau}_{=0} t_\tau + \xi_\tau^\top x_{\tau\tau} t_\tau^2 + \xi_\tau^\top x_\tau t_{\tau\tau} \stackrel{(3.29)}{=} \xi_\tau^\top x_{\tau\tau} t_\tau^2 + \frac{L^2}{t_\tau} t_{\tau\tau}$$

and therefore

$$|t_{\tau\tau}| \leq \frac{t_\tau}{L^2} \|\xi_\tau\| \|x_{\tau\tau}\| t_\tau^2 \stackrel{(3.28)}{\leq} \frac{\bar{c}_1 t_\tau^3}{L} \left((1 + \sqrt{2})\bar{v} + \bar{c}_0 \right). \quad (3.31)$$

Now we can bound

$$\begin{aligned} \|\xi_{\tau\tau}\| &\stackrel{(3.29)}{=} \|x_{tt} t_\tau^2 + x_t t_{\tau\tau}\| \\ &\leq \|x_{tt}\| t_\tau^2 + \|x_t\| |t_{\tau\tau}| \\ &\stackrel{(3.27)}{\leq} \bar{c}_1 \left((1 + \sqrt{2})\bar{v} + \bar{c}_0 \right) t_\tau^2 + (\bar{v} + \bar{c}_0) \frac{\bar{c}_1 t_\tau^3}{L} \left((1 + \sqrt{2})\bar{v} + \bar{c}_0 \right) \\ &\stackrel{(3.28)}{\leq} \bar{c}_1 t_\tau^2 \left((1 + \sqrt{2})\bar{v} + \bar{c}_0 \right) \left(1 + (\bar{v} + \bar{c}_0) \frac{t_\tau}{L} \right) \\ &\stackrel{(3.30)}{\leq} \frac{\bar{c}_1 L^2}{(\bar{v} - \bar{c}_0)^2} \left((1 + \sqrt{2})\bar{v} + \bar{c}_0 \right) \left(1 + \frac{\bar{v} + \bar{c}_0}{\bar{v} - \bar{c}_0} \right) \\ &= \frac{2\bar{v}\bar{c}_1 L^2}{(\bar{v} - \bar{c}_0)^3} \left((1 + \sqrt{2})\bar{v} + \bar{c}_0 \right), \end{aligned}$$

which completes the proof. \square

CHAPTER **4**

A Discrete-Continuous Algorithm for Globally Optimal Free Flight Trajectory Optimization

Borndörfer, R., Danecker, F., and Weiser, M.
22nd Symposium on Algorithmic Approaches for Transportation Modelling,
Optimization, and Systems (ATMOS 2022); 2:1–2:13; 106.
DOI: 10.4230/OASICS.ATMOS.2022.2.

This article is licensed under a Creative Commons Attribution 4.0
International License (<http://creativecommons.org/licenses/by/4.0/>).

Abstract We present an efficient algorithm that finds a globally optimal solution to the 2D Free Flight Trajectory Optimization Problem (aka Zermelo’s navigation problem) up to arbitrary precision in finite time. The algorithm combines a discrete and a continuous optimization phase. In the discrete phase, a set of candidate paths that densely covers the trajectory space is created on a directed auxiliary graph. Then Yen’s algorithm provides a promising set of discrete candidate paths which subsequently undergo a locally convergent refinement stage. Provided that the auxiliary graph is sufficiently dense, the method finds a path that lies within the convex domain around the global minimizer. From this starting point, the second stage will converge rapidly to the optimum. The density of the auxiliary graph depends solely on the wind field, and not on the accuracy of the solution, such that the method inherits the superior asymptotic convergence properties of the optimal control stage.

Contents

4.1	Introduction	153
4.2	The Free Flight Trajectory Optimization Problem	155
4.2.1	Continuous Point of View: Optimal Control	155
4.2.2	Discrete Point of View: Shortest Paths	159
4.2.3	Discrete-Continuous Point of View: DisCOptER	160
4.3	Towards Global Optimality	162
4.4	Conclusion	167

4.1 Introduction

Flight planning deals with finding the shortest flight path between two airports for an aircraft subject to a number of constraints, in particular, to wind conditions. The problem can be addressed from a discrete and from a continuous point of view and both approaches have received significant attention in the literature. Today's flight planning system follow the discrete approach, which treats the problem as a time-dependent shortest path problem in a world-wide 3D Airway Network, see [1] for a comprehensive survey, and a number of algorithms have been developed that address different aspects of the problem. For the most basic version, [2] and [3] suggested dynamic programming methods, [4] discusses graph preprocessing, and [5] and [6] present A*-type algorithms. [7] integrates overflight costs and [8] traffic restrictions. [9] investigates the free route case, in which the Airway Network can be enriched by additional, artificial waypoints and segments. This setting blends into the Free Flight Trajectory Optimization Problem, aka Zermelo's navigation problem, to find the (globally) time-optimal route from A to B with respect to wind conditions. This classic of continuous optimization is usually solved using direct or indirect methods from Optimal Control [10] (Chapter 2). These are highly efficient, but suffer from one key drawback, namely, they only converge locally. Such methods therefore depend on a sufficiently good starting point, which makes them, used as a standalone tool, incapable of meeting airlines' high expectations regarding the global optimality of routes. In other words, what is called an "optimal solution" in Control theory is only locally optimal, and not globally optimal in the sense of Discrete optimization.

As far as we know, Global Optimization has received little attention in this context so far, but inspiration can be drawn from related fields such as interstellar space mission design [11], robot motion planning [12–14], or even molecular structure optimization [15]. In all these cases, the central challenge is always to find the right balance between sufficient exploration of the search space on the one hand and accurate exploitation of promising regions on the other hand [16]. Two main types of approaches have been used to provide this balance, namely, *stochastic* and

deterministic algorithms. In both cases, finding solutions takes at least exponential time, the runtime increasing with the required accuracy.

Stochastic methods scan the search space with some sort of Multistart approach, i.e., a set of starting points is chosen from the search space more or less at random, and these are explored. The exploration may be enhanced by allowing the candidates (then called *agents*) to wander around with a certain (decreasing) probability (e.g., Simulated Annealing [11, 17]). The deeper investigation of promising areas can be implemented as a local optimization step (e.g., Monotonic Basin Hopping [18]) or via interaction of the candidates attracting each other to the best known solution (e.g., Particle Swarm Optimization [19]). Even though these methods have received a lot of attention over the last decades and show promising results in a variety of applications, they are generally not able to guarantee global optimality in finite time. At best, they will asymptotically converge to a global optimizer (e.g., PRM* or RRT* [12]).

Deterministic approaches are usually based on the principle of Branch and Bound and converge to the global optimizer up to arbitrary precision in finite time [20–23]. The complexity is generally exponential in the number of problem dimensions and the actual performance depends strongly on the quality of the lower bound.

We propose in this paper a efficient deterministic algorithm that finds the global optimizer of the Free Flight Trajectory Optimization Problem in finite time. It is not based on the Branch-and-Bound paradigm. Instead, a two-stage approach combines discrete and continuous optimization methods in a refinement of the concept of the hybrid algorithm DisCOptER [10] (Chapter 2). In the first stage, the search space is sampled by calculating discrete paths on a sufficiently dense artificial digraph. In the second stage, the candidate solutions are refined using efficient techniques from optimal control. Under mild assumptions, namely, the existence of an isolated global minimizer and bounded wind speeds and wind derivatives, the problem is convex in a certain neighborhood of the minimizer. A sufficiently dense graph then contains a path within this neighborhood. This path can be determined by means of Yen’s algorithm, and standard nonlinear programming methods will then efficiently produce the global optimizer up to any requested accuracy. In this way, our approach

focuses on the exploration of the relevant parts of the search space. Moreover, the density of the auxiliary graph depends solely on the convexity properties of the problem, i.e., on the wind field, and *not* on the required accuracy. Hence, the method inherits, on the one hand, the superior asymptotic convergence properties of the second stage, which, in turn, is the key to its efficiency. Typically, only a handful of paths have to be enumerated and investigated. On the other hand, the method also benefits from all advancements in the area of Discrete Flight Planning, e.g., [4, 5].

4.2 The Free Flight Trajectory Optimization Problem

As the Free Flight Trajectory Optimization Problem is ultimately looking for a smooth trajectory, we start our discussion from the Optimal Control point of view.

4.2.1 Continuous Point of View: Optimal Control

The Free Flight Trajectory Optimization Problem can be formally described as follows. Let a spatially heterogeneous, twice continuously differentiable wind field $w : \mathbb{R}^2 \rightarrow \mathbb{R}^2$ with a bounded magnitude $\|w\|_{L^\infty(\mathbb{R}^2)} < \bar{v}$ be given. A valid trajectory is any Lipschitz-continuous path $x : [0, T] \rightarrow \mathbb{R}^2$ with $\|x_t - w\| = \bar{v}$ almost everywhere, connecting the origin x_O and the destination x_D . Among those, we want to find one of minimal flight duration $T \in \mathbb{R}$ (flight duration is essentially proportional to fuel consumption [24]). This classic of optimal control is also known as Zermelo's navigation problem [25].

It can easily be shown that in case of bounded wind speed, the optimal trajectory cannot be arbitrarily longer than the straight connection of origin and destination. Hence every global minimizer is contained in an ellipse $\Omega \subset \mathbb{R}^2$ with focal points x_O and x_D .

Assume the flight trajectory $x \in H^1(0, 1) : [0, T] \rightarrow \mathbb{R}^2$ is given by a strictly monotonously increasing parametrization $t(\tau)$ on $(0, 1)$ as $x(t(\tau)) = \xi(\tau)$, such that $\xi : (0, 1) \rightarrow \mathbb{R}^2$ is a Lipschitz continuous path. Due to Rademacher's theorem, its derivative with respect to the time ξ_τ exists almost everywhere, and we assume

it not to vanish. Then, $t(\tau)$ is defined by the state equation $x_t = v + w \neq 0$ and the airspeed constraint $\|v\| = \bar{v}$, with $v \in L^2(0, 1)$ being the airspeed vector. Indeed,

$$\bar{v} = \|x_t - w\| \quad \text{and} \quad x_t t_\tau = \xi_\tau \neq 0$$

imply

$$\begin{aligned} & (t_\tau^{-1} \xi_\tau - w)^T (t_\tau^{-1} \xi_\tau - w) = \bar{v}^2 \\ \Leftrightarrow & t_\tau^{-2} \xi_\tau^T \xi_\tau - 2t_\tau^{-1} \xi_\tau^T w + w^T w - \bar{v}^2 = 0 \\ \Leftrightarrow & (\bar{v}^2 - w^T w) t_\tau^2 + 2\xi_\tau^T w t_\tau - \xi_\tau^T \xi_\tau = 0 \\ \Leftrightarrow & t_\tau = \frac{-\xi_\tau^T w + \sqrt{(\xi_\tau^T w)^2 + (\bar{v}^2 - w^T w)(\xi_\tau^T \xi_\tau)}}{\bar{v}^2 - w^T w} =: f(t, \xi, \xi_\tau) \end{aligned} \quad (4.1)$$

due to $t_\tau > 0$. The flight duration T is then given by integrating the ODE (4.1) from 0 to 1 as $T = t(1)$. Let us assume for ease of presentation that the wind w is stationary, i.e., independent of t , and thus $f(t, \xi, \xi_\tau) = f(\xi, \xi_\tau)$. Doing so, we obtain the simple integral

$$T(\xi) = \int_0^1 f(\xi(\tau), \xi_\tau(\tau)) d\tau. \quad (4.2)$$

Since the flight duration T as defined in (4.2) is based on a reparametrization $x(t) = \xi(\tau(t))$ of the path such that $\|x_t(t) - w(x(t))\| = \bar{v}$, the actual parametrization of ξ is irrelevant for the value of T . Calling two paths $\xi, \tilde{\xi}$ equivalent if there exists a Lipschitz-continuous bijection $r : (0, 1) \rightarrow (0, 1)$ such that $\xi(r(\tau)) = \tilde{\xi}(\tau)$, we can restrict the optimization to equivalence classes. Every equivalence class contains a representative with constant ground speed $\|\xi_\tau(\tau)\| = L$, that can be obtained from any $\tilde{\xi}$ with $\|\tilde{\xi}_\tau(\tau)\| \neq 0 \forall \tau$ via

$$\xi(\tau) := L \int_0^\tau \frac{\tilde{\xi}_\tau(t)}{\|\tilde{\xi}_\tau(t)\|} dt, \quad (4.3)$$

where $L := \int_0^1 \|\tilde{\xi}_\tau(\tau)\| d\tau$. Hence we will subsequently consider the following equivalent constrained minimization problem:

$$\min_{\xi \in X, L \in \mathbb{R}} T(\xi), \quad \text{s.t.} \quad \|\xi_\tau(\tau)\|^2 = L^2 \quad \forall \tau \in (0, 1); \quad (4.4)$$

here, the admissible set is the affine space

$$X = \{\xi \in H^1((0, 1), \mathbb{R}^2) \mid \xi(0) = x_O, \xi(1) = x_D\}. \quad (4.5)$$

Note that L also represents the path length of a solution, since

$$\int_0^1 \|\xi_\tau\| d\tau = L. \quad (4.6)$$

We finally express the constant ground speed requirement by means of a constraint $h(z) = 0$, where $z := (L, \xi) \in Z := \mathbb{R} \times X$ and

$$h : Z \rightarrow \Lambda := L^2(0, 1), \quad z \mapsto \xi_\tau^\top \xi_\tau - L^2 \quad (4.7)$$

for $L \leq L_{\max}$, with an arbitrary continuation for $L > L_{\max}$ that is linear in $\|\xi_\tau\|$. In order to take the boundary constraints $\xi(0) = x_O$, $\xi(1) = x_D$ into account, we restrict deviations $\delta\xi$ from the trajectory ξ to the space

$$\delta X := \{H^1((0, 1), \mathbb{R}^2) \mid \delta\xi(0) = \delta\xi(1) = 0\}. \quad (4.8)$$

The goal of the present paper is to find a isolated globally optimal solution ξ^{**} to (4.4) that satisfies $T(\xi^{**}) < T(\xi) \forall \xi \in X$, contrary to a local optimizer ξ^* that is only superior to trajectories in a certain neighborhood, $T(\xi^*) \leq T(\xi) \forall \xi \in \mathcal{N}(\xi^*) \subseteq X$. A isolated global minimizer satisfies the necessary *Karush-Kuhn-Tucker* (KKT) optimality conditions [26] given that it is a regular point, which is always the case since

$$h'(z) : \delta Z \mapsto \Lambda \quad \forall z \in Z, \quad \delta z \mapsto \xi_\tau^\top \delta\xi_\tau - L\delta L. \quad (4.9)$$

The KKT-conditions result from the variation of the Lagrangian

$$\mathcal{L}(z, \lambda) := T(\xi) + \langle \lambda, h(z) \rangle \quad (4.10)$$

with respect to z and λ :

$$0 = T'(\xi^{**})[\delta\xi, \delta\xi_\tau] + \int_0^1 \lambda^{**}(\delta\xi_\tau^\top \xi_\tau^{**})d\tau - L^{**}\delta L \int_0^1 \lambda^{**}d\tau \quad \forall \delta z \in \delta Z, \quad (4.11a)$$

$$0 = \int_0^1 \delta\lambda \left((\xi_\tau^{**})^\top \xi_\tau^{**} - (L^{**})^2 \right) d\tau \quad \forall \delta\lambda \in \Lambda, \quad (4.11b)$$

where $\delta z := (\delta L, \delta\xi)$ and $\delta Z := \mathbb{R} \times \delta X$. Consider the unconstrained problem $\min_{\xi \in X} T(\xi)$ and a global minimizer $\tilde{\xi}^{**}$. As discussed before, there is an equivalent route ξ^{**} that satisfies the constraint and hence – together with L from (4.6) – is a global minimizer of the constrained problem.

Lemma 4.1. — *Let (z^{**}, L^{**}) be a global minimizer of (4.4). Then, this solution together with*

$$\lambda^{**} = 0 \tag{4.12}$$

satisfies the necessary conditions (4.11).

Proof. Since ξ^{**} is also a global minimizer of the unconstrained problem, the necessary condition states that $T'(\xi^{**})[\delta\xi, \delta\xi_\tau] = 0$. The terms $\int_0^1 \lambda^{**}(\delta\xi_\tau^T \xi^{**}) d\tau$ and $\int_0^1 \lambda^{**} d\tau$ of (4.11a) both vanish for $\lambda^{**} = 0$. (4.11b) is satisfied because $\|\xi_\tau^{**}\| = L^{**} \forall \tau \in (0, 1)$. \square

Now we turn to the second order sufficient conditions for optimality. In general, a stationary point (z^*, λ^*) is a minimizer, iff the well known *Ladyzhenskaya–Babuška–Brezzi* (LBB) condition (e.g., [27]) is satisfied, which comprises a) the so called *inf-sup* condition

$$\inf_{\substack{\delta\lambda \in \Lambda \\ \delta\lambda \neq 0}} \sup_{\substack{\delta z \in \delta Z \\ \delta z \neq 0}} \frac{\langle \delta\lambda, h'(z)[\delta z] \rangle}{\|\delta z\|_{H^1} |\delta\lambda|_\Lambda} \geq C > 0 \tag{4.13}$$

and b) the requirement that the Lagrangian's Hessian regarding z , \mathcal{L}_{zz} , need be positive definite on the kernel of h' . Formally speaking, there must be a $\underline{\mathcal{B}} > 0$ such that

$$\mathcal{L}_{zz}(z^*)[\delta z]^2 \geq \underline{\mathcal{B}} \|\delta z\|_{L^2}^2$$

for any $\delta z \in \delta Z$ that satisfies

$$\langle \delta\lambda, h'(z^*)[\delta z] \rangle = 0 \quad \forall \delta\lambda \in \Lambda.$$

In our case, the second order sufficient condition is

$$T''(\xi^*)[\delta\xi, \delta\xi_\tau]^2 + 2 \int_0^1 \lambda^*(\delta\xi_\tau^T \delta\xi_\tau - \delta L^2) d\tau \geq \underline{\mathcal{B}}(\delta L^2 + \|\delta\xi\|_{L^2}^2 + \|\delta\xi_\tau\|_{L^2}^2)$$

for any $(\delta L, \delta\xi) \in \mathbb{R} \times \delta X$ such that

$$\int_0^1 \delta\lambda(\delta\xi_\tau^T \xi^* - L^* \delta L) d\tau = 0 \quad \forall \delta\lambda \in L^2(0, 1).$$

In case of a global minimizer z^{**} , this can be simplified using $\langle \lambda^{**}, h'' \rangle = 0$ from Lemma 4.1. Moreover, the constraint is equivalent to requiring that $\delta \xi_\tau^T \xi_\tau^{**} = L^{**} \delta L \quad \forall \tau \in (0, 1)$. With this, we conclude that for any isolated global minimizer (z^{**}, L^*) of (4.4) there exists a $\underline{\mathcal{B}} > 0$ such that

$$T''(\xi^{**})[\delta \xi, \delta \xi_\tau]^2 \geq \underline{\mathcal{B}} \left(\delta L^2 + \|\delta \xi\|_{L^2}^2 + \|\delta \xi_\tau\|_{L^2}^2 \right) \quad (4.14)$$

for any $\delta z \in \delta Z$ such that $\delta \xi_\tau^T \xi_\tau^{**} = L^{**} \delta L \quad \forall \tau \in (0, 1)$.

4.2.2 Discrete Point of View: Shortest Paths

If flight trajectories are restricted to airway segments connecting given waypoints, flight planning is a special kind of shortest path problem on a graph. It can be described as follows. Let $V \subset \mathbb{R}^2$ be a finite set of waypoints including x_O and x_D , and $A \subset V \times V$ a set of segments such that $G = (V, A)$ is a connected directed graph. A discrete flight path is a finite sequence $(x_i)_{0 \leq i \leq n}$ of waypoints with $(x_{i-1}, x_i) \in E$ for $i = 1, \dots, n$, connecting $x_0 = x_O$ with $x_n = x_D$. Shortest path problems on static graphs with non-negative weights are usually solved with the A^* variant of Dijkstra's algorithm [28].

Define a mapping $\Xi : (x_i)_{0 \leq i \leq n} \mapsto \xi \in X$ of discrete flight paths to continuous paths by piecewise linear interpolation

$$\xi(\tau) = x_{\lfloor n\tau \rfloor} + (n\tau - \lfloor n\tau \rfloor)(x_{\lceil n\tau \rceil} - x_{\lfloor n\tau \rfloor}), \quad (4.15)$$

resulting in polygonal chains, which are Lipschitz-continuous with piecewise constant derivative. Denote the image by $X_G := \text{im } \Xi \subset X$, i.e., X_G is the set of flight trajectories with constant ground speed in the Euclidean plane that can be realized by adhering to the airway network. The discrete flight planning problem then reads

$$\min_{\xi \in X_G} T(\xi). \quad (4.16)$$

With any $\xi \in X_G$ satisfying the constraint for constant ground speed, this differs from its continuous counterpart (4.4) essentially by the admissible set, which effectively acts as a particular discretization. The class of (h, ℓ) -dense graphs used in this work was introduced in [10] (Chapter 2) and is defined as follows.

Definition 4.1. — A digraph $G = (V, A)$ is said to be (h, ℓ) -dense in a convex set $\Omega \subset \mathbb{R}^2$ for $h, \ell \geq 0$, if it satisfies the following conditions:

1. containment: $V \subset \Omega$,
2. vertex density: $\forall p \in \Omega : \exists v \in V : \|p - v\| \leq h$,
3. local connectivity: $\forall u, v \in V, \|u - v\| \leq \ell + 2h : (u, v) \in E$.

Definition 4.2. — We call an (h, ℓ) -dense digraph rectangular, if the vertex positions can be described by,

$$x_{ij} = x_0 + \sqrt{2}h[i, j]^T \quad \text{for } i \in M \subseteq \mathbb{Z}, j \in N \subseteq \mathbb{Z} \quad (4.17)$$

with $x_{ij} \in \Omega$ and M, N being connected subsets of the integers.

An example for such a rectangular (h, ℓ) -dense airway digraph is shown in Figure 4.1 a). Note that, even for $\ell \rightarrow 0$, the minimum local connectivity length of $2h$ guarantees that a vertex is connected to all its direct neighbors. It is easy to show that any (h, ℓ) -dense digraph is connected, such that a path from origin to destination exists.

4.2.3 Discrete-Continuous Point of View: Hybrid Algorithm DisCOptER

In [10] (Chapter 2), a hybrid algorithm was proposed that combines the strengths of the discrete and the continuous approach to flight planning. In a nutshell, it works as follows: First, an artificial locally connected digraph of defined density is created, as in Definition 4.1 (blue dots in Figure 4.1 b), arcs omitted). The shortest path on this graph (red) serves as an initial guess for a subsequent refinement stage in which a suitable nonlinear programming formulation of the same problem is solved, leading to a continuous locally optimal solution (green). As follows from this paper, this solution is also globally optimal, provided that the graph is sufficiently dense.

In numerical experiments, we observed that even for scenarios that are far more challenging than any real world situation, a very sparse graph is already

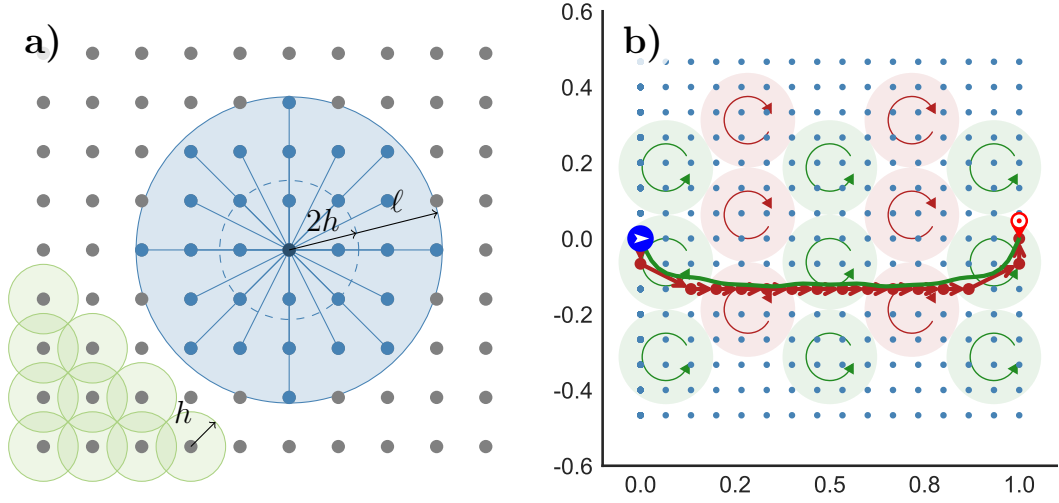


Figure 4.1: a) A rectangular (h, ℓ) -dense digraph. The center vertex (dark blue) is connected to all vertices in a circular neighborhood of radius $2h + \ell$ (light blue) with edges in both directions. b) Illustration of the classical hybrid algorithm DisCOptER. The planar wind field consists of 15 regularly aligned vortices indicated by the green and red discs. Blue dots: locally connected vertices of the (h, ℓ) -dense graph, see a). Red: Shortest path on the graph, Green: Continuous solution obtained via refinement.

sufficient to find the globally optimal solution, rendering the hybrid approach highly efficient. In case of the example illustrated in Figure 4.1 b), the global optimum was found using any graph with node spacing $h \leq \frac{1}{15\sqrt{2}}$, which corresponds to 16 or more nodes between origin and destination. Note that in similar scenarios with n vortices one can expect $\mathcal{O}(2^n)$ local minima.

We quickly recap the complexity analysis from [10] (Chapter 2). The novel algorithm DisCOptER was compared against the traditional, purely graph-based approach in terms of accuracy of the provided solution compared to the continuous optimum. Trajectories of the desired accuracy can in principle be obtained by solving the shortest path problem on a sufficiently dense, locally complete digraph, that can be characterized by its vertex density h and local connectivity radius ℓ , see Definition 4.1. An optimized combination of these properties is $h = \bar{\sigma}\ell^2/L^2$, where $\bar{\sigma}$ is an upper bound for the curvature of the optimal trajectory and L denotes its path length Theorem 3.4. Hence, ℓ^{-1} may serve as a suitable measure for the solution accuracy. The number of vertices $|V|$ in such a digraph is in $\mathcal{O}(\ell^{-4})$ and the number of arcs $|A|$ is in $\mathcal{O}(\ell^{-6})$. The complexity of solving the shortest path problem with

Dijkstra's algorithm is $\mathcal{O}(|A| + |V| \log |V|)$ and so the overall time complexity is in

$$\mathcal{O}(\ell^{-6}). \quad (4.18)$$

Since the required graph density is dictated exclusively by the wind conditions, the complexity of the hybrid algorithm approach is asymptotically inherited from the Optimal Control stage. Using a direct collocation method, the problem is discretized over the time domain with quasi equidistant steps $\delta\tau$. A comparable accuracy measure is then defined as $\ell := L\delta\tau$. Solving the first order necessary conditions – well known as *Karush-Kuhn-Tucker* (KKT) conditions – for the discretized problem via Newton's method rapidly yields a solution, provided that the starting point was already sufficiently close. Due to the problem structure each iteration step essentially involves a linear system of equations with an arrow-shaped matrix, which can be solved efficiently by specialized band-solvers. The overall time complexity of the hybrid algorithm is determined by the number of iterations and the cost of each step, which is in

$$\mathcal{O}(\ell^{-1}). \quad (4.19)$$

4.3 Towards Global Optimality

In terms of runtime the hybrid algorithm DisCOptER appears to be clearly superior to the traditional graph-based approach. One key question, however, remains: What is the right graph density? This section answers this question and presents a variant of the algorithm which is guaranteed to find a global minimizer in finite time by calculating not only one but multiple shortest paths. We exploit the fact that, by continuity, there is a sufficiently large neighborhood around the minimizer over which the objective function is convex, see Theorem 4.2. If started within this neighborhood, optimal control methods will quickly converge up to arbitrary precision. Using a sufficiently dense graph, as described in Lemma 4.3, we guarantee that there is a path that lies in this neighborhood of the global minimizer.

This path can be found by computing paths by Yen's algorithm [29], which computes

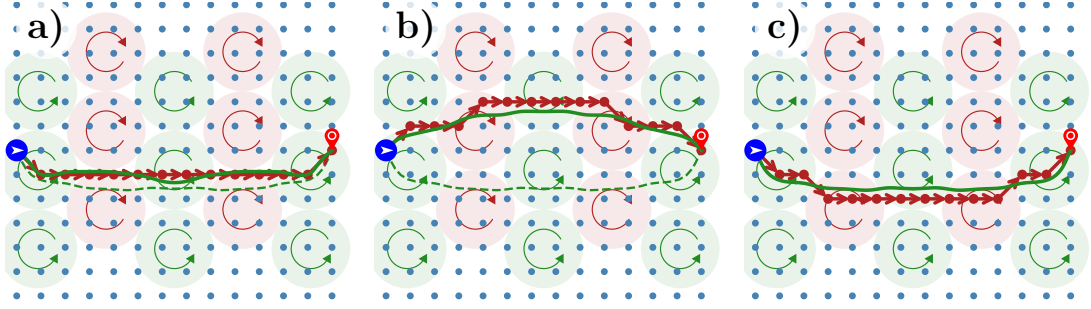


Figure 4.2: Illustration of the hybrid algorithm DisCOptER. The planar wind field consists of 15 regularly aligned vortices indicated by the green and red discs. Blue dots: locally connected vertices of the (h, ℓ) -dense graph, see Figure 4.1 a). Red: k^{th} shortest path on the graph, Green: Continuous solution obtained via refinement. a) Starting from the very shortest path the refinement stage does not converge. b) The 5^{th} shortest path on the graph leads to a local optimum. c) The 14^{th} shortest path on the graph finally leads to the global optimum.

shortest simple paths in the order of increasing travel time. A suitable stopping criterion is technically not necessary, but anyway provided in Theorem 4.4. The required graph density is dictated by the wind conditions. Adverse scenarios will require dense graphs leading to a large number of feasible paths that is, e.g., exponential in the number of vortices, cf. again the example in Fig. 4.2. The number will, however, always be finite and – most importantly – independent of the desired solution accuracy.

Theorem 4.2. — *Let $\|w(p)\| \leq \bar{c}_0 < \bar{v}/\sqrt{5}$, $\|w_x(p)\| \leq \bar{c}_1$, $\|w_{xx}(p)\| \leq \bar{c}_2$, and $\|w_{xxx}(p)\| \leq \bar{c}_3$ for every $p \in \Omega$. Moreover, let $z^{**} := (\xi^{**}, L^{**}) \in Z$ be a global minimizer of problem (4.4), that satisfies the necessary and sufficient conditions (4.11), (4.13), and (4.14) with $C > 0$ and $\underline{\mathcal{B}} > 0$. Then the problem (4.4) is convex in a neighborhood of z^{**} , i.e., there is a $R_C > 0$ exclusively depending on the wind conditions such that the LBB condition are satisfied for any $z \in Z$ with*

$$\|\Delta z\|_{H^1(0,1)} := \|z - z^{**}\|_{H^1(0,1)} \leq R_C. \quad (4.20)$$

Proof. According to (4.13), there is a $C > 0$ such that

$$\inf_{\substack{\delta\lambda \in \Lambda \\ \delta\lambda \neq 0}} \sup_{\substack{\delta z \in \delta Z \\ \delta z \neq 0}} \frac{\langle \delta\lambda, h'(z^{**})[\delta z] \rangle}{\|\delta z\|_{H^1} \|\delta\lambda\|_{\Lambda}} \geq C$$

with h as defined in (4.7). Moreover, it holds that

$$T''(\xi^{**})[\delta\xi, \delta\xi_\tau]^2 \geq \underline{\mathcal{B}} \left(\delta L^2 + \|\delta\xi\|_{L^2}^2 + \|\delta\xi_\tau\|_{L^2}^2 \right)$$

for any $\delta z \in \delta Z$ such that $\delta\xi_\tau^T \xi^{**} = L^{**} \delta L \quad \forall \tau \in (0, 1)$, see (4.14). Due to the continuity of the bilinear form, the *inf-sup* condition is satisfied for any z with $\|\Delta z\| \leq R_{C1}$, such that

$$\inf_{\substack{\delta\lambda \in \Lambda \\ \delta\lambda \neq 0}} \sup_{\substack{\delta z \in \delta Z \\ \delta z \neq 0}} \frac{\langle \delta\lambda, h'(z)[\delta z] \rangle}{\|\delta z\|_{H^1} \|\delta\lambda\|_\Lambda} \geq \frac{C}{2} > 0.$$

Similarly, the continuity of T as given in (4.2), guarantees that there is a $R_{C2} > 0$ such that

$$T''(\xi)[\delta\xi, \delta\xi_\tau]^2 \geq \frac{\underline{\mathcal{B}}}{2} \left(\delta L^2 + \|\delta\xi\|_{L^2}^2 + \|\delta\xi_\tau\|_{L^2}^2 \right)$$

for any $z \in Z$ such that $\|z - z^{**}\|_{H^1(0,1)} \leq R_{C2}$ and any $\delta z \in \delta Z$ such that $\xi_\tau^T \delta\xi_\tau = L \delta L \quad \forall \tau \in (0, 1)$. Consequently, the sufficient conditions are satisfied for any z with $\|\Delta z\| \leq R_C := \min(R_{C1}, R_{C2})$. \square

Providing a sufficiently (h, ℓ) -dense graph, we can guarantee that there is a discrete path within the convex neighborhood of the global minimizer $B_{R_C}(\xi^{**})$. The following Lemma involves a result from Lemma 3.6 stating that the curvature of a global minimizer of (4.4) is bounded by

$$\|\xi_{\tau\tau}^{**}\| \leq \bar{\sigma} := \frac{\bar{c}_1(L^{**})^2}{\bar{v} - \bar{c}_0} \left(\sqrt{2\bar{v}} + \frac{\bar{v} + \bar{c}_0}{\bar{v} - \bar{c}_0} \left((1 + \sqrt{2})\bar{v} + \bar{c}_0 \right) \right). \quad (4.21)$$

Lemma 4.3. — *Let (L^{**}, ξ^{**}) be a minimizer of (4.4). For any $R_C > 0$ there is a h small enough such that the corresponding (h, ℓ) -dense digraph contains a valid path ξ_R with $\|\xi^{**} - \xi_R\|_{H^1(0,1)} \leq R_C$. The connectivity length l shall here be given as $\ell = L^{**} \sqrt{h/\bar{\sigma}}$, which is an optimized choice as derived in Theorem 3.4.*

Proof. In Theorem 3.3, it was proved that for every $\xi \in X$ with $\|\xi_\tau\| = L$, there is a trajectory $\xi_R(\xi)$ on an (h, ℓ) -dense digraph with

$$\|\xi_R(\xi) - \xi\|_{H^1(0,1)} \leq 2\bar{\sigma} \frac{\ell}{L} + 2h \frac{L}{\ell} + 3h.$$

Since $\|\xi_{\tau}^{**}\| = L^{**}$, this bound holds for a global optimizer (L^{**}, ξ^{**}) of (4.4). Together with $\ell = L^{**}\sqrt{h/\bar{\sigma}}$ this reads

$$\|\xi_R(\xi) - \xi^{**}\|_{H^1(0,1)} \leq 4\sqrt{\bar{\sigma}h} + 3h,$$

which directly proves that $\|\xi_R(\xi) - \xi^{**}\|_{H^1(0,1)} \leq R_C$ for sufficiently small h . \square

Having defined a spatially bounded (h, ℓ) -dense digraph, we use Yen's algorithm [29] to enumerate paths in order of increasing travel time. Each generated discrete path $\xi_{G,i}$ undergoes a locally convergent refinement stage. If $\xi_{G,i}$ is the path on the graph that is closest to the minimizer ξ^{**} , then Theorem 4.2 and lemma 4.3 guarantee that it lies in the convex domain. For this reason we do not require the solver to incorporate any globalization strategies. Instead, the KKT system (4.11) can be solved via Newton's method, which either converges quadratically or is terminated in case of non-convexity.

Since any other local minimizer may be found as well, the preliminary solution shall be denoted as $\xi^*(\xi_{G,i})$ in Algorithm 2 and may replace the current best solution ξ_C if $T(\xi^*(\xi_{G,i})) < T(\xi_C)$.

A suitable stopping criterion builds on the following local error bound.

Theorem 4.4. — *Let (L^{**}, ξ^{**}) be a global minimizer of (4.4) and define $\Delta\xi := \xi - \xi^{**}$. Then there are constants $\bar{\mathcal{B}} > 0$ and $R_E > 0$ exclusively depending on the wind conditions, such that for any $\xi \in X$ with $\|\Delta\xi\|_{H^1} \leq R_E$, the error in the objective function T as defined in (4.2) is bounded by*

$$T(\xi) - T(\xi^{**}) \leq \frac{1}{2}\bar{\mathcal{B}}\|\Delta\xi\|_{H^1(0,1)}^2. \quad (4.22)$$

Proof. As shown in the proof of Theorem 3.2, the second directional derivative of T is bounded from above at a global minimizer. Let this bound be compactly given as

$$|T''(\xi)[\delta\xi, \delta\xi_{\tau}]^2| \leq 2\bar{\mathcal{B}}\|\delta\xi_{\tau}\|_{H^1(0,1)}^2$$

with some $\bar{\mathcal{B}} > 0$ that only depends on the wind conditions. Due to the continuity of T there is a $R_E > 0$ such that for any $\xi \in X$ with $\|\Delta\xi\|_{H^1} \leq R_E$, the second

directional derivative of T is bounded by

$$|T''(\xi)[\delta\xi, \delta\xi_\tau]^2| \leq \bar{\mathcal{B}}\|\delta\xi_\tau\|_{H^1(0,1)}^2.$$

We use this bound, the optimality of ξ^{**} , and Taylor's Theorem to validate that

$$\begin{aligned} T(\xi) &= T(\xi^{**}) + \underbrace{T'(\xi^{**})[\Delta\xi, \Delta\xi_\tau]}_{=0} + \int_0^1 (1-\nu)T''(\xi^{**} + \nu\Delta\xi)[\Delta\xi, \Delta\xi_\tau]^2 d\nu \\ &\leq T(\xi^{**}) + \frac{1}{2}\bar{\mathcal{B}}\|\Delta\xi\|_{H^1(0,1)}^2. \end{aligned}$$

□

Since we are only interested in discrete paths within the convex domain of the global minimizer $B_R(\xi^{**})$, the generation of new paths is terminated if the extra cost of the next discrete path cannot be compensated by convergence to a nearby local minimizer anymore, i.e., if

$$T(\xi_{G,i}) - T(\xi_C) \geq \frac{1}{2}\bar{\mathcal{B}}R^2 =: \epsilon, \quad (4.23)$$

where $\xi_{G,i}$ denotes the i th shortest path, ξ_C the current best guess and

$$R := \min(R_C, R_E).$$

Remark 4.1. — *We finally want to point out that the required graph density is exclusively dictated by the wind conditions and independent of the requested solution accuracy. Therefore, even though the enumeration of multiple discrete paths is certainly more expensive than finding the single shortest path as in the original DisCOpter concept, this difference vanishes asymptotically such that the proposed algorithm for global optimality inherits the superior convergence properties of the optimal control method given in Equation (4.19).*

Algorithm 2: This algorithm provides a globally optimal solution to the Free Flight trajectory optimization problem (4.4) in finite time.

Data: $x_O, x_D, \Omega, \bar{v}, w, \bar{c}_0, \bar{c}_1, \bar{c}_2, \bar{c}_3, C, \underline{\mathcal{B}}, \bar{\mathcal{B}}, R_E, R_C, TOL$
Result: (L_C, ξ_C) with $T(\xi_C) - T(\xi^{**}) \leq TOL$ and $\|\xi_\tau^{**}\| - L_C \leq TOL$

- 1 $(L_C, \xi_C) \leftarrow \text{None}; T_C \leftarrow \infty; i \leftarrow 0; R \leftarrow \min(R_C, R_E);$
- 2 $\epsilon \leftarrow$ Calculate the error bound for $\|\delta\xi\|_{H^1} \leq R$ from Theorem 4.4;
- 3 $(h, \ell) \leftarrow$ Calculate $h(R)$ and $\ell(h)$ as in Lemma 4.3;
- 4 Define a rectangular, spatially bounded (h, ℓ) -dense digraph covering Ω ;
- 5 **do**
- 6 Calculate the i th shortest path $\xi_{G,i}$;
- 7 **if** $T(\xi_{G,i}) - T_C \geq \epsilon$ **then**
- 8 | return (L_C, ξ_C) ;
- 9 **end**
- 10 /* Optimal Control stage */
- 10 $(converged, L^*, \xi^*) \leftarrow$ (Try to) Calculate a local minimizer starting from
- 11 $(L(\xi_{G,i}), \xi_{G,i})$ up to tolerance TOL ;
- 12 /* Update */
- 12 **if** $converged$ and $T(\xi^*) < T_C$ **then**
- 13 | $(L_C, \xi_C) \leftarrow (L^*, \xi^*)$;
- 14 | $T_C \leftarrow T(\xi^*)$;
- 15 **end**
- 16 $i \leftarrow i + 1$;
- 17 **while** $true$;

4.4 Conclusion

We presented a novel discrete-continuous algorithm that computes globally optimal solutions of the Free Flight Trajectory Optimization Problem in finite time to any desired accuracy. The main advantage of the method, and the key to its efficiency, is that the density of the discretization in the first graph-search stage of the algorithm depends only the problem data, and not on the desired accuracy. In this way, the algorithm inherits the superior asymptotic convergence properties of the second optimal control stage. A next step is a demonstration of computational efficiency. This requires improvements in the discrete part, in particular, an adaptive graph construction and the use of k -shortest path or k -dissimilar path algorithms that are, at least in practice, faster than Yen's algorithm, such as [30, 31] or [32], respectively.

Authors' Contributions

Conceptualization, R.B and M.W.; methodology, M.W.; software, F.D.; validation, F.D.; formal analysis, M.W.; investigation, F.D. and M.W.; resources, R.B., F.D. and M.W.; data curation, F.D.; writing-original draft preparation, F.D. and M.W.; writing-review and editing, R.B.; visualization, F.D.; supervision, R.B.; project administration, R.B. and M.W.; funding acquisition, R.B. and M.W. All authors have read and agreed to the published version of the manuscript.

References

- [1] S. E. Karisch, S. S. Altus, G. Stojković, and M. Stojković, “Operations,” in *Quantitative Problem Solving Methods in the Airline Industry*, Springer, 2011, ch. 6 – Operations, pp. 283–383. DOI: 10.1007/978-1-4614-1608-1_6.
- [2] H. M. de Jong, “Optimal Track Selection and 3-Dimensional Flight Planning,” Royal Netherlands Meteorological Institute, Tech. Rep., 1974.
- [3] H. K. Ng, B. Sridhar, and S. Grabbe, “Optimizing Aircraft Trajectories with Multiple Cruise Altitudes in the Presence of Winds,” *Journal of Aerospace Information Systems*, vol. 11, no. 1, pp. 35–47, 2014. DOI: 10.2514/1.I010084.
- [4] A. Schienle, P. Maristany de las Casas, and M. Blanco, “A Priori Search Space Pruning in the Flight Planning Problem,” in *19th Symposium on Algorithmic Approaches for Transportation Modelling, Optimization, and Systems (ATMOS 2019)*, vol. 75, Schloss Dagstuhl–Leibniz-Zentrum fuer Informatik, 2019, pp. 1–14. DOI: 10.4230/OASIcs.ATMOS.2019.8.
- [5] M. Blanco, R. Borndörfer, N.-D. Hoang, A. Kaier, A. Schienle, T. Schlechte, and S. Schlobach, “Solving Time Dependent Shortest Path Problems on Airway Networks Using Super-Optimal Wind,” in *16th Workshop on Algorithmic Approaches for Transportation Modelling, Optimization, and Systems (ATMOS 2016)*, vol. 54, Schloss Dagstuhl–Leibniz-Zentrum fuer Informatik, 2016, pp. 1–15. DOI: 10.4230/OASIcs.ATMOS.2016.12.
- [6] A. Knudsen, M. Chiarandini, and K. Larsen, “Heuristic Variants of A* Search for 3D Flight Planning,” in *Integration of Constraint Programming, Artificial Intelligence, and Operations Research*, Springer International Publishing, 2018, pp. 361–376. DOI: 10.1007/978-3-319-93031-2_26.

- [7] M. Blanco, R. Borndörfer, N. D. Hoàng, A. Kaier, P. Maristany de las Casas, S. Thomas, and S. Schlobach, “Cost Projection Methods for the Shortest Path Problem with Crossing Costs,” in *17th Workshop on Algorithmic Approaches for Transportation Modelling, Optimization, and Systems (ATMOS 2017)*, vol. 59, Schloss Dagstuhl–Leibniz-Zentrum fuer Informatik, 2017, pp. 1–14. DOI: 10.4230/OASIcs.ATMOS.2017.15.
- [8] A. N. Knudsen, M. Chiarandini, and K. S. Larsen, “Constraint Handling in Flight Planning,” in *Principles and Practice of Constraint Programming – 23rd International Conference*, 2017, pp. 354–369. DOI: 10.1007/978-3-319-66158-2_23.
- [9] C. K. Jensen, M. Chiarandini, and K. S. Larsen, “Flight Planning in Free Route Airspaces,” in *17th Workshop on Algorithmic Approaches for Transportation Modelling, Optimization, and Systems (ATMOS 2017)*, vol. 59, Schloss Dagstuhl–Leibniz-Zentrum fuer Informatik, 2017, pp. 1–14. DOI: 10.4230/OASIcs.ATMOS.2017.14.
- [10] R. Borndörfer, F. Danecker, and M. Weiser, “A Discrete-Continuous Algorithm for Free Flight Planning,” *Algorithms*, vol. 14, no. 1, p. 4, 2021. DOI: 10.3390/a14010004.
- [11] A. Cassioli, D. Izzo, D. Di Lorenzo, M. Locatelli, and F. Schoen, “Global Optimization Approaches for Optimal Trajectory Planning,” in *Modeling and Optimization in Space Engineering*. Springer New York, 2012, ch. 5, pp. 111–140. DOI: 10.1007/978-1-4614-4469-5_5.
- [12] S. Karaman and E. Frazzoli, “Sampling-Based Algorithms for Optimal Motion Planning,” *The International Journal of Robotics Research*, vol. 30, no. 7, pp. 846–894, 2011. DOI: 10.1177/0278364911406761.
- [13] T. T. Mac, C. Copot, D. T. Tran, and R. De Keyser, “Heuristic Approaches in Robot Path Planning: A Survey,” *Robotics and Autonomous Systems*, vol. 86, pp. 13–28, 2016. DOI: 10.1016/j.robot.2016.08.001.
- [14] O. Souissi, R. Benatitallah, D. Duvivier, A. Artiba, N. Belanger, and P. Feyzeau, “Path Planning: A 2013 Survey,” in *Proceedings of the 2013 International Conference on Industrial Engineering and Systems Management (IESM)*, 2013, pp. 1–8. [Online]. Available: <https://ieeexplore.ieee.org/document/6761521> (visited on 09/22/2023).
- [15] B. Hartke, “Global Optimization,” *Wiley Interdisciplinary Reviews: Computational Molecular Science*, vol. 1, no. 6, pp. 879–887, 2011. DOI: 10.1002/wcms.70.
- [16] M. Khajezadeh, M. R. Taha, A. El-Shafie, and M. Eslami, “A Survey on Meta-Heuristic Global Optimization Algorithms,” *Research Journal of Applied Sciences, Engineering and Technology*, vol. 3, no. 6, pp. 569–578, 2011. [Online]. Available: <https://maxwellsci.com/print/rjaset/v3-569-578.pdf> (visited on 09/22/2023).

- [17] M. Locatelli, “Simulated Annealing Algorithms for Continuous Global Optimization,” in *Handbook of Global Optimization*, Springer, 2002, pp. 179–229. DOI: 10.1007/978-1-4757-5362-2_6.
- [18] B. Addis, A. Cassioli, M. Locatelli, and F. Schoen, “A Global Optimization Method for the Design of Space Trajectories,” *Computational Optimization and Applications*, vol. 48, pp. 635–652, 2011. DOI: 10.1007/s10589-009-9261-6.
- [19] M. R. Bonyadi and Z. Michalewicz, “Particle Swarm Optimization for Single Objective Continuous Space Problems: A Review,” *Evolutionary Computation*, vol. 25, no. 1, pp. 1–54, 2017. DOI: 10.1162/EVCO_r_00180.
- [20] I. P. Androulakis, C. D. Maranas, and C. A. Floudas, “ α BB: A Global Optimization Method for General Constrained Nonconvex Problems,” *Journal of Global Optimization*, vol. 7, no. 4, pp. 337–363, 1995. DOI: 10.1007/BF01099647.
- [21] C. A. Floudas, *Deterministic Global Optimization: Theory, Methods and Applications*. Springer New York, 2000. DOI: 10.1007/978-1-4757-4949-6.
- [22] H. Diedam, “Global Optimal Control Using Direct Multiple Shooting,” Ph.D. dissertation, University of Heidelberg, 2015. DOI: 10.11588/heidok.00019744.
- [23] D. R. Jones, C. D. Perttunen, and B. E. Stuckman, “Lipschitzian Optimization without the Lipschitz Constant,” *J. Optim. Theory Appl.*, vol. 79, no. 1, pp. 157–181, 1993. DOI: 10.1007/BF00941892.
- [24] C. A. Wells, P. D. Williams, N. K. Nichols, D. Kalise, and I. Poll, “Reducing Transatlantic Flight Emissions by Fuel-Optimised Routing,” *Environ. Res. Letters*, vol. 16, no. 2, p. 025 002, 2021. DOI: 10.1088/1748-9326/abce82.
- [25] E. Zermelo, “Über das Navigationsproblem bei ruhender oder veränderlicher Windverteilung,” *ZAMM-Journal of Applied Mathematics and Mechanics/Zeitschrift für Angewandte Mathematik und Mechanik*, vol. 11(2), pp. 114–124, 1931. DOI: 10.1002/zamm.19310110205.
- [26] H. Kuhn and A. Tucker, “Nonlinear Programming,” in *Proceedings of the second Berkeley Symposium on Mathematical Statistics and Probability*, University of California Press, 1951, pp. 481–493.
- [27] D. Braess, *Finite Elemente*, 5th ed. Springer Spektrum Berlin, 2013. DOI: 10.1007/978-3-642-34797-9.
- [28] A. Madkour, W. G. Aref, F. U. Rehman, M. A. Rahman, and S. Basalamah, “A Survey of Shortest-Path Algorithms,” *Computing Research Repository*, 2017. DOI: 10.48550/arXiv.1705.02044.
- [29] J. Y. Yen, “Finding the k Shortest Loopless Paths in a Network,” *Management Science*, vol. 17, no. 11, pp. 712–716, 1971. DOI: 10.1287/mnsc.17.11.712.
- [30] G. Feng, “Finding k Shortest Simple Paths in Directed Graphs: A Node Classification Algorithm,” *Networks*, vol. 64, no. 1, pp. 6–17, 2014. DOI: 10.1002/net.21552.

- [31] D. Kurz and P. Mutzel, “A Sidetrack-Based Algorithm for Finding the k Shortest Simple Paths in a Directed Graph,” in *27th International Symposium on Algorithms and Computation (ISAAC 2016)*, vol. 64, Schloss Dagstuhl–Leibniz-Zentrum fuer Informatik, 2016, pp. 1–13. DOI: 10.4230/LIPIcs.ISAAC.2016.49.
- [32] A. Al Zoobi, D. Coudert, and N. Nisse, “On the Complexity of Finding k Shortest Dissimilar Paths in a Graph,” Inria; CNRS; I3S; Université Côte d’Azur, Research Report, 2021, p. 9. [Online]. Available: <https://hal.archives-ouvertes.fr/hal-03187276> (visited on 09/22/2023).

CHAPTER 5

Newton's Method for Global
Free Flight Trajectory Optimization

Borndörfer, R., Danecker, F., and Weiser, M.
Operations Research Forum 4, 63 (2023).
DOI: 10.1007/s43069-023-00238-z.

This article is licensed under a Creative Commons Attribution 4.0
International License (<http://creativecommons.org/licenses/by/4.0/>).

Abstract Globally optimal free flight trajectory optimization can be achieved with a combination of discrete and continuous optimization. A key requirement is that Newton's method for continuous optimization converges in a sufficiently large neighborhood around a minimizer. We show in this paper that, under certain assumptions, this is the case.

Contents

5.1	Introduction	175
5.2	The Free Flight Trajectory Optimization Problem	177
5.2.1	Notation	177
5.2.2	Problem Statement	177
5.3	Continuous Optimization: Newton-KKT	179
5.3.1	Optimality Conditions	179
5.3.2	Newton's Method	183
5.4	Proof of Convergence	183
5.4.1	Inf-Sup Condition	185
5.4.2	Positive Definiteness of the Lagrangian	187
5.4.3	Upper Bound for the Lagrangian	190
5.4.4	Invertibility of the KKT-Operator	193
5.4.5	Lipschitz Constant	194
5.4.6	Convergence of Newton's Method	199
5.5	Conclusion	201
5.A	Appendix	204
5.A.1	Global Bounds	204
5.A.2	Bounds in a Neighborhood of a Minimizer	217

5.1 Introduction

Around the world countries are implementing Free Flight airspaces that allow aircraft to choose their own route, as opposed to being restricted to a predetermined three-dimensional network. The primary factors that influence costs are time and fuel consumption, which are closely interrelated [1]. Based on the relative weights of these factors (cf. cost index) the optimal airspeed can be determined, which typically remains largely constant [2–4]. Additionally, the vertical flight path can usually be predetermined using aircraft performance data [5]. Consequently, the problem can be well approximated in a way proposed by Zermelo in 1931 [6], which involves finding the most efficient trajectory from point A to B for an aircraft flying at a constant airspeed in a given two-dimensional wind field.

The Free Flight Trajectory Optimization Problem is usually solved using direct or indirect methods from Optimal Control [5, 7–11]. These are highly efficient, but suffer from one key drawback: They only converge locally and are thus dependent on a sufficiently good starting point. This makes such methods, used as a standalone, incapable of meeting airlines' high expectations regarding the global optimality of routes.

In [12–14] (Chapters 2, 3 and 4) a deterministic two-stage algorithm was proposed that combines discrete and continuous optimization in order to find a globally optimal solution to the free flight trajectory optimization problem. With this approach the exponential complexity of other branch and bound based algorithms is circumvented.

The primary objective of the first stage is to obtain a finite sample in a systematic manner that adequately covers the search space. This deterministic approach eliminates the potential for infinite runtime, which may occur when using stochastic global optimization algorithms, such as Particle Swarm Optimization, Simulated Annealing, or Monotonic Basin Hopping [15–18].

One approach is to create a locally dense directed graph with a specific density determined by the node spacing h and connectivity length ℓ , thereby implicitly

defining the sample. The instances can then be selected in order of quality by applying Yen's algorithm [19] to calculate the k^{th} shortest paths.

Promising paths serve as initial guesses for a subsequent refinement stage in which a continuous solution to the problem is calculated up to the desired accuracy.

Analytical evidence and numerical experiments have demonstrated that the new hybrid algorithm has a time complexity of $\mathcal{O}(\ell^{-1})$, making it superior to the conventional purely discrete approach, which has a time complexity of $\mathcal{O}(\ell^{-6})$ [12] (Chapter 2). In this context, ℓ refers to the maximum arc length in a graph and the discretization length in a continuous optimization scenario. Thus, ℓ^{-1} serves as a comparable metric for the precision of the solution.

The present paper is concerned with the second stage. One way to generate a continuous solution is to apply Newton's method to the first order necessary conditions (the KKT-conditions) – an approach commonly referred to as Newton-KKT or Sequential Quadratic Programming (SQP) (see e.g., [20]). It is now shown that there is a quantifiable domain around a global optimum such that Newton-KKT converges if initialized accordingly.

Since the computational effort of the first graph-searching stage depends exclusively on the problem instance, i.e., the wind conditions, the algorithm asymptotically inherits the super fast convergence rates of the Newton-KKT method.

The paper is structured as follows. After defining the problem and introducing a formulation that is convenient for the analytical discussion in Section 5.2, we formally state the necessary and sufficient conditions as well as the Newton-KKT approach in Section 5.3. The proof of convergence is provided in Section 5.4 followed by a conclusion emphasizing the impact on previous and future work.

5.2 The Free Flight Trajectory Optimization Problem

5.2.1 Notation

Throughout this article lower case subscripts like e.g., x_t or ξ_τ , denote partial derivatives, while total derivatives are indicated by primes, e.g., T' or f' . Locally and globally optimal quantities are indicated by single and double superscript stars, respectively, e.g., ξ^* or ξ^{**} . If not stated otherwise, we assume $\|\cdot\|$ to denote the l^2 -norm. Accordingly, we use the following quantitative definition of the L^∞ -norm in terms of the l^2 -norm.

Definition 5.1. — *Let $f : \Omega \mapsto \mathbb{R}^n$. Then we define*

$$\|f\|_{L^\infty(\Omega)} := \inf\{C \geq 0 : \|f(x)\|_2 \leq C \text{ for a.a. } x \in \Omega\}. \quad (5.1)$$

5.2.2 Problem Statement

Neglecting any traffic flow restrictions, we consider Lipschitz-continuous flight paths $\xi \in C^{0,1}((0,1), \mathbb{R}^2)$ connecting origin $\xi(0) = x_O$ and destination $\xi(1) = x_D$. By Rademacher's theorem, such paths are almost everywhere differentiable, and moreover contained in the Sobolev space $W^{1,\infty}((0,1), \mathbb{R}^2)$.

A short calculation reveals that an aircraft traveling along such a path ξ with constant airspeed \bar{v} through a three times continuously differentiable wind field $w \in C^3(\mathbb{R}^2, \mathbb{R}^2)$ with bounded magnitude $\|w(x)\| < \bar{v}$ reaches the destination after a flight duration

$$T(\xi) = \int_0^1 f(\xi(\tau), \xi_\tau(\tau)) d\tau \quad (5.2)$$

with ξ_τ denoting the time derivative of ξ and

$$f(\xi, \xi_\tau) := t_\tau = \frac{-\xi_\tau^\top w + \sqrt{(\xi_\tau^\top w)^2 + (\bar{v}^2 - w^\top w)(\xi_\tau^\top \xi_\tau)}}{\bar{v}^2 - w^\top w}, \quad (5.3)$$

see [12–14] (Chapters 2, 3 and 4).

Among these paths ξ , we need to find one with minimal flight duration $T(\xi)$, since that is essentially proportional to fuel consumption [1]. This classic of optimal

control is known as Zermelo's navigation problem [6]. It can easily be shown that in case of bounded wind speed, the optimal trajectory cannot be arbitrarily longer than the straight connection of origin and destination. Hence, every global minimizer is contained in an ellipse $\Omega \subset \mathbb{R}^2$ with focal points x_O and x_D .

The flight duration T as defined in (5.2) is based on a time reparametrization from actual flight time $t \in [0, T]$ to pseudo-time $\tau \in [0, 1]$ according to the actual flight trajectory $x(t) = \xi(\tau(t))$ such that $\|x_t(t) - w(x(t))\| = \bar{v}$, where x_t denotes the so called ground speed, i.e., the derivative of position x with respect to the unscaled time t . As a consequence, the actual parametrization of ξ in terms of pseudo-time τ is irrelevant for the value of T . Calling two paths $\xi, \tilde{\xi}$ equivalent if there exists a Lipschitz-continuous bijection $r : (0, 1) \rightarrow (0, 1)$ such that $\xi(r(\tau)) = \tilde{\xi}(\tau)$, we can restrict the optimization to equivalence classes. Moreover, every equivalence class contains a representative with constant ground speed $\|\xi_\tau(\tau)\| = L$ for almost all τ , that can be obtained from any $\tilde{\xi}$ with $\|\tilde{\xi}_\tau(\tau)\| \neq 0 \forall \tau$ via

$$\xi(\tau) := L \int_0^\tau \frac{\tilde{\xi}_\tau(t)}{\|\tilde{\xi}_\tau(t)\|} dt, \quad L := \int_0^1 \|\tilde{\xi}_\tau(\tau)\| d\tau. \quad (5.4)$$

Hence, we introduce $z := (L, \xi) \in Z := \mathbb{R} \times X$ and the affine space of valid trajectories

$$X := \{\xi \in W^{1,\infty}((0, 1), \mathbb{R}^2) \mid \xi(0) = x_O, \xi(1) = x_D\}. \quad (5.5)$$

and subsequently consider the equivalent constrained minimization problem

$$\min_{z \in Z} T(\xi), \quad \text{s.t.} \quad h(z) = 0 \quad \text{for a.a. } \tau \in (0, 1) \quad (5.6)$$

with

$$h : Z \rightarrow \Lambda := L^\infty((0, 1), \mathbb{R}), \quad z \mapsto \xi_\tau^\top \xi_\tau - L^2. \quad (5.7)$$

If the constraint is satisfied, L also represents the path length, since

$$\int_0^1 \|\xi_\tau\| d\tau = L. \quad (5.8)$$

Note that $T : X \rightarrow \mathbb{R}$ is Fréchet differentiable with respect to the corresponding linear space

$$\delta X := W_0^{1,\infty}((0, 1), \mathbb{R}^2) \quad (5.9)$$

of directions $\delta\xi$ with zero boundary values, that consequently do not change origin and destination, equipped with the norm

$$\|\delta\xi\|_{X^\infty} = \|\delta\xi\|_{L^\infty(0,1)} + \|\delta\xi_\tau\|_{L^\infty(0,1)}. \quad (5.10)$$

Further, we define the linear space

$$\delta Z := \mathbb{R} \times \delta X \quad (5.11)$$

and equip the spaces Z and δZ with the norms

$$\|z\|_{Z^\infty} = |L| + \|\xi\|_{L^\infty(0,1)} + \|\xi_\tau\|_{L^\infty(0,1)}, \quad \text{and} \quad (5.12a)$$

$$\|z\|_{Z^2} = |L| + \|\xi\|_{L^2(0,1)} + \|\xi_\tau\|_{L^2(0,1)}. \quad (5.12b)$$

5.3 Continuous Optimization: Newton-KKT

In order to find a continuous solution to the free flight optimization problem (5.6) we apply Newton's method to the first order necessary conditions (the KKT-conditions), which is also known as sequential quadratic programming (SQP). Before we formally introduce Newton's method, we discuss the necessary and sufficient conditions for optimality, which also defines the goal of the presented algorithm.

5.3.1 Optimality Conditions

5.3.1.1 Necessary Conditions

The goal of the present paper is to find an isolated globally optimal solution ξ^{**} to (5.6) that satisfies

$$T(\xi^{**}) \leq T(\xi) \quad \forall \xi \in X, \quad (5.13)$$

contrary to a local optimizer ξ^* that is only superior to trajectories in a certain neighborhood,

$$T(\xi^*) \leq T(\xi) \quad \forall \xi \in \mathcal{N}(\xi^*) \subseteq X. \quad (5.14)$$

An isolated global minimizer satisfies the necessary *Karush-Kuhn-Tucker* (KKT) optimality conditions [21] given that it is a regular point, which is always the case, as confirmed by the following Theorem.

Theorem 5.1. — *Let $z = (L, \xi) \in Z$ with $L > 0$ and assume there is a direction $u \in \mathbb{R}^2$ and $c > 0$ such that $\xi_\tau^\top u \geq c$ almost everywhere. Then, $h'(z) : \delta Z \rightarrow L^\infty(0, 1)$ is surjective, i.e., z is regular.*

Proof. Let $f \in L^\infty(0, 1)$ be given and $b := \xi_\tau^\top u \geq c$. We set

$$\delta L = -\frac{\int_0^1 b^{-1} f/2 \, d\tau}{L \int_0^1 b^{-1} \, d\tau}$$

and

$$g = b^{-1}(f/2 + L\delta L), \quad \delta \xi_\tau = gu.$$

Due to $b \geq c$ almost everywhere, b^{-1} is bounded and hence $g, \xi_\tau \in L^\infty(0, 1)$. By construction, $\int_0^1 \delta \xi_\tau \, d\tau = 0$ holds, such that $\delta z = (\delta L, \delta \xi) \in \delta Z$. Now we obtain

$$\begin{aligned} h'(z)[\delta z] &= 2\xi_\tau^\top \delta \xi_\tau - 2L\delta L \\ &= 2bg - 2L\delta L \\ &= 2(f/2 + L\delta L) - 2L\delta L \\ &= f, \end{aligned}$$

and thus the claim. □

For $\lambda \in \Lambda^*$, the Lagrangian is defined as

$$\mathcal{L}(z, \lambda) := T(\xi) + \langle \lambda, h(z) \rangle. \quad (5.15)$$

The KKT-conditions guarantee for a regular minimizer z^{**} the existence of a Lagrange multiplier $\lambda^{**} \in \Lambda^*$, such that

$$\begin{aligned} 0 &= \mathcal{L}_z(z^{**}, \lambda^{**})[\delta z] & \forall \delta z \in \delta Z, \\ 0 &= \langle \delta \lambda, h(z^{**}) \rangle & \forall \delta \lambda \in \Lambda^* \end{aligned}$$

hold, where $\delta z := (\delta L, \delta \xi) \in \delta Z$. In our case, these necessary conditions read

$$0 = \underbrace{T'(\xi^{**})[\delta \xi]}_{=0 \text{ (5.18)}} + 2 \int_0^1 \lambda^{**} \left(\delta \xi_\tau^T \xi_\tau^{**} - \delta L L^{**} \right) d\tau \quad \forall \delta z \in \delta Z, \quad (5.16a)$$

$$0 = \int_0^1 \delta \lambda \left((\xi_\tau^{**})^T \xi_\tau^{**} - (L^{**})^2 \right) d\tau \quad \forall \delta \lambda \in \Lambda^*. \quad (5.16b)$$

Let us for a moment consider the unconstrained problem analogous to (5.6),

$$\min_{\xi \in X} T. \quad (5.17)$$

Any global minimizer $\tilde{\xi}^{**}$ of (5.17) is clearly non-isolated due to possible reparametrizations of the time. Let ξ^{**} denote the equivalent trajectory with constant ground speed, i.e., $\|\xi_\tau^{**}(\tau)\| = L^{**}$ for almost all τ . Both solutions $\tilde{\xi}^{**}, \xi^{**}$ satisfy the first order necessary condition

$$0 = T'(\xi^{**})[\delta \xi] \quad \forall \delta \xi \in \delta X. \quad (5.18)$$

Moreover, ξ^{**} – together with L^{**} from (5.8) – is a global minimizer of the constrained problem, which indicates that the ground-speed-constraint (5.7) is only weakly active. We confirm this by showing that the corresponding Lagrange multipliers λ^{**} vanish.

Lemma 5.2. — *Let $z^{**} = (\xi^{**}, L^{**})$ be a global minimizer of (5.6). Then, this solution together with*

$$\lambda^{**} = 0 \quad (5.19)$$

satisfies the necessary conditions (5.16).

Proof. Since ξ^{**} is also a global minimizer of the unconstrained problem, the necessary condition (5.18) states that $T'(\xi^{**})\delta \xi = 0$. The term $\int_0^1 \lambda^{**} \left(\delta \xi_\tau^T \xi_\tau^{**} - \delta L L^{**} \right) d\tau$ of (5.16a) vanishes for $\lambda^{**} = 0$. (5.16b) is satisfied because $\|\xi_\tau^{**}\| = L^{**}$ for almost all $\tau \in (0, 1)$. \square

5.3.1.2 Sufficient Conditions

Now we turn to the second order sufficient conditions for optimality. In general, a stationary point (z^*, λ^*) is a strict minimizer, if, in addition to the necessary conditions above, the well known *Ladyzhenskaya–Babuška–Brezzi* (LBB) condition (e.g., [22]) is satisfied, which comprise a) the so called *inf-sup* condition and b) the requirement that the Lagrangian's Hessian regarding z , \mathcal{L}_{zz} , need be positive definite on the kernel of h' .

The *inf-sup* condition states that for the minimizer z^* there is a $\kappa > 0$ such that

$$\inf_{\delta\lambda \neq 0 \in L^2(0,1)} \sup_{\delta z \in \delta Z^2} \frac{\langle \delta\lambda, h'(z^*)[\delta z] \rangle}{\|\delta\lambda\|_{L^2(0,1)} \|\delta z\|_{Z^2}} \geq \kappa. \quad (5.20)$$

Formally, the second part of the LBB condition requires that there is a $\underline{\mathcal{B}} > 0$ such that

$$\mathcal{L}_{zz}(z^*)[\delta z]^2 \geq \underline{\mathcal{B}} \|\delta z\|_{Z^2}^2$$

for any $\delta z \in \delta Z$ that satisfies

$$\langle \delta\lambda, h'(z^*)[\delta z] \rangle = 0 \quad \forall \delta\lambda \in L^2(0,1).$$

In the present case, this reads

$$T''(\xi^*)[\delta\xi]^2 + 2 \int_0^1 \lambda^* (\delta\xi_\tau^T \delta\xi_\tau - \delta L^2) d\tau \geq \underline{\mathcal{B}} \|\delta z\|_{Z^2}^2 \quad (5.21)$$

for any $\delta z \in \delta Z$ such that

$$\int_0^1 \delta\lambda \left(\delta\xi_\tau^T \xi_\tau^* - \delta L L^* \right) d\tau = 0 \quad \forall \delta\lambda \in L^2(0,1).$$

In case of a global minimizer $z^{**} = (\xi^{**}, L^{**})$, this can be reduced using $\lambda^{**} = 0$ from Lemma 5.2. Moreover, the constraint is equivalent to requiring that $\delta\xi_\tau^T \xi_\tau^{**} = \delta L L^{**}$ almost everywhere. With this, we conclude that for any isolated global minimizer z^{**} of (5.6) that satisfies the *inf-sup* condition, there exists a $\underline{\mathcal{B}} > 0$ such that

$$T''(\xi^{**})[\delta\xi, \delta\xi_\tau]^2 \geq \underline{\mathcal{B}} \|\delta z\|_{Z^2}^2 \quad (5.22)$$

for any $\delta z \in \delta Z$ such that $\delta\xi_\tau^T \xi_\tau^{**} = \delta L L^{**}$ almost everywhere.

It is important to note that the second order sufficient conditions are formulated in a L^2 -setting, while differentiability only holds in L^∞ . This is known as *two-norm-discrepancy* [23].

5.3.2 Newton's Method

In order to provide a more compact notation, we use $\chi = (z, \lambda) \in Z \times \Lambda^* =: Y$ in this context and define F as the total derivative of the Lagrangian,

$$F : Z \times \Lambda^* \mapsto \delta Z^* \times \Lambda, \quad F(\chi) := \mathcal{L}'(z, \lambda). \quad (5.23)$$

On Y we define the following norms,

$$\|\chi\|_{Y^\infty} = \|z\|_{Z^\infty} + \|\lambda\|_{L^\infty(0,1)} \quad \text{and} \quad (5.24a)$$

$$\|\chi\|_{Y^2} = \|z\|_{Z^2} + \|\lambda\|_{L^2(0,1)}. \quad (5.24b)$$

The problem is now to find a χ^{**} such that the first order necessary conditions for optimality as stated in (5.16) are satisfied, which translates to

$$F(\chi^{**}) = 0. \quad (5.25)$$

Applying Newton's method, we iteratively solve

$$F'(\chi^k)[\Delta\chi^k] = -F(\chi^k) \quad (5.26)$$

for $\Delta\chi^k$ and proceed with $\chi^{k+1} \leftarrow \chi^k + \Delta\chi^k$, starting with some initial value χ^0 .

In other words, in every iteration we need to find $(\Delta z^k, \Delta\lambda^k)$ such that

$$\begin{aligned} T''(\xi^k)[\delta\xi][\Delta\xi^k] + \langle \lambda^k, h''(z^k)[\delta z][\Delta z^k] \rangle + \langle \Delta\lambda^k, h'(z^k)[\delta z] \rangle \\ = -T'(\xi^k)[\delta\xi] - \langle \lambda^k, h'(z^k)[\delta z] \rangle \quad \forall \delta z \in \delta Z, \end{aligned} \quad (5.27a)$$

$$\langle \delta\lambda, h'(z^k)[\Delta z^k] \rangle = -\langle \delta\lambda, h(z^k) \rangle \quad \forall \delta\lambda \in \Lambda^*. \quad (5.27b)$$

5.4 Proof of Convergence

On the way to prove the existence of a non-empty domain $\mathcal{N}(\chi^{**}, R)$ such that Newton's method as defined in Section 5.3.2 converges to the corresponding global minimizer χ^{**} , if initialized with a starting point within this neighborhood, we first prove that the KKT-operator F' is invertible and that the Newton step $\Delta\chi^k$ is always well defined. Essentially, this is the case if the LBB condition as given in (5.20) and (5.22) is satisfied. Hence, we will show that there is a $R > 0$ such that

the *inf-sup* condition is satisfied and that the Lagrangian is positive definite on the kernel of the constraints for any $\chi \in \mathcal{N}(\chi^{**}, R)$. Further, we show that an affine covariant Lipschitz condition holds, which finally helps to complete the proof.

Before we get there, we recall Lemma 3.7 which provides a bound for the path length of a global minimizer.

Lemma 5.3. — *Let $z^{**}=(L^{**}, \xi^{**})$ be a global minimizer of (5.6), let $\|w\|_{L^\infty(\Omega)} \leq \bar{c}_0$, and define $\tilde{L} = \|x_D - x_O\|$. Then it holds that*

$$\tilde{L} \leq L^{**} \leq \frac{\bar{v} + \bar{c}_0}{\bar{v} - \bar{c}_0} \tilde{L}. \quad (5.28)$$

As most of the subsequent results hold in a L^∞ -neighborhood of a minimizer, we introduce the following notation.

Definition 5.2. — *We call the L^∞ -neighborhood of a point $z \in Z$ or $x \in Y$,*

$$\mathcal{N}(z, R) := \{\tilde{z} \in Z : \|\tilde{z} - z\|_{Z^\infty} \leq R\} \quad \text{or} \quad (5.29a)$$

$$\mathcal{N}(\chi, R) := \{\tilde{\chi} \in Y : \|\tilde{\chi} - \chi\|_{Y^\infty} \leq R\}, \quad (5.29b)$$

respectively.

Moreover, we provide three simple yet useful bounds that hold in such a L^∞ -neighborhood of a minimizer.

Lemma 5.4. — *Let $\chi^{**} = (z^{**}, \lambda^{**})$ be a global minimizer of (5.6) and the corresponding Lagrange multipliers. Then for every $\chi \in \mathcal{N}(\chi^{**}, R)$ it holds that*

$$L^{**} - R \leq L \leq L^{**} + R, \quad (5.30a)$$

$$L^{**} - R \leq \|\xi_\tau\|_{L^\infty(0,1)} \leq L^{**} + R, \quad (5.30b)$$

$$0 \leq \|\lambda\|_{L^\infty(0,1)} \leq R. \quad (5.30c)$$

Proof. The first two inequalities follow immediately, since a global minimizer satisfies the constraint from (5.6). The latter two are a direct consequence of Lemma 5.2. \square

5.4.1 Inf-Sup Condition

We now show that the *inf-sup* condition, introduced in (5.20), holds in a certain neighborhood around a global minimizer. First, however, we point out that deviations $\delta\xi$ and $\delta\xi_\tau$ from a trajectory are inherently related and that the former is always bounded by the latter.

Theorem 5.5 (Wirtinger's inequality). — *Let $\delta\xi \in H_0^1(0, 1)$. Then*

$$\|\delta\xi\|_{L^2(0,1)}^2 \leq \frac{1}{\pi} \|\delta\xi_\tau\|_{L^2(0,1)}^2 \quad (5.31)$$

holds.

Theorem 5.6. — *Let z^{**} be a global minimizer of (5.6). Further, let there be a constant $c > 0$ and some direction $u \in \mathbb{R}^2$ with $\|u\| = 1$ such that $u^\top \xi_\tau^{**} \geq c$ for almost all $\tau \in (0, 1)$. Then for any $z = (L, \xi) \in \mathcal{N}(z^{**}, R)$ with $R < c$ there is some $\kappa > 0$ such that*

$$\inf_{\lambda \neq 0 \in L^2(0,1)} \sup_{\delta z \in \delta Z} \frac{\langle \lambda, h'(z)[\delta z] \rangle}{\|\lambda\|_{L^2(0,1)} \|\delta z\|_{Z^2}} \geq \kappa$$

with

$$\kappa(R) = (c - R) \left[\frac{3}{8} + 2 \left(\frac{\bar{v} + \bar{c}_0}{\bar{v} - \bar{c}_0} + \frac{R}{\bar{L}} \right)^2 \right]^{-1/2}.$$

Proof. For $f \in L^2(0, 1)$ we define

$$\bar{f} := \int_0^1 f \, d\tau \in \mathbb{R} \quad \text{and} \quad \tilde{f} = f - \bar{f},$$

respectively, such that $(\bar{f}, \tilde{f})_{L^2(0,1)} = 0$ and

$$\|f\|_{L^2(0,1)}^2 = \|\tilde{f} + \bar{f}\|_{L^2(0,1)}^2 = \|\tilde{f}\|_{L^2(0,1)}^2 + \bar{f}^2.$$

With

$$\frac{\bar{v} + \bar{c}_0}{\bar{v} - \bar{c}_0} \tilde{L} + R \stackrel{(5.28)}{\geq} L^{**} + R \geq b := \xi_\tau^\top u \geq c - R \quad (5.32)$$

we choose $\delta\xi_\tau = \frac{1}{2}\tilde{\lambda}u$ and $\delta L = \frac{1}{2L}(\overline{b\tilde{\lambda}} - (c-R)\bar{\lambda})$. Note that $\delta\xi \in \delta X$ holds. For this choice, we obtain for $\delta z = (\delta L, \delta\xi)$

$$\begin{aligned}
\langle \lambda, h'(z)[\delta z] \rangle &= \int_0^1 (2\xi_\tau^\top \delta\xi_\tau \lambda - 2L\delta L\lambda) d\tau \\
&= \int_0^1 b\tilde{\lambda}\lambda d\tau - 2L\delta L\bar{\lambda} \\
&= \int_0^1 (b\tilde{\lambda}^2 + b\tilde{\lambda}\bar{\lambda}) d\tau - 2L\delta L\bar{\lambda} \\
&\stackrel{(5.32)}{\geq} (c-R)\|\tilde{\lambda}\|_{L^2(0,1)}^2 + \left(\int_0^1 b\tilde{\lambda} d\tau - 2L\delta L \right) \bar{\lambda} \\
&= (c-R)\|\tilde{\lambda}\|_{L^2(0,1)}^2 + \left(\int_0^1 b\tilde{\lambda} d\tau - \overline{b\tilde{\lambda}} + (c-R)\bar{\lambda} \right) \bar{\lambda} \\
&= (c-R) \left(\|\tilde{\lambda}\|_{L^2(0,1)}^2 + \bar{\lambda}^2 \right) \\
&= (c-R)\|\lambda\|_{L^2(0,1)}^2.
\end{aligned}$$

Moreover, we have

$$\|\delta\xi_\tau\|_{L^2(0,1)} \leq \frac{1}{2}\|\tilde{\lambda}\|_{L^2(0,1)}$$

and, since clearly $c \leq L^{**}$,

$$\begin{aligned}
|\delta L| &\leq \frac{1}{2L} \left(\|b\|_{L^2(0,1)}\|\tilde{\lambda}\|_{L^2(0,1)} + (c-R)|\bar{\lambda}| \right) \\
&\stackrel{(5.32)}{\leq} \frac{1}{\tilde{L}} \left((L^{**} + R)\|\tilde{\lambda}\|_{L^2(0,1)} + (c-R)|\bar{\lambda}| \right) \\
&\leq \left(\frac{\bar{v} + \bar{c}_0}{\bar{v} - \bar{c}_0} + \frac{R}{\tilde{L}} \right) \left(\|\tilde{\lambda}\|_{L^2(0,1)} + |\bar{\lambda}| \right),
\end{aligned}$$

which implies

$$\begin{aligned}
\|\delta z\|_{Z^2}^2 &\stackrel{(5.12b)}{=} \|\delta\xi\|_{L^2(0,1)}^2 + \|\delta\xi_\tau\|_{L^2(0,1)}^2 + \delta L^2 \\
&\stackrel{(5.31)}{\leq} \frac{3}{2}\|\delta\xi_\tau\|_{L^2(0,1)}^2 + \delta L^2 \\
&\leq \frac{3}{8}\|\tilde{\lambda}\|_{L^2(0,1)}^2 + \left(\frac{\bar{v} + \bar{c}_0}{\bar{v} - \bar{c}_0} + \frac{R}{\tilde{L}} \right)^2 \left(\|\tilde{\lambda}\|_{L^2(0,1)} + \bar{\lambda} \right)^2 \\
&\leq \frac{3}{8}\|\tilde{\lambda}\|_{L^2(0,1)}^2 + 2 \left(\frac{\bar{v} + \bar{c}_0}{\bar{v} - \bar{c}_0} + \frac{R}{\tilde{L}} \right)^2 \|\tilde{\lambda}\|_{L^2(0,1)}^2 + 2 \left(\frac{\bar{v} + \bar{c}_0}{\bar{v} - \bar{c}_0} + \frac{R}{\tilde{L}} \right)^2 \bar{\lambda}^2 \\
&\leq \left[\frac{3}{8} + 2 \left(\frac{\bar{v} + \bar{c}_0}{\bar{v} - \bar{c}_0} + \frac{R}{\tilde{L}} \right)^2 \right] \left(\|\tilde{\lambda}\|_{L^2(0,1)}^2 + \bar{\lambda}^2 \right) \\
&= \left[\frac{3}{8} + 2 \left(\frac{\bar{v} + \bar{c}_0}{\bar{v} - \bar{c}_0} + \frac{R}{\tilde{L}} \right)^2 \right] \|\lambda\|_{L^2(0,1)}^2.
\end{aligned}$$

Consequently,

$$\langle \lambda, h'(z)[\delta z] \rangle \geq (c - R) \left[\frac{3}{8} + 2 \left(\frac{\bar{v} + \bar{c}_0}{\bar{v} - \bar{c}_0} + \frac{R}{\bar{L}} \right)^2 \right]^{-1/2} \|\lambda\|_{L^2(0,1)} \|\delta z\|_{Z^2}$$

yields the claim. \square

5.4.2 Positive Definiteness of the Lagrangian

The next step in order to prove invertibility of the KKT-operator $F'(\chi)$, (5.26), is to show that the second partial derivative of the Lagrangian $\mathcal{L}(\chi)$, (5.15), with respect to the state z is positive definite on the kernel of the linearized constraints. On the way we derive a similar result for the objective $T(\xi)$, (5.2) for which we first derive an upper bound for its third derivative.

Lemma 5.7. — *Let $\|w\|_{L^\infty(\Omega)} \leq \bar{c}_0 \leq \bar{v}/\sqrt{5}$, $\|w_x\|_{L^\infty(\Omega)} \leq \bar{c}_1$, $\|w_{xx}\|_{L^\infty(\Omega)} \leq \bar{c}_2$, and $\|w_{xxx}\|_{L^\infty(\Omega)} \leq \bar{c}_3$ and define $\underline{v}^2 := \bar{v}^2 - \bar{c}_0^2$. Then, for any $\xi \in X$, the third directional derivative of f as given in (5.3) is bounded by*

$$\begin{aligned} & |f'''(\xi, \xi_\tau)[\delta\xi, \delta\xi_\tau]^2[\Delta\xi, \Delta\xi_\tau]| \\ & \leq \left(\bar{\gamma}_0 \|\xi_\tau\| \|\delta\xi\|^2 + \bar{\gamma}_2 \|\delta\xi\| \|\delta\xi_\tau\| + \frac{\bar{\gamma}_4}{\|\xi_\tau\|} \|\delta\xi_\tau\|^2 \right) \|\Delta\xi\| \\ & \quad + \left(\bar{\gamma}_1 \|\delta\xi\|^2 + \frac{\bar{\gamma}_3}{\|\xi_\tau\|} \|\delta\xi\| \|\delta\xi_\tau\| + \frac{\bar{\gamma}_5}{\|\xi_\tau\|^2} \|\delta\xi_\tau\|^2 \right) \|\Delta\xi_\tau\| \end{aligned} \quad (5.33)$$

with $\bar{\gamma}_i \geq 0$, $i \in 0, \dots, 5$, given as

$$\begin{aligned} \bar{\gamma}_0 &= \frac{2}{\underline{v}^4} (37\bar{c}_1^3 + 21\bar{c}_1\bar{c}_2\underline{v} + 2\bar{c}_3\underline{v}^2), & \bar{\gamma}_3 &= 40\frac{\bar{c}_1}{\underline{v}^2}, \\ \bar{\gamma}_1 &= \frac{1}{\underline{v}^3} (29\bar{c}_1^2 + 7\underline{v}\bar{c}_2), & \bar{\gamma}_4 &= 20\frac{\bar{c}_1}{\underline{v}^2}, \\ \bar{\gamma}_2 &= \frac{1}{\underline{v}^3} (57\bar{c}_1^2 + 13\underline{v}\bar{c}_2), & \bar{\gamma}_5 &= 18\frac{1}{\underline{v}}. \end{aligned} \quad (5.34)$$

The proof can again be found in the appendix. With this result we can derive a bound for the third directional derivative of T .

Theorem 5.8. — *Let (L^{**}, ξ^{**}) be a global minimizer of (5.6) and define $\tilde{L} := \|x_D - x_O\|$ and $\Delta\xi := \xi - \xi^{**}$. Moreover, let $\|w(p)\| \leq \bar{c}_0 \leq \bar{v}/\sqrt{5}$,*

$\|w_x(p)\| \leq \bar{c}_1$, $\|w_{xx}(p)\| \leq \bar{c}_2$, and $\|w_{xxx}(p)\| \leq \bar{c}_3$ for every $p \in \Omega$. Then, for any $\xi \in X$ with $\|\Delta\xi\|_{X^\infty} \leq R < \tilde{L}$, it holds that

$$|T'''(\xi)[\delta\xi]^2[\Delta\xi]| \leq \bar{\Gamma} \left(\|\delta\xi\|_{L^2(0,1)}^2 + \|\delta\xi_\tau\|_{L^2(0,1)}^2 \right) \|\Delta\xi\|_{C^{0,1}(0,1)}. \quad (5.35)$$

with $\|\Delta\xi\|_{C^{0,1}(0,1)} = \|\Delta\xi\|_{L^\infty(0,1)} + \|\Delta\xi_\tau\|_{L^\infty(0,1)}$ and

$$\bar{\Gamma} := \max \left\{ \left(\frac{\bar{v} + \bar{c}_0}{\bar{v} - \bar{c}_0} \tilde{L} + R \right) \bar{\gamma}_0 + \frac{\bar{\gamma}_2}{2}, \quad \frac{\bar{\gamma}_4}{\tilde{L} - R} + \frac{\bar{\gamma}_2}{2}, \right. \\ \left. \bar{\gamma}_1 + \frac{\bar{\gamma}_3}{2(\tilde{L} - R)}, \quad \frac{\bar{\gamma}_3}{2(\tilde{L} - R)} + \frac{\bar{\gamma}_5}{(\tilde{L} - R)^2} \right\} \quad (5.36)$$

and $\bar{\gamma}_0, \dots, \bar{\gamma}_5$ as given in Lemma 5.7 above.

Proof. From the definition of T in (5.2), we know that

$$T'''(\xi)[\delta\xi]^2[\Delta\xi] = \int_0^1 f'''(\xi, \xi_\tau)[\delta\xi, \delta\xi_\tau]^2[\Delta\xi, \Delta\xi_\tau] d\tau.$$

Inserting the bound from Lemmas 5.4 and 5.7 above and using Young's inequality yields

$$\begin{aligned} & |T'''(\xi)[\delta\xi]^2[\Delta\xi]| \\ & \leq \int_0^1 \left(\bar{\gamma}_0 \|\xi_\tau\| \|\delta\xi\|^2 + \bar{\gamma}_2 \|\delta\xi\| \|\delta\xi_\tau\| + \frac{\bar{\gamma}_4}{\|\xi_\tau\|} \|\delta\xi_\tau\|^2 \right) \|\Delta\xi\| \\ & \quad + \left(\bar{\gamma}_1 \|\delta\xi\|^2 + \frac{\bar{\gamma}_3}{\|\xi_\tau\|} \|\delta\xi\| \|\delta\xi_\tau\| + \frac{\bar{\gamma}_5}{\|\xi_\tau\|^2} \|\delta\xi_\tau\|^2 \right) \|\Delta\xi_\tau\| d\tau. \\ & \leq \|\Delta\xi\|_{L^\infty} \int_0^1 \bar{\gamma}_0 \|\xi_\tau\| \|\delta\xi\|^2 + \bar{\gamma}_2 \|\delta\xi\| \|\delta\xi_\tau\| + \frac{\bar{\gamma}_4}{\|\xi_\tau\|} \|\delta\xi_\tau\|^2 d\tau \\ & \quad + \|\Delta\xi_\tau\|_{L^\infty} \int_0^1 \bar{\gamma}_1 \|\delta\xi\|^2 + \frac{\bar{\gamma}_3}{\|\xi_\tau\|} \|\delta\xi\| \|\delta\xi_\tau\| + \frac{\bar{\gamma}_5}{\|\xi_\tau\|^2} \|\delta\xi_\tau\|^2 d\tau \\ & \stackrel{(5.30)}{\leq} \|\Delta\xi\|_{L^\infty} \int_0^1 \left(\frac{\bar{v} + \bar{c}_0}{\bar{v} - \bar{c}_0} \tilde{L} + R \right) \bar{\gamma}_0 \|\delta\xi\|^2 + \bar{\gamma}_2 \|\delta\xi\| \|\delta\xi_\tau\| + \frac{\bar{\gamma}_4}{\tilde{L} - R} \|\delta\xi_\tau\|^2 d\tau \\ & \quad + \|\Delta\xi_\tau\|_{L^\infty} \int_0^1 \bar{\gamma}_1 \|\delta\xi\|^2 + \frac{\bar{\gamma}_3}{\tilde{L} - R} \|\delta\xi\| \|\delta\xi_\tau\| + \frac{\bar{\gamma}_5}{(\tilde{L} - R)^2} \|\delta\xi_\tau\|^2 d\tau \\ & \stackrel{(Y)}{\leq} \|\Delta\xi\|_{L^\infty} \left[\left(\left(\frac{\bar{v} + \bar{c}_0}{\bar{v} - \bar{c}_0} \tilde{L} + R \right) \bar{\gamma}_0 + \frac{\bar{\gamma}_2}{2} \right) \|\delta\xi\|_{L^2}^2 + \left(\frac{\bar{\gamma}_4}{\tilde{L} - R} + \frac{\bar{\gamma}_2}{2} \right) \|\delta\xi_\tau\|_{L^2}^2 \right] \\ & \quad + \|\Delta\xi_\tau\|_{L^\infty} \left[\left(\bar{\gamma}_1 + \frac{\bar{\gamma}_3}{2(\tilde{L} - R)} \right) \|\delta\xi\|_{L^2}^2 + \left(\frac{\bar{\gamma}_3}{2(\tilde{L} - R)} + \frac{\bar{\gamma}_5}{(\tilde{L} - R)^2} \right) \|\delta\xi_\tau\|_{L^2}^2 \right] \\ & \stackrel{(5.36)}{\leq} \bar{\Gamma} \left(\|\delta\xi\|_{L^2(0,1)}^2 + \|\delta\xi_\tau\|_{L^2(0,1)}^2 \right) \|\Delta\xi\|_{C^{0,1}(0,1)}. \end{aligned}$$

□

Having bounded the third derivative of T , we can estimate the potential decay of T'' and thus derive a lower bound for the size of this neighborhood. Similarly, we can bound h'' and hence \mathcal{L}_{zz} .

Theorem 5.9. — *Let $\|w\|_{L^\infty(\Omega)} \leq \bar{c}_0 < \bar{v}/\sqrt{5}$, $\|w_x\|_{L^\infty(\Omega)} \leq \bar{c}_1$, $\|w_{xx}\|_{L^\infty(\Omega)} \leq \bar{c}_2$, and $\|w_{xxx}\|_{L^\infty(\Omega)} \leq \bar{c}_3$ and define $\tilde{L} := \|x_D - x_O\|$. Moreover, let $\chi^{**} := (z^{**}, \lambda^{**})$ be a globally optimal solution to problem (5.6), that satisfies the necessary and sufficient conditions (5.16), (5.20), and (5.22) with $\underline{\mathcal{B}} > 0$.*

Then there is a $0 < R < \min\left\{\frac{\underline{\mathcal{B}}}{2\bar{\Gamma}}, \frac{\underline{\mathcal{B}}}{40}, \frac{\tilde{L}}{2}\right\}$ with $\bar{\Gamma}$ from Theorem 5.8 such that

$$\mathcal{L}_{zz}(\chi)[\delta z]^2 \geq \frac{\underline{\mathcal{B}}}{4} \|\delta z\|_{Z^2}^2 \quad (5.37)$$

*holds for any $\chi \in \mathcal{N}(\chi^{**}, R)$ and any $\delta z \in \delta Z$ such that $\xi_\tau^T \delta \xi_\tau = L\delta L$ holds almost everywhere.*

Proof. Let $\Delta\xi := \xi - \xi^{**}$ and note that $\|\Delta\xi\|_{L^\infty(0,1)} \leq \|\Delta z\|_{Z^\infty} \leq R < \frac{\underline{\mathcal{B}}}{2\bar{\Gamma}}$. Then we obtain

$$\begin{aligned} T''(\xi)[\delta\xi, \delta\xi_\tau]^2 &= T''(\xi^{**})[\delta\xi, \delta\xi_\tau]^2 + \int_0^1 T'''(\xi + \nu\Delta\xi)[\delta\xi, \delta\xi_\tau]^2[\Delta\xi, \Delta\xi_\tau] d\nu \\ &\stackrel{(5.22)}{\geq} \underline{\mathcal{B}}\|\delta z\|_{Z^2}^2 + \int_0^1 T'''(\xi + \nu\Delta\xi)[\delta\xi, \delta\xi_\tau]^2[\Delta\xi, \Delta\xi_\tau] d\nu \\ &\stackrel{(5.35)}{\geq} \underline{\mathcal{B}}\|\delta z\|_{Z^2}^2 - \bar{\Gamma}(\|\delta\xi\|_{L^2(0,1)}^2 + \|\delta\xi_\tau\|_{L^2(0,1)}^2) \|\Delta z\|_{Z^\infty} \\ &\stackrel{(5.12b)}{\geq} \underline{\mathcal{B}}\|\delta z\|_{Z^2}^2 - \bar{\Gamma}\|\delta z\|_{Z^2}^2 \|\Delta z\|_{Z^\infty}, \\ &\geq \frac{\underline{\mathcal{B}}}{2} \|\delta z\|_{Z^2}^2. \end{aligned}$$

Further, we point out that

$$R \leq \frac{\tilde{L}}{2} \leq \frac{L^{**}}{2}, \quad (5.38)$$

which together with the bounds from Lemma 5.4 yields

$$\begin{aligned}
\langle h''(z)[\delta z]^2 \rangle &= \int_0^1 \lambda \left(\delta \xi_\tau^\top \delta \xi_\tau - \delta L^2 \right) d\tau \\
&= \int_0^1 \lambda \left(\|\delta \xi_\tau\|^2 - \left(\frac{\xi_\tau^\top \delta \xi_\tau}{L} \right)^2 \right) d\tau \\
&\geq -\|\lambda\|_{L^\infty(0,1)} \left(\|\delta \xi_\tau\|_{L^2(0,1)}^2 + \int_0^1 \frac{\|\xi_\tau\|^2 \|\delta \xi_\tau\|^2}{L^2} d\tau \right) \\
&\geq -\|\lambda\|_{L^\infty(0,1)} \left(\|\delta \xi_\tau\|_{L^2(0,1)}^2 + \frac{\|\xi_\tau\|_{L^\infty(0,1)}^2}{L^2} \int_0^1 \|\delta \xi_\tau\|^2 d\tau \right) \\
&\stackrel{(5.30)}{\geq} -R \left(\|\delta \xi_\tau\|_{L^2(0,1)}^2 + \frac{(L^{**} + R)^2}{(L^{**} - R)^2} \|\delta \xi_\tau\|_{L^2(0,1)}^2 \right) \\
&\geq -R \left(1 + \frac{(L^{**} + R)^2}{(L^{**} - R)^2} \right) \|\delta \xi_\tau\|_{L^2(0,1)}^2 \\
&\stackrel{(5.38)}{\geq} -10R \|\delta \xi_\tau\|_{L^2(0,1)}^2 \\
&\geq -\frac{\mathcal{B}}{4} \|\delta \xi_\tau\|_{L^2(0,1)}^2 \\
&\stackrel{(5.12b)}{\geq} -\frac{\mathcal{B}}{4} \|\delta z\|_{Z^2}^2.
\end{aligned}$$

Together, these bounds yield the claim with

$$\begin{aligned}
\mathcal{L}_{zz}(\chi)[\delta z]^2 &= T''(\xi)[\delta \xi]^2 + \langle h''(z)[\delta z]^2 \rangle \\
&\geq \frac{\mathcal{B}}{2} \|\delta z\|_{Z^2}^2 - \frac{\mathcal{B}}{4} \|\delta z\|_{Z^2}^2 \\
&\geq \frac{\mathcal{B}}{4} \|\delta z\|_{Z^2}^2.
\end{aligned}$$

□

5.4.3 Upper Bound for the Lagrangian

As a counterpart to the previous Lemma, we also derive an upper bound for L_{zz} close to a minimizer. Again we start with the underlying function f in order to bound the error in the objective function T .

Lemma 5.10. — *Let $\|w\|_{L^\infty(\Omega)} \leq \bar{c}_0 \leq \frac{\bar{v}}{\sqrt{5}}$, $\|w_x\|_{L^\infty(\Omega)} \leq \bar{c}_1$, and $\|w_{xx}\|_{L^\infty(\Omega)} \leq \bar{c}_2$. Moreover, let $\underline{v}^2 := \bar{v}^2 - \bar{c}_0^2$. Then, for any $\xi \in X$, the second directional derivative*

of f as given in (5.3) is bounded by

$$\begin{aligned}
|f''(\xi, \xi_\tau)[\delta\xi, \delta\xi_\tau][\tilde{\delta}\xi, \tilde{\delta}\xi_\tau]| &\leq \bar{\beta}_0 \|\xi_\tau\| \|\delta\xi\| \|\tilde{\delta}\xi\| \\
&\quad + \bar{\beta}_1 \left(\|\delta\xi\| \|\tilde{\delta}\xi_\tau\| + \|\delta\xi_\tau\| \|\tilde{\delta}\xi\| \right) \\
&\quad + \bar{\beta}_2 \|\xi_\tau\|^{-1} \|\delta\xi_\tau\| \|\tilde{\delta}\xi_\tau\|
\end{aligned} \tag{5.39}$$

with

$$\bar{\beta}_0 = 14 \frac{\bar{c}_1^2}{\underline{v}^3} + 4 \frac{\bar{c}_2}{\underline{v}^2}, \quad \bar{\beta}_1 = 7 \frac{\bar{c}_1}{\underline{v}^2}, \quad \text{and} \quad \bar{\beta}_2 = \frac{4}{\underline{v}}. \tag{5.40}$$

The proof can be found in the appendix.

Theorem 5.11. — *Let $z^{**} := (L^{**}, \xi^{**})$ be a global minimizer of (5.6) and $\Delta z := z - z^{**}$. Moreover, let $\|w\|_{L^\infty(\Omega)} \leq \bar{c}_0 \leq \bar{v}/\sqrt{5}$, $\|w_x\|_{L^\infty(\Omega)} \leq \bar{c}_1$, and $\|w_{xx}\|_{L^\infty(\Omega)} \leq \bar{c}_2$. Also define $\underline{v}^2 := \bar{v}^2 - \bar{c}_0^2$ and $\tilde{L} := \|x_D - x_O\|$. Then, for any $z \in \mathcal{N}(z^{**}, R)$, the second directional derivative of T as defined in (5.2) is bounded by*

$$|T''(\xi)[\Delta\xi]^2| \leq \bar{\mathcal{B}} \|\Delta z\|_{Z^2}^2 \tag{5.41}$$

with $\bar{\mathcal{B}} := \bar{\beta}_1 + \max \left\{ \left(\frac{\bar{v} + \bar{c}_0}{\bar{v} - \bar{c}_0} \tilde{L} + R \right) \bar{\beta}_0, \frac{\bar{\beta}_2}{L+R} \right\}$ and $\bar{\beta}_0, \bar{\beta}_1, \bar{\beta}_2$ as defined in Lemma 5.10.

Proof. From the definition of T in (5.2) we know that

$$T''(\xi)[\Delta\xi, \Delta\xi_\tau]^2 = \int_0^1 f''[\Delta\xi, \Delta\xi_\tau]^2 d\tau,$$

which, together with the bounds from Lemmas 5.4 and 5.10 as well as Young's

inequality, then leads to

$$\begin{aligned}
|T''(\xi)[\Delta\xi, \Delta\xi_\tau]^2| &\leq \int_0^1 \left(\bar{\beta}_0 \|\xi_\tau\| \|\Delta\xi\|^2 + 2\bar{\beta}_1 \|\Delta\xi\| \|\Delta\xi_\tau\| + \frac{\bar{\beta}_2}{\|\xi_\tau\|} \|\Delta\xi_\tau\|^2 \right) d\tau \\
&\stackrel{(5.30)}{\leq} \bar{\beta}_0 (L^{**} + R) \int_0^1 \|\Delta\xi\|^2 d\tau \\
&\quad + 2\bar{\beta}_1 \int_0^1 \|\Delta\xi\| \|\Delta\xi_\tau\| d\tau \\
&\quad + \frac{\bar{\beta}_2}{L^{**} + R} \int_0^1 \|\Delta\xi_\tau\|^2 d\tau \\
&\stackrel{(Y)}{\leq} \left((L^{**} + R)\bar{\beta}_0 + \bar{\beta}_1 \right) \|\Delta\xi\|_{L^2(0,1)}^2 \\
&\quad + \left(\bar{\beta}_1 + \frac{\bar{\beta}_2}{L^{**} + R} \right) \|\Delta\xi_\tau\|_{L^2(0,1)}^2 \\
&\stackrel{(5.28)}{\leq} \left(\left(\frac{\bar{v} + \bar{c}_0}{\bar{v} - \bar{c}_0} \tilde{L} + R \right) \bar{\beta}_0 + \bar{\beta}_1 \right) \|\Delta\xi\|_{L^2(0,1)}^2 \\
&\quad + \left(\bar{\beta}_1 + \frac{\bar{\beta}_2}{\tilde{L} + R} \right) \|\Delta\xi_\tau\|_{L^2(0,1)}^2 \\
&\leq \bar{\mathcal{B}} \left(\|\Delta\xi\|_{L^2(0,1)}^2 + \|\Delta\xi_\tau\|_{L^2(0,1)}^2 \right) \\
&\stackrel{(5.12b)}{\leq} \bar{\mathcal{B}} \|\Delta z\|_{Z^2}^2.
\end{aligned}$$

□

Theorem 5.12. — *Let $\chi^{**} = (z^{**}, \lambda^{**})$ be a global minimizer of (5.6) and the corresponding Lagrange multipliers. Then for every $\chi \in \mathcal{N}(\chi^{**}, R)$ and every $\delta z \in \delta Z$ it holds that*

$$|\mathcal{L}_{zz}(\chi)[\delta z]^2| \leq (\bar{\mathcal{B}} + R) \|\delta z\|_{Z^2}^2 \quad (5.42)$$

with $\bar{\mathcal{B}}(R)$ from Theorem 5.11.

Proof. Using the bound from Theorem 5.11 and Young's inequality, we get

$$\begin{aligned}
|\mathcal{L}_{zz}(\chi)[\delta z]^2| &= |T''(\xi)[\delta\xi]^2 + \langle h''(z)[\delta z]^2 \rangle| \\
&\stackrel{(5.41)}{\leq} \bar{\mathcal{B}} \|dz\|_{Z^2}^2 + \int_0^1 |\lambda (\delta\xi_\tau^T \delta\xi_\tau - \delta L^2)| d\tau \\
&\leq \bar{\mathcal{B}} \|dz\|_{Z^2}^2 + \|\lambda\|_{L^\infty(0,1)} \left(\|\delta\xi_\tau\|_{L^2(0,1)}^2 + \delta L^2 \right) \\
&\stackrel{(5.30)}{\leq} \bar{\mathcal{B}} \|dz\|_{Z^2}^2 + R \left(\|\delta\xi_\tau\|_{L^2(0,1)}^2 + \delta L^2 \right) \\
&\stackrel{(5.12b)}{\leq} (\bar{\mathcal{B}} + R) \|dz\|_{Z^2}^2.
\end{aligned}$$

□

5.4.4 Invertibility of the KKT-Operator

Using the previous three results, which together state the existence of a neighborhood around a minimizer such that the LBB condition is satisfied, we are now ready to prove that the KKT-operator F' is invertible.

Lemma 5.13. — *Let $\chi^{**} = (z^{**}, \lambda^{**})$ be a global minimizer of (5.6), that satisfies the first and second order conditions for optimality with some $\underline{\mathcal{B}} > 0$, and the corresponding Lagrange multipliers. Further, let there be a u with $\|u\| = 1$ such that $u^T \xi_\tau^{**} \geq c > 0$ for almost all $\tau \in (0, 1)$. Then for F as given in (5.23) it holds that*

$$\|F'(\chi)^{-1}\|_{Y^2} \leq \omega_1 \quad (5.43)$$

for every $\chi = (z, \lambda) \in \mathcal{N}(\chi^{**}, R)$ and

$$\omega_1 = \sqrt{2} \max \left\{ \frac{4}{\underline{\mathcal{B}}}, \frac{1}{\kappa} \left(1 + \frac{4(\overline{\mathcal{B}} + R)}{\underline{\mathcal{B}}} \right), \frac{\overline{\mathcal{B}} + R}{\kappa^2} \right\} \quad (5.44)$$

and $\overline{\mathcal{B}}(R)$ and $\kappa(R)$ as given in Theorem 5.11 and Theorem 5.6, respectively.

Proof. The proof builds on some prerequisites that have been established above and are briefly summarized.

i) In Theorem 5.6 it was proved that the *inf-sup* condition is satisfied:

$$\inf_{\delta\lambda \in L^2(0,1)} \sup_{\delta z \in \delta Z} \frac{\langle \delta\lambda, h'(z)[\delta z] \rangle}{\|\delta z\|_{Z^2} \|\delta\lambda\|_{L^2(0,1)}} \geq \kappa > 0.$$

ii) In Theorem 5.9 it was proved that \mathcal{L}_{zz} is positive definite on the kernel of the constraints, i.e.,

$$\mathcal{L}_{zz}(\chi)[\delta z]^2 = T''(\xi)[\delta\xi]^2 + \langle h''(z)[\delta z]^2 \rangle \geq \frac{\underline{\mathcal{B}}}{4} \|\delta z\|_{Z^2}^2$$

for all $\delta z \in \delta Z$ such that $h'(z)[\delta z] = 0$.

iii) In Theorem 5.12 it was proved that \mathcal{L}_{zz} is bounded from above as

$$|\mathcal{L}_{zz}(\chi)[\delta z]^2| = |T''(\xi)[\delta\xi]^2 + \langle h''(z)[\delta z]^2 \rangle| \leq (\overline{\mathcal{B}} + R) \|\delta z\|_{Z^2}^2.$$

Under these conditions, it follows from *Brezzi's Splitting Theorem* [22, Thm. 4.3] that $F'(x)$ is isomorphic. Further, it can be shown that for every right hand side $F(x)$ of the saddle point problem (5.26) there is exactly one solution $(\Delta z, \Delta \lambda)$ with

$$\begin{aligned}\|\Delta z\|_{Z^2} &\leq \frac{4}{\underline{\mathcal{B}}} \|T'(\xi) + \langle \lambda, h'(z) \rangle\|_{Z^2} \\ &\quad + \frac{1}{\kappa} \left(1 + \frac{4(\overline{\mathcal{B}} + R)}{\underline{\mathcal{B}}}\right) \|h(z)\|_{L^2(0,1)}, \\ \|\Delta \lambda\|_{L^2(0,1)} &\leq \frac{1}{\kappa} \left(1 + \frac{4(\overline{\mathcal{B}} + R)}{\underline{\mathcal{B}}}\right) \|T'(\xi) + \langle \lambda, h'(z) \rangle\|_{Z^2} \\ &\quad + \frac{\overline{\mathcal{B}} + R}{\kappa^2} \left(1 + \frac{4(\overline{\mathcal{B}} + R)}{\underline{\mathcal{B}}}\right) \|h(z)\|_{L^2(0,1)}.\end{aligned}$$

With $\|F(\chi)\| = \|T'(\xi) + \langle \lambda, h'(z) \rangle\|_{Z^2}^2 + \|h(z)\|_{L^2(0,1)}^2$ follows that

$$\begin{aligned}\|\Delta z\|_{Z^2} &\leq \sqrt{2} \max \left\{ \frac{4}{\underline{\mathcal{B}}}, \frac{1}{\kappa} \left(1 + \frac{4(\overline{\mathcal{B}} + R)}{\underline{\mathcal{B}}}\right) \right\} \|F(\chi)\|, \\ \|\Delta \lambda\|_{L^2(0,1)} &\leq \sqrt{2} \max \left\{ \frac{1}{\kappa} \left(1 + \frac{4(\overline{\mathcal{B}} + R)}{\underline{\mathcal{B}}}\right), \frac{\overline{\mathcal{B}} + R}{\kappa^2} \right\} \|F(\chi)\|,\end{aligned}$$

which directly yields

$$\|\Delta \chi\|_{Y^2}^2 \stackrel{(5.24b)}{=} \|\Delta z\|_{Z^2}^2 + \|\Delta \lambda\|_{L^2(0,1)}^2 \leq \omega_1^2 \|F(\chi)\|$$

with $\omega_1 = \sqrt{2} \max \left\{ \frac{4}{\underline{\mathcal{B}}}, \frac{1}{\kappa} \left(1 + \frac{4(\overline{\mathcal{B}} + R)}{\underline{\mathcal{B}}}\right), \frac{\overline{\mathcal{B}} + R}{\kappa^2} \right\}$. This completes the proof, since

$$\|F'(\chi)^{-1}\|_{Y^2} = \sup_{\|F(\chi)\|_{Y^2}} \frac{\|\Delta \chi\|_{Y^2}}{\|F(\chi)\|_{Y^2}} \leq \omega_1.$$

□

5.4.5 Lipschitz Constant

We are on the verge of presenting a Lipschitz constant for the free flight problem. To accomplish this, we introduce an additional bound in the form of a Lemma. This bound incorporates the constant $\hat{\mathcal{B}}$, which is derived in the appendix (Lemma 5.16). It serves to define an upper limit on the second derivative of f as defined in Equation (5.3). Its value is contingent upon the overall characteristics of the wind field.

Lemma 5.14. — *Let $\chi^{**} = (z^{**}, \lambda^{**})$ be a global minimizer of (5.6) and the corresponding Lagrange multipliers. For any $\chi_{i \in \{1,2\}} \in \mathcal{N}(\chi^{**}, R)$ there is a $\hat{\mathcal{B}}$ such that*

$$\|(F'(\chi_2) - F'(\chi_1))[\chi_2 - \chi_1]\|_{Y^2} \leq \omega_2 \|\chi_2 - \chi_1\|_{Y^2} \quad (5.45)$$

with

$$\omega_2 = (8 + \hat{\mathcal{B}})R. \quad (5.46)$$

Proof. From Lemma 5.4 it directly follows that

$$|L_2 - L_1| \leq 2R, \quad (5.47a)$$

$$\|\xi_{\tau,2} - \xi_{\tau,1}\|_{L^\infty(0,1)} \leq 2R, \quad (5.47b)$$

$$\|\lambda_2 - \lambda_1\|_{L^\infty(0,1)} \leq R. \quad (5.47c)$$

Using these bounds as well as the Cauchy-Schwarz inequality and Young's inequality,

we show that for any $\delta\chi \in \delta Z \times L^2(0, 1)$ with $\|\delta\chi\|_{L^2(0,1)} \leq 1$ it holds that

$$\begin{aligned}
& |\langle \lambda_2, h''(z_2)[z_2 - z_1, \delta z] \rangle - \langle \lambda_1, h''(z_1)[z_2 - z_1, \delta z] \rangle| \\
&= \left| \int_0^1 \lambda_2 (\delta \xi_\tau^\top (\xi_{\tau,2} - \xi_{\tau,1}) - \delta L(L_2 - L_1)) \right. \\
&\quad \left. - \lambda_1 (\delta \xi_\tau^\top (\xi_{\tau,2} - \xi_{\tau,1}) - \delta L(L_2 - L_1)) d\tau \right| \\
&= \left| \int_0^1 (\lambda_2 - \lambda_1) (\delta \xi_\tau^\top (\xi_{\tau,2} - \xi_{\tau,1}) - \delta L(L_2 - L_1)) d\tau \right| \\
&\leq \int_0^1 |\lambda_2 - \lambda_1| \|\delta \xi_\tau\| \|\xi_{\tau,2} - \xi_{\tau,1}\| d\tau \\
&\quad + |\delta L| |L_2 - L_1| \int_0^1 |\delta \lambda| d\tau \\
&\stackrel{(\text{CS})}{\leq} \left[\int_0^1 \|\delta \xi_\tau\|^2 d\tau \right]^{1/2} \left[\int_0^1 (\lambda_2 - \lambda_1)^2 \|\xi_{\tau,2} - \xi_{\tau,1}\|^2 d\tau \right]^{1/2} \\
&\quad + |\delta L| |L_2 - L_1| \|\lambda_2 - \lambda_1\|_{L^1} \\
&\stackrel{(5.47)}{\leq} \|\delta \xi_\tau\|_{L^2} \left[2R^2 \int_0^1 |\lambda_2 - \lambda_1| \|\xi_{\tau,2} - \xi_{\tau,1}\| d\tau \right]^{1/2} \\
&\quad + R |\delta L| |L_2 - L_1| \\
&\stackrel{(\text{CS})}{\leq} \sqrt{2}R \|\delta \xi_\tau\|_{L^2} \|\lambda_2 - \lambda_1\|_{L^2}^{1/2} \|\xi_{\tau,2} - \xi_{\tau,1}\|_{L^2}^{1/2} \\
&\quad + R |\delta L| |L_2 - L_1| \\
&\stackrel{(\text{Y})}{\leq} \frac{\sqrt{2}}{2} R \|\delta \xi_\tau\|_{L^2} [\|\lambda_2 - \lambda_1\|_{L^2} + \|\xi_{\tau,2} - \xi_{\tau,1}\|_{L^2}] \\
&\quad + R |\delta L| |L_2 - L_1| \\
&\leq \frac{\sqrt{2}}{2} R [\|\lambda_2 - \lambda_1\|_{L^2} + \|\xi_{\tau,2} - \xi_{\tau,1}\|_{L^2}] \\
&\quad + R |L_2 - L_1| \\
&\leq R \left[\|\lambda_2 - \lambda_1\|_{L^2} + \|\xi_{\tau,2} - \xi_{\tau,1}\|_{L^2} + \|\xi_2 - \xi_1\|_{L^2} + |L_2 - L_1| \right] \\
&\leq 2R \left[\|\lambda_2 - \lambda_1\|_{L^2}^2 + \|\xi_{\tau,2} - \xi_{\tau,1}\|_{L^2}^2 + \|\xi_2 - \xi_1\|_{L^2}^2 + |L_2 - L_1|^2 \right]^{1/2} \\
&\stackrel{(5.24b)}{=} 2R \|\chi_2 - \chi_1\|_{Y^2}
\end{aligned}$$

as well as

$$\begin{aligned}
& | \langle \lambda_2 - \lambda_1, (h'(z_2) - h'(z_1))[\delta z] \rangle | \\
&= \left| \int_0^1 (\lambda_2 - \lambda_1) \left((\xi_{\tau,2} - \xi_{\tau,1})^T \delta \xi_\tau - (L_2 - L_1) \delta L \right) d\tau \right| \\
&\leq \int_0^1 |\lambda_2 - \lambda_1| \|\xi_{\tau,2} - \xi_{\tau,1}\| \|\delta \xi_\tau\| d\tau \\
&\quad + |L_2 - L_1| |\delta L| \int_0^1 |\lambda_2 - \lambda_1| d\tau \\
&\stackrel{(CS)}{\leq} \left[\int_0^1 \|\delta \xi_\tau\|^2 d\tau \right]^{1/2} \left[\int_0^1 (\lambda_2 - \lambda_1)^2 \|\xi_{\tau,2} - \xi_{\tau,1}\|^2 d\tau \right]^{1/2} \\
&\quad + |L_2 - L_1| |\delta L| \|\lambda_2 - \lambda_1\|_{L^1} \\
&\stackrel{(5.47)}{\leq} \|\delta \xi_\tau\|_{L^2} \left[2R^2 \int_0^1 |\lambda_2 - \lambda_1| \|\xi_{\tau,2} - \xi_{\tau,1}\| d\tau \right]^{1/2} \\
&\quad + R|L_2 - L_1| |\delta L| \\
&\leq \sqrt{2}R \left[\int_0^1 (\lambda_2 - \lambda_1) \|\xi_{\tau,2} - \xi_{\tau,1}\| d\tau \right]^{1/2} \\
&\quad + R|L_2 - L_1| \\
&\stackrel{(CS)}{\leq} \sqrt{2}R \|\lambda_2 - \lambda_1\|_{L^2}^{1/2} \|\xi_{\tau,2} - \xi_{\tau,1}\|_{L^2}^{1/2} \\
&\quad + R|L_2 - L_1| \\
&\stackrel{(Y)}{\leq} \frac{\sqrt{2}}{2} R [\|\lambda_2 - \lambda_1\|_{L^2} + \|\xi_{\tau,2} - \xi_{\tau,1}\|_{L^2}] \\
&\quad + R|L_2 - L_1| \\
&\leq R \left[\|\lambda_2 - \lambda_1\|_{L^2} + \|\xi_{\tau,2} - \xi_{\tau,1}\|_{L^2} + \|\xi_2 - \xi_1\|_{L^2} + |L_2 - L_1| \right] \\
&\leq 2R \left[\|\lambda_2 - \lambda_1\|_{L^2}^2 + \|\xi_{\tau,2} - \xi_{\tau,1}\|_{L^2}^2 + \|\xi_2 - \xi_1\|_{L^2}^2 + |L_2 - L_1|^2 \right]^{1/2} \\
&\stackrel{(5.24b)}{=} 2R \|\chi_2 - \chi_1\|_{Y^2}
\end{aligned}$$

and

$$\begin{aligned}
& |\langle \delta\lambda, (h'(z_2) - h'(z_1))[z_2 - z_1] \rangle| \\
&= \left| \int_0^1 \delta\lambda ((\xi_{\tau,2} - \xi_{\tau,1})^\top (\xi_{\tau,2} - \xi_{\tau,1}) - (L_2 - L_1)^2) d\tau \right| \\
&\leq \int_0^1 |\delta\lambda| \|\xi_{\tau,2} - \xi_{\tau,1}\|^2 d\tau + (L_2 - L_1)^2 \int_0^1 |\delta\lambda| d\tau \\
&\stackrel{(5.47)}{\leq} 2R \int_0^1 |\delta\lambda| \|\xi_{\tau,2} - \xi_{\tau,1}\| d\tau + 2R|L_2 - L_1| \|\delta\lambda\|_{L^1} \\
&\stackrel{(\text{CS})}{\leq} 2R \left[\int_0^1 \delta\lambda^2 d\tau \right]^{1/2} \left[\int_0^1 \|\xi_{\tau,2} - \xi_{\tau,1}\|^2 d\tau \right]^{1/2} \\
&\quad + 2R|L_2 - L_1| \|\delta\lambda\|_{L^1} \\
&\leq 2R \|\delta\lambda\|_{L^2} \|\xi_{\tau,2} - \xi_{\tau,1}\|_{L^2} \\
&\quad + 2R|L_2 - L_1| \|\delta\lambda\|_{L^1} \\
&\leq 2R \|\xi_{\tau,2} - \xi_{\tau,1}\|_{L^2} + 2R|L_2 - L_1| \\
&\leq 2R \left[\|\lambda_2 - \lambda_1\|_{L^2} + \|\xi_{\tau,2} - \xi_{\tau,1}\|_{L^2} + \|\xi_2 - \xi_1\|_{L^2} + |L_2 - L_1| \right] \\
&\leq 4R \left[\|\lambda_2 - \lambda_1\|_{L^2}^2 + \|\xi_{\tau,2} - \xi_{\tau,1}\|_{L^2}^2 + \|\xi_2 - \xi_1\|_{L^2}^2 + |L_2 - L_1|^2 \right]^{1/2} \\
&\stackrel{(5.24b)}{=} 4R \|\chi_2 - \chi_1\|_{Y^2}.
\end{aligned}$$

As shown in Lemma 5.16 in the appendix, there is a $\hat{B} < \infty$ such that

$$|(f''(\xi_2) - f''(\xi_1)) [\xi_2 - \xi_1, \delta\xi]| \leq \hat{B} \sqrt{\|\xi_2 - \xi_1\|^2 + \|\xi_{\tau,2} - \xi_{\tau,1}\|^2} \sqrt{\|\delta\xi\|^2 + \|\delta\xi_\tau\|^2},$$

which provides the following bound, as

$$\begin{aligned}
& |(T''(\xi_2) - T''(\xi_1)) [\xi_2 - \xi_1, \delta\xi]| \\
&= \left| \int_0^1 (f''(\xi_2, \xi_{\tau,2}) - f''(\xi_1, \xi_{\tau,1})) [\xi_2 - \xi_1, \xi_{\tau,2} - \xi_{\tau,1}] [\delta\xi, \delta\xi_\tau] d\tau \right| \\
&\leq \hat{B}R \int_0^1 \left[\|\xi_2 - \xi_1\|^2 + \|\xi_{\tau,2} - \xi_{\tau,1}\|^2 \right]^{1/2} \left[\|\delta\xi\|^2 + \|\delta\xi_\tau\|^2 \right]^{1/2} d\tau \\
&\stackrel{(\text{CS})}{\leq} \hat{B}R \left[\int_0^1 \|\xi_2 - \xi_1\|^2 + \|\xi_{\tau,2} - \xi_{\tau,1}\|^2 d\tau \right]^{1/2} \left[\int_0^1 \|\delta\xi\|^2 + \|\delta\xi_\tau\|^2 d\tau \right]^{1/2} \\
&\leq \hat{B}R \left[\|\xi_2 - \xi_1\|_{L^2}^2 + \|\xi_{\tau,2} - \xi_{\tau,1}\|_{L^2}^2 \right]^{1/2} \left[\|\delta\xi\|_{L^2}^2 + \|\delta\xi_\tau\|_{L^2}^2 \right]^{1/2} \\
&\stackrel{(5.24b)}{\leq} \hat{B}R \|\chi_2 - \chi_1\|_{Y^2} \|\delta\chi\|_{Y^2} \\
&\leq \hat{B}R \|\chi_2 - \chi_1\|_{Y^2}.
\end{aligned}$$

Finally, we use the bounds derived above to show that for any δx with $\|\delta x\|_{Y^2} \leq 1$ it holds that

$$\begin{aligned}
|(F'(\chi_2) - F'(\chi_1))[\chi_2 - \chi_1, \delta\chi]| &= |(T''(\xi_2) - T''(\xi_1))[\delta\xi, \xi_2 - \xi_1] \\
&\quad + \langle \lambda_2, h''(z_2)[\delta z, z_2 - z_1] \rangle \\
&\quad - \langle \lambda_1, h''(z_1)[\delta z, z_2 - z_1] \rangle \\
&\quad + \langle \lambda_2 - \lambda_1, (h'(z_2) - h'(z_1))[\delta z] \rangle \\
&\quad + \langle \delta\lambda, (h'(z_2) - h'(z_1))[z_2 - z_1] \rangle| \\
&\leq \hat{\mathcal{B}}R\|\chi_2 - \chi_1\|_{Y^2} \\
&\quad + 2R\|\chi_2 - \chi_1\|_{Y^2} \\
&\quad + 2R\|\chi_2 - \chi_1\|_{Y^2} \\
&\quad + 4R\|\chi_2 - \chi_1\|_{Y^2} \\
&\leq \omega_2\|\chi_2 - \chi_1\|_{Y^2}
\end{aligned}$$

with

$$\omega_2(R) = (8 + \hat{\mathcal{B}})R.$$

This directly yields the claim, as

$$\begin{aligned}
\|(F'(\chi_2) - F'(\chi_1))[\chi_2 - \chi_1]\|_{Y^2} &= \sup_{\|\delta\chi\|_{Y^2}=1} |(F'(\chi_2) - F'(\chi_1))[\chi_2 - \chi_1, \delta\chi]| \\
&\leq \omega_2\|\chi_2 - \chi_1\|_{Y^2}.
\end{aligned} \tag{5.48}$$

□

5.4.6 Convergence of Newton's Method

We are now ready to connect the results outlined above to prove that the Newton-KKT method applied to the free flight optimization problem (5.6) converges to a global minimizer as characterized in Section 5.3.1 provided that there is a $u \in \mathbb{R}^2$ with $\|u\| = 1$ such that $u^T \xi_\tau^{**} \geq c$. Roughly speaking, the optimal route needs to head towards the destination, dominating any route that involves flying the opposite direction. It is intuitively clear that this holds even for relatively strong wind conditions.

Theorem 5.15. — *Let $\chi^{**} = (z^{**}, \lambda^{**})$ be a global solution of (5.6) that satisfies the first and second order conditions for optimality with $\underline{\mathcal{B}} > 0$. Moreover, let there be a $c > 0$ and a $u \in \mathbb{R}^2$ with $\|u\| = 1$ such that $u^\top \xi_\tau^{**} \geq c$ for almost all $\tau \in (0, 1)$. Finally, let $\omega := \omega_1 \omega_2$, as given in Lemmas 5.13 and 5.14.*

*Then there is a $R_C > 0$, such that the ordinary Newton iterates defined in Section 5.3.2 converge to χ^{**} at an estimated rate*

$$\|\chi^{k+1} - \chi^{**}\|_{Y^2} \leq \frac{\omega}{2} \|\chi^k - \chi^{**}\|_{Y^2}, \quad (5.49)$$

*if initialized with $\chi^0 \in \mathcal{N}(\chi^{**}, R_C)$ and provided that the iterates χ^k remain in $\mathcal{N}(\chi^{**}, R_C)$. Moreover, χ^{**} is unique in $\mathcal{N}(\chi^{**}, R_C)$.*

Proof. In Theorems 5.6, 5.9 and 5.12 we showed that the *inf-sup* condition is satisfied, that, $\mathcal{L}_{zz}(\chi)$ is positive definite on the kernel of the constraint for all $x \in \mathcal{N}(\chi^{**}, R_C)$, and that it is bounded from above. Consequently, $F'(\chi)$ is invertible with

$$\|F'(\chi)^{-1}\| \leq \omega_1 \quad \forall \chi \in \mathcal{N}(\chi^{**}, R_C),$$

as confirmed in Lemma 5.13. Further, it follows from Lemmas 5.13 and 5.14 that

$$\begin{aligned} & \|F'(\chi_1)^{-1}(F'(\chi_2) - F'(\chi_1))[\chi_2 - \chi_1]\|_{Y^2} \\ & \leq \|F'(\chi_1)^{-1}\|_{Y^2} \|(F'(\chi_2) - F'(\chi_1))[\chi_2 - \chi_1]\|_{Y^2} \\ & \leq \omega_1 \omega_2 \|\chi_2 - \chi_1\|_{Y^2} \\ & \leq \omega \|\chi_2 - \chi_1\|_{Y^2} \end{aligned}$$

for $\chi_1, \chi_2 \in \mathcal{N}(\chi^{**}, R_C)$. It is clear that since ω_1 is bounded and $\omega_2 = (8 + \hat{\mathcal{B}})R$, there is a $R_C > 0$ such that $\omega := \omega_1 \omega_2 < 2$. We now define $e_k := \chi^k - \chi^{**}$ and

proceed for $\mu \in (0, 1)$ as follows:

$$\begin{aligned}
& \|\chi^k + \mu\Delta\chi^k - \chi^{**}\|_{Y^2} \\
&= \|e_k - \mu F'(\chi^k)^{-1} F(\chi^k)\|_{Y^2} \\
&= \|e_k - \mu F'(\chi^k)^{-1} (F(\chi^k) - \underbrace{F(\chi^{**})}_{=0})\|_{Y^2} \\
&= \|(1 - \mu)e_k - \mu F'(\chi^k)^{-1} \int_{s=0}^1 (F'(\chi^k - se_k) - F'(\chi^k)) e_k ds\|_{Y^2} \\
&\leq (1 - \mu) \|e_k\|_{Y^2} + \frac{\mu}{2} \omega \|e_k\|_{Y^2},
\end{aligned}$$

which yields the claim with $\mu = 1$ as

$$\|e_{k+1}\|_{Y^2} \leq \frac{\omega}{2} \|e_k\|_{Y^2}.$$

In order to prove uniqueness in $\mathcal{N}(\chi^{**}, R_C)$, assume there is a second solution $\chi^* \neq \chi^{**}$ with $F(\chi^*) = 0$ and $\chi^* \in \mathcal{N}(\chi^{**}, R_C)$. Initialized with $\chi^0 := \chi^*$ it certainly holds that $\chi^1 = \chi^*$. However, from (5.49) we obtain

$$\|\chi^1 - \chi^{**}\|_{Y^2} \leq \frac{\omega}{2} \|\chi^0 - \chi^{**}\|_{Y^2} < \|\chi^0 - \chi^{**}\|_{Y^2},$$

due to $\omega < 2$, which yields a contradiction. \square

5.5 Conclusion

It has been demonstrated that the Newton-KKT method can be used to solve the free flight trajectory optimization problem under certain conditions. These conditions are i) the requirement for the iterates to remain within a L^∞ -neighborhood of the solution, and ii) a starting point that is sufficiently close to the solution. Such a suitable starting point can be found efficiently by calculating shortest paths on a specific graph [13] (Chapter 4). Hence an important tool for efficient deterministic global optimization of the free flight problem has been established.

Authors' Contributions

Conceptualization, R.B and M.W.; methodology, F.D. and M.W.; validation, F.D.; formal analysis, F.D. and M.W.; investigation, F.D. and M.W.; resources, R.B., F.D. and M.W.; writing-original draft preparation, F.D. and M.W.; writing-review and editing, R.B.; supervision, R.B.; project administration, R.B. and M.W.; funding acquisition, R.B. and M.W..

All authors have read and agreed to the published version of the manuscript.

References

- [1] C. A. Wells, P. D. Williams, N. K. Nichols, D. Kalise, and I. Poll, "Reducing Transatlantic Flight Emissions by Fuel-Optimised Routing," *Environ. Res. Letters*, vol. 16, no. 2, p. 025 002, 2021. DOI: 10.1088/1748-9326/abce82.
- [2] S. E. Karisch, S. S. Altus, G. Stojković, and M. Stojković, "Operations," in *Quantitative Problem Solving Methods in the Airline Industry*, Springer, 2011, ch. 6 – Operations, pp. 283–383. DOI: 10.1007/978-1-4614-1608-1_6.
- [3] A. Alizadeh, M. Uzun, E. Koyuncu, and G. Inalhan, "Optimal En-Route Trajectory Planning based on Wind Information," *IFAC-PapersOnLine*, vol. 51, no. 9, pp. 180–185, 2018, 15th IFAC Symposium on Control in Transportation Systems (CTS). DOI: 10.1016/j.ifacol.2018.07.030.
- [4] W. Rumler, T. Günther, U. Weißhaar, and H. Fricke, "Flight Profile Variations due to the Spreading Practice of Cost Index Based Flight Planning," in *4th International Conference on Research in Air Transportation, Budapest*, 2010. [Online]. Available: <https://de.scribd.com/document/150317383/Flight-Profile-Variations-Due-to-Spreading-Practice-of-CI-Planning> (visited on 09/22/2023).
- [5] H. K. Ng, B. Sridhar, and S. Grabbe, "Optimizing Aircraft Trajectories with Multiple Cruise Altitudes in the Presence of Winds," *Journal of Aerospace Information Systems*, vol. 11, no. 1, pp. 35–47, 2014. DOI: 10.2514/1.I010084.
- [6] E. Zermelo, "Über das Navigationsproblem bei ruhender oder veränderlicher Windverteilung," *ZAMM-Journal of Applied Mathematics and Mechanics/Zeitschrift für Angewandte Mathematik und Mechanik*, vol. 11(2), pp. 114–124, 1931. DOI: 10.1002/zamm.19310110205.
- [7] J. T. Betts, *Practical Methods for Optimal Control and Estimation Using Nonlinear Programming (Second Edition)*. Siam (Society for Industrial and Applied Mathematics, Philadelphia), 2011. DOI: 10.1137/1.9780898718577.

- [8] A. Dreves, M. Gerds, M. Sama, and A. D'Ariano, *Free Flight Trajectory Optimization and Generalized Nash Equilibria in Conflicting Situations*, 2017.
- [9] B. Geiger, J. Horn, A. DeLullo, A. Niessner, and L. Long, "Optimal Path Planning of UAVs Using Direct Collocation with Nonlinear Programming," in *AIAA Guidance, Navigation, and Control Conference and Exhibit*, American Institute of Aeronautics and Astronautics, Inc., 2006. DOI: 10.2514/6.2006-6199.
- [10] B. Girardet, L. Lapasset, D. Delahaye, C. Rabut, and Y. Brenier, "Generating Optimal Aircraft Trajectories with respect to Weather Conditions," in *2nd International Conference on Interdisciplinary Science for Innovative Air Traffic Management (ISIATM)*, 2013. [Online]. Available: <https://hal-enac.archives-ouvertes.fr/hal-00867818> (visited on 09/22/2023).
- [11] B. Girardet, L. Lapasset, D. Delahaye, and C. Rabut, "Wind-Optimal Path Planning: Application to Aircraft Trajectories," in *13th International Conference on Control Automation Robotics Vision (ICARCV)*, 2014, pp. 1403–1408. DOI: 10.1109/ICARCV.2014.7064521.
- [12] R. Borndörfer, F. Danecker, and M. Weiser, "A Discrete-Continuous Algorithm for Free Flight Planning," *Algorithms*, vol. 14, no. 1, p. 4, 2021. DOI: 10.3390/a14010004.
- [13] R. Borndörfer, F. Danecker, and M. Weiser, "A Discrete-Continuous Algorithm for Globally Optimal Free Flight Trajectory Optimization," in *22nd Symposium on Algorithmic Approaches for Transportation Modelling, Optimization, and Systems (ATMOS 2022)*, vol. 106, Schloss Dagstuhl – Leibniz-Zentrum für Informatik, 2022, pp. 1–13. DOI: 10.4230/OASIcs.ATMOS.2022.2.
- [14] R. Borndörfer, F. Danecker, and M. Weiser, "Error Bounds for Discrete-Continuous Free Flight Trajectory Optimization," *Journal of Optimization Theory and Applications*, vol. 198, no. 2, pp. 830–856, 2023. DOI: 10.1007/s10957-023-02264-7.
- [15] M. Locatelli, "Simulated Annealing Algorithms for Continuous Global Optimization," in *Handbook of Global Optimization*, Springer, 2002, pp. 179–229. DOI: 10.1007/978-1-4757-5362-2_6.
- [16] A. Cassioli, D. Izzo, D. Di Lorenzo, M. Locatelli, and F. Schoen, "Global Optimization Approaches for Optimal Trajectory Planning," in *Modeling and Optimization in Space Engineering*. Springer New York, 2012, ch. 5, pp. 111–140. DOI: 10.1007/978-1-4614-4469-5_5.
- [17] B. Addis, A. Cassioli, M. Locatelli, and F. Schoen, "A Global Optimization Method for the Design of Space Trajectories," *Computational Optimization and Applications*, vol. 48, pp. 635–652, 2011. DOI: 10.1007/s10589-009-9261-6.
- [18] M. R. Bonyadi and Z. Michalewicz, "Particle Swarm Optimization for Single Objective Continuous Space Problems: A Review," *Evolutionary Computation*, vol. 25, no. 1, pp. 1–54, 2017. DOI: 10.1162/EVC0_r_00180.

- [19] J. Y. Yen, “Finding the k Shortest Loopless Paths in a Network,” *Management Science*, vol. 17, no. 11, pp. 712–716, 1971. DOI: 10.1287/mnsc.17.11.712.
- [20] J. Nocedal and S. J. Wright, *Numerical Optimization*. Springer, 2006. DOI: 10.1007/978-0-387-40065-5.
- [21] H. Maurer and J. Zowe, “First and Second Order Necessary and Sufficient Optimality Conditions for Infinite-Dimensional Programming Problems,” *Math. Programming*, vol. 16, pp. 98–110, 1979. DOI: 10.1007/BF01582096.
- [22] D. Braess, *Finite Elemente*, 5th ed. Springer Spektrum Berlin, 2013. DOI: 10.1007/978-3-642-34797-9.
- [23] E. Casas and F. Tröltzsch, “Second Order Optimality Conditions and Their Role in PDE Control,” *Jahresbericht der Deutschen Mathematiker-Vereinigung*, vol. 117, no. 1, pp. 3–44, 2015. DOI: 10.1365/s13291-014-0109-3.

5.A Appendix

5.A.1 Global Bounds

The derivative $f = t_\tau$ of parametrized time as defined in (5.3) consists of two terms, the tailwind term

$$f_1 = -\frac{\xi_\tau^\top w}{g}, \quad (5.50)$$

$$g = \bar{v}^2 - w^\top w, \quad (5.51)$$

and the length term

$$f_2 = g^{-1} \left((\xi_\tau^\top w)^2 + g(\xi_\tau^\top \xi_\tau) \right)^{1/2}. \quad (5.52)$$

At each time τ , we obtain

$$\underline{v}^2 := \bar{v}^2 - \bar{c}_0^2 \leq g \leq \bar{v}^2. \quad (5.53)$$

The directional derivatives of g in direction $\delta\xi$ and $\Delta\xi \in \delta X$ read

$$g'\delta\xi = -2w^T w_x \delta\xi \quad (5.54)$$

$$\Rightarrow \|g'\| \leq 2\bar{c}_0\bar{c}_1 \quad (5.55)$$

$$\delta\xi^T g'' \delta\xi = -2\delta\xi^T w_x^T w_x \delta\xi - 2w_{xx}[w, \delta\xi, \delta\xi] \quad (5.56)$$

$$\Rightarrow \|g''\| \leq 2(\bar{c}_1^2 + \bar{c}_0\bar{c}_2). \quad (5.57)$$

$$g'''[\delta\xi, \delta\xi, \Delta\xi] = -6w_{xx}[w_x \delta\xi, \delta\xi, \Delta\xi] - 2w_{xxx}[w, \delta\xi, \delta\xi, \Delta\xi] \quad (5.58)$$

$$\Rightarrow \|g'''\| \leq 2(3\bar{c}_1\bar{c}_2 + \bar{c}_0\bar{c}_3). \quad (5.59)$$

For the tailwind term, we consider

$$f'_1(\xi, \xi_\tau)[\delta\xi, \delta\xi_\tau] = g^{-2}(\xi_\tau^T w)(g'\delta\xi) - g^{-1}\xi_\tau^T w_x \delta\xi - g^{-1}w^T \delta\xi_\tau, \quad (5.60)$$

which is bounded by

$$|f'_1(\xi, \xi_\tau)[\delta\xi, \delta\xi_\tau]| \leq \left(2\frac{\bar{c}_0^2\bar{c}_1}{\underline{v}^4} + \frac{\bar{c}_1}{\underline{v}^2}\right) \|\xi_\tau\| \|\delta\xi\| + \frac{\bar{c}_0}{\underline{v}^2} \|\delta\xi_\tau\|. \quad (5.61)$$

The second directional derivatives is

$$\begin{aligned} f''_1(\xi, \xi_\tau)[\delta\xi, \delta\xi_\tau][\tilde{\delta\xi}, \tilde{\delta\xi}_\tau] &= -2g^{-3}(g'\tilde{\delta\xi})(\xi_\tau^T w)(g'\delta\xi) &+ g^{-2}(\tilde{\delta\xi}_\tau^T w)(g'\delta\xi) \\ &+ g^{-2}(\xi_\tau^T w_x \tilde{\delta\xi})(g'\delta\xi) &+ g^{-2}(\xi_\tau^T w)(\delta\xi^T g'' \tilde{\delta\xi}) \\ &+ g^{-2}(g'\tilde{\delta\xi})(\xi_\tau^T w_x \delta\xi) &- g^{-1}(\tilde{\delta\xi}_\tau w_x \delta\xi) \\ &- g^{-1}w_{xx}[\xi_\tau, \delta\xi, \tilde{\delta\xi}] &+ g^{-2}(g'\tilde{\delta\xi})(w^T \delta\xi_\tau) \\ &- g^{-1}(\delta\xi_\tau^T w_x \tilde{\delta\xi}) & \end{aligned} \quad (5.62)$$

and in particular

$$\begin{aligned} f''_1(\xi, \xi_\tau)[\delta\xi, \delta\xi_\tau]^2 &= -2g^{-3}(g'\delta\xi)^2(\xi_\tau^T w) &+ 2g^{-2}(g'\delta\xi)(\xi_\tau^T w_x \delta\xi) \\ &+ g^{-2}(\delta\xi^T g'' \delta\xi)(\xi_\tau^T w) &- g^{-1}w_{xx}[\xi_\tau, \delta\xi, \delta\xi] \\ &- 2g^{-1}(\delta\xi_\tau^T w_x \delta\xi) &+ 2g^{-2}(\delta\xi_\tau^T w)(g'\delta\xi), \end{aligned} \quad (5.63)$$

which yields

$$\begin{aligned}
|f_1''(\xi, \xi_\tau)[\delta\xi, \delta\xi_\tau][\tilde{\delta\xi}, \tilde{\delta\xi}_\tau]| \leq & \left[8\frac{\bar{c}_0^3\bar{c}_1^2}{\underline{v}^6} + 6\frac{\bar{c}_0\bar{c}_1^2}{\underline{v}^4} + 2\frac{\bar{c}_0^2\bar{c}_2}{\underline{v}^4} + \frac{\bar{c}_2}{\underline{v}^2} \right] \|\xi_\tau\| \|\delta\xi\| \|\tilde{\delta\xi}\| \\
& + \left[2\frac{\bar{c}_0^2\bar{c}_1}{\underline{v}^4} + \frac{\bar{c}_1}{\underline{v}^2} \right] \|\delta\xi_\tau\| \|\tilde{\delta\xi}\| \\
& + \left[2\frac{\bar{c}_0^2\bar{c}_1}{\underline{v}^4} + \frac{\bar{c}_1}{\underline{v}^2} \right] \|\delta\xi\| \|\tilde{\delta\xi}_\tau\|
\end{aligned} \tag{5.64}$$

and

$$\begin{aligned}
|f_1''(\xi, \xi_\tau)[\delta\xi, \delta\xi_\tau]^2| \leq & \left[8\frac{\bar{c}_0^3\bar{c}_1^2}{\underline{v}^6} + 6\frac{\bar{c}_0\bar{c}_1^2}{\underline{v}^4} + 2\frac{\bar{c}_0^2\bar{c}_2}{\underline{v}^4} + \frac{\bar{c}_2}{\underline{v}^2} \right] \|\xi_\tau\| \|\delta\xi\|^2 \\
& + \left[4\frac{\bar{c}_0^2\bar{c}_1}{\underline{v}^4} + 2\frac{\bar{c}_1}{\underline{v}^2} \right] \|\delta\xi\| \|\delta\xi_\tau\|,
\end{aligned} \tag{5.65}$$

respectively. Finally, the third directional derivative is

$$\begin{aligned}
& f_1'''(\xi, \xi_\tau)[\delta\xi, \delta\xi_\tau]^2[\Delta\xi, \Delta\xi_\tau] \\
& = 6g^{-4}(g'\Delta\xi)(g'\delta\xi)^2(\xi_\tau^T w) - 4g^{-3}(g'\delta\xi)(\Delta\xi^T g''\delta\xi)(\xi_\tau^T w) \\
& \quad - 2g^{-3}(g'\Delta\xi)(\delta\xi^T g''\delta\xi)(\xi_\tau^T w) + g^{-2}g'''[\delta\xi, \delta\xi, \Delta\xi](\xi_\tau^T w) \\
& \quad - 2g^{-3}(g'\delta\xi)^2(\xi_\tau^T w_x \Delta\xi) + g^{-2}(\delta\xi^T g''\delta\xi)(\xi_\tau^T w_x \Delta\xi) \\
& \quad - 4g^{-3}(g'\Delta\xi)(g'\delta\xi)(\xi_\tau^T w_x \delta\xi) + 2g^{-2}(\Delta\xi^T g''\delta\xi)(\xi_\tau^T w_x \delta\xi) \\
& \quad + 2g^{-2}(g'\delta\xi)w_{xx}[\xi_\tau, \delta\xi, \Delta\xi] + g^{-2}(g'\Delta\xi)w_{xx}[\xi_\tau, \delta\xi, \delta\xi] \\
& \quad - g^{-1}w_{xxx}[\xi_\tau, \delta\xi, \delta\xi, \Delta\xi] \\
& \quad - 2g^{-3}(g'\delta\xi)^2(\Delta\xi^T w) + g^{-2}(\delta\xi^T g''\delta\xi)(\Delta\xi^T w) \\
& \quad + 2g^{-2}(g'\delta\xi)(\Delta\xi^T w_x \delta\xi) - g^{-1}w_{xx}[\Delta\xi_\tau, \delta\xi, \delta\xi] \\
& \quad - 4g^{-3}(g'\Delta\xi)(g'\delta\xi)(\delta\xi_\tau^T w) + 2g^{-2}(\Delta\xi^T g''\delta\xi)(\delta\xi_\tau^T w) \\
& \quad + 2g^{-2}(g'\delta\xi)(\delta\xi_\tau^T w_x \Delta\xi) + 2g^{-2}(g'\Delta\xi)(\delta\xi_\tau^T w_x \delta\xi) \\
& \quad - 2g^{-1}w_{xx}[\delta\xi_\tau, \delta\xi, \Delta\xi],
\end{aligned} \tag{5.66}$$

which is bounded by

$$\begin{aligned}
& |f_1'''(\xi, \xi_\tau)[\delta\xi, \delta\xi_\tau]^2[\Delta\xi, \Delta\xi_\tau]| \\
& \leq \frac{\|\xi_\tau\|}{\underline{v}} \left[\frac{\bar{c}_1^3}{\underline{v}^3} \left(48 \frac{\bar{c}_0^4}{\underline{v}^4} + 48 \frac{\bar{c}_0^2}{\underline{v}^2} + 6 \right) \right. \\
& \quad + \frac{\bar{c}_1 \bar{c}_2}{\underline{v}^2} \left(24 \frac{\bar{c}_0^3}{\underline{v}^3} + 18 \frac{\bar{c}_0}{\underline{v}} \right) \\
& \quad \left. + \frac{\bar{c}_3}{\underline{v}} \left(2 \frac{\bar{c}_0^2}{\underline{v}^2} + 1 \right) \right] \|\delta\xi\|^2 \|\Delta\xi\| \\
& \quad + \left[\frac{\bar{c}_1^2}{\underline{v}^3} \left(8 \frac{\bar{c}_0^3}{\underline{v}^3} + 6 \frac{\bar{c}_0}{\underline{v}} \right) + \frac{\bar{c}_2}{\underline{v}^2} \left(2 \frac{\bar{c}_0^2}{\underline{v}^2} + 1 \right) \right] \|\delta\xi\|^2 \|\Delta\xi_\tau\| \\
& \quad + \left[\frac{\bar{c}_1^2}{\underline{v}^3} \left(16 \frac{\bar{c}_0^3}{\underline{v}^3} + 12 \frac{\bar{c}_0}{\underline{v}} \right) + \frac{\bar{c}_2}{\underline{v}^2} \left(4 \frac{\bar{c}_0^2}{\underline{v}^2} + 2 \right) \right] \|\delta\xi\| \|\delta\xi_\tau\| \|\Delta\xi\|. \tag{5.67}
\end{aligned}$$

Before we turn to the length term f_2 , we first consider the term

$$F := (\xi_\tau^\top w)^2 + g(\xi_\tau^\top \xi_\tau) \tag{5.68}$$

with

$$\underline{v}^2 \|\xi_\tau\|^2 \leq F \leq \|\xi_\tau\|^2 \bar{v}^2.$$

We also note that

$$\frac{g}{F} \leq \frac{1}{\|\xi_\tau\|^2}.$$

Then

$$\begin{aligned}
F'(\xi, \xi_\tau)[\delta\xi, \delta\xi_\tau] &= 2(\xi_\tau^\top w)((\delta\xi_\tau^\top w) + (\xi_\tau^\top w_x \delta\xi)) \\
& \quad + (g' \delta\xi)(\xi_\tau^\top \xi_\tau) + 2g(\xi_\tau^\top \delta\xi_\tau), \tag{5.69}
\end{aligned}$$

which is bounded by

$$|F'(\xi, \xi_\tau)[\delta\xi, \delta\xi_\tau]| \leq 2\bar{v}^2 \|\xi_\tau\| \|\delta\xi_\tau\| + 4\bar{c}_0 \bar{c}_1 \|\xi_\tau\|^2 \|\delta\xi\|, \tag{5.70}$$

The second derivative is

$$\begin{aligned}
F''(\xi, \xi_\tau)[\delta\xi, \delta\xi_\tau][\tilde{\delta}\xi, \tilde{\delta}\xi_\tau] &= 2(\xi_\tau^\top w)(\delta\xi_\tau^\top w_x \tilde{\delta}\xi) && + 2(\xi_\tau^\top w_x \tilde{\delta}\xi)(\delta\xi_\tau^\top w) \\
&+ 2(\tilde{\delta}\xi_\tau^\top w)(\delta\xi_\tau^\top w) && + 2(\xi_\tau^\top w_x \tilde{\delta}\xi)(\xi_\tau^\top w_x \delta\xi) \\
&+ 2(\xi_\tau^\top w)w_{xx}[\xi_\tau, \delta\xi, \tilde{\delta}\xi] && + 2(\tilde{\delta}\xi_\tau^\top w)(\xi_\tau^\top w_x \delta\xi) \\
&+ 2(\xi_\tau^\top w)(\tilde{\delta}\xi_\tau^\top w_x \delta\xi) && + (\tilde{\delta}\xi_\tau^\top g'' \delta\xi)(\xi_\tau^\top \xi_\tau) \\
&+ 2(g' \delta\xi)(\tilde{\delta}\xi_\tau^\top \xi_\tau) && + 2(g' \tilde{\delta}\xi)(\xi_\tau^\top \delta\xi_\tau) \\
&+ 2g(\tilde{\delta}\xi_\tau^\top \delta\xi_\tau) && \tag{5.71}
\end{aligned}$$

and in particular

$$\begin{aligned}
F''(\xi, \xi_\tau)[\delta\xi, \delta\xi_\tau]^2 &= 4(\xi_\tau^\top w)(\delta\xi_\tau^\top w_x \delta\xi) && + 4(\delta\xi_\tau^\top w)(\xi_\tau^\top w_x \delta\xi) \\
&+ 2(\delta\xi_\tau^\top w)^2 && + 2(\xi_\tau^\top w_x \delta\xi)^2 \\
&+ 2(\xi_\tau^\top w)w_{xx}[\xi_\tau, \delta\xi, \delta\xi] && + (\delta\xi_\tau^\top g'' \delta\xi)(\xi_\tau^\top \xi_\tau) \\
&+ 4(g' \delta\xi)(\delta\xi_\tau^\top \xi_\tau) && + 2g(\delta\xi_\tau^\top \delta\xi_\tau), \tag{5.72}
\end{aligned}$$

which yields

$$\begin{aligned}
|F''(\xi, \xi_\tau)[\delta\xi, \delta\xi_\tau][\tilde{\delta}\xi, \tilde{\delta}\xi_\tau]| &\leq (4\bar{c}_1^2 + 4\bar{c}_0\bar{c}_2) \|\xi_\tau\|^2 \|\delta\xi\| \|\tilde{\delta}\xi\| \\
&+ 8\bar{c}_0\bar{c}_1 \|\xi_\tau\| \|\delta\xi\| \|\tilde{\delta}\xi_\tau\| \\
&+ 8\bar{c}_0\bar{c}_1 \|\xi_\tau\| \|\delta\xi_\tau\| \|\tilde{\delta}\xi\| \\
&+ 2\bar{v}^2 \|\delta\xi_\tau\| \|\tilde{\delta}\xi_\tau\| \tag{5.73}
\end{aligned}$$

and

$$\begin{aligned}
|F''(\xi, \xi_\tau)[\delta\xi, \delta\xi_\tau]^2| &\leq (4\bar{c}_1^2 + 4\bar{c}_0\bar{c}_2) \|\xi_\tau\|^2 \|\delta\xi\|^2 \\
&+ 16\bar{c}_0\bar{c}_1 \|\xi_\tau\| \|\delta\xi\| \|\delta\xi_\tau\| \\
&+ 2\bar{v}^2 \|\delta\xi_\tau\|^2, \tag{5.74}
\end{aligned}$$

respectively. The third derivative is

$$\begin{aligned}
F'''(\xi, \xi_\tau)[\delta\xi, \delta\xi_\tau]^2[\tilde{\delta\xi}, \tilde{\delta\xi}_\tau] &= 4(\tilde{\delta\xi}_\tau^\top w)(\delta\xi_\tau^\top w_x \delta\xi) && + 4(\xi_\tau^\top w_x \tilde{\delta\xi})(\delta\xi_\tau^\top w_x \delta\xi) \\
&+ 4(\xi_\tau^\top w)w_{xx}[\delta\xi_\tau, \delta\xi, \tilde{\delta\xi}] && + 4(\delta\xi_\tau^\top w_x \tilde{\delta\xi})(\xi_\tau^\top w_x \delta\xi) \\
&+ 4(\delta\xi_\tau^\top w)(\tilde{\delta\xi}_\tau^\top w_x \delta\xi) && + 4(\delta\xi_\tau^\top w)w_{xx}[\xi_\tau, \delta\xi, \tilde{\delta\xi}] \\
&+ 4(\delta\xi_\tau^\top w)(\delta\xi_\tau^\top w_x \tilde{\delta\xi}) && + 4(\xi_\tau^\top w_x \delta\xi)(\tilde{\delta\xi}_\tau^\top w_x \delta\xi) \\
&+ 4(\xi_\tau^\top w_x \delta\xi)w_{xx}[\xi_\tau, \delta\xi, \tilde{\delta\xi}] && + 2(\tilde{\delta\xi}_\tau^\top w)w_{xx}[\xi_\tau, \delta\xi, \delta\xi] \\
&+ 2(\xi_\tau^\top w_x \tilde{\delta\xi})w_{xx}[\xi_\tau, \delta\xi, \delta\xi] && + 2(\xi_\tau^\top w)w_{xxx}[\xi_\tau, \delta\xi, \delta\xi, \tilde{\delta\xi}] \\
&+ 2(\xi_\tau^\top w)w_{xx}[\tilde{\delta\xi}_\tau, \delta\xi, \delta\xi] && + g'''[\delta\xi, \delta\xi, \tilde{\delta\xi}](\xi_\tau^\top \xi_\tau) \\
&+ 2(\delta\xi_\tau^\top g'' \delta\xi)(\tilde{\delta\xi}_\tau^\top \xi_\tau) && + 4(\tilde{\delta\xi}_\tau^\top g'' \delta\xi)(\delta\xi_\tau^\top \xi_\tau) \\
&+ 4(g' \delta\xi)(\delta\xi_\tau^\top \tilde{\delta\xi}_\tau) && + 2(g' \tilde{\delta\xi})(\delta\xi_\tau^\top \delta\xi_\tau), \tag{5.75}
\end{aligned}$$

which is bounded by

$$\begin{aligned}
|F'''(\xi, \xi_\tau)[\delta\xi, \delta\xi_\tau]^2[\tilde{\delta\xi}, \tilde{\delta\xi}_\tau]| &\leq 4\|\xi_\tau\|^2(\bar{c}_0\bar{c}_3 + 3\bar{c}_1\bar{c}_2)\|\delta\xi\|^2\|\tilde{\delta\xi}\| \\
&+ 8\|\xi_\tau\|(\bar{c}_1^2 + \bar{c}_0\bar{c}_2)\|\delta\xi\|^2\|\tilde{\delta\xi}_\tau\| \\
&+ 16\|\xi_\tau\|(\bar{c}_1^2 + \bar{c}_0\bar{c}_2)\|\delta\xi\|\|\delta\xi_\tau\|\|\tilde{\delta\xi}\| \\
&+ 16\bar{c}_0\bar{c}_1\|\delta\xi\|\|\delta\xi_\tau\|\|\tilde{\delta\xi}_\tau\| \\
&+ 8\bar{c}_0\bar{c}_1\|\delta\xi_\tau\|^2\|\tilde{\delta\xi}\|. \tag{5.76}
\end{aligned}$$

For the length term $f_2 = g^{-1}\sqrt{F}$, we thus obtain

$$f_2'(\xi, \xi_\tau)[\delta\xi, \delta\xi_\tau] = -g^{-2}(g' \delta\xi)F^{1/2} + \frac{1}{2}g^{-1}F^{-1/2}F'[\delta\xi, \delta\xi_\tau], \tag{5.77}$$

which is bounded by

$$|f_2'(\xi, \xi_\tau)[\delta\xi, \delta\xi_\tau]| \leq \left(2\frac{\bar{c}_0\bar{c}_1\bar{v}}{v^4} + 4\frac{\bar{c}_0\bar{c}_1}{v^3}\right)\|\xi_\tau\|\|\delta\xi\| + 2v^{-3}\bar{v}^2\|\delta\xi_\tau\|. \tag{5.78}$$

The second derivative is

$$\begin{aligned}
f_2''(\xi, \xi_\tau)[\delta\xi, \delta\xi_\tau][\tilde{\delta}\xi, \tilde{\delta}\xi_\tau] &= 2g^{-3}(g'\tilde{\delta}\xi)(g'\delta\xi)F^{1/2} \\
&\quad - g^{-2}(\delta\xi^T g''\tilde{\delta}\xi)F^{1/2} \\
&\quad - \frac{1}{2}g^{-2}(g'\delta\xi)F^{-1/2}F'[\tilde{\delta}\xi, \tilde{\delta}\xi_\tau] \\
&\quad - \frac{1}{2}g^{-2}(g'\tilde{\delta}\xi)F^{-1/2}F'[\delta\xi, \delta\xi_\tau] \\
&\quad + \frac{1}{2}g^{-1}F^{-1/2}F''[\delta\xi, \delta\xi_\tau][\tilde{\delta}\xi, \tilde{\delta}\xi_\tau] \\
&\quad - \frac{1}{4}g^{-1}F^{-3/2}F'[\delta\xi, \delta\xi_\tau]F'[\tilde{\delta}\xi, \tilde{\delta}\xi_\tau] \tag{5.79}
\end{aligned}$$

and in particular

$$\begin{aligned}
f_2''(\xi, \xi_\tau)[\delta\xi, \delta\xi_\tau]^2 &= 2g^{-3}(g'\delta\xi)^2F^{1/2} \\
&\quad - g^{-2}(\delta\xi^T g''\delta\xi)F^{1/2} \\
&\quad - g^{-2}(g'\delta\xi)F^{-1/2}F'[\delta\xi, \delta\xi_\tau] \\
&\quad + \frac{1}{2}g^{-1}F^{-1/2}F''[\delta\xi, \delta\xi_\tau]^2 \\
&\quad - \frac{1}{4}g^{-1}F^{-3/2}(F'[\delta\xi, \delta\xi_\tau])^2, \tag{5.80}
\end{aligned}$$

which yields

$$\begin{aligned}
&|f_2''(\xi, \xi_\tau)[\delta\xi, \delta\xi_\tau][\tilde{\delta}\xi, \tilde{\delta}\xi_\tau]| \\
&\leq \left[8\frac{\bar{c}_0^2\bar{c}_1^2\bar{v}}{v^6} + 12\frac{\bar{c}_0^2\bar{c}_1^2}{v^5} + 2\frac{(\bar{c}_1^2 + \bar{c}_0\bar{c}_2)\bar{v}}{v^4} + 2\frac{\bar{c}_1^2 + \bar{c}_0\bar{c}_2}{v^3} \right] \|\xi_\tau\| \|\delta\xi\| \|\tilde{\delta}\xi\| \\
&\quad + \left[4\frac{\bar{c}_0\bar{c}_1\bar{v}^2}{v^5} + 4\frac{\bar{c}_0\bar{c}_1}{v^3} \right] \|\delta\xi\| \|\tilde{\delta}\xi_\tau\| \\
&\quad + \left[4\frac{\bar{c}_0\bar{c}_1\bar{v}^2}{v^5} + 4\frac{\bar{c}_0\bar{c}_1}{v^3} \right] \|\delta\xi_\tau\| \|\tilde{\delta}\xi\| \\
&\quad + \left[\frac{\bar{v}^4}{v^5} + \frac{\bar{v}^2}{v^3} \right] \|\xi_\tau\|^{-1} \|\delta\xi_\tau\| \|\tilde{\delta}\xi_\tau\| \tag{5.81}
\end{aligned}$$

and

$$\begin{aligned}
& |f_2''(\xi, \xi_\tau)[\delta\xi, \delta\xi_\tau]^2| \\
& \leq \left[8 \frac{\bar{c}_0^2 \bar{c}_1^2 \bar{v}}{\underline{v}^6} + 12 \frac{\bar{c}_0^2 \bar{c}_1^2}{\underline{v}^5} + 2 \frac{(\bar{c}_1^2 + \bar{c}_0 \bar{c}_2) \bar{v}}{\underline{v}^4} + 2 \frac{\bar{c}_1^2 + \bar{c}_0 \bar{c}_2}{\underline{v}^3} \right] \|\xi_\tau\| \|\delta\xi\|^2 \\
& \quad + \left[8 \frac{\bar{c}_0 \bar{c}_1 \bar{v}^2}{\underline{v}^5} + 8 \frac{\bar{c}_0 \bar{c}_1}{\underline{v}^3} \right] \|\delta\xi\| \|\delta\xi_\tau\| \\
& \quad + \left[\frac{\bar{v}^4}{\underline{v}^5} + \frac{\bar{v}^2}{\underline{v}^3} \right] \|\xi_\tau\|^{-1} \|\delta\xi_\tau\|^2
\end{aligned} \tag{5.82}$$

The third derivative is

$$\begin{aligned}
f_2'''(\xi, \xi_\tau)[\delta\xi, \delta\xi_\tau]^2[\tilde{\delta\xi}, \tilde{\delta\xi}_\tau] = & -6g^{-4}(g'\tilde{\delta\xi})(g'\delta\xi)^2F^{1/2} \\
& + 4g^{-3}(g'\delta\xi)(\tilde{\delta\xi}^T g''\delta\xi)F^{1/2} \\
& + g^{-3}(g'\delta\xi)^2F^{-1/2}F'[\tilde{\delta\xi}, \tilde{\delta\xi}_\tau] \\
& + 2g^{-3}(g'\tilde{\delta\xi})(\delta\xi^T g''\delta\xi)F^{1/2} \\
& - g^{-2}g'''[\delta\xi, \delta\xi, \tilde{\delta\xi}]F^{1/2} \\
& - \frac{1}{2}g^{-2}(\delta\xi^T g''\delta\xi)F^{-1/2}F'[\tilde{\delta\xi}, \tilde{\delta\xi}_\tau] \\
& + g^{-3}(g'\tilde{\delta\xi})(g'\delta\xi)F^{-1/2}F'[\delta\xi, \delta\xi_\tau] \\
& - \frac{1}{2}g^{-2}(\tilde{\delta\xi}^T g''\delta\xi)F^{-1/2}F'[\delta\xi, \delta\xi_\tau] \\
& + \frac{1}{4}g^{-2}(g'\delta\xi)F^{-3/2}F'[\delta\xi, \delta\xi_\tau]F'[\tilde{\delta\xi}, \tilde{\delta\xi}_\tau] \\
& - \frac{1}{2}g^{-2}(g'\delta\xi)F^{-1/2}F''[\delta\xi, \delta\xi_\tau][\tilde{\delta\xi}, \tilde{\delta\xi}_\tau] \\
& + g^{-3}(g'\tilde{\delta\xi})(g'\delta\xi)F^{-1/2}F'[\delta\xi, \delta\xi_\tau] \\
& - \frac{1}{2}g^{-2}(\tilde{\delta\xi}g''\delta\xi)F^{-1/2}F'[\delta\xi, \delta\xi_\tau] \\
& + \frac{1}{4}g^{-2}(g'\delta\xi)F^{-3/2}F'[\delta\xi, \delta\xi_\tau]F'[\tilde{\delta\xi}, \tilde{\delta\xi}_\tau] \\
& - \frac{1}{2}g^{-2}(g'\delta\xi)F^{-1/2}F''[\delta\xi, \delta\xi_\tau][\tilde{\delta\xi}, \tilde{\delta\xi}_\tau] \\
& + \frac{1}{4}g^{-2}(g'\tilde{\delta\xi})F^{-3/2}(F'[\delta\xi, \delta\xi_\tau])^2 \\
& + \frac{3}{8}g^{-1}F^{-5/2}(F'[\delta\xi, \delta\xi_\tau])^2F'[\tilde{\delta\xi}, \tilde{\delta\xi}_\tau] \\
& - \frac{1}{2}g^{-1}F^{-3/2}F'[\delta\xi, \delta\xi_\tau]F''[\delta\xi, \delta\xi_\tau][\tilde{\delta\xi}, \tilde{\delta\xi}_\tau] \\
& - \frac{1}{2}g^{-2}(g'\tilde{\delta\xi})F^{-1/2}F''[\delta\xi, \delta\xi_\tau]^2 \\
& - \frac{1}{4}g^{-1}F^{-3/2}F''[\delta\xi, \delta\xi_\tau]^2F'[\tilde{\delta\xi}, \tilde{\delta\xi}_\tau] \\
& + \frac{1}{2}g^{-1}F^{-1/2}F'''[\delta\xi, \delta\xi_\tau]^2[\tilde{\delta\xi}, \tilde{\delta\xi}_\tau], \tag{5.83}
\end{aligned}$$

which is bounded by

$$\begin{aligned}
& |f_2'''(\xi, \xi_\tau)[\delta\xi, \delta\xi_\tau]^2[\tilde{\delta}\xi, \tilde{\delta}\xi_\tau]| \\
& \leq \frac{2\|\xi_\tau\|}{\underline{v}} \left[\frac{\bar{c}_3}{\underline{v}} \left(\frac{\bar{c}_0}{\underline{v}} + \frac{\bar{v}\bar{c}_0}{\underline{v}^2} \right) \right. \\
& \quad + \frac{3\bar{c}_1\bar{c}_2}{\underline{v}^2} \left(1 + \frac{\bar{v}}{\underline{v}} + 6\frac{\bar{c}_0^2}{\underline{v}^2} + 4\frac{\bar{v}\bar{c}_0^2}{\underline{v}^3} \right) \\
& \quad \left. + \frac{6\bar{c}_1^3}{\underline{v}^3} \left(3\frac{\bar{c}_0}{\underline{v}} + 2\frac{\bar{v}\bar{c}_0}{\underline{v}^2} + 8\frac{\bar{c}_0^3}{\underline{v}^3} + 4\frac{\bar{v}\bar{c}_0^3}{\underline{v}^4} \right) \right] \|\delta\xi\|^2 \|\tilde{\delta}\xi\| \\
& + \frac{4}{\underline{v}} \left[\frac{\bar{c}_1^2}{\underline{v}^2} \left(1 + \frac{\bar{v}^2}{\underline{v}^2} + 9\frac{\bar{c}_0^2}{\underline{v}^2} + 7\frac{\bar{c}_0^2\bar{v}^2}{\underline{v}^4} \right) \right. \\
& \quad \left. + \frac{\bar{c}_2}{\underline{v}} \left(\frac{\bar{c}_0}{\underline{v}} + \frac{\bar{v}^2\bar{c}_0}{\underline{v}^3} + \frac{\bar{c}_0^3}{\underline{v}^3} \right) \right] \|\delta\xi\|^2 \|\tilde{\delta}\xi_\tau\| \\
& + \frac{8}{\underline{v}} \left[\frac{\bar{c}_1^2}{\underline{v}^2} \left(1 + \frac{\bar{v}^2}{\underline{v}^2} + 9\frac{\bar{c}_0^2}{\underline{v}^2} + 7\frac{\bar{c}_0^2\bar{v}^2}{\underline{v}^4} \right) \right. \\
& \quad \left. + \frac{\bar{c}_2}{\underline{v}} \left(\frac{\bar{c}_0}{\underline{v}} + \frac{\bar{v}^2\bar{c}_0}{\underline{v}^3} + \frac{\bar{c}_0^3}{\underline{v}^3} \right) \right] \|\delta\xi\| \|\delta\xi_\tau\| \|\tilde{\delta}\xi\| \\
& + \frac{8\bar{c}_0\bar{c}_1}{\|\xi_\tau\|\underline{v}^3} \left(1 + 3\frac{\bar{v}^2}{\underline{v}^2} + 2\frac{\bar{v}^4}{\underline{v}^4} \right) \|\delta\xi\| \|\delta\xi_\tau\| \|\tilde{\delta}\xi_\tau\| \\
& + \frac{4\bar{c}_0\bar{c}_1}{\|\xi_\tau\|\underline{v}^3} \left(1 + 3\frac{\bar{v}^2}{\underline{v}^2} + 2\frac{\bar{v}^4}{\underline{v}^4} \right) \|\delta\xi_\tau\|^2 \|\tilde{\delta}\xi\| \\
& + \frac{3\bar{v}^4}{\|\xi_\tau\|^2\underline{v}^5} \left(1 + \frac{\bar{v}^2}{\underline{v}^2} \right) \|\delta\xi_\tau\|^2 \|\tilde{\delta}\xi_\tau\|. \tag{5.84}
\end{aligned}$$

Lemma 5.7. — Let $\|w\|_{L^\infty(\Omega)} \leq \bar{c}_0 \leq \bar{v}/\sqrt{5}$, $\|w_x\|_{L^\infty(\Omega)} \leq \bar{c}_1$, $\|w_{xx}\|_{L^\infty(\Omega)} \leq \bar{c}_2$, and $\|w_{xxx}\|_{L^\infty(\Omega)} \leq \bar{c}_3$ and define $\underline{v}^2 := \bar{v}^2 - \bar{c}_0^2$. Then, for any $\xi \in X$, the third directional derivative of f as given in (5.3) is bounded by

$$\begin{aligned}
& |f'''(\xi, \xi_\tau)[\delta\xi, \delta\xi_\tau]^2[\Delta\xi, \Delta\xi_\tau]| \\
& \leq \left(\bar{\gamma}_0 \|\xi_\tau\| \|\delta\xi\|^2 + \bar{\gamma}_2 \|\delta\xi\| \|\delta\xi_\tau\| + \frac{\bar{\gamma}_4}{\|\xi_\tau\|} \|\delta\xi_\tau\|^2 \right) \|\Delta\xi\| \\
& \quad + \left(\bar{\gamma}_1 \|\delta\xi\|^2 + \frac{\bar{\gamma}_3}{\|\xi_\tau\|} \|\delta\xi\| \|\delta\xi_\tau\| + \frac{\bar{\gamma}_5}{\|\xi_\tau\|^2} \|\delta\xi_\tau\|^2 \right) \|\Delta\xi_\tau\| \tag{5.33}
\end{aligned}$$

with $\bar{\gamma}_i \geq 0$, $i \in 0, \dots, 5$, given as

$$\begin{aligned}
\bar{\gamma}_0 &= \frac{2}{\underline{v}^4} (37\bar{c}_1^3 + 21\bar{c}_1\bar{c}_2\underline{v} + 2\bar{c}_3\underline{v}^2), & \bar{\gamma}_3 &= 40\frac{\bar{c}_1}{\underline{v}^2}, \\
\bar{\gamma}_1 &= \frac{1}{\underline{v}^3} (29\bar{c}_1^2 + 7\underline{v}\bar{c}_2), & \bar{\gamma}_4 &= 20\frac{\bar{c}_1}{\underline{v}^2}, \\
\bar{\gamma}_2 &= \frac{1}{\underline{v}^3} (57\bar{c}_1^2 + 13\underline{v}\bar{c}_2), & \bar{\gamma}_5 &= 18\frac{1}{\underline{v}}. \tag{5.34}
\end{aligned}$$

Proof. We obtain f by adding f_1 and f_2 . The third derivative of f can thus be bounded using (5.67), (5.84), and the triangle inequality.

$$\begin{aligned}
& |f'''[\delta\xi, \delta\xi_\tau]^2[\Delta\xi, \Delta\xi_\tau]| \\
& \leq \frac{\|\xi_\tau\|}{\underline{v}} \left[\frac{\bar{c}_3}{\underline{v}} \left(1 + 2\frac{\bar{c}_0}{\underline{v}} + 2\frac{\bar{v}\bar{c}_0}{\underline{v}^2} + 2\frac{\bar{c}_0^2}{\underline{v}^2} \right) \right. \\
& \quad + 6\frac{\bar{c}_1\bar{c}_2}{\underline{v}^2} \left(1 + 1\frac{\bar{v}}{\underline{v}} + 3\frac{\bar{c}_0}{\underline{v}} + 6\frac{\bar{c}_0^2}{\underline{v}^2} + 4\frac{\bar{v}\bar{c}_0^2}{\underline{v}^3} + 4\frac{\bar{c}_0^3}{\underline{v}^3} \right) \\
& \quad \left. + 6\frac{\bar{c}_1^3}{\underline{v}^3} \left(1 + 6\frac{\bar{c}_0}{\underline{v}} + 4\frac{\bar{v}\bar{c}_0}{\underline{v}^2} + 8\frac{\bar{c}_0^2}{\underline{v}^2} + 16\frac{\bar{c}_0^3}{\underline{v}^3} + 8\frac{\bar{v}\bar{c}_0^3}{\underline{v}^4} + 8\frac{\bar{c}_0^4}{\underline{v}^4} \right) \right] \|\delta\xi\|^2 \|\Delta\xi\| \\
& + \frac{1}{\underline{v}} \left[2\frac{\bar{c}_1^2}{\underline{v}^2} \left(2 + 3\frac{\bar{c}_0}{\underline{v}} + 2\frac{\bar{v}^2}{\underline{v}^2} + 18\frac{\bar{c}_0^2}{\underline{v}^2} + 4\frac{\bar{c}_0^3}{\underline{v}^3} + 14\frac{\bar{c}_0^2\bar{v}^2}{\underline{v}^4} \right) \right. \\
& \quad \left. + \frac{\bar{c}_2}{\underline{v}} \left(1 + 4\frac{\bar{c}_0}{\underline{v}} + 2\frac{\bar{c}_0^2}{\underline{v}^2} + 4\frac{\bar{v}^2\bar{c}_0}{\underline{v}^3} + 4\frac{\bar{c}_0^3}{\underline{v}^3} \right) \right] \|\delta\xi\|^2 \|\Delta\xi_\tau\| \\
& + \frac{1}{\underline{v}} \left[4\frac{\bar{c}_1^2}{\underline{v}^2} \left(2 + 4\frac{\bar{c}_0^3}{\underline{v}^3} + 3\frac{\bar{c}_0}{\underline{v}} + 2\frac{\bar{v}^2}{\underline{v}^2} + 18\frac{\bar{c}_0^2}{\underline{v}^2} + 14\frac{\bar{c}_0^2\bar{v}^2}{\underline{v}^4} \right) \right. \\
& \quad \left. + 2\frac{\bar{c}_2}{\underline{v}} \left(1 + 4\frac{\bar{c}_0}{\underline{v}} + 2\frac{\bar{c}_0^2}{\underline{v}^2} + 4\frac{\bar{v}^2\bar{c}_0}{\underline{v}^3} + 4\frac{\bar{c}_0^3}{\underline{v}^3} \right) \right] \|\delta\xi\| \|\delta\xi_\tau\| \|\Delta\xi\| \\
& + \frac{8\bar{c}_0\bar{c}_1}{\|\xi_\tau\|\underline{v}^3} \left(1 + 3\frac{\bar{v}^2}{\underline{v}^2} + 2\frac{\bar{v}^4}{\underline{v}^4} \right) \|\delta\xi\| \|\delta\xi_\tau\| \|\Delta\xi_\tau\| \\
& + \frac{4\bar{c}_0\bar{c}_1}{\|\xi_\tau\|\underline{v}^3} \left(1 + 3\frac{\bar{v}^2}{\underline{v}^2} + 2\frac{\bar{v}^4}{\underline{v}^4} \right) \|\delta\xi_\tau\|^2 \|\Delta\xi\| \\
& + \frac{3\bar{v}^4}{\|\xi_\tau\|^2\underline{v}^5} \left(1 + \frac{\bar{v}^2}{\underline{v}^2} \right) \|\delta\xi_\tau\|^2 \|\Delta\xi_\tau\|.
\end{aligned}$$

With $\frac{\bar{c}_0}{\bar{v}} \leq \frac{1}{\sqrt{5}}$, we note that

$$\frac{\bar{c}_0}{\underline{v}} \leq \frac{1}{2}, \quad \frac{\bar{v}}{\underline{v}} \leq \sqrt{\frac{3}{2}}, \quad \text{and} \quad \frac{\bar{v}}{\underline{v}} \leq \frac{\sqrt{5}}{2}$$

and obtain

$$\begin{aligned}
|f'''[\delta\xi, \delta\xi_\tau]^2[\Delta\xi, \Delta\xi_\tau]| &\leq \frac{\|\xi_\tau\|}{\underline{v}} \left[\frac{\bar{c}_3}{\underline{v}} \left(\frac{5}{2} + \sqrt{\frac{3}{2}} \right) \right. \\
&\quad + 6 \frac{\bar{c}_1 \bar{c}_2}{\underline{v}^2} \left(\frac{9}{2} + 2\sqrt{\frac{3}{2}} \right) \\
&\quad \left. + 6 \frac{\bar{c}_1^3}{\underline{v}^3} \left(\frac{17}{2} + 3\sqrt{\frac{3}{2}} \right) \right] \|\delta\xi\|^2 \|\Delta\xi\| \\
&\quad + \frac{1}{\underline{v}} \left[\frac{57}{2} \frac{\bar{c}_1^2}{\underline{v}^2} + \frac{13}{2} \frac{\bar{c}_2}{\underline{v}} \right] \|\delta\xi\|^2 \|\Delta\xi_\tau\| \\
&\quad + \frac{1}{\underline{v}} \left[57 \frac{\bar{c}_1^2}{\underline{v}^2} + 13 \frac{\bar{c}_2}{\underline{v}} \right] \|\delta\xi\| \|\delta\xi_\tau\| \|\Delta\xi\| \\
&\quad + 40 \frac{\bar{c}_1}{\|\xi_\tau\| \underline{v}^2} \|\delta\xi\| \|\delta\xi_\tau\| \|\Delta\xi_\tau\| \\
&\quad + 20 \frac{\bar{c}_1}{\|\xi_\tau\| \underline{v}^2} \|\delta\xi_\tau\|^2 \|\Delta\xi\| \\
&\quad + \frac{135}{8 \|\xi_\tau\|^2 \underline{v}} \|\delta\xi_\tau\|^2 \|\Delta\xi_\tau\|,
\end{aligned}$$

Rounding up the values yields the bound

$$\begin{aligned}
|f'''[\delta\xi, \delta\xi_\tau]^2[\Delta\xi, \Delta\xi_\tau]| &\leq \frac{\|\xi_\tau\|}{\underline{v}} \left[4 \frac{\bar{c}_3}{\underline{v}} + 42 \frac{\bar{c}_1 \bar{c}_2}{\underline{v}^2} + 74 \frac{\bar{c}_1^3}{\underline{v}^3} \right] \|\delta\xi\|^2 \|\Delta\xi\| \\
&\quad + \frac{1}{\underline{v}} \left[29 \frac{\bar{c}_1^2}{\underline{v}^2} + 7 \frac{\bar{c}_2}{\underline{v}} \right] \|\delta\xi\|^2 \|\Delta\xi_\tau\| \\
&\quad + \frac{1}{\underline{v}} \left[57 \frac{\bar{c}_1^2}{\underline{v}^2} + 13 \frac{\bar{c}_2}{\underline{v}} \right] \|\delta\xi\| \|\delta\xi_\tau\| \|\Delta\xi\| \\
&\quad + 40 \frac{\bar{c}_1}{\|\xi_\tau\| \underline{v}^2} \|\delta\xi\| \|\delta\xi_\tau\| \|\Delta\xi_\tau\| \\
&\quad + 20 \frac{\bar{c}_1}{\|\xi_\tau\| \underline{v}^2} \|\delta\xi_\tau\|^2 \|\Delta\xi\| \\
&\quad + 18 \frac{1}{\|\xi_\tau\|^2 \underline{v}} \|\delta\xi_\tau\|^2 \|\Delta\xi_\tau\|.
\end{aligned}$$

□

Lemma 5.10. — *Let $\|w\|_{L^\infty(\Omega)} \leq \bar{c}_0 \leq \frac{\bar{v}}{\sqrt{5}}$, $\|w_x\|_{L^\infty(\Omega)} \leq \bar{c}_1$, and $\|w_{xx}\|_{L^\infty(\Omega)} \leq \bar{c}_2$. Moreover, let $\underline{v}^2 := \bar{v}^2 - \bar{c}_0^2$. Then, for any $\xi \in X$, the second directional derivative*

of f as given in (5.3) is bounded by

$$\begin{aligned}
|f''(\xi, \xi_\tau)[\delta\xi, \delta\xi_\tau][\tilde{\delta}\xi, \tilde{\delta}\xi_\tau]| &\leq \bar{\beta}_0 \|\xi_\tau\| \|\delta\xi\| \|\tilde{\delta}\xi\| \\
&\quad + \bar{\beta}_1 \left(\|\delta\xi\| \|\tilde{\delta}\xi_\tau\| + \|\delta\xi_\tau\| \|\tilde{\delta}\xi\| \right) \\
&\quad + \bar{\beta}_2 \|\xi_\tau\|^{-1} \|\delta\xi_\tau\| \|\tilde{\delta}\xi_\tau\|
\end{aligned} \tag{5.39}$$

with

$$\bar{\beta}_0 = 14 \frac{\bar{c}_1^2}{\underline{v}^3} + 4 \frac{\bar{c}_2}{\underline{v}^2}, \quad \bar{\beta}_1 = 7 \frac{\bar{c}_1}{\underline{v}^2}, \quad \text{and} \quad \bar{\beta}_2 = \frac{4}{\underline{v}}. \tag{5.40}$$

Proof. We obtain f by adding f_1 and f_2 . The second derivative of f can thus be bounded using (5.64), (5.81), and the triangle inequality.

$$\begin{aligned}
|f''(\xi, \xi_\tau)[\delta\xi, \delta\xi_\tau][\tilde{\delta}\xi, \tilde{\delta}\xi_\tau]| &\leq \left[8\bar{c}_0^2\bar{c}_1^2 \frac{\bar{c}_0 + \bar{v}}{\underline{v}^6} + 12 \frac{\bar{c}_0^2\bar{c}_1^2}{\underline{v}^5} \right. \\
&\quad + 2 \frac{\bar{c}_1^2\bar{v} + \bar{c}_0\bar{c}_2\bar{v} + 3\bar{c}_0\bar{c}_1^2 + \bar{c}_0^2\bar{c}_2}{\underline{v}^4} \\
&\quad \left. + 2 \frac{\bar{c}_1^2 + \bar{c}_0\bar{c}_2}{\underline{v}^3} + \frac{\bar{c}_2}{\underline{v}^2} \right] \|\xi_\tau\| \|\delta\xi\| \|\tilde{\delta}\xi\| \\
&\quad + \left[4 \frac{\bar{c}_0\bar{c}_1\bar{v}^2}{\underline{v}^5} + 2 \frac{\bar{c}_0^2\bar{c}_1}{\underline{v}^4} + 4 \frac{\bar{c}_0\bar{c}_1}{\underline{v}^3} + \frac{\bar{c}_1}{\underline{v}^2} \right] \|\delta\xi_\tau\| \|\tilde{\delta}\xi\| \\
&\quad + \left[4 \frac{\bar{c}_0\bar{c}_1\bar{v}^2}{\underline{v}^5} + 2 \frac{\bar{c}_0^2\bar{c}_1}{\underline{v}^4} + 4 \frac{\bar{c}_0\bar{c}_1}{\underline{v}^3} + \frac{\bar{c}_1}{\underline{v}^2} \right] \|\delta\xi\| \|\tilde{\delta}\xi_\tau\| \\
&\quad + \left[\frac{\bar{v}^4}{\underline{v}^5} + \frac{\bar{v}^2}{\underline{v}^3} \right] \|\xi_\tau\|^{-1} \|\delta\xi_\tau\| \|\tilde{\delta}\xi_\tau\|.
\end{aligned}$$

With $\frac{\bar{c}_0}{\bar{v}} \leq \frac{1}{\sqrt{5}}$, we note that

$$\frac{\bar{c}_0}{\underline{v}} \leq \frac{1}{2}, \quad \frac{\bar{v}}{\underline{v}} \leq \sqrt{\frac{3}{2}}, \quad \text{and} \quad \frac{\bar{v}}{\underline{v}} \leq \frac{\sqrt{5}}{2}$$

and obtain

$$\begin{aligned}
|f''(\xi, \xi_\tau)[\delta\xi, \delta\xi_\tau][\tilde{\delta}\xi, \tilde{\delta}\xi_\tau]| &\leq \left[\left(9 + 4\sqrt{\frac{3}{2}} \right) \frac{\bar{c}_1^2}{\underline{v}^3} + 4 \frac{\bar{c}_2}{\underline{v}^2} \right] \|\xi_\tau\| \|\delta\xi\| \|\tilde{\delta}\xi\| \\
&\quad + \frac{13\bar{c}_1}{2\underline{v}^2} \|\delta\xi_\tau\| \|\tilde{\delta}\xi\| \\
&\quad + \frac{13\bar{c}_1}{2\underline{v}^2} \|\delta\xi\| \|\tilde{\delta}\xi_\tau\| \\
&\quad + \frac{15}{4\underline{v}} \|\xi_\tau\|^{-1} \|\delta\xi_\tau\| \|\tilde{\delta}\xi_\tau\|.
\end{aligned}$$

Rounding up the values yields the bound

$$\begin{aligned}
|f'''(\xi, \xi_\tau)[\delta\xi, \delta\xi_\tau][\tilde{\delta}\xi, \tilde{\delta}\xi_\tau]| &\leq \left[14\frac{\bar{c}_1^2}{v^3} + 4\frac{\bar{c}_2}{v^2}\right] \|\xi_\tau\| \|\delta\xi\| \|\tilde{\delta}\xi\| \\
&\quad + 7\frac{\bar{c}_1}{v^2} \|\delta\xi_\tau\| \|\tilde{\delta}\xi\| \\
&\quad + 7\frac{\bar{c}_1}{v^2} \|\delta\xi\| \|\tilde{\delta}\xi_\tau\| \\
&\quad + \frac{4}{v} \|\xi_\tau\|^{-1} \|\delta\xi_\tau\| \|\tilde{\delta}\xi_\tau\|.
\end{aligned}$$

□

5.A.2 Bounds in a Neighborhood of a Minimizer

Below we derive bounds that hold in a L^∞ -neighborhood of a global minimizer. Let $x^{**} = (z^{**}, \lambda^{**})$ be a global minimizer of (5.6) and the corresponding Lagrange multipliers. Moreover, let $x_1, x_2 \in \mathcal{N}(x^{**}, R)$ and define $\Delta x := x_2 - x_1$. Then it holds that $\|\Delta x\|_{Y^\infty} \leq 2R$ and consequently

$$\|\Delta\xi\|_{L^\infty(0,1)} \stackrel{(5.24a)}{\leq} 2R, \quad (5.85)$$

$$\|\Delta\xi_\tau\|_{L^\infty(0,1)} \stackrel{(5.24a)}{\leq} 2R. \quad (5.86)$$

Let $\|w\|_{L^\infty(\Omega)} \leq \bar{c}_0$, $\|w_x\|_{L^\infty(\Omega)} \leq \bar{c}_1$, $\|w_{xx}\|_{L^\infty(\Omega)} \leq \bar{c}_2$, and $\|w_{xxx}\|_{L^\infty(\Omega)} \leq \bar{c}_3$, then the following bounds hold,

$$|w(\xi_2) - w(\xi_1)| = \left| \int_0^1 w_x(\xi_1 + \mu\delta\xi)[\delta\xi]d\mu \right| \leq \bar{c}_1 \|\delta\xi\| \leq 2R\bar{c}_1, \quad (5.87)$$

$$\|w_x(\xi_2) - w_x(\xi_1)\| = \left| \int_0^1 w_{xx}(\xi_1 + \mu\delta\xi)d\mu \right| \leq \bar{c}_2 \|\delta\xi\| \leq 2R\bar{c}_2, \quad (5.88)$$

$$\|w_{xx}(\xi_2) - w_{xx}(\xi_1)\| = \left| \int_0^1 w_{xxx}(\xi_1 + \mu\delta\xi)d\mu \right| \leq \bar{c}_3 \|\delta\xi\| \leq 2R\bar{c}_3. \quad (5.89)$$

Moreover, we show that

$$\begin{aligned}
|g(\xi_2) - g(\xi_1)| &= |\bar{v}^2 - w(\xi_2)^T w(\xi_2) - \bar{v}^2 + w(\xi_1)^T w(\xi_1)| \\
&= |w(\xi_2)^T w(\xi_2) - w(\xi_1)^T w(\xi_1)| \\
&\leq 2\bar{c}_0\bar{c}_1\|\delta\xi\| \\
&\leq 4R\bar{c}_0\bar{c}_1,
\end{aligned} \tag{5.90}$$

$$\begin{aligned}
|g(\xi_2)^2 - g(\xi_1)^2| &= |(g(\xi_2) - g(\xi_1))(g(\xi_2) + g(\xi_1))| \\
&\leq (2\bar{c}_0\bar{c}_1\|\delta\xi\|)(2\bar{v}^2) \\
&\leq 4\bar{c}_0\bar{c}_1\bar{v}^2\|\delta\xi\| \\
&\leq 8R\bar{c}_0\bar{c}_1\bar{v}^2,
\end{aligned} \tag{5.91}$$

$$\begin{aligned}
|g(\xi_2)^3 - g(\xi_1)^3| &= |g(\xi_2) - g(\xi_1)| |g(\xi_1)^2 + 2g(\xi_1)g(\xi_2) + g(\xi_2)^2| \\
&\leq (2\bar{c}_0\bar{c}_1\|\delta\xi\|)(4\bar{v}^4) \\
&\leq 8\bar{c}_0\bar{c}_1\bar{v}^4\|\delta\xi\| \\
&\leq 16R\bar{c}_0\bar{c}_1\bar{v}^4,
\end{aligned} \tag{5.92}$$

$$\begin{aligned}
|g'(\xi_2) - g'(\xi_1)| &= \left| \int_0^1 g''(\xi_1 + \mu\delta\xi)[\delta\xi]d\mu \right| \\
&\leq 2(\bar{c}_1^2 + \bar{c}_0\bar{c}_2)\|\delta\xi\| \\
&\leq 4R(\bar{c}_1^2 + \bar{c}_0\bar{c}_2),
\end{aligned} \tag{5.93}$$

$$\begin{aligned}
\|g''(\xi_2) - g''(\xi_1)\| &= \left| \int_0^1 g'''(\xi_1 + \mu\delta\xi)d\mu \right| \\
&\leq 2(3\bar{c}_1\bar{c}_2 + \bar{c}_0\bar{c}_3)\|\delta\xi\| \\
&\leq 2R(3\bar{c}_1\bar{c}_2 + \bar{c}_0\bar{c}_3).
\end{aligned} \tag{5.94}$$

Furthermore, with F as given in (5.68), and (5.30) we get

$$\underline{v}^2(L^{**} - R)^2 \leq \underline{v}^2\|\xi_\tau\|^2 \leq F \leq \|\xi_\tau\|^2\bar{v}^2 \leq (L^{**} + R)^2\bar{v}^2$$

and

$$\begin{aligned}
|F'(\xi, \xi_\tau)[\delta\xi, \delta\xi_\tau]| &\leq 2\bar{v}^2\|\xi_\tau\|\|\delta\xi_\tau\| + 4\bar{c}_0\bar{c}_1\|\xi_\tau\|^2\|\delta\xi\| \\
&\leq 2\bar{v}^2(L^{**} + R)\|\delta\xi_\tau\| + 4\bar{c}_0\bar{c}_1(L^{**} + R)^2\|\delta\xi\|.
\end{aligned} \tag{5.95}$$

This yields

$$\begin{aligned}
& |F(\xi_2, \xi_{\tau,2})^{1/2} - F(\xi_1, \xi_{\tau,1})^{1/2}| \\
& \leq \frac{1}{2} \left| \int_0^1 F(\xi_1 + \mu\delta\xi)^{-1/2} F'(\xi_1 + \mu\delta\xi) d\mu \right| \\
& \leq \frac{\bar{v}^2(L^{**} + R)}{\underline{v}(L^{**} - R)} \|\delta\xi_\tau\| + \frac{2\bar{c}_0\bar{c}_1(L^{**} + R)^2}{\underline{v}(L^{**} - R)} \|\delta\xi\|, \tag{5.96}
\end{aligned}$$

$$\begin{aligned}
& |F(\xi_2, \xi_{\tau,2})^{-1/2} - F(\xi_1, \xi_{\tau,1})^{-1/2}| \\
& \leq \frac{1}{2} \left| \int_0^1 F(\xi_1 + \mu\delta\xi)^{-3/2} F'(\xi_1 + \mu\delta\xi) d\mu \right| \\
& \leq \frac{\bar{v}^2(L^{**} + R)}{\underline{v}^3(L^{**} - R)^3} \|\delta\xi_\tau\| + \frac{2\bar{c}_0\bar{c}_1(L^{**} + R)^2}{\underline{v}^3(L^{**} - R)^3} \|\delta\xi\|, \tag{5.97}
\end{aligned}$$

$$\begin{aligned}
& |F(\xi_2, \xi_{\tau,2})^{-3/2} - F(\xi_1, \xi_{\tau,1})^{-3/2}| \\
& \leq \frac{3}{2} \left| \int_0^1 F(\xi_1 + \mu\delta\xi)^{-5/2} F'(\xi_1 + \mu\delta\xi) d\mu \right| \\
& \leq \frac{\bar{v}^2(L^{**} + R)}{\underline{v}^5(L^{**} - R)^5} \|\delta\xi_\tau\| + \frac{2\bar{c}_0\bar{c}_1(L^{**} + R)^2}{\underline{v}^5(L^{**} - R)^5} \|\delta\xi\|. \tag{5.98}
\end{aligned}$$

For f_1 as defined in (5.50), we obtain

$$\begin{aligned}
& (f_1''(\xi_2, \xi_{\tau,2}) - f_1''(\xi_1, \xi_{\tau,1}))[\Delta\xi, \Delta\xi_\tau][\delta\xi, \delta\xi_\tau] \\
&= g(\xi_1)^{-3}g(\xi_2)^{-3} \left[-2g(\xi_1)^3(g'(\xi_2)\delta\xi)(\xi_{\tau,2}^T w(\xi_2))(g'(\xi_2)\Delta\xi) \right. \\
&\quad + 2g(\xi_2)^3(g'(\xi_1)\delta\xi)(\xi_{\tau,1}^T w(\xi_1))(g'(\xi_1)\Delta\xi) \\
&\quad + g(\xi_1)^3g(\xi_2)(\delta\xi_\tau^T w(\xi_2))(g'(\xi_2)\Delta\xi) \\
&\quad - g(\xi_2)^3g(\xi_1)(\delta\xi_\tau^T w(\xi_1))(g'(\xi_1)\Delta\xi) \\
&\quad + g(\xi_1)^3g(\xi_2)(\xi_{\tau,2}^T w_x(\xi_2)\delta\xi)(g'(\xi_2)\Delta\xi) \\
&\quad - g(\xi_2)^3g(\xi_1)(\xi_{\tau,1}^T w_x(\xi_1)\delta\xi)(g'(\xi_1)\Delta\xi) \\
&\quad + g(\xi_1)^3g(\xi_2)(\xi_{\tau,2}^T w(\xi_2))(\Delta\xi^T g''(\xi_2)\delta\xi) \\
&\quad - g(\xi_2)^3g(\xi_1)(\xi_{\tau,1}^T w(\xi_1))(\Delta\xi^T g''(\xi_1)\delta\xi) \\
&\quad + g(\xi_1)^3g(\xi_2)(g'(\xi_2)\delta\xi)(\xi_{\tau,2}^T w_x(\xi_2)\Delta\xi) \\
&\quad - g(\xi_2)^3g(\xi_1)(g'(\xi_1)\delta\xi)(\xi_{\tau,1}^T w_x(\xi_1)\Delta\xi) \\
&\quad - g(\xi_1)^3g(\xi_2)^2(\delta\xi_\tau w_x(\xi_2)\Delta\xi) \\
&\quad + g(\xi_2)^3g(\xi_1)^2(\delta\xi_\tau w_x(\xi_1)\Delta\xi) \\
&\quad - g(\xi_1)^3g(\xi_2)^2 w_{xx}(\xi_2)[\xi_{\tau,2}, \Delta\xi, \delta\xi] \\
&\quad + g(\xi_2)^3g(\xi_1)^2 w_{xx}(\xi_1)[\xi_{\tau,1}, \Delta\xi, \delta\xi] \\
&\quad + g(\xi_1)^3g(\xi_2)(g'(\xi_2)\delta\xi)(w(\xi_2)^T \Delta\xi_\tau) \\
&\quad - g(\xi_2)^3g(\xi_1)(g'(\xi_1)\delta\xi)(w(\xi_1)^T \Delta\xi_\tau) \\
&\quad - g(\xi_1)^3g(\xi_2)^2(\Delta\xi_\tau^T w_x(\xi_2)\delta\xi) \\
&\quad \left. + g(\xi_2)^3g(\xi_1)^2(\Delta\xi_\tau^T w_x(\xi_1)\delta\xi) \right].
\end{aligned}$$

Using the bounds from above we finally obtain

$$\begin{aligned}
& |(f_1''(\xi_2, \xi_{\tau,2}) - f_1''(\xi_1, \xi_{\tau,1}))[\Delta\xi, \Delta\xi_\tau][\delta\xi, \delta\xi_\tau]| \\
&\leq \hat{\beta}_1 R \sqrt{\|\Delta\xi\|^2 + \|\Delta\xi_\tau\|^2} \sqrt{\|\delta\xi\|^2 + \|\delta\xi_\tau\|^2} \quad (5.99)
\end{aligned}$$

with

$$\begin{aligned}
\hat{\beta}_1 = \frac{4}{\underline{\nu}^{12}} & \left(5 + 80\bar{c}_0\bar{c}_1\bar{\nu}^4 + 8\bar{c}_0\bar{c}_1\bar{\nu}^2 + 12\bar{c}_0\bar{c}_1 + 16\bar{c}_0\bar{c}_2 + 4\bar{c}_0\bar{c}_3 \right. \\
& \left. + 16\bar{c}_1^2 + 12\bar{c}_1\bar{c}_2 + 4\bar{c}_1 + 4\bar{c}_2 + 2\bar{c}_3 \right). \quad (5.100)
\end{aligned}$$

For f_2 as defined in (5.52) we obtain

$$\begin{aligned}
& (f_2''(\xi_2, \xi_{\tau,2}) - f_2''(\xi_1, \xi_{\tau,1}))[\Delta\xi, \Delta\xi_\tau][\delta\xi, \delta\xi_\tau] \\
&= g(\xi_1)^{-3}g(\xi_2)^{-3} \left[2g(\xi_1)^3(g'(\xi_2)\delta\xi)(g'(\xi_2)\Delta\xi)F(\xi_2)^{1/2} \right. \\
&\quad - 2g(\xi_2)^3(g'(\xi_1)\delta\xi)(g'(\xi_1)\Delta\xi)F(\xi_1)^{1/2} \\
&\quad - g(\xi_2)g(\xi_1)^3(\Delta\xi^T g''(\xi_2)\delta\xi)F(\xi_2)^{1/2} \\
&\quad + g(\xi_1)g(\xi_2)^3(\Delta\xi^T g''(\xi_1)\delta\xi)F(\xi_1)^{1/2} \\
&\quad - \frac{1}{2}g(\xi_2)g(\xi_1)^3(g(\xi_2)'\Delta\xi)F(\xi_2)^{-1/2}F'(\xi_2)[\delta\xi, \delta\xi_\tau] \\
&\quad + \frac{1}{2}g(\xi_1)g(\xi_2)^3(g(\xi_1)'\Delta\xi)F(\xi_1)^{-1/2}F'(\xi_1)[\delta\xi, \delta\xi_\tau] \\
&\quad - \frac{1}{2}g(\xi_2)g(\xi_1)^3(g'(\xi_2)\delta\xi)F(\xi_2)^{-1/2}F'(\xi_2)[\Delta\xi, \Delta\xi_\tau] \\
&\quad + \frac{1}{2}g(\xi_1)g(\xi_2)^3(g'(\xi_1)\delta\xi)F(\xi_1)^{-1/2}F'(\xi_1)[\Delta\xi, \Delta\xi_\tau] \\
&\quad + \frac{1}{2}g(\xi_2)^2g(\xi_1)^3F(\xi_2)^{-1/2}F''(\xi_2)[\Delta\xi, \Delta\xi_\tau][\delta\xi, \delta\xi_\tau] \\
&\quad - \frac{1}{2}g(\xi_1)^2g(\xi_2)^3F(\xi_1)^{-1/2}F''(\xi_1)[\Delta\xi, \Delta\xi_\tau][\delta\xi, \delta\xi_\tau] \\
&\quad - \frac{1}{4}g(\xi_2)^2g(\xi_1)^3F(\xi_2)^{-3/2}F'(\xi_2)[\Delta\xi, \Delta\xi_\tau]F'(\xi_2)[\delta\xi, \delta\xi_\tau] \\
&\quad \left. + \frac{1}{4}g(\xi_1)^2g(\xi_2)^3F(\xi_1)^{-3/2}F'(\xi_1)[\Delta\xi, \Delta\xi_\tau]F'(\xi_1)[\delta\xi, \delta\xi_\tau] \right]
\end{aligned}$$

Using the bounds from above, this yields

$$\begin{aligned}
& |(f_2''(\xi_2, \xi_{\tau,2}) - f_2''(\xi_1, \xi_{\tau,1}))[\delta\xi, \delta\xi_\tau][\tilde{\delta}\xi, \tilde{\delta}\xi_\tau]| \\
&\leq \hat{\beta}_2 R \sqrt{\|\Delta\xi\|^2 + \|\Delta\xi_\tau\|^2} \sqrt{\|\delta\xi\|^2 + \|\delta\xi_\tau\|^2} \quad (5.101)
\end{aligned}$$

with

$$\begin{aligned}
\hat{\beta}_2 = \frac{4}{\underline{v}^{12}} & \left[20 + 10\bar{c}_1 + 7\bar{c}_2 + \bar{c}_3 + 10\bar{c}_0\bar{c}_1 + 36\bar{c}_0\bar{c}_1\bar{v}^2 + 88\bar{c}_0\bar{c}_1\bar{v}^4 \right. \\
& + 20\bar{c}_0\bar{c}_2 + 8\bar{c}_0\bar{c}_3 + 20\bar{c}_1^2 + 24\bar{c}_1\bar{c}_2 \\
& + \left(\frac{3}{\underline{v}(L^{**} - R)} + \frac{6}{\underline{v}^3(L^{**} - R)^3} + \frac{6}{\underline{v}^5(L^{**} - R)^5} \right) \\
& \left. \left(\bar{v}^2(L^{**} + R) + 2\bar{c}_0\bar{c}_1(L^{**} + R)^2 \right) \right]. \quad (5.102)
\end{aligned}$$

Lemma 5.16. — *Let ξ^{**}, L^{**} be a global minimizer of (5.6). Moreover, let ξ_1, ξ_2 be given such that $\|\xi_i - \xi^{**}\|_{C^{0,1}(0,1)} \leq R$ and define $\Delta\xi := \xi_1 - \xi_2$. Then there is a $\hat{\mathcal{B}} < \infty$ such that*

$$\begin{aligned} & |(f''(\xi_2, \xi_{\tau,2}) - f''(\xi_1, \xi_{\tau,1}))[\Delta\xi, \Delta\xi_{\tau}][\delta\xi, \delta\xi_{\tau}]| \\ & \leq \hat{\mathcal{B}}R\sqrt{\|\Delta\xi\|^2 + \|\Delta\xi_{\tau}\|^2}\sqrt{\|\delta\xi\|^2 + \|\delta\xi_{\tau}\|^2}. \end{aligned} \quad (5.103)$$

Proof. With (5.99) and (5.101) we obtain

$$\begin{aligned} & |(f''(\xi_2, \xi_{\tau,2}) - f''(\xi_1, \xi_{\tau,1}))[\Delta\xi, \Delta\xi_{\tau}][\delta\xi, \delta\xi_{\tau}]| \\ & \leq |(f''_1(\xi_2, \xi_{\tau,2}) - f''_1(\xi_1, \xi_{\tau,1}))[\Delta\xi, \Delta\xi_{\tau}][\delta\xi, \delta\xi_{\tau}]| \\ & \quad + |(f''_2(\xi_2, \xi_{\tau,2}) - f''_2(\xi_1, \xi_{\tau,1}))[\Delta\xi, \Delta\xi_{\tau}][\delta\xi, \delta\xi_{\tau}]| \\ & \leq \hat{B}R\sqrt{\|\Delta\xi\|^2 + \|\Delta\xi_{\tau}\|^2}\sqrt{\|\delta\xi\|^2 + \|\delta\xi_{\tau}\|^2} \end{aligned}$$

with $\hat{\mathcal{B}} = \hat{\beta}_1 + \hat{\beta}_2$. □

CHAPTER 6

Convergence Properties of Newton's Method for Globally Optimal Free Flight Trajectory Optimization

Borndörfer, R., Danecker, F., and Weiser, M.
23rd Symposium on Algorithmic Approaches for Transportation Modelling,
Optimization, and Systems (ATMOS 2023); 3:1–3:6; 115.
DOI: 10.4230/OASICS.ATMOS.2023.3.

This article is licensed under a Creative Commons Attribution 4.0
International License (<http://creativecommons.org/licenses/by/4.0/>).

Abstract The algorithmic efficiency of Newton-based methods for Free Flight Trajectory Optimization is heavily influenced by the size of the domain of convergence. We provide numerical evidence that the convergence radius is much larger in practice than what the theoretical worst case bounds suggest. The algorithm can be further improved by a convergence-enhancing domain decomposition.

Contents

6.1	Introduction	225
6.2	The Free Flight Trajectory Optimization Problem	226
6.3	Numerical Results	227
6.3.1	Size of the Convergence Radius	229
6.3.2	Relevance of the Error Terms	230
6.3.3	Algorithmic Improvement	231
6.4	Conclusion	232

6.1 Introduction

Today, aircraft are required to take routes in the airway network, a 3D graph over the surface of the earth. Such routes are longer and less fuel efficient than unconstrained routes. Air traffic associations in many places, in particular, in Europe and in the US, are therefore investigating options to introduce Free Flight aviation regimes that allows such routes, in an attempt to reduce congestion, travel times, and fuel consumption. By giving pilots more freedom to choose their routes, taking into account factors such as weather conditions, wind patterns, and individual aircraft performance, Free Flight can improve overall efficiency and operational flexibility. For a more comprehensive and detailed discussion of the problem and an overview of solution approaches, we kindly direct the reader to our previous publications [1–4] (Chapters 2, 3, 4 and 5) and the references therein.

In [1, 2] (Chapters 2 and 4), we introduced an algorithm that combines Discrete and Continuous Optimization techniques to obtain a globally optimal trajectory under Free Flight conditions. The approach involves constructing a discrete approximation of the problem in the form of a sufficiently dense graph, which implicitly generates a pool of potential candidate paths. These paths (i) can be efficiently explored using state-of-the-art shortest path algorithms, and (ii) provide suitable initial solutions for a locally convergent continuous optimization approach. Specifically, we proposed the application of Newton's method to the first-order necessary conditions, an algorithm that is known as Newton-KKT method or Sequential Quadratic Programming (SQP) [4] (Chapter 5).

The efficiency of this hybrid method hinges on the graph density that is required to guarantee that a discrete candidate path lies within the domain of convergence of the continuous optimizer. The size of the domain of convergence depends on the wind conditions, and directly impacts the computational efficiency of the algorithm: A smaller convergence radius requires a denser graph and thus more discrete candidate paths that need to be considered.

In this article we provide numerical evidence that the convergence radius exceeds the theoretical lower bound. This finding greatly enhances the robustness, the speed, and the practical applicability of the proposed approach beyond the theoretical guarantees that are currently known. Furthermore, our investigation confirms that the norm that was introduced in our previous papers to quantify the size of the domain of convergence is an appropriate choice. It effectively captures the characteristics of the domain and provides meaningful insights into its extent. We finally propose a nonlinear domain decomposition-inspired algorithmic modification to increase the convergence radius and enhance optimization performance.

6.2 The Free Flight Trajectory Optimization Problem

The vertical component of a flight trajectory is primarily governed by aircraft-specific performance data and the corresponding reduction in weight due to fuel burn, allowing for a relatively precise determination beforehand. In contrast, the horizontal component is predominantly influenced by external factors, with wind conditions being a crucial factor. As a result, a common approach involves optimizing each component separately (e.g., [5]). In this paper, we concentrate on the optimization of the horizontal trajectory.

Neglecting any traffic flight restrictions, we consider flight paths in the Sobolev-Space

$$X = \{\xi \in W^{1,\infty}((0, 1), \mathbb{R}^2) \mid \xi(0) = x_O, \xi(1) = x_D\}. \quad (6.1)$$

connecting origin x_O and destination x_D . A short calculation reveals that an aircraft travelling along such a path ξ with constant airspeed \bar{v} through a three times continuously differentiable wind field $w \in C^3(\mathbb{R}^2, \mathbb{R}^2)$ of bounded magnitude $\|w\|_{L^\infty} < \bar{v}$ reaches the destination after a flight duration

$$T(\xi) = \int_0^1 f(\xi(\tau), \xi_\tau(\tau)) d\tau, \quad (6.2)$$

where ξ_τ denotes the time derivative of ξ and

$$f(\xi, \xi_\tau) := t_\tau = \frac{-\xi_\tau^\top w + \sqrt{(\xi_\tau^\top w)^2 + (\bar{v}^2 - w^\top w)(\xi_\tau^\top \xi_\tau)}}{\bar{v}^2 - w^\top w}, \quad (6.3)$$

see [1–4] (Chapters 2, 3, 4 and 5).

Among these paths ξ , we need to find one with minimal flight duration $T(\xi)$, since that is essentially proportional to fuel consumption [6]. This classic of optimal control is known as Zermelo's navigation problem [7].

Since the flight duration T as defined in (6.2) is based on a time reparametrization from actual flight time $t \in [0, T]$ to pseudo-time $\tau \in (0, 1)$ according to the actual flight trajectory $x(t) = \xi(\tau(t))$ such that $\|x_t(t) - w(x(t))\| = \bar{v}$, the actual parametrization of ξ in terms of pseudo-time τ is irrelevant for the value of T and we can restrict the optimization to finding the representative with constant ground speed $\|\xi_\tau(\tau)\|$. Hence, we will subsequently consider the constrained minimization problem

$$\min_{\xi \in X, L \in \mathbb{R}} T(\xi), \quad \text{s.t.} \quad \|\xi_\tau(\tau)\|^2 = L^2 \quad \text{for a.a. } \tau \in (0, 1). \quad (6.4)$$

If the constraint is satisfied, L can be interpreted as the path length.

6.3 Numerical Results

In the following we explore three key aspects of Free Flight Optimization numerically: the gap between the empirical convergence radius and its theoretical lower bound, the suitability of the norm used in previous works for assessing convergence accurately, and an algorithmic approach for increasing the convergence radius.

These points will be studied on a benchmark example of crossing a wind field consisting of 15 regularly aligned disjoint vortices from $x_O = (0, 0)$ to $x_D = (1, 0)$ at an airspeed of $\bar{v} = 1$, see Figure 6.1 a). The wind speed attains its maximum at the center of a vortex with $\|w\|_{L^\infty} \leq \frac{1}{2}\bar{v}$ and decreases monotonically to 0 towards the boundary. A formal definition is given in [1] (Chapter 2).

Traversing a vortex, there are two locally optimal options; using the tailwind on one side or avoiding the headwind with a detour on the other side (cf. [1], Chapter 2, example b)). Hence, there may be roughly $\mathcal{O}(2^n)$ locally optimal routes in a wind

field with n vortices, posing a challenging problem for global optimization; moreover, a wind field setting of this complexity will rarely if ever be encountered in practice.

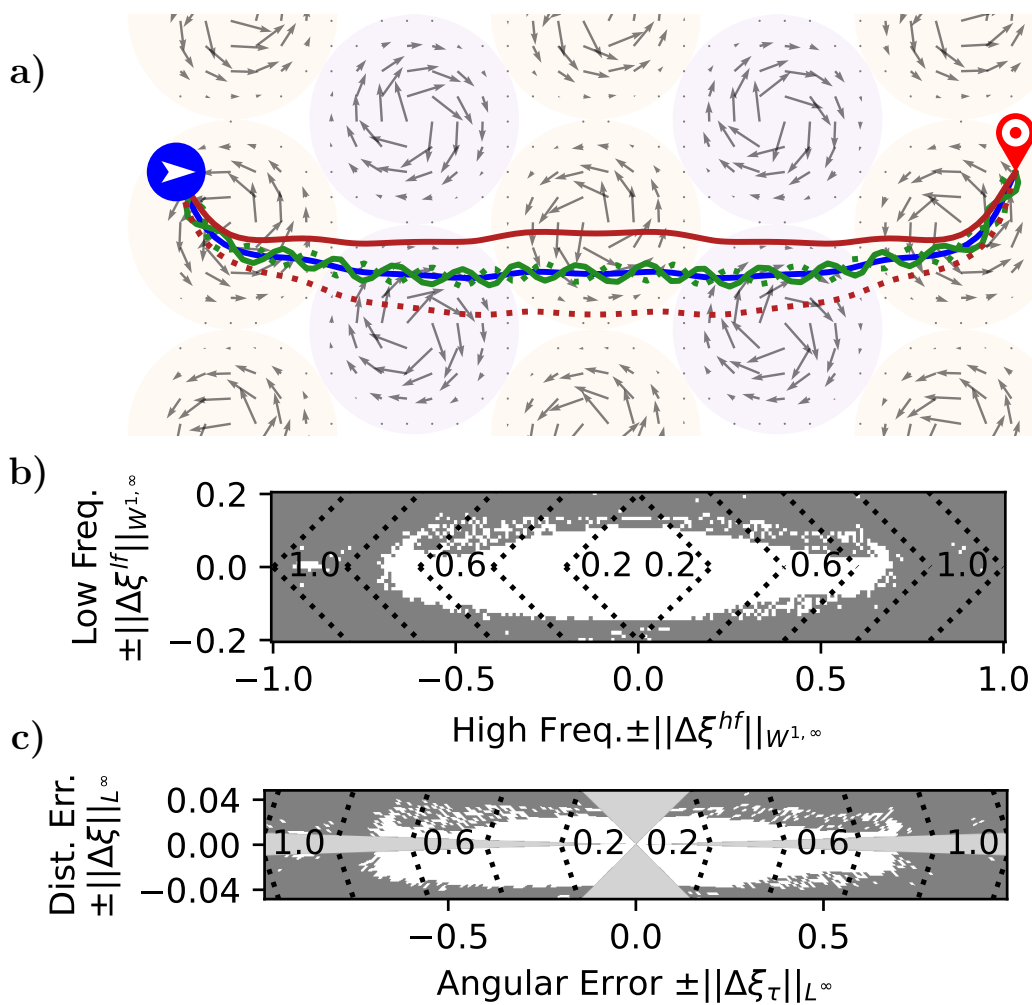


Figure 6.1: a) The extremes of the sampled part of the two-dimensional subspace are shown. Blue: globally optimal route ξ^{**} , green: high-frequency deviation $\xi^{**} + \Delta\xi^{hf}$, red: low-frequency deviation $\xi^{**} + \Delta\xi^{lf}$. b) Empirical domain of convergence. White: Newton's method converged back to the global optimum, gray: it did not. Dashed lines: constant combined norm $\|\Delta\xi\|_{W^{1,\infty}}$. For the purpose of illustration the sign is chosen based on the direction of the respective deviation. c) Via an affine transformation, each of the quadrants of b) is mapped into the space spanned by angular and distance error.

6.3.1 Size of the Convergence Radius

It has been shown in [4] (Chapter 5) that there is a positive convergence radius R_C such that the Newton-KKT method initialized with ξ converges to a minimizer ξ^{**} if

$$\underbrace{\|\xi - \xi^{**}\|_{L^\infty(0,1)}}_{\text{distance err.}} + \underbrace{\|(\xi - \xi^{**})_\tau\|_{L^\infty(0,1)}}_{\text{angular err.}} + |L - L^{**}| + \|\lambda - \lambda^{**}\|_{L^\infty(0,1)} \leq R_C. \quad (6.5)$$

Since the constraint in (6.4) is only weakly active, the Lagrangian Multiplier can directly be initialized with $\lambda = \lambda^{**} = 0$ (see [4], Chapter 5). Moreover, L can reasonably be initialized with the path length of the candidate route. Hence we concentrate on the first two terms which we will refer to as *distance* and *angular error*. Note that higher order derivatives (e.g., curvature) do not affect the overall travel time (6.2). In the following we examine a two-dimensional affine subspace of the trajectory space that allows us to separate the individual impact of these error terms (see discussion in Section 6.3.2);

$$M := \xi^{**} + \mathbb{R}\Delta\xi^{\text{hf}} + \mathbb{R}\Delta\xi^{\text{lf}}, \quad (6.6)$$

which is anchored at the global optimum ξ^{**} and spanned by a low- and a high-frequency deviation, both of the form

$$\Delta\xi^f(\tau) = n(\tau) \sin(k^f \pi \tau), \quad f \in \{\text{hf}, \text{lf}\} \quad (6.7)$$

with $k^{\text{lf}} = 1$, $k^{\text{hf}} = 30$ and $n(\tau) \in \mathbb{R}^2$ denoting a unit vector perpendicular to the optimal direction of flight $\xi_\tau^{**}(\tau)$. The norm of such a deviation reads

$$\|\Delta\xi^f\|_{W^{1,\infty}(0,1)} = \|\Delta\xi^f\|_{L^\infty(0,1)} + \|\Delta\xi_\tau^f\|_{L^\infty(0,1)} = 1 + k^f \pi$$

and consequently

$$\begin{aligned} \|\Delta\xi\|_{W^{1,\infty}(0,1)} &= \|a^{\text{hf}} \Delta\xi^{\text{hf}} + a^{\text{lf}} \Delta\xi^{\text{lf}}\|_{W^{1,\infty}(0,1)} \\ &= |a^{\text{hf}}|(1 + k^{\text{hf}} \pi) + |a^{\text{lf}}|(1 + k^{\text{lf}} \pi). \end{aligned}$$

From this subspace M candidates ξ are sampled around the global optimum and used as starting points in order to solve the optimization problem (6.4) via the

Newton-KKT method as described in [4] (Chapter 5). Figure 6.1 a) shows the global optimum in blue and the extremes of the sampled region in red and green, solid and dotted, respectively. Figure 6.1 b) shows whether the procedure converged back to the optimum (white) or not (gray) with the abscissa and ordinate indicating the Sobolev-norm of the high- and low-frequency deviation, respectively. The total Sobolev-distance (6.8a) is indicated by dotted contour lines. It can be shown that even under mild wind conditions, $R_C \approx 10^{-8}$ holds. Our numerical experiments, however, reveal that the domain of convergence is consistently larger than 10^{-1} – several orders of magnitude larger than the theoretical guaranty.

6.3.2 Relevance of the Error Terms

With the same norm, a low-frequent deviation introduces mostly distance error, while a deviation with high frequency results in significant angular error. This observation allows transforming each quadrant of Figure 6.1 b) into the space of distance and angular error via

Distance error:

$$\|\Delta\xi\|_{L^\infty} = |a^{\text{lf}}| + |a^{\text{hf}}| = \frac{1}{1 + k^{\text{lf}}\pi} \|\Delta\xi^{\text{lf}}\|_{W^{1,\infty}} + \frac{1}{1 + k^{\text{hf}}\pi} \|\Delta\xi^{\text{hf}}\|_{W^{1,\infty}}, \quad (6.8a)$$

Angular error:

$$\|\Delta\xi_\tau\|_{L^\infty} = |a^{\text{lf}}| k^{\text{lf}}\pi + |a^{\text{hf}}| k^{\text{hf}}\pi = \frac{k^{\text{lf}}\pi}{1 + k^{\text{lf}}\pi} \|\Delta\xi^{\text{lf}}\|_{W^{1,\infty}} + \frac{k^{\text{hf}}\pi}{1 + k^{\text{hf}}\pi} \|\Delta\xi^{\text{hf}}\|_{W^{1,\infty}}, \quad (6.8b)$$

as shown in Figure 6.1 c). Note that both deviations contribute to angular and distance errors. As a result, cones around the axes (depicted as light gray regions) cannot be represented using deviations of the specified form.

Both error terms are significant. A viable route can have a large distance error if it is far from the optimum (Figure 6.1 a), red paths), but it should exhibit parallel behavior for a small angular error. On the other hand, if the candidate path zig-zags around the optimum, it will have a substantial angular error (Figure 6.1 a), green paths), but it cannot deviate significantly from the optimal path, leading to a lower distance error.

In terms of distance error, the extent of the domain of convergence is largely determined by the wind field. At each vortex there are two locally optimal options; passing left or right. At some point one will inevitably enter the convergence region of the next local optimum.

6.3.3 Algorithmic Improvement

Our approach focuses on candidate routes with a high angular error, as exemplified by the red route in Figure 6.2. This is of importance for the discrete-continuous algorithm, since graph-based shortest paths tend to zig-zag around an optimizer [3] (Chapter 3).

It is intuitively clear that on a local scale, an optimal trajectory is nearly straight. We exploit this for reducing high-frequency errors by solving local trajectories on an overlapping decomposition of the time domain, thus realizing a nonlinear alternating Schwarz method [8].

We select equidistant points along the initial route, such that the distance between consecutive points is smaller than significant wind field structures. In the example, the route was obtained by imposing a large, high-frequency deviation as before and divided into 11 segments, deliberately not a divisor of the frequency. This initial route lies outside the convergence region (see Figure 6.2).

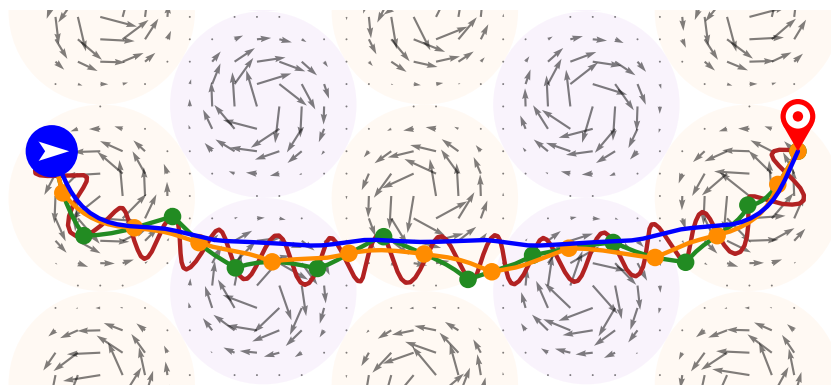


Figure 6.2: The initial guess (red) is divided into segments, on which the trajectory is locally optimized (green). This process is repeated, and the resulting trajectory (orange) is the initial guess for the optimization of the entire route. Starting from the smoothed guess (orange), Newton's method converges to the global optimizer (blue), while from the initial guess (red) it does not.

In the first step, we calculate the optimal routes on all subintervals (depicted in green). Next, utilizing this refined segment, we repeat the process with shifted waypoints (depicted in orange). A significant portion of the oscillation has been smoothed out, resulting in a notable reduction of the angular error. Using this refined segment as a starting point for optimizing the entire route leads us to the desired optimum (blue). Figure 6.3 reveals, that this improvement enlarges the convergence region significantly.

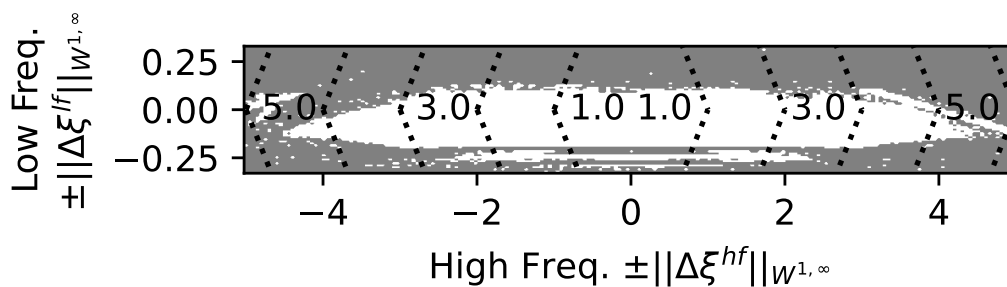


Figure 6.3: The approach has led to a significant increase of the domain of convergence (cf. Fig. 6.1 b)).

6.4 Conclusion

The recently proposed Discrete-Continuous Hybrid Algorithm for Free Flight Trajectory Optimization relies on the existence of a sufficiently large domain of convergence around a global minimizer. In our study, we have presented compelling evidence that this condition is satisfied even under highly challenging conditions and that the measure we have proposed for assessing it is appropriate. Furthermore, we have introduced a domain decomposition method to expand the convergence region, which is expected to significantly enhance the practical performance of the hybrid approach.

Authors' Contributions

Conceptualization, R.B., F.D., and M.W.; methodology, F.D. and M.W.; validation, F.D.; formal analysis, F.D. and M.W.; investigation, F.D.; resources, R.B., F.D. and M.W.; writing-original draft preparation, F.D. and M.W.; writing-review and

editing, R.B.; supervision, R.B.; project administration, R.B. and M.W.; funding acquisition, R.B. and M.W..

All authors have read and agreed to the published version of the manuscript.

References

- [1] R. Borndörfer, F. Danecker, and M. Weiser, “A Discrete-Continuous Algorithm for Free Flight Planning,” *Algorithms*, vol. 14, no. 1, p. 4, 2021. DOI: 10.3390/a14010004.
- [2] R. Borndörfer, F. Danecker, and M. Weiser, “A Discrete-Continuous Algorithm for Globally Optimal Free Flight Trajectory Optimization,” in *22nd Symposium on Algorithmic Approaches for Transportation Modelling, Optimization, and Systems (ATMOS 2022)*, vol. 106, Schloss Dagstuhl – Leibniz-Zentrum für Informatik, 2022, pp. 1–13. DOI: 10.4230/OASIcs.ATMOS.2022.2.
- [3] R. Borndörfer, F. Danecker, and M. Weiser, “Error Bounds for Discrete-Continuous Free Flight Trajectory Optimization,” *Journal of Optimization Theory and Applications*, vol. 198, no. 2, pp. 830–856, 2023. DOI: 10.1007/s10957-023-02264-7.
- [4] R. Borndörfer, F. Danecker, and M. Weiser, “Newton's Method for Global Free Flight Trajectory Optimization,” *Operations Research Forum*, vol. 4, no. 3, p. 63, 2023. DOI: 10.1007/s43069-023-00238-z.
- [5] H. K. Ng, B. Sridhar, and S. Grabbe, “Optimizing Aircraft Trajectories with Multiple Cruise Altitudes in the Presence of Winds,” *Journal of Aerospace Information Systems*, vol. 11, no. 1, pp. 35–47, 2014. DOI: 10.2514/1.1010084.
- [6] C. A. Wells, P. D. Williams, N. K. Nichols, D. Kalise, and I. Poll, “Reducing Transatlantic Flight Emissions by Fuel-Optimised Routing,” *Environ. Res. Letters*, vol. 16, no. 2, p. 025002, 2021. DOI: 10.1088/1748-9326/abce82.
- [7] E. Zermelo, “Über das Navigationsproblem bei ruhender oder veränderlicher Windverteilung,” *ZAMM-Journal of Applied Mathematics and Mechanics/Zeitschrift für Angewandte Mathematik und Mechanik*, vol. 11(2), pp. 114–124, 1931. DOI: 10.1002/zamm.19310110205.
- [8] P. L. Lions, “On the Schwarz Alternating Method. I,” in *1st International Symposium on Domain Decomposition Methods for Partial Differential Equations*, SIAM, 1988, pp. 1–42.

CHAPTER **7**

Appendix

Contents

7.1	A Priori Estimates	237
7.1.1	Still Air	238
7.1.2	Moderate Wind Conditions	239
7.2	Efficiently Harvesting the Benefits of Free Flight . . .	249
7.2.1	Graph-Based Routing	249
7.2.2	DisCOptER	252
7.2.3	Wind Conditions	253
7.2.4	Origin-Destination Pairs	254
7.2.5	Results	254
7.2.6	Supplementary Material	258
7.3	Errata	261
7.3.1	Notational improvements	261
7.3.2	Continuity of the objective function	261

7.1 A Priori Estimates

The DisCOptER algorithm, developed in this work, relies fundamentally on the existence of a sufficiently large region surrounding the global optimum, within which the ordinary Newton-KKT method can converge. We reconsider Theorem 5.15, which proved that this condition holds true if two key assumptions are met.

Theorem 5.15. — *Let $\chi^{**} = (z^{**}, \lambda^{**})$ be a global solution of (5.6) that satisfies the first and second order conditions for optimality with $\underline{\mathcal{B}} > 0$. Moreover, let there be a $c > 0$ and a $u \in \mathbb{R}^2$ with $\|u\| = 1$ such that $u^T \xi_\tau^{**} \geq c$ for almost all $\tau \in (0, 1)$. Finally, let $\omega := \omega_1 \omega_2$, as given in Lemmas 5.13 and 5.14.*

*Then there is a $R_C > 0$, such that the ordinary Newton iterates defined in Section 5.3.2 converge to χ^{**} at an estimated rate*

$$\|\chi^{k+1} - \chi^{**}\|_{Y^2} \leq \frac{\omega}{2} \|\chi^k - \chi^{**}\|_{Y^2}, \quad (5.49)$$

*if initialized with $\chi^0 \in \mathcal{N}(\chi^{**}, R_C)$ and provided that the iterates χ^k remain in $\mathcal{N}(\chi^{**}, R_C)$. Moreover, χ^{**} is unique in $\mathcal{N}(\chi^{**}, R_C)$.*

The first assumption asserts the existence of a direction u and a constant $c > 0$, in which the globally optimal trajectory consistently points, such that

$$u^T \xi_\tau^{**} \geq c \quad \text{for almost all } \tau \in (0, 1).$$

The second originates from the sufficient conditions for optimality and essentially requires the second derivative of the objective's Hessian to be strictly positive definite on the kernel of the constraints, characterized by the constant $\underline{\mathcal{B}} > 0$.

In this section it will be shown, that these conditions are satisfied and that the involved constants can be calculated from a priori known global bounds on the wind conditions if the wind is not too rough. With this in place, the DisCOptER algorithm converges deterministically and yields a globally optimal solution.

We will start by examining the simpler scenario of still air, demonstrating that the requirements are met under these conditions. Subsequently, we will extend the discussion to the more complex case of moderate wind conditions.

7.1.1 Still Air

If there is no wind at all, the objective function of (5.6) reduces to

$$T(\xi) = \int_0^1 \frac{\|\xi_\tau\|}{\bar{v}} d\tau \stackrel{(5.6)}{=} \frac{L}{\bar{v}}$$

for feasible (ξ, L) . It is easy to see that the optimum is the one trajectory that minimizes the path length L , which of course is the straight line. With $\tilde{L} := \|x_D - x_O\|$ denoting the distance from origin to destination and $u := \frac{x_D - x_O}{\tilde{L}}$ the unit vector in this direction, the solution can be expressed as

$$\xi^{**}(\tau) = x_O + \tau \tilde{L} u, \quad L^{**} = \tilde{L}. \quad (7.1)$$

First it shall be confirmed that this solution is a stationary point, i.e., that the necessary conditions for optimality as given in (5.16) are satisfied. With the Lagrangian multipliers $\lambda^{**} = 0$ as of (5.19) it holds that

$$\begin{aligned} T'(\xi^{**})[\delta\xi] + 2 \int_0^1 \underbrace{\lambda^{**}}_{=0 \text{ (5.19)}} \left(\delta\xi_\tau^\top \xi_\tau^{**} - \delta L L^{**} \right) d\tau &= \frac{2}{\bar{v}} \int_0^1 \delta\xi_\tau^\top \xi_\tau^{**} d\tau \\ &= \frac{2}{\bar{v}} \tilde{L} u^\top \underbrace{\int_0^1 \delta\xi_\tau d\tau}_{=0 \text{ (5.9)}} = 0 \end{aligned}$$

for any $\delta z \in \delta Z$. Moreover, for any $\delta\lambda \in \Lambda^*$ it holds that

$$\int_0^1 \delta\lambda \left((\xi_\tau^{**})^\top \xi_\tau^{**} - (L^{**})^2 \right) d\tau = \int_0^1 \delta\lambda \left(\tilde{L}^2 \underbrace{u^\top u}_{=1} - \tilde{L}^2 \right) d\tau = 0,$$

which completes the necessary conditions.

Further, it can be shown that this simple instance of the free flight trajectory optimization problem is locally convex in the sense that the LBB condition as previously described in Section 5.3.1.2 is satisfied. It is easy to see that

$$\xi_\tau^\top u \geq \frac{\tilde{L}^2}{2} > 0 \quad \forall \tau \in (0, 1) \quad (7.2)$$

for every $z \in \mathcal{N}(z^{**}, \frac{\tilde{L}}{2})$. Consequently, the inf-sup condition is satisfied for any such z , as shown in Theorem 5.6.

It remains to show that the second directional derivative of T , now given by

$$T''(\xi)[\delta\xi, \delta\xi_\tau]^2 = \int_0^1 \frac{\|\xi_\tau\|^2 \|\delta\xi_\tau\|^2 - (\xi_\tau^\top \delta\xi_\tau)^2}{\bar{v} \|\xi_\tau\|^3} d\tau,$$

is strictly positive for any $z \in Z$ and any $\delta z \in \delta Z$ that satisfies $\xi_\tau^\top \delta\xi_\tau = L\delta L$.

Obviously, T'' is in general non-negative and vanishes only if $\delta\xi_\tau$ is collinear to ξ_τ . These directions, however, do not maintain origin and destination and are hence not contained in δX as described in (5.9).

In order to verify this, assume there was such a direction $\delta\xi_\tau = a(\tau)\xi_\tau$ with some $a : (0, 1) \mapsto \mathbb{R}$. From $\xi_\tau^\top \delta\xi_\tau = L\delta L$ follows that $\delta\xi_\tau = \frac{L\delta L}{\|\xi_\tau\|^2} \xi_\tau$, which reveals a contradiction, since

$$0 \stackrel{!}{\underset{(5.9)}}{=} \int_0^1 \delta\xi_\tau d\tau = L\delta L \int_0^1 \frac{1}{\|\xi_\tau\|^2} d\tau \neq 0.$$

Consequently, it can be concluded that in this simple case the problem is convex for any $z \in \mathcal{N}(z^{**}, R)$. I.e., the straight connection is the only minimizer in this neighborhood. Furthermore, this implies that all the prerequisites of Theorem 5.15 are satisfied. Hence, the defined Newton-KKT approach converges locally and consequently the discrete-continuous hybrid algorithm DisCOptER developed in this work converges globally.

7.1.2 Moderate Wind Conditions

In contrast to the case of zero wind, realistic wind fields often exhibit a large number of local minima which necessitates efficient and robust global optimization algorithms.

The convergence Theorem 5.15 relies on the existence of constants u , c , and $\underline{\mathcal{B}}$. These constants serve two vital purposes: qualitatively, they establish the existence of a domain of convergence, and quantitatively, they determine its size. It will now be shown that such constants do exist and can be calculated from a priori assumptions regarding the wind conditions, if those are sufficiently mild in terms of actual speed as well as spatial derivatives.

This analysis can be divided into two primary components, similar to the case of no wind. First, it will be established that the angle between the optimal

trajectory and the straight connection remains bounded, thereby providing values for the constants c and u . This, in conjunction with previous findings, verifies the satisfaction of the inf-sup condition (5.20). Secondly, it will be demonstrated that the objective functional T is indeed positive definite on the kernel of the constraints, as described in equation (5.22).

Lemma 7.1. — *Let $z^{**} = (\xi^{**}, L^{**})$ be a globally optimal solution of (5.6) and $u := \frac{x_D - x_O}{\tilde{L}}$ denote the unit vector from origin to destination. Moreover, let the wind speed be bounded by*

$$\|w\|_{L^\infty(\Omega)} \leq \bar{c}_0 < \frac{\pi - 2}{\pi + 2} \bar{v}. \quad (7.3)$$

Then there is a $c > 0$ such that

$$u^T \xi_\tau^{**}(\tau) \geq c \quad \forall \tau \in (0, 1). \quad (7.4)$$

Proof. W.l.o.g. assume that the problem is posed such that $u = [1, 0]^T$. With $\alpha(\tau)$ denoting the angle between u and the ground speed vector $\xi_\tau^{**}(\tau)$, the latter can be written as

$$\xi_\tau^{**}(\tau) = L^{**} \begin{bmatrix} \cos(\alpha(\tau)) \\ \sin(\alpha(\tau)) \end{bmatrix},$$

due to $\|\xi_\tau^{**}\| \stackrel{(5.6)}{=} L^{**}$. As stated in Lemma 5.3 the path length L^{**} of a global minimizer is bounded by

$$L^{**} \leq \frac{\bar{v} + \bar{c}_0}{\bar{v} - \bar{c}_0} \tilde{L} < \frac{\pi}{2} \tilde{L}.$$

According to Bellman's principle of optimality, any subpath taken from an optimal trajectory is also optimal. As a consequence, the minimizer's turning rate is bounded, $|\alpha_\tau(\tau)| \leq \bar{\alpha}_\tau$, and can be determined by creating a path with a constant maximum curvature, which is a circular segment that stretches from the starting point to the destination, with a length of $L^S = \frac{\bar{v} + \bar{c}_0}{\bar{v} - \bar{c}_0} \tilde{L}$ (see Figure 7.1). Then it holds that

$$\frac{L^S}{\tilde{L}} = \frac{\bar{\alpha}_\tau/2}{\sin(\bar{\alpha}_\tau/2)} \quad \Rightarrow \quad |\alpha_\tau(\tau)| \leq \bar{\alpha}_\tau < \pi.$$

In order to construct a case in which the optimum trajectory maximizes the angle α between ξ_τ^{**} and u , assume that the maximum is attained right at the start, i.e., $\alpha(0) = \bar{\alpha}$ and that the angle is decreased at maximum rate throughout, i.e.,

$$\xi_\tau(\tau) = L \begin{bmatrix} \cos(\bar{\alpha} - \tau\bar{\alpha}_\tau) \\ \sin(\bar{\alpha} - \tau\bar{\alpha}_\tau) \end{bmatrix}. \quad (7.5)$$

This describes exactly the circular segment depicted in Figure 7.1. Let $v := [0, 1]^T$ be a unit vector perpendicular to u , then any trajectory connecting origin and destination satisfies

$$\tilde{L} = \int_0^1 u^T \xi_\tau d\tau \quad \text{and} \quad 0 = \int_0^1 v^T \xi_\tau d\tau.$$

Insertion of (7.5) into the second equation yields

$$\begin{aligned} 0 &= L \int_0^1 \sin(\bar{\alpha} - \tau\bar{\alpha}_\tau) d\tau \\ &= \frac{L}{\bar{\alpha}_\tau} (\cos(\bar{\alpha} - \bar{\alpha}_\tau) - \cos(\bar{\alpha})) \\ &= \frac{2L}{\bar{\alpha}_\tau} \sin(\bar{\alpha}_\tau/2) \sin(\bar{\alpha} - \bar{\alpha}_\tau/2). \end{aligned}$$

As $|\bar{\alpha}_\tau| < \pi$, the only solution is

$$\bar{\alpha} = \frac{\bar{\alpha}_\tau}{2} - \frac{\pi}{2} < \frac{\pi}{2},$$

which completes the proof, since

$$u^T \xi_\tau = L^{**} \cos \alpha \geq L^{**} \cos \bar{\alpha} > 0.$$

□

With Theorem 5.6, it follows directly that the inf-sup condition is satisfied for z^{**} and any $z \in \mathcal{N}(z^{**}, R)$.

In order to proceed with the second part of the LBB condition, another supporting Lemma is required. Starting at a feasible point (L, ξ) , we are only interested in the subspace tangential to the constraints, i.e., in directions $\delta z \in \delta Z$ that satisfy $\delta \xi_\tau^T \xi_\tau = \delta L L$. As discussed in Section 7.1.1, directions $\delta \xi_\tau$ parallel to ξ_τ are not contained in δX_τ . It will now be show that the angle between $\delta \xi_\tau$ and ξ_τ , measured in the L^2 -norm, cannot get arbitrarily small.

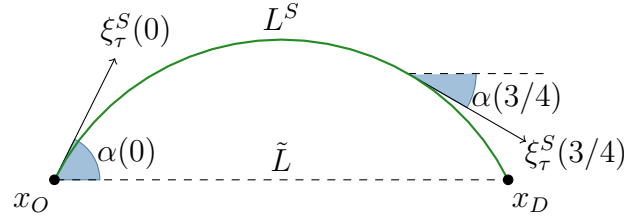


Figure 7.1: Illustration of the maximum angle between the straight line from x_O to x_D and the ground speed vector ξ_τ .

Lemma 7.2. — Let $\xi \in X$ be a feasible point of (5.6), i.e., $\|\xi_\tau\| = L$ f.a.a. $\tau \in (0, 1)$. Moreover, define $\tilde{L} := \|x_D - x_O\|$. Then it holds that

$$\|\delta\xi_\tau^\top \xi_\tau\|_{L^2(0,1)}^2 \leq \frac{(L/\tilde{L})^4}{(L/\tilde{L})^2 + 1} \tilde{L}^2 \|\delta\xi_\tau\|_{L^2(0,1)}^2 \quad (7.6)$$

for any $\delta z \in \delta Z$ such that $\delta\xi_\tau^\top \xi_\tau = \delta L L$.

Proof. With respect to the flight direction ξ_τ a direction $\delta\xi_\tau$ can be divided into a tangential component $\delta\xi_\tau^\parallel = a(\tau)\xi_\tau$ with $a(\tau) : (0, 1) \mapsto \mathbb{R}$ and a perpendicular component $\delta\xi_\tau^\perp$ with $\xi_\tau^\top \delta\xi_\tau^\perp = 0$, such that $\delta\xi_\tau = \delta\xi_\tau^\perp + \delta\xi_\tau^\parallel$. From $\delta\xi_\tau^\top \xi_\tau = \delta L L$ immediately follows that

$$\begin{aligned} L\delta L &= \xi_\tau^\top \delta\xi_\tau = \xi_\tau^\top (\delta\xi_\tau^\perp + \delta\xi_\tau^\parallel) = \xi_\tau^\top \delta\xi_\tau^\parallel = a\xi_\tau^\top \xi_\tau \stackrel{(5.6)}{=} aL^2 \\ \Rightarrow a(\tau) &= \frac{\delta L}{L} = \text{const.} \end{aligned}$$

Hence,

$$\delta\xi_\tau^\parallel = \frac{\delta L}{L} \xi_\tau \quad (7.7)$$

$$\Rightarrow \|\delta\xi_\tau^\parallel\|_{L^2(0,1)}^2 = \int_0^1 \|\delta\xi_\tau^\parallel\|^2 d\tau \stackrel{(7.7)}{=} \frac{\delta L^2}{L^2} \int_0^1 \|\xi_\tau\|^2 d\tau \stackrel{(5.8)}{=} \delta L^2. \quad (7.8)$$

For any $\delta\xi \in \delta X$ it holds that $0 \stackrel{(5.9)}{=} \int \delta\xi_\tau d\tau = \int \delta\xi_\tau^\perp d\tau + \int \delta\xi_\tau^\parallel d\tau$, which yields

$$\begin{aligned}
\int_0^1 \|\delta\xi_\tau^\perp\|^2 d\tau &\geq \left(\left\| \int_0^1 \delta\xi_\tau^\perp d\tau \right\| \right)^2 \\
&= \left(\left\| \int_0^1 \delta\xi_\tau^\parallel d\tau \right\| \right)^2 \\
&\stackrel{(7.7)}{=} \frac{\delta L^2}{L^2} \left(\left\| \int_0^1 \xi_\tau d\tau \right\| \right)^2 \\
&= \frac{\tilde{L}^2}{L^2} \delta L^2 \\
&\stackrel{(7.8)}{=} \frac{\tilde{L}^2}{L^2} \|\delta\xi_\tau^\parallel\|_{L^2(0,1)}^2,
\end{aligned} \tag{7.9}$$

since $\|\delta\xi_\tau^\parallel\|_{L^2(0,1)}^2 = \int_0^1 \|\delta\xi_\tau^\parallel\|^2 d\tau = \delta L^2$. Due to the orthogonality of $\delta\xi_\tau^\parallel$ and $\delta\xi_\tau^\perp$, the Pythagorean equation $\|\delta\xi_\tau\|^2 = \|\delta\xi_\tau^\perp\|^2 + \|\delta\xi_\tau^\parallel\|^2$ holds, which leads to

$$\begin{aligned}
\|\delta\xi_\tau^\parallel\|_{L^2(0,1)}^2 &= \|\delta\xi_\tau\|_{L^2(0,1)}^2 - \|\delta\xi_\tau^\perp\|_{L^2(0,1)}^2 \\
&\stackrel{(7.9)}{\leq} \|\delta\xi_\tau\|_{L^2(0,1)}^2 - \frac{\tilde{L}^2}{L^2} \|\delta\xi_\tau^\parallel\|_{L^2(0,1)}^2 \\
&\leq \frac{L^2}{L^2 + \tilde{L}^2} \|\delta\xi_\tau\|_{L^2(0,1)}^2.
\end{aligned} \tag{7.10}$$

With this, everything is in place to prove the claim

$$\begin{aligned}
\|\delta\xi_\tau^\top \xi_\tau\|_{L^2(0,1)}^2 &= \int_0^1 (\delta\xi_\tau^\top \xi_\tau)^2 d\tau \\
&= \int_0^1 (\xi_\tau^\top \delta\xi_\tau^\parallel)^2 d\tau \\
&\stackrel{(5.6)}{=} L^2 \int_0^1 \|\delta\xi_\tau^\parallel\|^2 d\tau \\
&\stackrel{(7.10)}{\leq} \frac{L^4}{L^2 + \tilde{L}^2} \|\delta\xi_\tau\|_{L^2(0,1)}^2.
\end{aligned}$$

□

As a first step on the way to a lower bound for T'' a general lower bound for the second directional derivative of f is provided in the following Lemma.

Lemma 7.3. — *Let $\|w\|_{L^\infty(\Omega)} \leq \bar{c}_0$, $\|w_x\|_{L^\infty(\Omega)} \leq \bar{c}_1$, and $\|w_{xx}\|_{L^\infty(\Omega)} \leq \bar{c}_2$ and define $\underline{v}^2 := \bar{v}^2 - \bar{c}_0^2$ as well as $\bar{\bar{v}}^2 := \bar{v}^2 + \bar{c}_0^2$. Then, for any $z \in Z$, the second*

directional derivative of f as defined in (5.3) is bounded from below by

$$\begin{aligned} f(\xi, \xi_\tau)''[\delta\xi, \delta\xi_\tau]^2 &\geq -\underline{\beta}_0 \frac{\|\xi_\tau\| \|\delta\xi\|^2}{\bar{v} \tilde{L}^2} - \underline{\beta}_1 \frac{\|\delta\xi\| \|\delta\xi_\tau\|}{\tilde{L} \bar{v}} + \underline{\beta}_2 \frac{\|\delta\xi_\tau\|^2}{\bar{v} \|\xi_\tau\|} \\ &\quad - \underline{\beta}_3 \frac{\|\delta\xi_\tau\| |\xi_\tau^T \delta\xi_\tau|}{\bar{v} \|\xi_\tau\|^2} - \underline{\beta}_4 \frac{(\xi_\tau^T \delta\xi_\tau)^2}{\bar{v} \|\xi_\tau\|^3}, \end{aligned} \quad (7.11)$$

where $\beta_i \in \mathbb{R}^+$, $i \in 0 \dots 4$, with

$$\begin{aligned} \underline{\beta}_0 &= \tilde{L}^2 \bar{v} \left[\frac{\bar{c}_1^2}{\bar{v}^3} \left(8 \frac{\bar{c}_0^3}{\bar{v}^3} + 12 \frac{\bar{c}_0^2}{\bar{v}^2} + 6 \frac{\bar{c}_0}{\bar{v}} + 1 \right) \right. \\ &\quad \left. + \frac{\bar{c}_2}{\bar{v}^2} \left(2 \frac{\bar{c}_0^2}{\bar{v}^2} + 2 \frac{\bar{v} \bar{c}_0}{\bar{v}^2} + 2 \frac{\bar{c}_0}{\bar{v}} + 1 \right) \right], \end{aligned} \quad (7.12a)$$

$$\underline{\beta}_1 = \frac{\tilde{L} \bar{v} \bar{c}_1}{\bar{v}^2} \left(8 \frac{\bar{c}_0^3}{\bar{v}^3} + 4 \frac{\bar{c}_0^2}{\bar{v}^2} + 8 \frac{\bar{c}_0}{\bar{v}} + 2 \right), \quad (7.12b)$$

$$\underline{\beta}_2 = \frac{\bar{v}}{\bar{v}} \left(\frac{\bar{v}}{\bar{v}} - \frac{\bar{c}_0^4}{\bar{v}^4} \right), \quad (7.12c)$$

$$\underline{\beta}_3 = \frac{2 \bar{v} \bar{c}_0^2}{\bar{v}^3}, \quad (7.12d)$$

$$\underline{\beta}_4 = \frac{\bar{v}}{\bar{v}}. \quad (7.12e)$$

Proof. As outlined in the Appendix of Chapter 5, f , as defined in (5.3), consists of two terms, the tailwind term

$$f_1 = -\frac{\xi_\tau^T w}{g}, \quad \text{with} \quad (7.13)$$

$$g = \bar{v}^2 - w^T w, \quad (7.14)$$

and the length term

$$f_2 = g^{-1} \left((\xi_\tau^T w)^2 + g(\xi_\tau^T \xi_\tau) \right)^{1/2}. \quad (7.15)$$

Consequently, we obtain f'' by adding f_1'' and f_2'' from (5.63) and (5.80) as

$$\begin{aligned}
f''(\xi, \xi_\tau)[\delta\xi, \delta\xi_\tau]^2 &= (f_1'' + f_2'')[\delta\xi, \delta\xi_\tau]^2 \\
&= -2g^{-3}(g'\delta\xi)^2(\xi_\tau^\top w) && + g^{-2}(\delta\xi^\top g''\delta\xi)(\xi_\tau^\top w) \\
&\quad + 2g^{-2}(g'\delta\xi)(\xi_\tau^\top w_x\delta\xi) && - g^{-1}w_{xx}[\xi_\tau, \delta\xi, \delta\xi] \\
&\quad + 2g^{-2}(g'\delta\xi)(\delta\xi_\tau^\top w) && - 2g^{-1}(\delta\xi_\tau^\top w_x\delta\xi), \\
&\quad + 2g^{-3}(g'\delta\xi)^2 F^{1/2} && - g^{-2}(\delta\xi^\top g''\delta\xi)F^{1/2} \\
&\quad - g^{-2}(g'\delta\xi)F^{-1/2}F'[\delta\xi, \delta\xi_\tau] && + \frac{1}{2}g^{-1}F^{-1/2}F''[\delta\xi, \delta\xi_\tau]^2 \\
&\quad - \frac{1}{4}g^{-1}F^{-3/2}(F'[\delta\xi, \delta\xi_\tau])^2.
\end{aligned}$$

Using the previously derived bounds for g and F , as well as their derivatives, yields the claimed lower bound

$$\begin{aligned}
f(\xi, \xi_\tau)''[\delta\xi, \delta\xi_\tau]^2 &\geq -\left[\frac{\bar{c}_1^2}{\underline{v}^3}\left(8\frac{\bar{c}_0^3}{\underline{v}^3} + 12\frac{\bar{c}_0^2}{\underline{v}^2} + 6\frac{\bar{c}_0}{\underline{v}} + 1\right)\right. \\
&\quad \left. + \frac{\bar{c}_2}{\underline{v}^2}\left(2\frac{\bar{c}_0^2}{\underline{v}^2} + 2\frac{\bar{v}\bar{c}_0}{\underline{v}^2} + 2\frac{\bar{c}_0}{\underline{v}} + 1\right)\right]\|\xi_\tau\|\|\delta\xi\|^2 \\
&\quad - \frac{\bar{c}_1}{\underline{v}^2}\left(8\frac{\bar{c}_0^3}{\underline{v}^3} + 4\frac{\bar{c}_0^2}{\underline{v}^2} + 8\frac{\bar{c}_0}{\underline{v}} + 2\right)\|\delta\xi\|\|\delta\xi_\tau\| \\
&\quad + \frac{1}{\|\xi_\tau\|}\left(\frac{1}{\bar{v}} - \frac{\bar{c}_0^4}{\underline{v}^5}\right)\|\delta\xi_\tau\|^2 \\
&\quad - 2\frac{\bar{c}_0^2}{\underline{v}^3\|\xi_\tau\|^2}\|\delta\xi_\tau\|\|\xi_\tau^\top\delta\xi_\tau\| \\
&\quad - \frac{1}{\underline{v}\|\xi_\tau\|^3}(\xi_\tau^\top\delta\xi_\tau)^2.
\end{aligned}$$

□

This directly leads to the following theorem.

Theorem 7.4. — *Let (L^{**}, ξ^{**}) be a global minimizer of (5.6). Moreover, let the wind speed be bounded as usual with sufficiently small $\bar{c}_0, \bar{c}_1, \bar{c}_2$. Then there is a $\underline{\mathcal{B}} > 0$ such that*

$$T''(\xi^{**})[\delta\xi, \delta\xi_\tau]^2 \geq \underline{\mathcal{B}}\|\delta z\|_{Z^2}^2 \quad (7.16)$$

for any $\delta z \in \delta Z$ such that $\delta\xi_\tau^\top \xi_\tau^{**} = \delta L L^{**}$.

Proof. It was shown in Lemma 5.3, that an optimal trajectory cannot be arbitrarily longer than the straight connection. More precisely,

$$\tilde{L} \leq L^{**} \leq \frac{\bar{v} + \bar{c}_0}{\bar{v} - \bar{c}_0} \tilde{L} \quad (7.17)$$

with $\tilde{L} := \|x_D - x_O\|$. Further, the proof involves a few bounds regarding components of δz . Wirtinger's inequality is one of them (refer to Theorem 5.5);

$$\|\delta\xi\|_{L^2(0,1)}^2 \leq \frac{1}{\pi} \|\delta\xi_\tau\|_{L^2(0,1)}^2. \quad (7.18)$$

Since $\delta\xi_\tau^T \xi_\tau^{**} = \delta L L^{**}$, it holds that

$$|\delta L| \leq \int_0^1 \frac{\|\delta\xi_\tau\|_{L^{**}}}{L^{**}} d\tau \leq \|\delta\xi_\tau\|_{L^2(0,1)}. \quad (7.19)$$

Using the two bounds above, it follows that the magnitudes of the components of δz are inherently linked and can be represented by one of them;

$$\|\delta z\|_{Z^2}^2 \stackrel{(5.12b)}{=} \|\delta\xi\|_{L^2(0,1)}^2 + \|\delta\xi_\tau\|_{L^2(0,1)}^2 + \delta L^2 \stackrel{\substack{(5.31) \\ (7.19)}}{\leq} \frac{2\pi + 1}{\pi} \|\delta\xi_\tau\|_{L^2(0,1)}^2. \quad (7.20)$$

Finally, the proof is completed combining the definition of T from (5.2), the bounds

from Lemmas 7.2 and 7.3, and Young's inequality;

$$\begin{aligned}
T''(\xi^{**})[\delta\xi, \delta\xi_\tau]^2 &\stackrel{(5.2)}{=} \int_0^1 f''(\xi^{**}, \xi_\tau^{**})[\delta\xi, \delta\xi_\tau]^2 d\tau \\
&\stackrel{(7.11)}{=} \int_0^1 -\underline{\beta}_0 \frac{L^{**}}{\bar{v}} \frac{\|\delta\xi\|^2}{\tilde{L}^2} - \underline{\beta}_1 \frac{\|\delta\xi\| \|\delta\xi_\tau\|}{\tilde{L} \bar{v}} + \underline{\beta}_2 \frac{\|\delta\xi_\tau\|^2}{\bar{v} L^{**}} \\
&\quad - \underline{\beta}_3 \frac{\|\delta\xi_\tau\| |\delta\xi_\tau^\top \xi_\tau^{**}|}{\bar{v} (L^{**})^2} - \underline{\beta}_4 \frac{(\delta\xi_\tau^\top \xi_\tau^{**})^2}{\bar{v} (L^{**})^3} d\tau \\
&\stackrel{(Y)}{\geq} \int_0^1 \left(-\underline{\beta}_0 \frac{L^{**}}{\bar{v}} - \frac{\underline{\beta}_1}{2} \right) \frac{\|\delta\xi\|^2}{\tilde{L}^2} + \left(-\frac{\underline{\beta}_1}{2} + \underline{\beta}_2 \frac{\bar{v}}{L^{**}} - \frac{\underline{\beta}_3}{2} \right) \frac{\|\delta\xi_\tau\|^2}{\bar{v}^2} \\
&\quad - \left(\underline{\beta}_3 \frac{\bar{v}}{2L^{**}} + \underline{\beta}_4 \right) \frac{(\delta\xi_\tau^\top \xi_\tau^{**})^2}{\bar{v} (L^{**})^3} d\tau \\
&\stackrel{(7.6)}{\geq} \left[-\frac{\bar{v} L^{**}}{\pi \tilde{L}^2} \underline{\beta}_0 - \left(\frac{\bar{v}^2}{\pi \tilde{L}^2} + 1 \right) \frac{\underline{\beta}_1}{2} + \frac{\bar{v}}{L^{**}} \underline{\beta}_2 \right. \\
&\quad \left. - \left(1 + \frac{\bar{v}^2 / \tilde{L}^2}{(L^{**} / \tilde{L})^2 + 1} \right) \frac{\underline{\beta}_3}{2} - \frac{\bar{v} L^{**} / \tilde{L}^2}{(L^{**} / \tilde{L})^2 + 1} \underline{\beta}_4 \right] \frac{\|\delta\xi_\tau\|_{L^2(0,1)}^2}{\bar{v}^2} \\
&\stackrel{(5.28)}{\geq} \frac{\pi}{2\pi + 1} \left[-\frac{\bar{v} + \bar{c}_0}{\bar{v} - \bar{c}_0} \frac{\bar{v}}{\pi \tilde{L}} \underline{\beta}_0 - \left(\frac{\bar{v}^2}{\pi \tilde{L}^2} + 1 \right) \frac{\underline{\beta}_1}{2} + \frac{\bar{v} - \bar{c}_0}{\bar{v} + \bar{c}_0} \frac{\bar{v}}{\tilde{L}} \underline{\beta}_2 \right. \\
&\quad \left. - \left(1 + \frac{\bar{v}^2}{2\tilde{L}^2} \right) \frac{\underline{\beta}_3}{2} - \frac{\bar{v} + \bar{c}_0}{\bar{v} - \bar{c}_0} \frac{\bar{v}}{2\tilde{L}} \underline{\beta}_4 \right] \frac{\|\delta z\|_{Z^2}^2}{\bar{v}^2}.
\end{aligned}$$

Due to $\underline{\beta}_0, \dots, \underline{\beta}_4 \geq 0$ as given in (7.12), the bracket contains only one positive term. Further inspection reveals that every term is monotonically decreasing in $\bar{c}_0, \bar{c}_1, \bar{c}_2$. Since for $\bar{c}_0, \bar{c}_1, \bar{c}_2 = 0$ the bracket reduces to

$$\left[0 + 0 + \frac{\bar{v}}{\tilde{L}} + 0 - \frac{\bar{v}}{2\tilde{L}} \right] = \frac{\bar{v}}{2\tilde{L}} > 0,$$

it holds that

$$T''(\xi^{**})[\delta\xi, \delta\xi_\tau]^2 \geq \underline{\mathcal{B}} \|\delta z\|_{Z^2}^2$$

with $\underline{\mathcal{B}} > 0$ for sufficiently mild wind (small $\bar{c}_0, \bar{c}_1, \bar{c}_2$). \square

Thorough analysis of the lower bound at a global minimizer (L^{**}, ξ^{**}) revealed that the second derivative of the objective functional T'' is indeed strictly positive definite on the kernel of the constraints, given that the wind is sufficiently mild

along the trajectory. Furthermore, this characteristic extends to the Hessian of the Lagrangian because the constraint is locally bounded (refer to Theorem 5.9).

Given that the inf-sup condition is also satisfied, we can deduce that the minimizer is isolated. Consequently, the DisCOptER algorithm developed in this work can be effectively employed to determine this global minimizer.

7.2 Efficiently Harvesting the Benefits of Free Flight

In this section we present a comprehensive comparison between graph-based routing and our DisCOptER algorithm for solving the Free Flight Trajectory Optimization Problem under conditions closely resembling real-world scenarios. Specifically, we explore routing between European capital airports while considering realistic wind conditions on a spherical Earth.

Our investigation yields two significant findings. Firstly, the DisCOptER algorithm demonstrates exceptional performance, successfully identifying the globally optimal route without requiring the fallback strategy of iterating through multiple shortest paths.

Secondly, we demonstrate that the efficiency of graph-based routing can be substantially improved by focusing on high angular resolution during the graph construction. Unsurprisingly, increasing the resolution of the underlying graph leads to convergence of the corresponding discrete shortest path towards the continuous solution provided by the DisCOptER algorithm. Importantly, however, the proposed method improves the convergence rate compared to the naive approach of constructing a locally complete graph.

Throughout the study, we model the Earth as a perfect sphere with a radius of 6,371 kilometers. Geographical spherical coordinates will be represented in the format (λ, ϕ) , where $\lambda \in]-180^\circ, 180^\circ]$ denotes the longitude and $\phi \in [-90^\circ, 90^\circ]$ represents the latitude in degrees. Additionally, all angular measures are assumed to be in degrees, and trigonometric functions are applied accordingly.

7.2.1 Graph-Based Routing

EUROCONTROL frequently publishes the *"Free Route Airspace (FRA) points list for the European Civil Aviation Conference (ECAC) and neighbouring States"*¹. Utilizing this data for planar routing, we ignore the fact that many waypoints are

¹<https://www.eurocontrol.int/publication/free-route-airspace-fra-points-list-ecac-area>

As discussed in the introduction (refer to Section 1.4.1), the angular resolution provided by the graph significantly influences the solution quality. This motivates the construction of a locally dense digraph with predefined angular resolution. For each waypoint, we divide its surroundings into n_a equisized sections. Within each section, we create an arc from the given waypoint to the nearest waypoint in that section, as illustrated in Figure 7.3. If no waypoint lies within a particular section, no arc is created. This approach ensures that each waypoint has at most (and most of the time, exactly) n_a outgoing arcs.

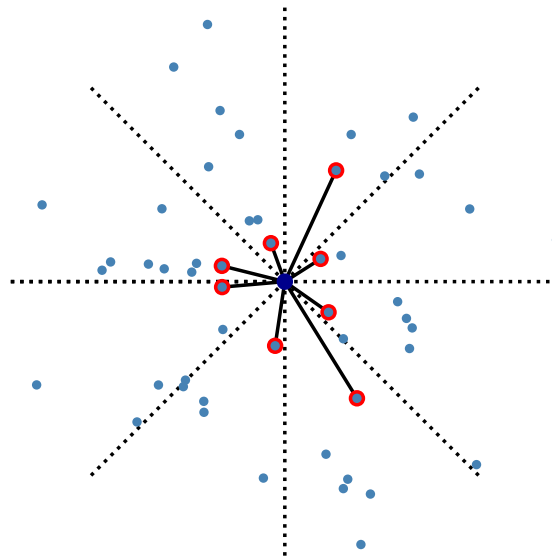


Figure 7.3: The considered waypoint is in the center. $n_a = 8$ successor nodes are determined by considering the closest waypoint in each of the n_a sectors (red nodes).

It is well known that alternative approaches to Dijkstra’s algorithm, such as the A* method, are more efficient for calculating the shortest path on a given digraph (refer to Section 1.4.1). However, achieving consistent and comparable results with the DisCOptER method necessitates precise computation of arc costs, which in turn incurs significant computational overhead. In fact, the effort required for the graph creation exceeds the query time for finding the shortest path by far, rendering the choice of the algorithm little impactful.

Moreover, it is essential to acknowledge that the comparability between the method outlined above and real-world routing is inherently limited for two primary reasons. Firstly, the Free Flight Trajectory Optimization Problem, as introduced

in Section 1.3, already incorporates several simplifications, which were discussed in detail in Section 1.2. Secondly, the challenge lies in the scarcity of precise and publicly available data regarding the current status of free routing airspaces. This dearth of information makes it challenging to construct a truly realistic representation for evaluation purposes.

7.2.2 DisCOptER

The DisCOptER method developed in this work consists of two steps. Firstly, a coarse path is calculated as the shortest path on a specifically designed graph. Subsequently, this path serves as initial guess for a refinement stage, in which a continuous trajectory is generated using the ordinary Newton-KKT method with a direct collocation approach.

For this study, we construct a "rectangular" graph with a node spacing of $h = \lceil d(x_O, x_D)/3^\circ \rceil$ on the great circle segment between departure and destination airport (one node per 3° of distance or about 333 km), where $d : \mathbb{R}^2 \times \mathbb{R}^2 \mapsto [0^\circ, 180^\circ]$ is the great circle distance,

$$d(x_1, x_2) = 2 \arccos(\sin \phi_1 \sin \phi_2 + \cos \phi_1 \cos \phi_2 \cos(\lambda_2 - \lambda_1)). \quad (7.21)$$

Additionally, for each node position, 9 nodes are placed along the perpendicular great circle segment, covering a range of $\pm 4^\circ$ ($\approx \pm 444$ km). Any two nodes within a great circle distance of at most $9h/4$ are connected by arcs in both directions (roughly 2 neighboring nodes in each direction). Depending on the distance from origin to destination, the resulting graph contains 36–117 nodes with on average 16–22 outgoing arcs per node.

In the direct collocation approach we use a discretization of 50 equidistant time steps. An illustration of this method for two exemplary flights is presented in Figure 7.6.

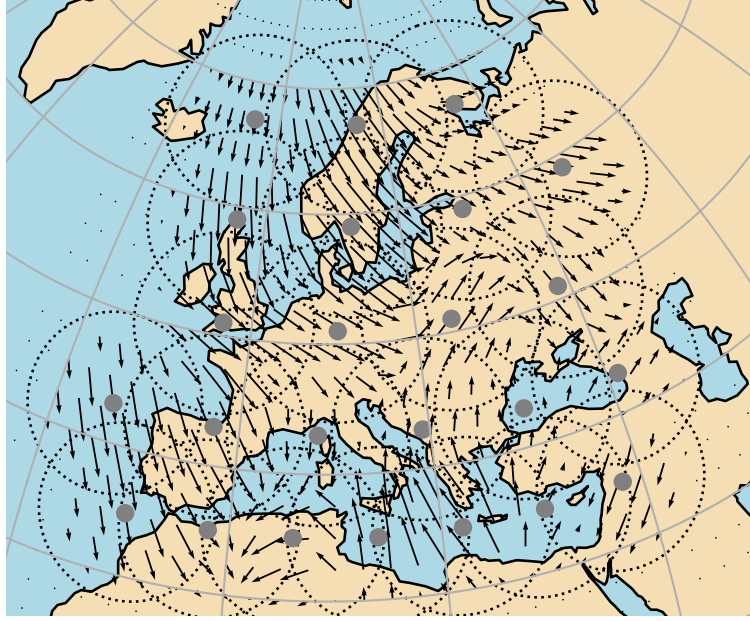


Figure 7.4: Illustration of the wind conditions. The dots and dashed lines illustrate the underlying radial basis functions.

7.2.3 Wind Conditions

The wind field used for this investigation is described by 24 basis functions with a compact support, each of which is characterized by the spherical coordinates of its center $c_i = [\lambda_i, \phi_i]^T \in \mathbb{R}^2$, its weight vector $[\eta_i, \nu_i]^T \in \mathbb{R}^2$ independently defining the longitudinal and latitudinal wind speed components, and its radius $R_i \in \mathbb{R}^+$ which is uniformly set to 7° . Center coordinates and weights are given in Table 7.1. Figure 7.4 illustrates this wind field. Formally, the wind at a point x is obtained as

$$w(x) = \bar{w} \sum_i f\left(\frac{d(x, c_i)}{R_i}\right) \begin{bmatrix} \eta_i \\ \nu_i \end{bmatrix}, \quad (7.22)$$

where $f : \mathbb{R}^+ \mapsto [0, 1]$ is the underlying radial basis function given as

$$f(r) = \begin{cases} \exp\left(-\frac{r^2}{1-r^2}\right) & \text{if } r < 1, \\ 0 & \text{otherwise.} \end{cases} \quad (7.23)$$

With the parameters detailed below in Table 7.1, the wind speed is bounded with $\|w\|_{L^\infty} \leq \bar{w} = 0.3\bar{v}$, where \bar{v} denotes the airspeed. Since we analyze only relative improvements in this investigation, absolute values are not relevant, but with an airspeed of $\bar{v} = 800$ km/h this translates to a maximum wind speed of 240 km/h.

7.2.4 Origin-Destination Pairs

As detailed in Table 7.2, 27 European capital airports were considered in this analysis, excluding peripheral regions such as the Canary Islands or Iceland. These are either not or insufficiently covered by the FRA waypoints, such that their inclusion would certainly introduce significant bias into the results.

Considering flight connections between every pair of airports with a great circle distance of at least 1,000 kilometers in both directions, we have compiled a list comprising exactly $n_c = 500$ connections. The distribution of these distances is presented in Figure 7.5.

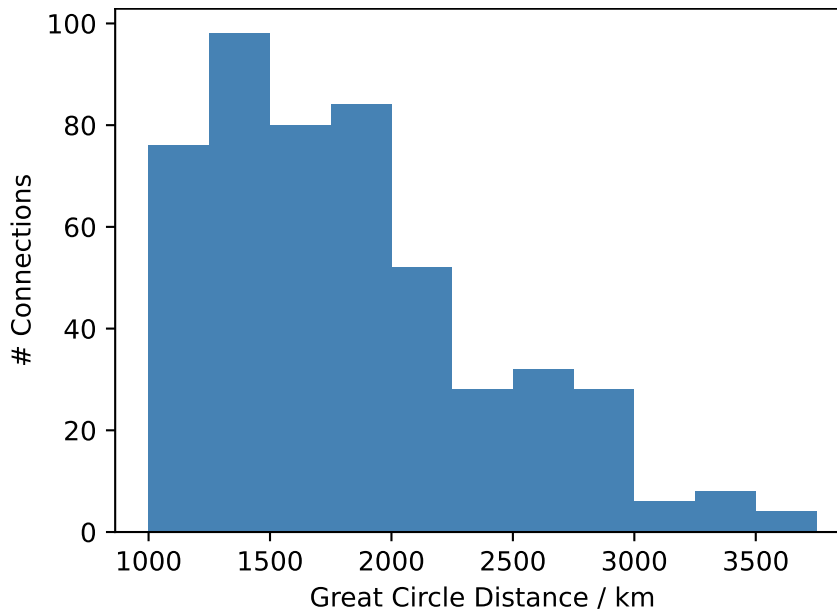


Figure 7.5: Distribution of the great circle distance in the set of 500 connections.

7.2.5 Results

For each of the 500 connections, we employ two distinct methods to calculate trajectories.

Firstly, we compute the shortest path on a locally connected directed graph with specified angular resolution, as detailed above in Section 7.2.1.

Secondly, we utilize the DisCOptER algorithm, introduced in this work, configured with parameters outlined before in Section 7.2.2.

Two exemplary instances of this process are depicted in Figure 7.6. Blue dots represent the FRA waypoints, and the blue path signifies the shortest path on the constructed graph. Orange dots represent the nodes generated during the discrete stage of the DisCOptER algorithm, and the orange path represents the corresponding shortest path, which serves as an initial guess for the subsequent nonlinear optimization stage. The continuous trajectory obtained through this process is depicted in green.

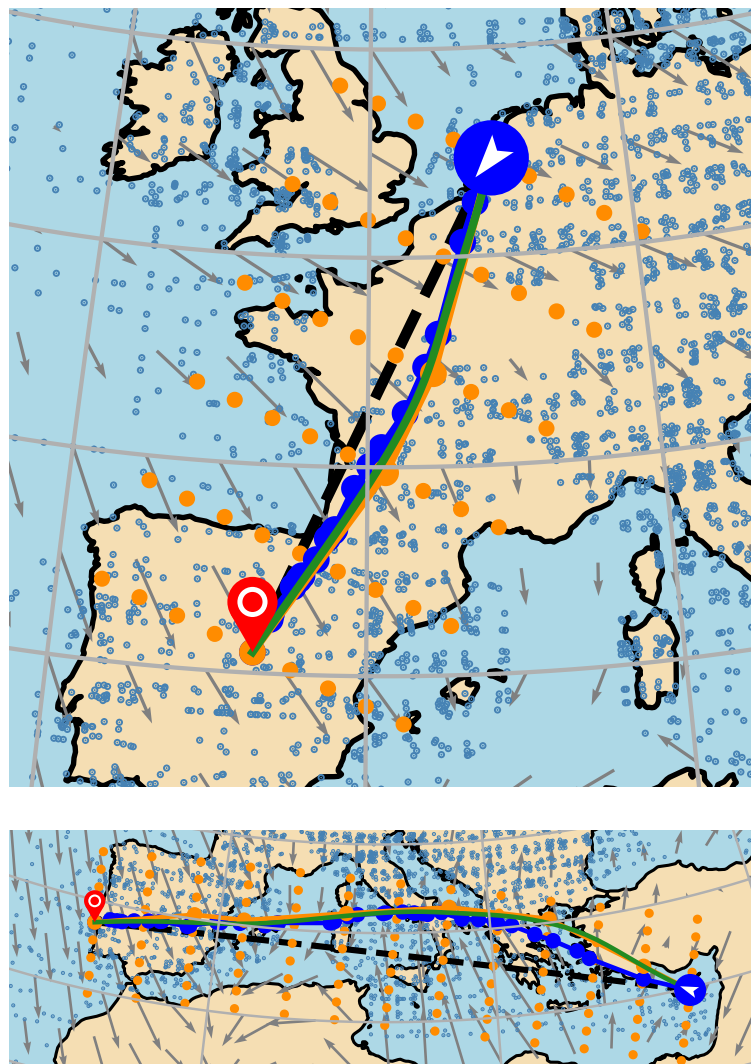


Figure 7.6: Exemplary flights. Top: AMS (Amsterdam Airport Schiphol, Netherlands) to MAD (Adolfo Suárez Madrid-Barajas Airport, Spain). Bottom: LCA (Larnaca International Airport, Cyprus) to LIS (Humberto Delgado Airport, Portugal). Black dashed line: great circle segment, blue route: graph-based path, orange: nodes used by the DisCOptER algorithm and corresponding shortest path, green: refined trajectory found with the DisCOptER algorithm (globally optimal).

The evaluation revealed that the DisCOptER algorithm consistently identifies the globally optimal solution across all instances without resorting to iterating through multiple shortest paths; even though the utilized graph is very sparse. Furthermore, this achievement is typically accomplished with a maximum of 4 Newton steps, while 93% of all instances required not more than 2 steps.

In the graph-based approach, the quality of the solution is directly linked to the angular resolution. Let $T_{G,i}(n_a)$ denote the travel time on the shortest path in a graph with angular resolution defined by n_a for flight i . Moreover, let T_i^{**} be the globally minimal travel time for this instance. Then,

$$\epsilon_{G,i}(n_a) := \frac{T_{G,i}(n_a)}{T_i^{**}} - 1 \quad (7.24)$$

denotes the relative gap for flight i between the shortest path and the global optimum concerning the overall travel time. Figure 7.7 illustrates this gap for all instances and various values of n_a .

Clearly, a low angular resolution, such as $n_a = 9$, results in significantly suboptimal routes with a gap of up to 10%. Conversely, increasing the angular resolution rapidly enhances the results. With $n_a = 36$, all routes are within 2% of the global optimum, and 87% are within 0.5%.

In Section 2.2.3 and especially in Chapter 3 the efficiency of routing on locally dense graphs was investigated. In contrast to the present case, it was assumed that each node was connected to every other nodes within a certain connectivity radius ℓ . It was shown that the approximation error of such graphs scales quadratically with the inverse of the connectivity radius and impacts the travel time on the resulting shortest path again quadratically. Hence, with $T_{D,i}(\ell)$ denoting the travel time on the shortest path on a locally densely connected digraph with connectivity radius ℓ , it holds that

$$\epsilon_{D,i}(\ell) = \frac{T_{D,i}(\ell)}{T_i^{**}} - 1 \in \mathcal{O}(\ell^{-4}). \quad (7.25)$$

Moreover, it is important to note that, on a fixed set of nodes, the computational effort of Dijkstra's algorithm, C_D , scales linearly with the number of arcs n_a , which,

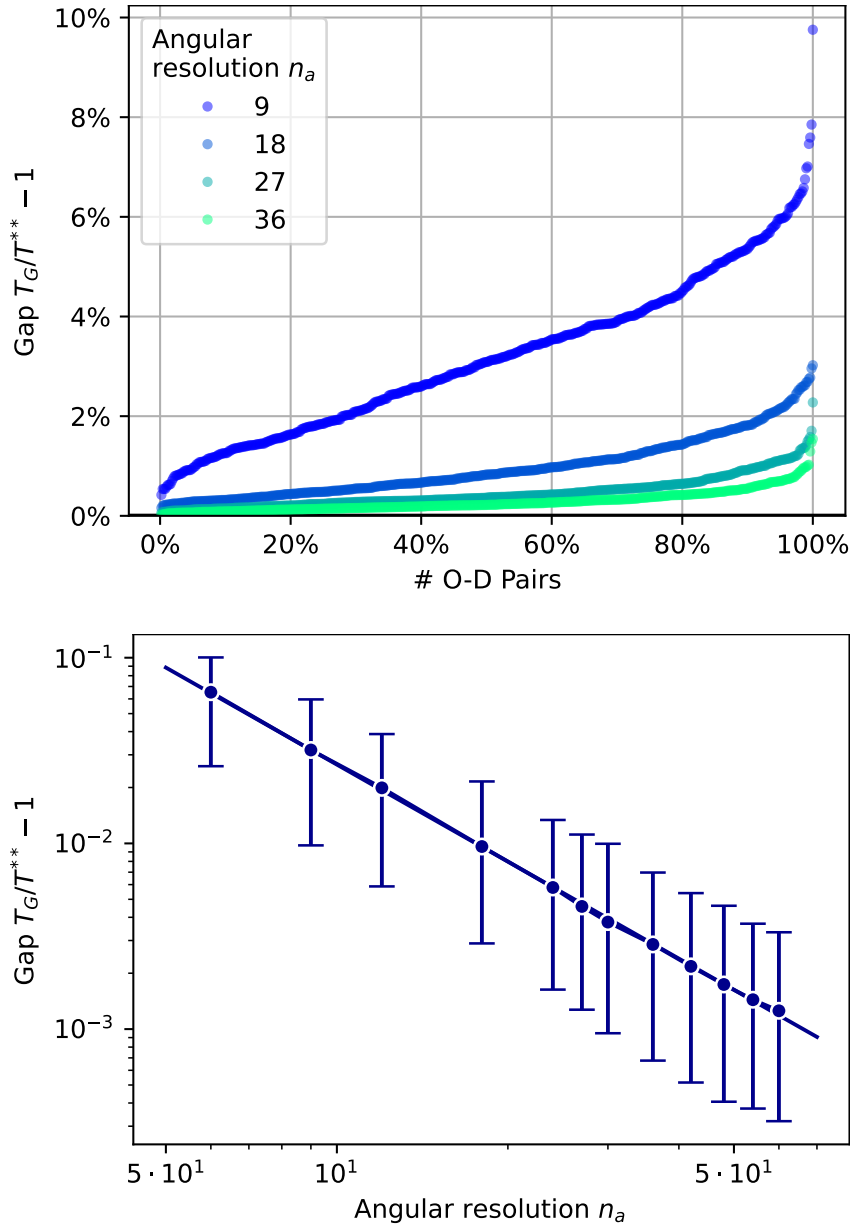


Figure 7.7: Relative difference of the travel time on the best graph-based route compared to the global optimum. Top: sorted results for the set of 500 flights. Bottom: mean gap for various angular resolution and fitted regression line, given in (7.27). Error bars indicate the 5% and 95% percentiles, respectively.

in turn, scales quadratically with the connectivity radius ℓ . Therefore,

$$C_D \in \mathcal{O}(\epsilon^{-1/2}). \quad (7.26)$$

The bottom image of Figure 7.7 demonstrates that the presented method of creating a graph with defined angular resolution improves upon this. It can be

clearly seen that the mean gap

$$\bar{\epsilon}_G(n_a) = \frac{1}{n_c} \sum_i \epsilon_{G,i}(n_a)$$

scales more favorably than quadratically with the inverse angular resolution,

$$\bar{\epsilon}_G(n_a) \approx 0.37 n_a^{-1.74}. \quad (7.27)$$

Following the same argument as above, this leads to a computational effort of

$$C_G \in \mathcal{O}(\epsilon^{-1/1.74}), \quad (7.28)$$

making the proposed method efficient for constructing a trajectory-oriented graph, based on provided waypoints.

7.2.6 Supplementary Material

Below, the parameters that define the wind field can be found in Table 7.1. Additionally, Table 7.2 provides a list of the airports considered in this study.

Center coordinates		Weights	
$\lambda / ^\circ$	$\phi / ^\circ$	η	ν
-10.00	35.00	-0.136	0.063
-13.75	43.00	-0.204	0.133
-2.00	35.00	-0.061	0.095
-2.75	43.00	-0.150	0.129
-3.50	51.00	-0.069	0.194
-4.25	59.00	-0.179	0.076
-5.00	67.00	-0.105	0.016
6.00	35.00	-0.071	-0.160
8.25	43.00	-0.086	-0.008
10.50	51.00	-0.057	0.160
12.75	59.00	-0.123	0.210
15.00	67.00	-0.125	0.166
14.00	35.00	0.210	-0.007
19.25	43.00	0.097	0.031
24.50	51.00	0.074	0.123
29.75	59.00	-0.048	0.081
35.00	67.00	-0.006	0.068
22.00	35.00	0.187	-0.126
30.25	43.00	0.060	0.007
38.50	51.00	-0.111	0.063
46.75	59.00	-0.050	0.127
30.00	35.00	0.080	0.080
41.25	43.00	0.039	0.089
38.00	35.00	-0.112	-0.111

Table 7.1: Center coordinates and weights of the wind function defined in Section 7.2.3.

IATA Code	Name	$\lambda / ^\circ$	$\phi / ^\circ$
AMS	Amsterdam Airport Schiphol	4.74	52.33
ARN	Stockholm Arlanda Airport	17.94	59.65
ATH	Athens International Airport	23.95	37.94
BER	Berlin-Brandenburg Airport	13.49	52.37
BFS	Belfast International Airport	-6.23	54.65
BUD	Budapest Ferenc Liszt International Airport	19.25	47.44
CDG	Paris Charles de Gaulle Airport	5.88	45.64
CPH	Copenhagen Airport	12.65	55.61
CWL	Cardiff Airport	-3.34	51.40
DUB	Dublin Airport	-6.24	53.43
EDI	Edinburgh Airport	-3.36	55.95
FCO	Leonardo da Vinci-Fiumicino Airport	12.23	41.82
HEL	Helsinki Airport	24.95	60.32
LCA	Larnaca International Airport	33.62	34.87
LHR	Heathrow Airport	-0.46	51.47
LIS	Humberto Delgado Airport	-9.13	38.77
LUX	Luxembourg Airport	6.21	49.63
MAD	Adolfo Suárez Madrid-Barajas Airport	-3.57	40.50
MLA	Malta International Airport	14.49	35.85
OSL	Oslo Airport	11.10	60.20
RIX	Riga International Airport	23.97	56.92
SOF	Sofia International Airport	23.41	42.70
SPU	Split Airport	16.30	43.54
VIE	Vienna International Airport	16.58	48.10
VNO	Vilnius International Airport	25.29	54.63
WAW	Warsaw Chopin Airport	20.97	52.16
ZRH	Zurich Airport	8.55	47.46

Table 7.2: List of considered European capital airports.

7.3 Errata

I would like to express my sincere gratitude to the reviewers of my thesis for their invaluable time and effort in carefully reviewing my work. Their insightful comments, constructive feedback, and rigorous evaluation have undoubtedly contributed to the refinement and improvement of this research. I will thoroughly address each point raised in the subsequent sections.

7.3.1 Notational improvements

In Chapter 5, particularly in Lemma 5.3, we acknowledge the lack of clear differentiation between the domain space Y^2 and its dual space $(Y^2)^*$, which may have caused confusion among readers.

Furthermore, the valuable feedback provided by the reviewer has significantly enhanced the readability of the article. One notable improvement was the reformulation of the constraint in (5.7) in a slightly different manner. While these changes were minor and did not alter the main findings, they notably improved the overall clarity of the manuscript.

In light of these enhancements, we have decided to publish an updated version of the article on arXiv². We believe that these revisions will contribute to a better understanding of the presented research and its implications.

7.3.2 Continuity of the objective function

In Theorem 4.4 it was assumed that the second derivative of the travel time function T was continuous in the neighborhood of a minimizer in $H^1(0, 1)$.

However, it later became evident that this continuity only holds in $W^{1,\infty}(0, 1)$. Despite the seemingly minor difference, this distinction carries intricate implications. While continuity is established solely in the L^∞ -setting, other properties such as the invertibility of the KKT-operator require an L^2 -norm. This problem, commonly referred to as two-norm-discrepancy, has been discussed extensively in Chapter 5.

²R. Borndörfer, F. Danecker, M. Weiser; Newton's Method for Global Free Flight Trajectory Optimization; DOI: 10.48550/arXiv.2302.04748.

Although the continuity of T'' has been assumed, it has never been explicitly stated. This omission will be rectified below.

Lemma 7.5. — *The second total derivative of the travel time function T as given in (5.2) can be given as*

$$T''(\xi)[\delta\xi, \Delta\xi] = \int_0^1 f_1''(\xi(\tau), \xi_\tau(\tau)) + f_2''(\xi(\tau), \xi_\tau(\tau)) d\tau \quad (7.29)$$

with f_1'', f_2'' as defined in (5.62) and (5.79), respectively. For any $0 < \underline{\eta} < \bar{\eta}$, this derivative is continuous for all $\xi \in X$ such that $\underline{\eta} \leq \|\xi_\tau(\tau)\| \leq \bar{\eta}$ for almost all $\tau \in (0, 1)$.

Proof. Analogously to the considerations in Section 5.A it can be shown that there are constants $\tilde{\beta}_1, \tilde{\beta}_2 < \infty$, which depend on the usual global bounds on the wind field, such that

$$\begin{aligned} & |(f_k''(\xi_2, \xi_{\tau,2}) - f_k''(\xi_1, \xi_{\tau,1})) [\Delta\xi, \Delta\xi_\tau][\delta\xi, \delta\xi_\tau]| \\ & \leq \tilde{\beta}_k (\|\xi_2 - \xi_1\| + \|\xi_{\tau,2} - \xi_{\tau,1}\|) (\|\delta\xi\| + \|\delta\xi_\tau\|) (\|\Delta\xi\| + \|\Delta\xi_\tau\|) \end{aligned}$$

for $k \in \{1, 2\}$. Using these bounds, it can easily be shown that

$$\begin{aligned} & |T''(\xi_2)[\delta\xi, \Delta\xi] - T''(\xi_1)[\delta\xi, \Delta\xi]| \\ & \leq \left| \int_0^1 (f_1''(\xi_2(\tau), \xi_{\tau,2}(\tau)) - f_1''(\xi_1(\tau), \xi_{\tau,1}(\tau))) [\Delta\xi, \Delta\xi_\tau][\delta\xi, \delta\xi_\tau] d\tau \right| \\ & \quad + \left| \int_0^1 (f_2''(\xi_2(\tau), \xi_{\tau,2}(\tau)) - f_2''(\xi_1(\tau), \xi_{\tau,1}(\tau))) [\Delta\xi, \Delta\xi_\tau][\delta\xi, \delta\xi_\tau] d\tau \right| \\ & \leq \tilde{\mathcal{B}} \|\delta\xi\|_{C^{0,1}(0,1)} \|\Delta\xi\|_{C^{0,1}(0,1)} \|\xi_2 - \xi_1\|_{C^{0,1}(0,1)}, \end{aligned}$$

with $\tilde{\mathcal{B}} = \tilde{\beta}_1 + \tilde{\beta}_2$ which proves the claim. \square

It is important to note, that continuity of T'' is only required in a \mathcal{L}^∞ neighborhood of a minimizer. Under these circumstances, the assumptions of Lemma 7.5 are satisfied as confirmed in Lemma 5.4.

CHAPTER **8**

Conclusion

In the course of this thesis, we have introduced an innovative algorithm and demonstrated its exceptional efficiency in the pursuit of highly accurate globally optimal solutions for the Free Flight Trajectory Optimization Problem. Beyond its immediate application in flight planning, this methodology possesses broad-ranging versatility with the potential for diverse implementations in various path planning tasks. The applicability extends to routing of autonomous underwater vehicles (AUVs), ships, sailing boats, unmanned aerial vehicles (UAVs), drones, or robots as well as many other domains characterized by complex trajectory optimization challenges.

However, the significance of this work goes beyond the practical efficiency of the developed algorithm. It encompasses a profound exploration of the problem's duality, viewed through the lenses of classical path planning and optimal control. In this research, we have illuminated the intricate interplay between discrete and continuous optimization perspectives, unveiling that neither perspective inherently supersedes the other. Instead, their hybridization emerges as the most potent approach for solving challenging optimization problems like the Free Flight Trajectory Optimization Problem.

Central to this revelation lies the pivotal choice of the optimal switch-over point, exemplified here by the question for the right graph density in our algorithm. Through an in-depth examination of the unique attributes inherent to both discrete and continuous optimization paradigms, we have provided conclusive answers to this question.

Looking forward, several entry points beckon for future exploration: First and foremost, the results presented in Chapter 3 underscore the potential for substantial advancements by integrating local wind information into the algorithm. This insight motivates the development of adaptive algorithms, which could significantly enhance the algorithm's ability to navigate through complex wind patterns.

The application of Yen's algorithm as a fall-back strategy to provide alternative candidate paths, while rigorous, is well known to yield redundant results. To mitigate this, the exploration of alternative approaches like " k dissimilar path algorithms"

holds promise, enforcing the generation of genuinely different paths. Ideally, this would be combined with a posteriori estimators to assess the size of the convergence region surrounding an already discovered (local) optimum.

Furthermore, the scope of future work encompasses the potential replacement of the two fundamental optimization methods employed in the DisCOptER algorithm. Instead of utilizing a static graph in the first stage, exploring the integration of Rapidly-exploring Random Trees (RRT) or similar techniques could yield novel insights and trade-offs between optimality and efficiency. Similarly, in the second stage, the ordinary Newton's method might be substituted with Trust Region-based methods, offering pragmatic efficiency at the potential expense of guaranteed global optimality. The selection of these approaches should be meticulously tailored to individual applications, carefully weighing the trade-offs between optimality and practicality.

The DisCOptER algorithm is a versatile tool, ready to address a broad class of problems. Its solid theoretical foundation, as established in this thesis, ensures its robustness and applicability across various domains. This framework can be employed to overcome intricate optimization challenges and pave the way for further efficient and innovative solutions in the field of trajectory planning and beyond.